

CAPITAL UNIVERSITY OF SCIENCE AND
TECHNOLOGY, ISLAMABAD



Sliding Mode Based Robust Control Design Framework for Underactuated Mechanical Systems

by

Ibrahim Shah

A thesis submitted in partial fulfillment for the
degree of Doctor of Philosophy

in the

Faculty of Engineering

Department of Electrical Engineering

2018

**Sliding Mode Based Robust Control Design
Framework for Underactuated Mechanical
Systems**

By

Ibrahim Shah
(PE131010)

Dr. Shihua Li

School of Automation, Southeast University, China

Dr Ibrahim Beklan Kucukdemiral

Glasgow Caledonian University, UK

Dr. Fazal ur Rehman

(Thesis Supervisor)

Dr. Noor Muhammad Khan

(Head, Department of Electrical Engineering)

Dr. Imtiaz Ahmad Taj

(Dean, Faculty of Engineering)

**DEPARTMENT OF ELECTRICAL ENGINEERING
CAPITAL UNIVERSITY OF SCIENCE AND TECHNOLOGY
ISLAMABAD**

2018

Copyright © 2018 by Ibrahim Shah

All rights reserved. No part of this thesis may be reproduced, distributed, or transmitted in any form or by any means, including photocopying, recording, or other electronic or mechanical methods, by any information storage and retrieval system without the prior written permission of the author.

DEDICATED TO MY PARENTS



**CAPITAL UNIVERSITY OF SCIENCE & TECHNOLOGY
ISLAMABAD**

Expressway, Kahuta Road, Zone-V, Islamabad
Phone: +92-51-111-555-666 Fax: +92-51-4486705
Email: info@cust.edu.pk Website: <https://www.cust.edu.pk>

CERTIFICATE OF APPROVAL

This is to certify that the research work presented in the thesis, entitled “**Sliding Mode Based Robust Control Design Framework for Underactuated Mechanical Systems**” was conducted under the supervision of **Dr. Fazal ur Rehman**. No part of this thesis has been submitted anywhere else for any other degree. This thesis is submitted to the **Department of Electrical Engineering, Capital University of Science and Technology** in partial fulfillment of the requirements for the degree of Doctor in Philosophy in the field of **Electrical Engineering**. The open defence of the thesis was conducted on **November 06, 2018**.

Student Name: Mr. Ibrahim Shah (PE131010)

6/11/18

The Examining Committee unanimously agrees to award PhD degree in the mentioned field.

Examination Committee :

(a) External Examiner 1: Dr. Laiq Khan
Professor
COMSATS University, Abbottabad

(b) External Examiner 2: Dr. Abdul Qayyum Khan
Associate Professor
PIEAS, Islamabad

(c) Internal Examiner : Dr. Aamir Iqbal Bhatti
Professor
CUST, Islamabad

Supervisor Name : Dr. Fazal ur Rehman
Professor
CUST, Islamabad

Name of HoD : Dr. Noor Muhammad Khan
Professor
CUST, Islamabad

Name of Dean : Dr. Imtiaz Ahmad Taj
Professor
CUST, Islamabad

AUTHOR'S DECLARATION

I, **Mr. Ibrahim Shah** (Registration No. PE-131010), hereby state that my PhD thesis titled, '**Sliding Mode Based Robust Control Design Framework for Underactuated Mechanical Systems**' is my own work and has not been submitted previously by me for taking any degree from Capital University of Science and Technology, Islamabad or anywhere else in the country/ world.

At any time, if my statement is found to be incorrect even after my graduation, the University has the right to withdraw my PhD Degree.

A handwritten signature in black ink, appearing to read 'Ibrahim Shah', with the date '06/11/18' written below it.

(**Mr. Ibrahim Shah**)

Dated: 06 November, 2018

Registration No : PE-131010

PLAGIARISM UNDERTAKING

I solemnly declare that research work presented in the thesis titled “**Sliding Mode Based Robust Control Design Framework for Underactuated Mechanical Systems**” is solely my research work with no significant contribution from any other person. Small contribution/ help wherever taken has been duly acknowledged and that complete thesis has been written by me.

I understand the zero tolerance policy of the HEC and Capital University of Science and Technology towards plagiarism. Therefore, I as an author of the above titled thesis declare that no portion of my thesis has been plagiarized and any material used as reference is properly referred/ cited.

I undertake that if I am found guilty of any formal plagiarism in the above titled thesis even after award of PhD Degree, the University reserves the right to withdraw/ revoke my PhD degree and that HEC and the University have the right to publish my name on the HEC/ University Website on which names of students are placed who submitted plagiarized thesis.



6/11/18

(Mr. Ibrahim Shah)

Registration No. PE-131010

Dated: 06 November, 2018

List of Publications

1. **Ibrahim Shah**, Fazal ur Rehman, "Smooth Higher-Order Sliding Mode Control of a Class of Underactuated Mechanical Systems," *Arabian Journal for Science and Engineering*, vol. 42, issue 12, pp. 5147–5164, 2017, DOI 10.1007/s13369-017-2617-9, **Impact Factor = 0.865**
2. **Ibrahim Shah**, Fazal ur Rehman, "Smooth Second Order Sliding Mode Control of a Class of Underactuated Mechanical Systems," *IEEE Access*, vol. 6, pp. 1-13, 2018, DOI 10.1109/ACCESS.2018.2806568, **Impact Factor = 3.244**

Acknowledgements

In the name of Allah, The Most Gracious, The Dispenser of Grace. All praise is due to Allah alone, Who granted me with the opportunity and abilities to pursue my post graduate research and study. All respect is due to the Holy Prophet Muhammad (P.B.U.H), the last messenger of Allah, whose life is the perfect model for all human beings and Whose teachings are the source of guidance in all disciplines of life.

I am extremely grateful to my research adviser, Dr. Fazal ur Rehman, for his valuable guidance, strong encouragement and kind support towards my research and study. His strong mathematical background, clear concepts of systems and control theory have always been the foremost sources of motivation and inspiration for my research. In fact, pursuing research in control systems would not have been realized without Dr. Rehman's continued motivation, guidance, and advice.

I would like to thank all the teachers of Electrical Engineering Department at CUST, with special mention of Dr. Aamer Iqbal Bhatti, Dr. Imtiaz Taj, Dr. Raza Samar, Dr. Noor Muhammad Khan, and Mr. Tahir Awan, for imparting up-to-date and state-of-the-art knowledge, with devotion and sincerity, to all who come to CUST to seek education and carry out research.

Special thanks are due to Dr. Muhammad Mansoor Ahmad whose clear vision, great leadership, and endless efforts made CUST an excellent center for postgraduate research and study in the country.

Many thanks go to my research colleagues Waseem Abbasi, Sami Uddin, Sarfaraz, Nazim Saddiqi for technical discussion, encouraging remarks and fruitful suggestions. Sincere gratitude is due to Usama and Umair of FPGA and Microelectronics Lab for his sincere help and utmost cooperation.

Special thanks go to my colleagues and classmate Sultan Mehmood, Ali Syed and Sajid Ali for their sincere help and encouragement.

Special thanks also goes to Dr. Yosuf Zafar of the Embedded Systems Design Group (ESDG) for motivating me towards higher study and for his extraordinary help and cooperation in facilitating me with an occasion to pursue my research. I

am also thankful to all scientists, engineers and staff members of ESDG for their utmost helps during all stages of my higher study. May Allah bless them all.

I wish to thank my parent organization, Pakistan Atomic Energy Commission, for allowing me and granting study leave to complete my higher study. Higher Education Commission of Pakistan also deserves thanks for funding my study at CUST.

Above all, I am highly grateful to my family for their encouragement, for letting me ignore the many beautiful moments of life enjoying with them and for letting me ignore them when they needed me to be with them at many many occasions during all this process of long research.

Abstract

Underactuated mechanical systems have increasing number of practical applications, theoretical importance as nonlinear benchmark systems, and obvious advantages such as low cost and low weight. However, complex nonlinear behavior makes the control design problem a difficult task and the presence of uncertainties makes it further challenging. Hence, enhanced performance and robustness to uncertainties become critical issues in designing control for these systems.

Increasing practical applications and theoretical importance, make the design of a comprehensive robust control framework for underactuated mechanical systems an important problem. The explicit consideration of uncertainties in the design framework and its capabilities to effectively control the highly nonlinear dynamics will enhance the advantages of these systems. SMC techniques remain the only nonlinear control techniques that can better achieves these objectives.

In this research work, the author proposes a sliding mode based robust control design framework for underactuated mechanical systems. The framework is comprehensive applicable to classes of systems in a unified but simply-to-apply way. The framework is built on three sliding mode design solutions to the problem.

First, a standard SMC design is proposed for underactuated mechanical systems. The control laws take explicitly into account both the matched and unmatched uncertainties. Generic expressions for the sliding mode dynamics are derived. Analytic expressions for the sliding parameters are also given which characterize the desired performance. The main results are general and based on the Euler-Lagrange representation of these systems. Moreover, the discontinuous terms explicitly embedded in the control for the rejection of matched and unmatched uncertainties provide a better insight and understanding into the complex nature of uncertainties in these systems.

Second, to address the chattering associated with standard SMC, the author proposes the use of super-twisting algorithm for underactuated mechanical systems. This treatment is based on linear sliding mode surfaces and use some the results derived for the standard SMC.

Third, novel nonlinear sliding manifolds based on the *Lagrangian zero dynamics* are proposed for underactuated mechanical systems. The application of smooth higher order sliding mode control is proposed to enforce sliding mode in the manifold that guarantees stability of the overall dynamics of the system. The relative degree of these systems, in general, is not 1, and hence, leaving the designer with the choice of using higher order sliding mode control. The proposed design framework remarkably simplifies the control design problem of underactuated mechanical systems.

Finally, the nature of dynamics and singularities are hurdles in the global convergence of some underactuated mechanical systems. To overcome these hurdles, the author address the swingup control problems of these systems in a classical way and demonstrate successful swingup and balancing using the proposed higher order sliding mode control.

The proposed control design framework is validated for the following benchmark underactuated mechanical systems and achieve enhanced performance with the added advantage of remarkable robustness to uncertainties.

1. The Inertia-Wheel Pendulum
2. The Translational Oscillator with Rotational Actuator
3. The Acrobot
4. The Furuta Pendulum
5. The Overhead Crane
6. The Cart-Pole System
7. The Pendubot
8. The Beam-and-Ball System

Keywords: Underactuated Mechanical Systems, Nonlinear Systems, Nonlinear Sliding Surfaces, Sliding Mode Control, Higher Order Sliding Mode.

Contents

Author's Declaration	v
Plagiarism Undertaking	vi
List of Publications	vii
Acknowledgements	viii
Abstract	x
List of Figures	xvi
List of Tables	xx
Abbreviations	xxi
Symbols	xxii
1 Introduction	1
1.1 Background and Motivation	1
1.2 Problem Statement and Research Objectives	6
1.3 Research Contributions	8
1.4 Overview of This Thesis	10
2 Literature Review	12
2.1 Introduction	12
2.2 Theoretical Challenges in the Control of Underactuated Mechanical Systems	13
2.3 Modeling Approaches for Underactuated Mechanical Systems	14
2.4 Analytical Tools for Underactuated Mechanical Systems	17
2.4.1 Exact Feedback Linearization	17
2.4.2 Collocated Partial Feedback Linearization	18
2.4.3 Non-collocated Partial Feedback Linearization	19
2.4.4 Normal Forms	20
2.5 Control Design Approaches for Underactuated Mechanical Systems	21

3	Preliminaries	25
3.1	General n Degrees of Freedom (nDOF) Underactuated Mechanical Systems	25
3.2	Two Degrees of Freedom (2DOF) Underactuated Mechanical Systems	26
3.3	Three Degrees of Freedom (3DOF) Underactuated Mechanical Systems	27
3.4	Some Benchmark Underactuated Mechanical Systems	28
3.5	Sliding Mode Control and Observation	37
3.5.1	Standard Sliding Mode Control	39
3.5.2	Higher Order Sliding Mode (HOSM) Control	40
3.5.3	Sliding Mode Observation	41
3.5.4	The Benchmark Nonlinear Control Design Problem	42
4	Standard SMC Design for Underactuated Mechanical Systems	54
4.1	Problem Formulation	55
4.2	Standard SMC Design for Class-I Underactuated Mechanical Systems	57
4.2.1	Control Law Design	59
4.2.2	Application to Class-I Underactuated Mechanical Systems .	62
4.2.2.1	The Inertia-Wheel Pendulum (IWP)	63
4.2.2.2	Performance Analysis of The IWP	66
4.2.2.3	The TORA System	71
4.2.2.4	Performance Analysis of The TORA System	73
4.3	Standard SMC Design for Class-II Underactuated Mechanical Systems	79
4.3.1	Control Law Design	81
4.3.2	Application to Class-II Underactuated Mechanical Systems .	82
4.3.2.1	The Beam-and-Ball System	82
4.3.2.2	Performance Analysis of The Beam-and-Ball System	85
4.3.2.3	The Cart-Pole System	93
4.3.2.4	Performance Analysis of The Cart-Pole System . . .	95
4.3.2.5	The Overhead Crane	101
4.3.2.6	Performance Analysis of The Overhead Crane . . .	102
4.4	Chapter Summary and Conclusions	106
5	HOSM Design for Underactuated Mechanical Systems	108
5.1	HOSM Design for Class-I Underactuated Mechanical Systems . . .	109
5.1.1	Control Law Design	110
5.1.2	Application to Class-I Underactuated Mechanical Systems .	112
5.1.2.1	The Inertia-Wheel Pendulum	112
5.1.2.2	Performance Analysis of The IWP	112
5.1.2.3	The TORA System	115
5.1.2.4	Performance Analysis of The TORA System	115
5.2	HOSM Design for Class-II Underactuated Mechanical Systems . . .	117
5.2.1	Control Law Design	118
5.2.2	Application to Class-II Underactuated Mechanical Systems .	119
5.2.2.1	The Beam-and-Ball System	119

5.2.2.2	Performance Analysis of The Beam-and-Ball System	120
5.2.2.3	The Cart-Pole System	123
5.2.2.4	Performance Analysis of The Cart-Pole System	123
5.2.2.5	The Overhead Crane	125
5.2.2.6	Performance Analysis of The Overhead Crane	125
5.3	Chapter Summary and Conclusions	127
6	Smooth HOSM Design for Underactuated Mechanical Systems	128
6.1	Problem Formulation	129
6.2	Smooth HOSM Design for Class-I Underactuated Mechanical Systems	131
6.2.1	Nonlinear Sliding Manifolds and Control Law Design	133
6.2.2	Application to Class-I Underactuated Mechanical Systems	137
6.2.2.1	The Inertia-Wheel Pendulum (IWP)	137
6.2.2.2	Performance Analysis of The IWP	139
6.2.2.3	The TORA System	141
6.2.2.4	Performance Analysis of The TORA System	142
6.2.2.5	The Acrobot	144
6.2.2.6	Performance Analysis of The Acrobot	146
6.3	Smooth HOSM Design for Class-II Underactuated Mechanical Systems	149
6.3.1	Nonlinear Sliding Manifold and Control Law Design	151
6.3.2	Application to Class-II Underactuated Mechanical Systems	151
6.3.2.1	The Furuta Pendulum	151
6.3.2.2	Performance Analysis of The Furuta Pendulum	153
6.3.2.3	The Overhead Crane	155
6.3.2.4	Performance Analysis of The Overhead Crane	156
6.3.2.5	The Cart-Pole System	159
6.3.2.6	Performance Analysis of The Cart-Pole System	160
6.3.2.7	The Pendubot	162
6.3.2.8	Performance Analysis of The Pendubot	164
6.3.2.9	The Beam-and-Ball System	166
6.3.2.10	Performance Analysis of The Beam-and-Ball System	167
6.4	Comparison of Proposed Control Design Strategies	172
6.5	Novelty Highlights	178
6.6	Chapter Summary and Conclusions	180
7	Swingup and Balancing of Underactuated Mechanical Systems	182
7.1	Class-I Underactuated Mechanical Systems	183
7.1.1	Inertia-Wheel Pendulum (IWP)	183
7.1.2	The Acrobot	188
7.2	Class-II Underactuated Mechanical Systems	198
7.2.1	The Furuta Pendulum	198
7.2.2	Pendubot	202
7.3	Chapter Summary and Conclusions	211

8 Conclusion and Future Work	212
8.1 Conclusion	213
8.2 Future Work	214
Bibliography	215

List of Figures

3.1	Schematics of Class-I Underactuated Mechanical Systems	31
3.2	Schematics of Class-II Underactuated Mechanical Systems	35
3.3	The Magnetic Levitation System	36
3.4	3DOF Underactuated Mechanical Systems	38
3.5	Open loop response of the TORA system to $q(0) = [0.025, 0, 0, 0]^T$ in the presence of disturbance and parametric variations.	47
3.6	Closed loop response of the TORA system with SMC law (3.29) with $D_0 = 0$, $q(0) = [0.025, 0, 0, 0]^T$	48
3.7	Closed loop response of the TORA system with SMC law (3.29) with $D_0 = 0.02$, $q(0) = [0.025, 0, 0, 0]^T$	49
3.8	Closed loop response of the TORA system with HOSM control law (3.29), $q(0) = [0.025, 0, 0, 0]^T$	53
4.1	IWP - variation of γ_2 in Eq. (4.38) with design constants a , b , c , and its lower limit γ_{2c} , in Eq. (4.37).	65
4.2	IWP - Closed loop response with SMC law (4.12) ($\Gamma = 2000.0$, $D_1 = 0$, $D_2 = 0$), $q(0) = [\pi, 0, 0, 0]^T$,	68
4.3	IWP - Closed loop response with SMC law (4.12) ($\Gamma = 2000.0$, $D_1 = 0.2$, $D_2 = 0.2$), $q(0) = [\pi, 0, 0, 0]^T$,	69
4.4	IWP - Unmatched and matched disturbances $d_1(t)$, $d_2(t)$ and effective disturbances $\bar{d}_1(t)$, $\bar{d}_2(t)$ on unactuated variable q_1 and actuated variable q_2	70
4.5	TORA - variation of γ_2 (a) and q_{2c} (b) with design constants a and c , taking $b = 1$	74
4.6	TORA - Open loop response to $q(0) = [0.025, 0, 0, 0]^T$ in the pres- ence of disturbance.	75
4.7	TORA - Closed loop response with SMC law (4.12) ($\Gamma = 1.0$, $D_1 =$ 0 , $D_2 = 0$), $q(0) = [0.025, 0, 0, 0]^T$	76
4.8	TORA - Closed loop response with SMC law (4.12) ($\Gamma = 1.0$, $D_1 =$ 0.05 , $D_2 = 0.025$), $q(0) = [0.025, 0, 0, 0]^T$	77
4.9	TORA - Unmatched and matched disturbances $d_1(t)$, $d_2(t)$ and the effective disturbances $\bar{d}_1(t)$, $\bar{d}_2(t)$ on unactuated variable q_1 and actuated variable q_2	78
4.10	The Beam-and-Ball - Closed loop response with SMC law (4.54) ($\Gamma = 5.0$, $D_1 = 0$, $D_2 = 0$), $q(0) = [-0.6, 0, 1.0, 0]^T$	87
4.11	The Beam-and-Ball - Closed loop response with SMC law (4.54) ($\Gamma = 5.0$, $D_1 = 0$, $D_2 = 0$), $q(0) = [1.3, 0, 3.0, 0]^T$	87

4.12	The Beam-and-Ball - Closed loop response with SMC law (4.54) ($\Gamma = 2.5.0, D_1 = 0, D_2 = 0$), $q(0) = [1.5, 0, 6.0, 0]^T$	88
4.13	The Beam-and-Ball - Closed loop response with SMC law (4.54) ($\Gamma = 2.5.0, D_1 = 0.5, D_2 = 0$), $q(0) = [1.5, 0, 6.0, 0]^T$	89
4.14	The Beam-and-Ball - Closed loop response with SMC law (4.54) ($\Gamma = 2.5.0, D_1 = 0.5, D_2 = 0.025$), $q(0) = [1.5, 0, 6.0, 0]^T$	90
4.15	The Beam-and-Ball - Matched and unmatched disturbances $d_1(t)$, $d_2(t)$ and the effective disturbances $\bar{d}_1(t)$, $\bar{d}_2(t)$ on actuated variable q_1 and unactuated variable q_2	91
4.16	The Beam-and-Ball - Closed loop tracking response with SMC law (4.54) ($\Gamma = 2.5.0, D_1 = 0, D_2 = 0$), $q(0) = [0, 0, 0, 0]^T$	92
4.17	The Cart-Pole - variation of q_{2c} Eq. (4.73) with design constants a , b , and c through the design parameter γ_2 , Eq. (4.70b).	95
4.18	The Cart-Pole - Closed loop response with SMC law (4.54) ($\Gamma = 0.75.0, D_1 = 0, D_2 = 0$), $q(0) = [5, 0, \pi/3, 0]^T$	98
4.19	The Cart-Pole - Closed loop response with SMC law (4.54) ($\Gamma = 0.75.0, D_1 = 2, D_2 = 2$), $q(0) = [5, 0, \pi/3, 0]^T$	99
4.20	The Cart-Pole - Matched and unmatched disturbances $d_1(t)$, $d_2(t)$ and the effective disturbances $\bar{d}_1(t)$, $\bar{d}_2(t)$ on actuated variable q_1 and unactuated variable q_2	100
4.21	The Overhead Crane - Closed loop response with SMC law (4.54) ($\Gamma = 0.75, D_1 = 2, D_2 = 2$), $q(0) = [0, 0, 0, 0]^T$	104
4.22	The Overhead Crane - Matched and unmatched disturbances $d_1(t)$, $d_2(t)$ and the effective disturbances $\bar{d}_1(t)$, $\bar{d}_2(t)$ on actuated variable q_1 and unactuated variable q_2	105
5.1	IWP - Closed loop response with STA control law (5.14) ($\lambda_1 = -0.01, \lambda_2 = -0.02$), $q(0) = [\pi, 0, 0, 0]^T$,	114
5.2	TORA - Closed loop response with STA control law (5.14) ($\lambda_1 = 0.075, \lambda_2 = 0.050$), $q(0) = [0.025, 0, 0, 0]^T$	116
5.3	The Beam-and-Ball - Closed loop response with STA control law (5.14) ($\lambda_1 = -4.0, \lambda_2 = -0.5$), $q(0) = [-0.6, 0, 1.0, 0]^T$	121
5.4	The Beam-and-Ball - Closed loop response with STA control law (5.14) ($\lambda_1 = -4.0, \lambda_2 = -0.5$), $q(0) = [1.3, 0, 3.0, 0]^T$	121
5.5	The Beam-and-Ball - Closed loop response with STA control law (5.14) ($\lambda_1 = -4.0, \lambda_2 = -0.5$), $q(0) = [1.3, 0, 3.0, 0]^T$	122
5.6	The Cart-Pole - Closed loop response with STA control law (5.14) ($\lambda_1 = -35.0, \lambda_2 = -2.5$), $q(0) = [5, 0, \pi/3, 0]^T$	124
5.7	The Overhead Crane - Closed loop response with STA control law (5.14) ($\lambda_1 = -100.0, \lambda_2 = -0.5$), $q(0) = [0, 0, 0, 0]^T$	126
6.1	IWP - Closed loop response with control law (6.25) ($K_1 = 500, K_2 = 400$) and observer (6.26) ($\lambda_1 = 2, \lambda_2 = 3$), sliding parameters ($\alpha = 3, \beta = 2$), $q(0) = [\pi()/3, 0, 0, 0]^T$	140

6.2	TORA - Closed loop response with control law (6.25) ($K_1 = 20$, $K_2 = 25$) and observer (6.26) ($\lambda_1 = 1.5$, $\lambda_2 = 2$), sliding parameters ($\alpha = 1.5$, $\beta = 0$), $q(0) = [0.025, 0, 0, 0]^T$	143
6.3	Acrobot - Closed loop response with control law (6.25) ($K_1 = 75$, $K_2 = 50$) and observer (6.26) ($\lambda_1 = 1$, $\lambda_2 = 3$), sliding parameters ($\alpha = 8$, $\beta = 16$), $q(0) = [-\frac{\pi}{6}, 0, \frac{\pi}{3}, 0]^T$	148
6.4	Furuta Pendulum - Closed loop response with control law (6.25) ($K_1 = 25$, $K_2 = 20$) and observer (6.26) ($\lambda_1 = 1$, $\lambda_2 = 3$), sliding parameters ($\alpha = 0.3061$, $\beta = 0.2041$), $q(0) = [-5, 0, \frac{\pi}{6}, 0]^T$	154
6.5	The Overhead Crane - Closed loop response with control law (6.25) ($K_1 = 1$, $K_2 = 1.6$) and observer (6.26) ($\lambda_1 = 1$, $\lambda_2 = 3$), sliding parameters ($\alpha = 0.2041$, $\beta = 0.1020$), $q(0) = [0, 0, 0, 0]^T$	158
6.6	The Cart-Pole - Closed loop response with control law (6.25) ($K_1 = 20$, $K_2 = 15$) and observer (6.26) ($\lambda_1 = 3$, $\lambda_2 = 5$), sliding parameters ($\alpha = 0.1531$, $\beta = 0.0510$), $q(0) = [5, 0, \pi/3, 0]^T$	161
6.7	Pendubot - Closed loop response with control law (6.25) ($K_1 = 125$, $K_2 = 100$) and observer (6.26) ($\lambda_1 = 3$, $\lambda_2 = 5$), sliding parameters ($\alpha = 8$, $\beta = 16$), $q(0) = [-\frac{\pi}{6}, 0, \frac{\pi}{4}, 0]^T$	165
6.8	The Beam-and-Ball - Closed loop response with control law (6.25) ($K_1 = 5$, $K_2 = 6$) and observer (6.26) ($\lambda_1 = 4$, $\lambda_2 = 5$), sliding parameters ($\alpha = 1.5$, $\beta = 1.5$), $q(0) = [-0.6, 0, 1.0, 0]^T$	169
6.9	The Beam-and-Ball - Closed loop response with control law (6.25) ($K_1 = 5$, $K_2 = 6$) and observer (6.26) ($\lambda_1 = 4$, $\lambda_2 = 5$), sliding parameters ($\alpha = 1.5$, $\beta = 1.5$), $q(0) = [1.5, 0, 10.0, 0]^T$	170
6.10	The Beam-and-Ball - Closed loop tracking response with control law (6.25) ($K_1 = 5$, $K_2 = 6$) and observer (6.26) ($\lambda_1 = 4$, $\lambda_2 = 5$), sliding parameters ($\alpha = 1.5$, $\beta = 1.5$), $q(0) = [0, 0, 0, 0]^T$	171
6.11	IWP - Comparison of SMC law (4.12) ($\Gamma = 2000.0$), STA law (5.14) ($\lambda_1 = -0.01$, $\lambda_2 = -0.02$) and SSOSM law (6.25) ($K_1 = 500$, $K_2 = 400$), $q(0) = [\pi/3, 0, 0, 0]^T$	173
6.12	TORA - Comparison of SMC law (4.12) ($\Gamma = 1$), STA law (5.14) ($\lambda_1 = 0.075$, $\lambda_2 = 0.050$) and SSOSM law (6.25) ($K_1 = 500$, $K_2 = 400$), $q(0) = [0.025, 0, 0, 0]^T$	174
6.13	The Beam-and-Ball - Comparison of SMC law (4.12) ($\Gamma = 2.5$), STA law (5.14) ($\lambda_1 = -4.0$, $\lambda_2 = -0.5$) and SSOSM law (6.25) ($K_1 = 5$, $K_2 = 6$), $q(0) = [1.3, 0, 3.0, 0]^T$	175
6.14	The Cart-Pole - Comparison of SMC law (4.12) ($\Gamma = 0.75$), STA law (5.14) ($\lambda_1 = -35.0$, $\lambda_2 = -2.5$) and SSOSM law (6.25) ($K_1 = 20$, $K_2 = 15$), $q(0) = [5, 0, \pi/3, 0]^T$	176
6.15	The Overhead Crane - Comparison of SMC law (4.12) ($\Gamma = 0.45$), STA law (5.14) ($\lambda_1 = -80.0$, $\lambda_2 = -0.5$) and SSOSM law (6.25) ($K_1 = 1$, $K_2 = 1.6$), $q(0) = [0, 0, 0, 0]^T$	177
7.1	IWP - Closed loop response with control law (7.6) ($K_d = 11$, $K_p = 30$), $q(0) = [\pi, 0, 0, 0]^T$	186

7.2	IWP - Swingup with control law (7.6) ($K_d = 11, K_p = 30$) and balancing with HOSM control law (6.25) ($K_1 = 500, K_2 = 400$) and observer (6.26) ($\lambda_1 = 2, \lambda_2 = 3$), sliding parameters ($\alpha = 3, \beta = 2$), $q(0) = [\pi, 0, 0, 0]^T$	187
7.3	Acrobot - Closed loop response with control law (7.12) ($K_d = 3, K_p = 2$), $q(0) = [\pi, 0, 0, 0]^T$	191
7.4	Acrobot - Closed loop response with control law (7.12) ($K_d = 1, K_p = 20$), $q(0) = [\pi, 0, 0, 0]^T$	192
7.5	Acrobot - Swingup with control law (7.12) ($K_d = 1, K_p = 20$) and balancing with HOSM control law (6.25) ($K_1 = 75, K_2 = 50$) and observer (6.26) ($\lambda_1 = 1, \lambda_2 = 3$), sliding parameters ($\alpha = 8, \beta = 16$), $q(0) = [\pi, 0, 0, 0]^T$	193
7.6	Acrobot - Closed loop response with control law (7.17) ($K_d = 12, K_p = 36$), $q(0) = [\pi, 0, 2\pi, 0]^T$	196
7.7	Acrobot - Swingup with control law (7.17) ($K_d = 12, K_p = 36$) and balancing with HOSM control law (6.25) ($K_1 = 75, K_2 = 50$) and observer (6.26) ($\lambda_1 = 1, \lambda_2 = 3$), sliding parameters ($\alpha = 8, \beta = 16$), $q(0) = [\pi, 0, 2\pi, 0]^T$	197
7.8	Furuta Pendulum - Closed loop response with control law (7.24) ($K_d = 8, K_p = 10$), $q(0) = [-5, 0, \pi, 0]^T$	200
7.9	Furuta Pendulum - Swingup with control law (7.24) ($K_d = 8, K_p = 10$) and balancing with HOSM control law (6.25) ($K_1 = 8, K_2 = 10$) and observer (6.26) ($\lambda_1 = 1, \lambda_2 = 3$), sliding parameters ($\alpha = 8, \beta = 16$), $q(0) = [-5, 0, \pi, 0]^T$	201
7.10	Pendubot - Closed loop response with control law (7.30) ($K_d = 10, K_p = 125$), $q(0) = [\pi, 0, 0, 0]^T$	205
7.11	Pendubot - Swingup with control law (7.30) ($K_d = 10, K_p = 125$) and balancing with HOSM control law (6.25) ($K_1 = 125, K_2 = 100$) and observer (6.26) ($\lambda_1 = 3, \lambda_2 = 5$), sliding parameters ($\alpha = 8, \beta = 16$), $q(0) = [\pi, 0, 0, 0]^T$	206
7.12	Pendubot - Closed loop response with control law (7.35) ($K_d = 4.3, K_p = 6$), $q(0) = [\pi, 0, \frac{\pi}{2}0, 0]^T$	209
7.13	Pendubot - Swingup with control law (7.35) ($K_d = 4.3, K_p = 6$) and balancing with HOSM control law (6.25) ($K_1 = 125, K_2 = 100$) and observer (6.26) ($\lambda_1 = 3, \lambda_2 = 5$), sliding parameters ($\alpha = 8, \beta = 16$), $q(0) = [\pi, 0, \frac{\pi}{2}0, 0]^T$	210

List of Tables

4.1	The Euler-Lagrange Equation (4.5) for IWP and TORA System . . .	62
6.1	Lagrangian Zero Dynamic Function $f(z, \dot{z}, \xi, \dot{\xi})$ in Eqs. (6.9), (6.52)	178
6.2	Nonlinear Sliding Manifolds in Transformed Coordinates $(z, \dot{z}, \xi, \dot{\xi})$	178
6.3	Nonlinear Sliding Manifolds in Actual Coordinates $(q_1, \dot{q}_1, q_2, \dot{q}_2)$. . .	178
6.4	Control Coefficient $b(q_1, \dot{q}_1, q_2, \dot{q}_2)$ in Eq. (6.24)	179

Abbreviations

2DOF	Two Degrees Of Freedom
3DOF	Three Degrees Of Freedom
FOSM	First Order Sliding Mode
HOSM	Higher Order Sliding Mode
IDA-PBC	Interconnection and Damping Assignment-Passivity Based Control
IWP	Inertia-Wheel Pendulum
<i>n</i>DOF	<i>n</i> Degrees Of Freedom
PBC	Passivity Based Control
PFL	Partial Feedback Linearization
RTA	Real Twisting Algorithm
SMC	Sliding Mode Control
SOSM	Second Order Sliding Mode
SSOSM	Smooth Second Order Sliding Mode
SRTA	Smooth Real Twisting Algorithm
SSTA	Smooth Super-Twisting Algorithm
STA	Super-Twisting Algorithm
TORA	Translational Oscillator with Rotational Actuator
UMS	Underactuated Mechanical System
VSS	Variable Structure System
VTOL	Vertical Take Off and Landing

Symbols

m	mass
g	acceleration due to gravity
L	Length
F	Force
τ	Torque
\mathcal{L}	Lagrangian
\mathcal{H}	Hamiltonian
\mathcal{E}	Total Energy

Chapter 1

Introduction

This chapter introduces the research work carried out in this thesis. First, building upon the background, the author explains how motivation for this work was developed and then clearly identifies the research problem and defines research objectives. Novel contributions this research adds to the existing body of scientific knowledge are summarized. The chapter concludes with an overview of this thesis.

1.1 Background and Motivation

Mechanical Systems are among the oldest systems invented by humans to be used as helping systems in their daily life. Today mechanical systems are used in almost every aspect of practical life. The range of these systems is broad and the applications are diverse, for example; the basic ones such as a wheel, a pulley, and an on-off valve on a water line, simple systems such as a sewing machine, a bicycle, large systems such as the initial steam engine, and the more complex and sophisticated systems such as today's industrial systems, automobiles, robots, aerospace systems, and marine systems.

With the passage of time, as these systems became more common in use and more complex in structure and functionality, their manual operation became tedious

and less productive. Humans started thinking to somehow *regulate or automate* these systems for better output both quantitatively and qualitatively. This need and realization of regulation or automation led to the development of **Mechanical Control Systems** and hence the application of **Control Theory** in the field of **Mechanics**. Water level regulator for steam boiler by I. Pulzunov in 1765, and *flyball governor* for controlling the speed of steam engine, *an all-mechanical system*, by James Watt in 1769, can be cited to be the first reported use of **Automatic Feedback Control** in mechanical systems. State-of-the-art research and developments in control theory on one front and advances in technologies like electrical, analog and digital electronics, microprocessors, and computers on the other front, made it possible to design and develop more sophisticated mechanical control systems. The results of these achievements by humans are numerous and their impacts are enormous as reflected by the use of high performance and quality systems in today's practical life.

Traditionally, from control point of view, mechanical control systems have been studied under the following subclasses:

1. **Fully Actuated Mechanical Systems:** Number of control actuators is equal to the number of degrees to be controlled.
2. **Underactuated Mechanical Systems:** Number of control actuators is less than the number of degrees to be controlled.
3. **Nonholonomic Systems:** Systems have nonintegrable first order constraints on their velocities.

The control problem of fully actuated mechanical systems is not a big issue. The reason is that the matured and established nonlinear control technique of exact *feedback linearization* [1] is applicable that renders the system linear and then linear control methods such as pole placement or frequency domain analysis can be used to design the control.

Interest in the control of nonholonomic systems started in the 70's and established

as a matured standalone field in the 90's [2]. Historically, nonholonomic systems are the most widely studied mechanical systems as evident by the vast amount of literature, and, in fact, are still the subject of active research in the control community. The most important reason, which led to this research and other interesting control problems, is the fact that nonholonomic systems *fail* the famous necessary condition of Brockett [3] for the existence of *smooth continuous time invariant state feedback control laws* for stabilization. In fact, the origin of research interest in underactuated mechanical systems can be traced back to nonholonomic systems due to the initial realization that nonholonomic systems obey *first order (velocity or kinematic) constraints* while underactuated mechanical systems obey *second order (acceleration or dynamic) constraints* [4–6].

Motivated by theoretical challenges in the beginning, research in the control and analysis of underactuated mechanical systems started in the 90's [4–10]. In the last decade, research shifted from theoretical nature to practical one when the usefulness of underactuated mechanical systems was realized in diverse applications of scientific and engineering importance. The broad application areas of underactuated mechanical systems include robotics, industry, aerospace systems and marine systems. Apart from practical applications, underactuated mechanical systems have been of great importance and interest in research and education of control theory as prototype systems for high order nonlinear complex systems. Both theoretical importance and practical usefulness have contributed to research activities focused on the control and analysis of underactuated mechanical systems in the last two decades [11, 12].

Underactuation arises due to less number of control actuators than the number of degrees to be controlled. Reasons of underactuation may be natural due to dynamics of the system itself or intentional/artificial for some useful practical purpose, for example:

- natural dynamics; aircraft, helicopter, underwater vehicle
- actuator failure
- low cost

- low weight
- low power consumption, important in some applications like aerospace
- low system level complexity
- low risk/damage to human/objects, if hit by (at the cost of high vulnerability to disturbances)
- creating prototype/benchmark nonlinear system for education and research.

Examples of practical underactuated mechanical systems include the following:

- robotics; flexible-link joints, mobile robots, and other kinds of manipulators.
- aerospace; aircraft, spacecrafts, helicopters, space robots, satellites, space exploration systems
- marine; ships, underwater vehicles and surface vessels
- industrial: object manipulation and transportation
- education and research: The Inertia-Wheel Pendulum, The TORA System, The Acrobot, The Furuta Pendulum, The Overhead Crane, The Cart-Pole System, The Pendubot, and The Beam-and-Ball System.

However, the benefits of underactuation are associated with difficult control design and often poor system performance. The reason is that complex nonlinear behavior, nonholonomic nature, and control coupling in the actuated and underactuated parts of the dynamics make control design a difficult problem. On one hand, linear controllers, based on the standard Jacobian linearized model of the system around an equilibrium point, have very small region of attraction due to strong nonlinear dynamics of the system and hence are of little practical use. On the other hand, due to underactuation, the established nonlinear control techniques such as input-output and feedback linearization, and in some cases direct backstepping, are not applicable. The presence of external disturbances and model uncertainties

and makes this difficult problem further challenging.

The complexity of dynamics and the uniqueness of required design technique have dictated the research to a system by system approach for underactuated mechanical systems, for example,

1. The Inertia-Wheel Pendulum [13–15]
2. The TORA System [16–26]
3. The Acrobot [27–31]
4. The Furuta Pendulum [32–36]
5. The Overhead Crane [37–43]
6. The Cart-Pole System [44–51]
7. The Pendubot [52–62],.
8. The Beam-and-Ball System [63–69]

There are some excellent class based design approaches for mechanical systems, for example, energy based [9], Controlled Lagrangian [70, 71], IDA-PBC [72], hybrid [73, 74], and equivalent-input-disturbance approach [75], but these techniques lack robustness. Still, there are excellent standard and second order sliding mode approaches, for example, [76–80] but these approaches suffers from chattering that is not desired and even practically not applicable in mechanical systems.

Due to absence of direct independent control actuators for some of the degrees of freedom, underactuated mechanical systems are more vulnerable to disturbances. Furthermore, the effects of both matched and unmatched disturbances are coupled, similar to the control itself, to the actuated and unactuated parts of the dynamics. Standard SMC provides a good measure of the effects of disturbance and the way to make system response robust to these effects. Analysis of the effects of disturbance with standard SMC can be used to get insight into the adverse effects of disturbance coupled in the unactuated and actuated parts of the dynamics.

The above discussion and analysis clarifies that the benefits of underactuated mechanical systems are numerous but their realization in practical applications is limited due to difficult control design problem. There are excellent research works in the literature but most are limited to a system by system approach as mentioned above, or lack robustness or suffers from chattering, and hence, there is a strong basis and need to investigate a novel robust and chattering free smooth control design approach applicable to classes of underactuated mechanical systems in a unified but simple to apply way. In summary, practical importance of underactuated mechanical systems and the theoretically challenging nature of the control problem motivates for investigating a comprehensive control design framework based on smooth higher order sliding modes for the realization of above mentioned benefits in high performance control applications.

1.2 Problem Statement and Research Objectives

Underactuated mechanical systems have theoretical and practical importance with the added advantages of underactuation. But the benefits associated with underactuation come at a greater cost of difficult control design due to complex nonlinear behavior and control coupling. Lack of direct actuators for some of the degrees of freedom makes underactuated mechanical systems more susceptible to internal model uncertainties and unknown external disturbances. Greater probability of mismatch between the real plant and its mathematical model on which control synthesis is based results in model uncertainties and external disturbances are always common in real world applications. So designing robust nonlinear control schemes to effectively control the complex nonlinear behavior of underactuated mechanical systems in the presence of model uncertainties and external disturbances becomes an obviously important control problem. Solving this challenging control problem will help in the realization of full advantages and usefulness of underactuated mechanical systems in high performance control applications.

Sliding mode control [81–83], which can efficiently control higher order complex

nonlinear dynamics and also provides robustness to internal model uncertainties and unknown external disturbances, remains the only nonlinear control technique that can provide solution to the above mentioned control design problem. There are other nonlinear control techniques developed for mechanical systems for example energy based [9], Controlled Lagrangian [70, 71], IDA-PBC [72], hybrid [73, 74], and equivalent-input-disturbance approach [75] but these techniques lack robustness. Furthermore, the excellent standard and second order sliding mode approaches, for example, [76–80], suffers from chattering that causes wear and tear in mechanical systems, and hence, practically not applicable.

The research objective in this work is to investigate, using sliding mode control theory, a comprehensive and unified but yet simple to apply high performance robust control design framework for underactuated mechanical systems. The framework must be general and hence applicable to whole class of underactuated mechanical systems instead to a specific system. Since chattering is undesired and even practically not applicable, especially, in mechanical control systems, the framework must consider smooth control action. Finally, the framework is numerically validated for the following benchmark underactuated mechanical systems

1. The Inertia-Wheel Pendulum
2. The TORA System
3. The Acrobot
4. The Furuta Pendulum
5. The Overhead Crane
6. The Cart-Pole System
7. The Pendubot
8. The Beam-and-Ball System

1.3 Research Contributions

The main contributions, this research work adds to the existing body of scientific knowledge, are summarized as below:

- A comprehensive and unified but simple-to-apply robust control design framework, based on the application of sliding mode control theory, is proposed for underactuated mechanical systems.
- First, generic standard sliding mode control laws are proposed for the two classes of underactuated mechanical systems. The control laws take explicitly into account both the matched and unmatched uncertainties. The control laws use linear sliding manifolds based on the actuated and unactuated configuration variables. Generic expressions, describing the sliding mode dynamics in each class of systems, are derived. Analytic expressions, for performance design parameters of the sliding manifold, are derived in closed form. These expressions enable the designer to choose stable sliding parameters, in terms of system physical parameters, for the achievement of desired performance in an intuitively simple way. The main results of this treatment are general. The control laws and expressions for the sliding mode dynamics are based on the general Euler-Lagrange equations of underactuated mechanical systems instead of a specific system. The effects of matched and unmatched uncertainties on system stability are analyzed. Furthermore, to reduce chattering and achieve smooth control desired and demanded for mechanical systems, the application of super-twisting algorithm is investigated using the results of this treatment.
- Second, to address the chattering associated with standard SMC, the author proposes the use of super-twisting algorithm for underactuated mechanical systems. This treatment is based on linear sliding mode surfaces and use some the results derived for the standard SMC.

- Third, to achieve global convergence of underactuated mechanical systems, nonlinear sliding manifolds are proposed. Exploiting the existing transformation techniques, the dynamics of the two classes of underactuated mechanical systems are transformed into an actuated/unactuated nonlinear subsystem and an unactuated/actuated linear subsystem. The nonlinear subsystem represents the *Lagrangian zero dynamics* of underactuated mechanical system. Nonlinear sliding manifolds for the Lagrangian zero dynamics are introduced and the application of smooth higher order sliding mode control is proposed to enforce sliding mode in the manifold that guarantees stability of the overall dynamics of underactuated mechanical system. The author finds that the relative degree of underactuated mechanical systems, in general, is not 1, and hence, standard sliding mode is not applicable. This leaves the designer with the choice of using higher order sliding mode. However, this obstacle turns out to be a blessing as higher order sliding mode are smooth as compared to standard sliding mode. Furthermore, to provide robustness against uncertainties the use of well known existing observers is identified. The proposed design framework remarkably simplifies the control design problem of underactuated mechanical systems in general and of a class of them in specific. The dynamics of this later class are in the nontriangular quadratic normal form and which would otherwise be quite challenging.
- Finally, the swingup control problem of underactuated mechanical systems is investigated in a more comprehensive way using the collocated and non-collocated partial feedback linearization. Successful swingup and balancing by HOSM control is demonstrated for benchmark underactuated mechanical systems.
- The proposed design framework is validated for the following benchmark underactuated mechanical systems:
 1. The Inertia-Wheel Pendulum
 2. The TORA System
 3. The Acrobot

4. The Furuta Pendulum
 5. The Overhead Crane
 6. The Cart-Pole System
 7. The Pendubot
 8. The Beam-and-Ball System
- The results are improved to and in agreement with the existing standard works reported in the literature.
-

1.4 Overview of This Thesis

The overview of the rest of this thesis is as follows:

Chapter 2 presents a rigorous and thorough literature review of underactuated mechanical systems from control point of view. Theoretical challenges in the control of underactuated mechanical systems are discussed. Different analytical tools and control design techniques developed over the past years are reviewed.

Chapter 3 presents some preliminaries including dynamical modeling of underactuated mechanical systems, simplifying analytical tool, collocated and noncollocated partial feedback linearization, and transformation to desired normal forms. A brief introduction to sliding mode control from application point of view is also presented here.

Chapter 4 presents standard SMC design for underactuated mechanical systems based on linear sliding manifolds. The associated expressions for sliding mode dynamics and analytic expressions, in closed form, for performance design parameters of the sliding manifold are derived here. The design procedure is demonstrated for benchmark underactuated mechanical systems.

Chapter 5 investigates the application of HOSM based on super-twisting algorithm for underactuated mechanical systems in order to reduce chattering inherently

present in the standard SMC. The design procedure is demonstrated for benchmark underactuated mechanical systems.

Chapter 6 propose nonlinear sliding manifolds for underactuated mechanical systems and the application of smooth HOSM control to enforce sliding mode in the manifold. The design procedure is demonstrated for benchmark underactuated mechanical systems.

Chapter 7 addresses the swingup control problem of underactuated mechanical systems. The chapter demonstrates successful swingup and balancing for benchmark underactuated mechanical systems.

Chapter 8 concludes this research and outline possible future work.

Chapter 2

Literature Review

This chapter presents a rigorous literature review of underactuated mechanical systems from control point of view. Theoretical challenges in the control of underactuated mechanical systems are discussed. Different analytical tools and control design techniques developed over the past years are reviewed.

2.1 Introduction

Analysis and control of underactuated mechanical systems remains one of the active areas of research in the last two decades. Research interest in these systems started with the study of nonholonomic mechanical systems. Analysis and control of nonholonomic mechanical systems [2, 84] started in the early 80's and became a matured and established area of research in the mid 90's. Study and research in nonholonomic systems generated some interesting control problems. Being nonholonomic in nature, it was proved that these systems were not stabilizable by smooth continuous time invariant state feedback control laws [3], [85].

As some of these nonholonomic mechanical systems were inherently underactuated, the interest shifted towards the analysis and control of underactuated mechanical systems in the 90's with the first applications mainly in robot manipulators [4, 7, 8, 86–92]. This interest got momentum when the use of underactuated

mechanical systems became increasingly common in scientific and engineering applications such as robotics, aerospace systems and marine systems. These developments led to the establishment of research in underactuated mechanical systems as one of the most active field both from technological and theoretical point of view and research in the control and analysis of underactuated mechanical systems started as a field [5, 6, 9, 10, 72, 73, 93–96].

Nonholonomic mechanical systems have first order (kinematic or velocity) constraints. As parts of the dynamics of an underactuated mechanical system can be written as second order (dynamic or acceleration) constraints, in contrast to nonholonomic mechanical systems, underactuated mechanical systems were also called mechanical control systems with second order nonholonomic constraints [4–6].

2.2 Theoretical Challenges in the Control of Underactuated Mechanical Systems

Underactuation, i.e. fewer number of independent control actuators than the configuration variables to be controlled, fundamentally makes the control problem of underactuated mechanical systems a highly challenging task. Moreover, strong non linear behavior, nonholonomic constraints, and input coupling adds extra design difficulties to this challenging control problem. Feedback linearization is an important analytical and design tool used as initial step in the design of nonlinear control for nonlinear dynamical systems [1]. However due to underactuation. *exact feedback linearization* for underactuated mechanical systems is not possible. This can be seen from the dynamical equations of motions for underactuated mechanical systems where the control input matrix is non invertible, and hence, an explicit change of control is not possible that implies the exact feedback linearization does not exist.

In [8, 9], it was shown that for a certain class of underactuated mechanical systems, the dynamics can be partitioned into an unactuated subsystem and an actuated

subsystem and a *partial feedback linearization* of the actuated subsystem is possible. But still, the unactuated subsystem remains nonlinear and coupled to the linearized actuated subsystem.

Later on, in [94], it was shown that an explicit change of coordinates is possible to decouple the two subsystems in an actuated one and an unactuated one. But still, the decoupled systems are strongly nonlinear and, as mentioned, this is for a special class of underactuated mechanical systems not all the systems.

2.3 Modeling Approaches for Underactuated Mechanical Systems

A brief introduction to dynamical modeling of underactuated mechanical systems will help to understand the difficulties of the control problem and to fully appreciate the analytical tools and the design techniques developed over the years. Usually, Newton's second law is used to arrive at the equations of motion of a dynamical systems but for mechanical systems other representations are useful and easy to work with. Different but equivalent representations, which have been the basis of different control design approaches in the past, are reviewed in the following.

Euler-Lagrange Representation:

The Euler-Lagrange equations of motion of an n degrees of freedom mechanical control system are [97]:

$$\frac{d}{dt} \frac{\partial \mathcal{L}}{\partial \dot{q}} - \frac{\partial \mathcal{L}}{\partial q} = F(q)u \quad (2.1)$$

where $\mathcal{L}(q, \dot{q})$ is the *Lagrangian* of the mechanical system, $F(q) \in \mathfrak{R}^{n \times m}$ is the control input matrix, $u \in \mathfrak{R}^m$ is the control input vector, and $q \in \mathfrak{R}^n$ is the configuration vector in generalized coordinates. The case, $m = \text{rank}(F) = n$, represents a fully actuated mechanical system, and, the case, $m = \text{rank}(F) < n$, characterizes an underactuated mechanical system.

The vector form of Eq. (2.1) is:

$$M(q)\ddot{q} + C(q, \dot{q})\dot{q} + G(q) = F(q)u \quad (2.2)$$

where $M(q)$ is the positive definite symmetric inertia matrix, $G(q)$ have gravitational terms and $C(q, \dot{q})\dot{q}$ have centrifugal and Coriolis terms.

The *Lagrangian* $\mathcal{L}(q, \dot{q})$ of the system is defined as below:

$$\mathcal{L}(q, \dot{q}) = K(q, \dot{q}) - V(q) = \frac{1}{2}\dot{q}^T M(q)\dot{q} - V(q) \quad (2.3)$$

which is the difference between kinetic energy, $K(q, \dot{q})$, and potential energy, $V(q)$.

Note that in Eq. (2.2) the matrices $M(q)$ and $C(q, \dot{q})$ are related as:

$$X = \dot{M}(q) - 2C(q, \dot{q}) \quad (2.4)$$

where X is a skew symmetric matrix such that $V^T X V = 0$ and $V \in \mathcal{R}^n$ is an arbitrary vector and V^T is its transpose.

Since the inertia matrix $M(q)$ is symmetric, we have:

$$\dot{M}(q) = C(q, \dot{q}) + C^T(q, \dot{q}) \quad (2.5)$$

Legendre Normal Form Representation:

Taking the Legendre transform of $\mathcal{L}(q, \dot{q})$ in Eq. (2.3) with respect to \dot{q} , we have:

$$p = \frac{\partial \mathcal{L}}{\partial \dot{q}} = M(q)\dot{q} \quad (2.6)$$

Using Eqs. (2.2), (2.5) and (2.6) we have:

$$\begin{aligned} \dot{q} &= M^{-1}(q)qp \\ \dot{p} &= -G(q) + \bar{C}^T(q, p)M^{-1}(q)p + F(q)u \end{aligned} \quad (2.7)$$

where $\bar{C}^T(q, p) = C^T(q, M^{-1}(q)p)$.

Eq. (2.7) is the *Legendre Normal Form* of mechanical control system in Eq. (2.1). Eqs. (2.1) and (2.7) are two different but equivalent representation of the same mechanical control system. Eq. (2.1) is a second order ODE and Eq. (2.7) is first order ODE that is more appropriate for controllability and observability analysis of mechanical control systems.

Defining $x = [x_1, x_2]^T = [q, p]^T$, Eq. (2.7) can be cast into the most familiar form of:

$$\dot{x} = f(x) + g(x)u \quad (2.8)$$

that is *affine* in control u [1] and many nonlinear analytical tools for analysis and control design exist for such systems.

Hamiltonian Representation:

The *Hamiltonian* $\mathcal{H}(q, p)$ of a mechanical control systems is defined as:

$$\mathcal{H}(q, p) = \frac{1}{2}p^T M^{-1}(q)p + V(q) \quad (2.9)$$

Using Eq. (2.9), the *Hamiltonian* representation of a mechanical system is obtained as:

$$\begin{aligned} \dot{q} &= \frac{\partial \mathcal{H}(q, p)}{\partial p} \\ \dot{p} &= -\frac{\partial \mathcal{H}(q, p)}{\partial q} + F(q)u \end{aligned} \quad (2.10)$$

Energy Representation:

Still another property of interest used in energy based control methods is the total *Energy* $\mathcal{E}(q, \dot{q})$ of a conservative mechanical control system defined as follows:

$$\mathcal{E}(q, \dot{q}) = K(q, \dot{q}) + V(q) = \frac{1}{2}\dot{q}^T M(q)\dot{q} + V(q) \quad (2.11)$$

The time rate of change of $\mathcal{E}(q, \dot{q})$ is:

$$\dot{\mathcal{E}}(q, \dot{q}) = \dot{q}^T \left[F(q)u - \frac{\partial P(\dot{q})}{\partial \dot{q}} \right] \quad (2.12)$$

where $P(\dot{q})$ represents the dissipation term of underactuated mechanical system.

2.4 Analytical Tools for Underactuated Mechanical Systems

The following state of the art analytical tools were developed for underactuated mechanical systems over the year. These tools were used in most works as initial simplifying design steps.

2.4.1 Exact Feedback Linearization

The vector form of the Euler-Lagrange equations (2.1) of a mechanical control system is:

$$M(q)\ddot{q} + C(q, \dot{q})\dot{q} + G(q) = F(q)u \quad (2.13)$$

First, noting that for the fully actuated case, since $F(q)$ is invertible, redefining the control u as:

$$u = F^{-1}(q) [M(q)v + C(q, \dot{q})\dot{q} + G(q)] \quad (2.14)$$

and defining state variables as $x = [x_1, x_2]^T = [q, \dot{q}]^T$, we can write (2.13) as:

$$\begin{aligned} \dot{x}_1 &= x_2 \\ \dot{x}_2 &= v \end{aligned} \quad (2.15)$$

which is a linear equation, a vector double integrator, and hence, the fully actuated mechanical control system can be rendered *exact feedback linearizable*. But this is not the case for the unactuated case since $F(q)$ is not invertible and we cannot find the control transformation (2.14), and hence, cannot arrive at Eq. (2.15).

2.4.2 Collocated Partial Feedback Linearization

As mentioned above, due to underactuation, exact feedback linearization is not applicable in the case of underactuated mechanical systems. However, for certain classes of underactuated mechanical systems, a partial feedback linearization is possible. The most important and initial work on linearization of underactuated mechanical systems is the collocated Partial Feedback Linearization (PFL) due to Spong [8, 9]. This linearization has been used by many researchers as an initial step in the design of control for underactuated mechanical systems [9, 27, 73].

Consider for the special underactuation case of $F(q) = [0, I_m]^T$, then partitioning the configuration vector q as $q = [q_1, q_2]^T$, where $q_1 \in \mathfrak{R}^{(n-m)}$ and $q_2 \in \mathfrak{R}^{(m)}$ are the unactuated and the actuated configuration vectors, and partitioning the inertia matrix $M(q)$ accordingly, the dynamics in (2.13) can be written as:

$$\begin{aligned} m_{11}(q)\ddot{q}_1 + m_{12}(q)\ddot{q}_2 + c_1(q, \dot{q}) + g_1(q) &= 0 \\ m_{21}(q)\ddot{q}_1 + m_{22}(q)\ddot{q}_2 + c_2(q, \dot{q}) + g_2(q) &= u \end{aligned} \quad (2.16)$$

where $c_1(q, \dot{q})$ and $c_2(q, \dot{q})$ contain Coriolis and centrifugal, and $g_1(q)$ and $g_2(q)$ contain the gravitational terms.

By defining the invertible control transformation for u in (2.16) as:

$$u = ((m_{22} - m_{21}m_{11}^{-1}m_{12}))v + c_2(q, \dot{q}) + g_2(q) - m_{21}m_{11}^{-1}(c_1(q, \dot{q}) + g_1(q)) \quad (2.17)$$

Eq. (2.16) can be written as:

$$\begin{aligned} \ddot{q}_1 &= -m_{11}^{-1}(c_1(q, \dot{q}) + g_1(q)) - m_{11}^{-1}m_{12}v \\ \ddot{q}_2 &= v \end{aligned} \quad (2.18)$$

where the second part is a linear double integrator subsystem.

Defining $[q_1, p_1, q_2, p_2]^T = [q_1, \dot{q}_1, q_2, \dot{q}_2]^T$ as state variables for (2.18), the state

space representation of (2.18) can be written as:

$$\begin{aligned}
 \dot{q}_1 &= p_1 \\
 \dot{p}_1 &= f_0(q, p) + g_0(q)v \\
 \dot{q}_2 &= p_2 \\
 \dot{p}_2 &= v
 \end{aligned} \tag{2.19}$$

where

$$\begin{aligned}
 f_0(q, p) &= -m_{11}^{-1}(c_1(q, \dot{q}) + g_1(q)) \\
 g_0(q) &= -m_{11}^{-1}m_{12}
 \end{aligned} \tag{2.20}$$

Thus any underactuated mechanical system in the form (2.16) can be partially linearized as in (2.19) into a *nonlinear* unactuated subsystem (q_1, p_1) and a *linear* actuated subsystem (q_2, p_2) . But still, both the subsystems are coupled, through the new control input v , that poses difficulties in the control design for underactuated mechanical systems in the form of (2.16).

2.4.3 Non-located Partial Feedback Linearization

Another linearization due to Olfati-Saber [94] in which the unactuated subsystem is linearized is called non-located Partial Feedback Linearization (PFL). This linearization also has been used by many researchers as an initial step in the design of control for underactuated mechanical systems [54, 96, 98].

Consider for the special underactuation case of (2.16) and define the invertible control transformation for u as:

$$u = ((m_{21} - m_{22}m_{12}^{-1}m_{11}))v + c_2(q, \dot{q}) + g_2(q) - m_{22}m_{12}^{-1}(c_1(q, \dot{q}) + g_1(q)) \tag{2.21}$$

Eq. (2.16) can be written as:

$$\begin{aligned}
 \ddot{q}_1 &= v \\
 \ddot{q}_2 &= -m_{12}^{-1}(c_2(q, \dot{q}) + g_2(q)) - m_{12}^{-1}m_{11}v
 \end{aligned} \tag{2.22}$$

where the first part is a linear double integrator subsystem.

Defining $[q_1, p_1, q_2, p_2]^T = [q_1, \dot{q}_1, q_2, \dot{q}_2]^T$ as state variables for (2.22), the state space representation of (2.22) can be written as:

$$\begin{aligned}\dot{q}_1 &= p_1 \\ \dot{p}_1 &= v \\ \dot{q}_2 &= p_2 \\ \dot{p}_2 &= f_0(q, p) + g_0(q)v\end{aligned}\tag{2.23}$$

where now

$$\begin{aligned}f_0(q, p) &= -m_{12}^{-1}(c_2(q, \dot{q}) + g_2(q)) \\ g_0(q) &= -m_{12}^{-1}m_{11}\end{aligned}\tag{2.24}$$

Thus any underactuated mechanical system in the form (2.16) can be partially linearized as in (2.23) into a *linear* actuated subsystem (q_1, p_1) and a *nonlinear* actuated subsystem (q_2, p_2) . But still, both the subsystems are coupled, through the new control input v , that again poses difficulties in the control design for underactuated mechanical systems of the form (2.16).

Apart from these two cases, a partial feedback linearization for the input coupling case of $F(q) = [F_1(q), F_2(q)]^T$ is possible that can be found in [94].

2.4.4 Normal Forms

Noting above that although the dynamics of underactuated mechanical system are partially linearized into a set of nonlinear subsystems and a set of linear subsystems as in Eqs. (2.19) and (2.23). But still, the nonlinear and linear subsystems are coupled through the new control v , i.e., v appears in both the systems. This causes difficulties in control design for underactuated mechanical systems. An important task is the decoupling of these two systems.

Using the control input transformation (2.17) or (2.21) and an explicit change of coordinates [96] the dynamics in Eq. (2.13) of an underactuated mechanical

system can be partially linearized and and decoupled into the following form:

$$\begin{aligned}\ddot{z} &= f(z, \dot{z}, \xi, \dot{\xi}) \\ \ddot{\xi} &= v\end{aligned}\tag{2.25}$$

where $f(z, \dot{z}, \xi, \dot{\xi})$ is either in the *strict feedback normal form* or in the *nontriangular quadratic normal form*.

Although partially linearized and decoupled, control design for the *nontriangular quadratic normal form* (2.25) is quite difficult with traditional nonlinear techniques. The proposed design framework makes this difficult control problem much simple. The Furuta Pendulum, the Cart-Pole system, the Overhead Crane, the Beam-and-Ball system, and the Pendubot are examples of underactuated mechanical systems in this category.

2.5 Control Design Approaches for Underactuated Mechanical Systems

Different control design approaches, developed and used over the years for underactuated mechanical systems, are reviewed in this section.

- *Energy and Passivity Based Control:*

For an underactuated mechanical system, the total energy and its time rate of change are given, respectively, by equations (2.11) and (2.12). Each desired equilibrium state of an underactuated mechanical system represent a total equilibrium energy. In Energy and Passivity Based Control (PBC) methods the total energy, as given by (2.11), is regulated to the equivalent value of the desired equilibrium state thus achieving regulation of the system states to the desired values. This method is mainly used for the set-point regulation of underactuated mechanical systems. Applications of these methods can be found in the works of [9, 27, 50, 74, 99–105].

- *Controlled Lagrangian:*

In the Euler-Lagrange based formulation of underactuated mechanical systems, the dynamical equation of motions are given by (2.1) with the *Lagrangian* $\mathcal{L}(q, \dot{q})$ defined in (2.3). In this formulation, each equilibrium state of an underactuated mechanical system corresponds to specific equilibrium state of the Lagrangian. In Controlled Lagrangian method, the Lagrangian of underactuated mechanical system is regulated, by modifying the inertia matrix and the potential energy function, to the desired equilibrium state by the use of control input, and then to ensure the passivity of the system, damping is injected into the system. Application of Controlled Lagrangian to underactuated mechanical systems can be found in [70, 71].

- *IDA-PBC:*

In the Hamiltonian based formulation of underactuated mechanical systems, the dynamical equation of motions are given by (2.10) with the *Hamiltonian* $\mathcal{H}(q, \dot{q})$ defined in (2.9). In this formulation each equilibrium state of an underactuated mechanical system corresponds to specific equilibrium state of the Hamiltonian. In the IDA-PBC method the Hamiltonian of the underactuated mechanical system is regulated, by modifying the inertia matrix, the potential energy function and the interconnection matrix, to the desired equilibrium state by the use of control input and then to ensure the passivity of the system, damping is injected into the system [106]. Application of IDA-PBC to underactuated mechanical systems can be found in [72, 107].

- *Backstepping Control:*

Backstepping [108] is a powerful nonlinear recursive design techniques for nonlinear systems. In each recursive step, an intermediate signal is treated as virtual control and control Lyapunov function is chosen to find the desired value of virtual control. The last recursive step gives the final desired value of the actual control. Backstepping Control has been used for global tracking of underactuated mechanical systems. Application of Backstepping Control to underactuated mechanical systems can be found in [109–115].

- *Adaptive and Robust Control:*

Discrepancies always exist between the physical system and its mathematical model on which control synthesis is based. These discrepancies arise due to uncertain parameters, unmodeled dynamics, parametric variations, and external disturbances. For acceptable performance, the controller should be robust to such discrepancies. Adaptive Control is the classic and traditional method to incorporate the effects of such discrepancies in the control action by online estimation of the parameters. In other words, the controller has the capabilities to adapt to the changing dynamics of the plant. The other control scheme is the Robust Control based on fixed control structures to overcome the effects of fixed structured and unstructured uncertainties. Applications of these methods to underactuated mechanical systems can be found in [7, 88–90, 116]

- *Fuzzy Control:*

Originally proposed in 1965, in Fuzzy Control the control decision making is made somehow fuzzy using artificial intelligence techniques. Fuzzy Control techniques can handle uncertain and imprecise control applications. The model based approach of Fuzzy Control has been used in the control applications of underactuated mechanical systems. Often, fuzzy techniques are used in combination with other control techniques like adaptive, sliding mode, and combination thereof, for example. Applications of Fuzzy Control to underactuated mechanical systems can be found in [117–124].

- *Optimal Control:*

In Optimal Control, the design procedure is based on finding a control law that minimizes or maximizes a cost function or objective function. Optimization of energy or time are two approaches in Optimal Control. Applications of Optimal Control to underactuated mechanical systems can be found in [125–130].

- *Sliding Mode Control:*

Sliding Mode Control is the most powerful robust control technique against parametric uncertainties, unmodeled plant dynamics and external disturbances. In SMC, first, a sliding surface is designed with desired dynamics and then a control law is selected to force system states to the sliding surface. After reaching the surface, system states slide, along the surface, to the desired values or origin and remain there under the action of the control. During sliding and at the desired values after sliding, system dynamics depend only on the parameters of the surface and system motion is robust to parameter variations. Robustness to external disturbance is ensured through a discontinuous term in the control law or through estimation by observer and then cancellation by the control law. Apart from robustness, SMC techniques can easily control higher order and complex nonlinear plants. Due to these promising control features, SMC has been used by researchers for the control of underactuated mechanical system. Application of SMC to underactuated mechanical systems can be found in [41, 65, 76–78, 131–137]

In summary, there are many excellent research works on the subject. Most works address the control problem of a specific underactuated mechanical system. There is a strong need for class based control design approaches that are robust and also provide smooth control action which is especially required for mechanical control systems. Due to slow response of mechanical systems, high (theoretically infinite) frequency of the control action in standard SMC is not possible that results in loss of accuracy, and hence, degraded system performance. This provides strong basis and need for a smooth robust sliding mode design framework that addresses the problem in a unified and comprehensive way.

Chapter 3

Preliminaries

This chapter presents some preliminaries related to underactuated mechanical systems and the application of sliding mode control. An illustrative design example of a benchmark underactuated mechanical system is presented to show the level of difficulty arising in the control design and to show how the application of SMC theory can help to solve this difficult control problem in a relatively simple way.

3.1 General n Degrees of Freedom (nDOF) Underactuated Mechanical Systems

As mentioned in Chapter 2, the dynamical equations of motion of an n degrees of freedom mechanical control system are given by Euler-Lagrange equation as below [97]:

$$\frac{d}{dt} \frac{\partial \mathcal{L}}{\partial \dot{q}} - \frac{\partial \mathcal{L}}{\partial q} = F(q)u \quad (3.1)$$

where $q \in \mathfrak{R}^n$ is the configuration vector in generalized coordinates, $F(q) = [f_1(q), \dots, f_m(q)]^T \in \mathfrak{R}^{n \times m}$ is the control input matrix, $u \in \mathfrak{R}^m$ is the control input vector. Furthermore, $\mathcal{L}(q, \dot{q})$ is the *Lagrangian* of the system defined as below:

$$\mathcal{L}(q, \dot{q}) = K(q, \dot{q}) - V(q) = \frac{1}{2} \dot{q}^T M(q) \dot{q} - V(q) \quad (3.2)$$

where $K(q, \dot{q})$ is the kinetic energy of the system and $V(q)$ is the potential energy.

The vector form of the dynamics in (3.1) is:

$$M(q)\ddot{q} + C(q, \dot{q})\dot{q} + G(q) = F(q)u \quad (3.3)$$

where $M(q)$ is the positive definite symmetric inertia matrix, $G(q)$ have gravitational terms and $C(q, \dot{q})\dot{q}$ have centrifugal and Coriolis terms. The case, $m = \text{rank}(F) = n$, represents a fully actuated mechanical system, and, the case, $m = \text{rank}(F) < n$, characterizes an underactuated mechanical system.

For the general case, $F(q) = [F_1(q), F_2(q)]^T$, and partitioning $q = [q_1, q_2]^T$ according to $F(q)$, where $q_1 \in \mathfrak{R}^{(n-m)}$ and $q_2 \in \mathfrak{R}^m$, dynamics (3.3) are written as:

$$\begin{aligned} m_{11}(q)\ddot{q}_1 + m_{12}(q)\ddot{q}_2 + c_1(q, \dot{q}) + g_1(q) &= F_1(q)u \\ m_{12}(q)\ddot{q}_1 + m_{22}(q)\ddot{q}_2 + c_2(q, \dot{q}) + g_2(q) &= F_2(q)u \end{aligned} \quad (3.4)$$

where $u \in \mathfrak{R}^m$ is the vector of control inputs produced by m actuators, $c_1(q, \dot{q}) \in \mathfrak{R}^{(n-m)}$ and $c_2(q, \dot{q}) \in \mathfrak{R}^m$ are the centrifugal and Coriolis terms, $g_1(q) \in \mathfrak{R}^{(n-m)}$ and $g_2(q) \in \mathfrak{R}^m$ are the gravitational terms, and

$$M(q) = \begin{bmatrix} m_{11}(q) & m_{12}(q) \\ m_{21}(q) & m_{22}(q) \end{bmatrix}$$

is the positive definite and symmetric inertia matrix.

3.2 Two Degrees of Freedom (2DOF) Underactuated Mechanical Systems

For 2DOF underactuated mechanical system, $n = 2$ and $m = 1$, so in system in (3.4), $q \in \mathfrak{R}^2$, $u \in \mathfrak{R}^1$, $q_1 \in \mathfrak{R}^1$, and $q_2 \in \mathfrak{R}^1$. Assume $M(q) = M(q_2)$. Depending upon whether $F_1(q) = 0$ or $F_2(q) = 0$, system in (3.4) takes one of the following

two forms:

$$\begin{aligned} m_{11}(q_2)\ddot{q}_1 + m_{12}(q_2)\ddot{q}_2 + c_1(q, \dot{q}) + g_1(q) &= 0 \\ m_{21}(q_2)\ddot{q}_1 + m_{22}(q_2)\ddot{q}_2 + c_2(q, \dot{q}) + g_2(q) &= u \end{aligned} \quad (3.5)$$

for $F_1(q) = 0$ and $F_2(q) = I_1$, and

$$\begin{aligned} m_{11}(q_2)\ddot{q}_1 + m_{12}(q_2)\ddot{q}_2 + c_1(q, \dot{q}) + g_1(q) &= u \\ m_{21}(q_2)\ddot{q}_1 + m_{22}(q_2)\ddot{q}_2 + c_2(q, \dot{q}) + g_2(q) &= 0 \end{aligned} \quad (3.6)$$

for $F_1(q) = I_1$ and $F_2(q) = 0$.

Remark 3.1. Systems in the form of (3.5) in which the shape variable (variable appearing in the inertia matrix) q_2 is actuated were classified as *Class-I* underactuated mechanical systems in [94]. The Inertial-Wheel Pendulum (IWP), the TORA system, and the Acrobot are examples of *Class-I* underactuated mechanical systems.

Remark 3.2. Systems in the form of (3.6) in which the shape variable (variable appearing in the inertia matrix) q_2 is unactuated were classified as *Class-II* underactuated mechanical systems in [94]. The Furuta Pendulum, the Overhead Crane, the Cart-Pole system, the Pendubot, and the Beam-and-Ball system are examples of *Class-II* underactuated mechanical systems.

3.3 Three Degrees of Freedom (3DOF) Underactuated Mechanical Systems

For 3DOF underactuated mechanical systems, $n = 3$ and $m = 1$ or $m = 2$ in (3.1) or in (3.3).

For $m = 1$, $u \in \mathfrak{R}^1$ and $F(q) = [f_1(q), f_2(q), f_3(q)]^T \in \mathfrak{R}^{3 \times 1}$. As $q \in \mathfrak{R}^3$, depending upon the configuration of $F(q)$, we have three degrees of freedom underactuated mechanical systems with one independent actuator. Examples are three link manipulators with one actuator. The location of the actuator lead to different underactuated systems.

For $m = 2$, $u \in \mathfrak{R}^2$ and $F(q) = \begin{bmatrix} f_{11}(q) & f_{12}(q) & f_{13}(q) \\ f_{21}(q) & f_{22}(q) & f_{23}(q) \end{bmatrix}^T \in \mathfrak{R}^{3 \times 2}$. As $q \in \mathfrak{R}^3$, depending upon the configuration of $F(q)$, we have three degrees of freedom underactuated mechanical systems with two independent actuators. Surface Vessel and the Vertical Take Off and Landing (VTOL) aircraft are examples of this category.

3.4 Some Benchmark Underactuated Mechanical Systems

This section briefly discusses some benchmark underactuated mechanical systems that have been widely studied in the literature.

A. Class-I Underactuated Mechanical Systems:

The dynamics of *Class-I* underactuated mechanical systems are governed by Equation 3.5 as:

$$\begin{aligned} m_{11}(q_2)\ddot{q}_1 + m_{12}(q_2)\ddot{q}_2 + c_1(q, \dot{q}) + g_1(q) &= 0 \\ m_{21}(q_2)\ddot{q}_1 + m_{22}(q_2)\ddot{q}_2 + c_2(q, \dot{q}) + g_2(q) &= u \end{aligned} \quad (3.7)$$

In all these systems, the configuration vector q_1 is unactuated and the configuration vector q_2 , which appears in the inertia matrix, is actuated.

1. The Acrobot (The Tip Robot):

Figure 3.1a shows the Acrobot. It is a two link underactuated manipulator. The single actuator is at the elbow. The control problem for the Acrobot is to stabilize it at the upward unstable equilibrium position, i.e., $q_1 = 0$, $q_2 = 0$. Some works on the Acrobot can be referred to as [27–31].

For the dynamics of the Acrobot in Eq. (3.7) we have:

$$\begin{aligned}
m_{11}(q_2) &= m_1\ell_1^2 + m_2(L_1^2 + \ell_2^2) + I_1 + I_2 + 2m_2L_1\ell_2 \cos(q_2) \\
m_{12}(q_2) &= m_2\ell_2^2 + I_2 + m_2L_1\ell_2 \cos(q_2) \\
m_{21}(q_2) &= m_{12} \\
m_{22}(q_2) &= m_2\ell_2^2 + I_2 \\
c_1(q, \dot{q}) &= -m_2L_1\ell_2 \sin(q_2)(2\dot{q}_1\dot{q}_2 + \dot{q}_2^2) \\
c_2(q, \dot{q}) &= m_2L_1\ell_2 \sin(q_2)\dot{q}_1^2 \\
g_1(q) &= -(m_1\ell_1 + m_2L_1)g \sin(q_1) - m_2\ell_2g \sin(q_1 + q_2) \\
g_2(q) &= -m_2\ell_2g \sin(q_1 + q_2)
\end{aligned} \tag{3.8}$$

2. The TORA System:

Figure 3.1b shows the TORA system. The actuator is at the pendulum. The control problem for the TORA is to stabilize it at the equilibrium position, i.e., $q_1 = 0, q_2 = 0$. The control problem of the TORA system is a benchmark problem for nonlinear control design [16]. Some works on the TORA system can be referred to as [16–26].

For the dynamics of the TORA system in Eq. (3.7) we have:

$$\begin{aligned}
m_{11}(q_2) &= m_1 + m_2 \\
m_{12}(q_2) &= m_2r \cos(q_2) \\
m_{21}(q_2) &= m_{12}(q_2) \\
m_{22}(q_2) &= I_2 + m_2r^2 \\
c_1(q, \dot{q}) &= -m_2r \sin(q_2)\dot{q}_2^2 \\
c_2(q, \dot{q}) &= 0 \\
g_1(q_1, q_2) &= kq_1 \\
g_2(q_1, q_2) &= m_2rg \sin(q_2)
\end{aligned} \tag{3.9}$$

3. The Inertia-Wheel Pendulum (IWP):

Figure 3.1c shows the IWP. The actuator is at the Wheel. The control

problem for the IWP is to stabilize it at the upward unstable equilibrium position, i.e., $q_1 = 0$. The final equilibrium value of q_2 is not important. Some works on the IWP can be referred to as [13–15].

For the dynamics of the IWP in Eq. (3.7) we have:

$$\begin{aligned}
m_{11}(q_2) &= I_1 + I_2 + m_1 l_1^2 + m_2 L_1^2 \\
m_{12}(q_2) &= I_2 \\
m_{21}(q_2) &= m_{12}(q_2) \\
m_{22}(q_2) &= m_{12}(q_2) \\
c_1(q, \dot{q}) &= 0 \\
c_2(q, \dot{q}) &= 0 \\
g_1(q_1, q_2) &= -(m_1 l_1 + m_2 L_1)g \sin(q_1) \\
g_2(q_1, q_2) &= 0
\end{aligned} \tag{3.10}$$

Remark 3.3. The inertia matrix $M(q)$ of the IWP does not depend on the configuration vector q and hence is referred to as the *Flat* 2DOF underactuated mechanical system.

B. Class-II Underactuated Mechanical Systems:

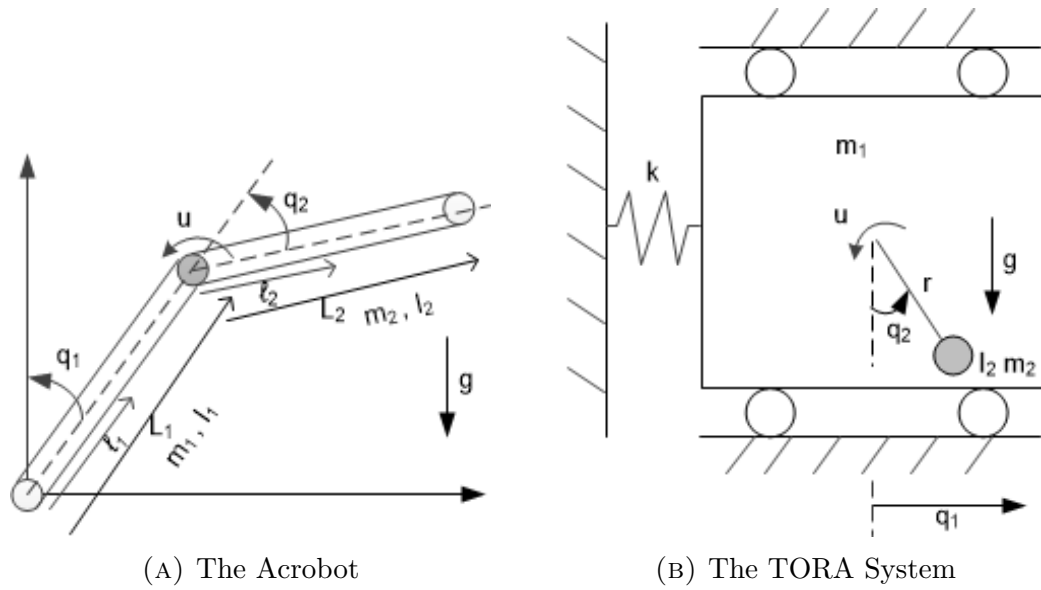
The dynamics of *Class-II* Underactuated Mechanical Systems are governed by Equation 3.6 as:

$$\begin{aligned}
m_{11}(q_2)\ddot{q}_1 + m_{12}(q_2)\ddot{q}_2 + c_1(q, \dot{q}) + g_1(q) &= u \\
m_{21}(q_2)\ddot{q}_1 + m_{22}(q_2)\ddot{q}_2 + c_2(q, \dot{q}) + g_2(q) &= 0
\end{aligned} \tag{3.11}$$

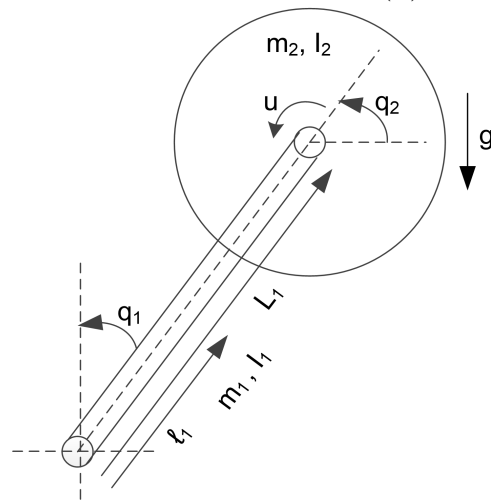
In all these systems, the configuration vector q_1 is actuated and the configuration vector q_2 , which appears in the inertia matrix, is unactuated.

1. The Pendubot (Pendulum Robot):

The Pendubot is shown in Fig. 3.2a. It is a two link underactuated manipulator. The single actuator is at the shoulder. The control task for the



(A) The Acrobot (B) The TORA System



(C) The Inertia-Wheel Pendulum

FIGURE 3.1: Schematics of Class-I Underactuated Mechanical Systems

Pendubot is to stabilize it at the upward unstable equilibrium position i.e. $q_1 = 0, q_2 = 0$. Some works on the Pendubot can be referred to [52–62].

For the dynamics of the Pendubot in Eq. (3.11) we have:

$$\begin{aligned}
m_{11}(q_2) &= m_1 \ell_1^2 + m_2(L_1^2 + \ell_2^2) + I_1 + I_2 + 2m_2 L_1 \ell_2 \cos(q_2) \\
m_{12}(q_2) &= m_2 \ell_2^2 + I_2 + m_2 L_1 \ell_2 \cos(q_2) \\
m_{21}(q_2) &= m_{12} \\
m_{22}(q_2) &= m_2 \ell_2^2 + I_2 \\
c_1(q, \dot{q}) &= -m_2 L_1 \ell_2 \sin(q_2)(2\dot{q}_1 \dot{q}_2 + \dot{q}_2^2) \\
c_2(q, \dot{q}) &= m_2 L_1 \ell_2 \sin(q_2) \dot{q}_1^2 \\
g_1(q) &= -(m_1 \ell_1 + m_2 L_1)g \sin(q_1) - m_2 \ell_2 g \sin(q_1 + q_2) \\
g_2(q) &= -m_2 \ell_2 g \sin(q_1 + q_2)
\end{aligned} \tag{3.12}$$

2. The Furuta Pendulum:

The Furuta Pendulum is shown in Fig. 3.2b. The actuator is at the rotating arm. The control problem is to stabilize the pendulum at its upward unstable equilibrium position $q_2 = 0$ by the rotating the horizontal arm. Some works on the Furuta Pendulum can be referred to [32–36].

For the dynamics of the Furuta Pendulum in Eq. (3.11) we have:

$$\begin{aligned}
m_{11}(q_2) &= I_1 + m_1 l_1^2 + m_2 L_1^2 + m_2 l_2^2 \sin^2(q_2) \\
m_{12}(q_2) &= m_2 L_1 l_2 \cos(q_2) \\
m_{21}(q_2) &= m_{12}(q_2) \\
m_{22}(q_2) &= I_2 + m_2 l_2^2 \\
c_1(q, \dot{q}) &= 2m_2 l_2^2 \sin(q_2) \cos(q_2) \dot{q}_1 \dot{q}_2 - m_2 L_1 l_2 \sin(q_2) \dot{q}_2^2 \\
c_2(q, \dot{q}) &= -m_2 l_2^2 \sin(q_2) \cos(q_2) \dot{q}_1^2 \\
g_1(q_1, q_2) &= 0 \\
g_2(q_1, q_2) &= -m_2 l_2 g \sin(q_2)
\end{aligned} \tag{3.13}$$

3. The Cart-Pole System:

Figure 3.2c shows the Cart-Pole System. The actuator is at the Cart. The control task for the Cart-Pole System is to stabilize the Pole (pendulum) at

the upward unstable equilibrium position $q_2 = 0$ and tracking the position of the Cart from any initial position q_{10} to any other desired position q_{1des} . Some works on the Cart-Pole system can be referred to [44–51].

For the dynamics of the Cart-Pole system in Eq. (3.11) we have:

$$\begin{aligned}
 m_{11}(q_2) &= m_1 + m_2 \\
 m_{12}(q_2) &= m_2 \ell_2 \cos(q_2) \\
 m_{21}(q_2) &= m_{12}(q_2) \\
 m_{22}(q_2) &= I_2 + m_2 \ell_2^2 \\
 c_1(q, \dot{q}) &= -m_2 \ell_2 \sin(q_2) \dot{q}_2^2 \\
 c_2(q, \dot{q}) &= 0 \\
 g_1(q_1, q_2) &= 0 \\
 g_2(q_1, q_2) &= -m_2 \ell_2 g \sin(q_2)
 \end{aligned} \tag{3.14}$$

4. The Overhead Crane:

Figure 3.2d shows the Overhead Crane. The actuator is at the Crane trolley. The control problem for the Overhead Crane is to track, as quickly as possible, the position of the Crane trolley from any initial position q_{10} to any other desired position q_{1des} and keeping the free swings of the Load angle q_2 as minimum as possible. Some work on the Overhead Crane can be referred to [37–43].

For the dynamics of the Overhead Crane in Eq. (3.11) we have:

$$\begin{aligned}
m_{11}(q_2) &= M + m \\
m_{12}(q_2) &= mL \cos(q_2) \\
m_{21}(q_2) &= m_{12}(q_2) \\
m_{22}(q_2) &= I_2 + mL^2 \\
c_1(q, \dot{q}) &= -mL \sin(q_2) \dot{q}_2^2 \\
c_2(q, \dot{q}) &= 0 \\
g_1(q_1, q_2) &= 0 \\
g_2(q_1, q_2) &= mLg \sin(q_2)
\end{aligned} \tag{3.15}$$

5. *The Beam-and-Ball System:*

Figure 3.2e shows the well known Beam-and-Ball system. The actuator is at the Beam. The control problem for the Beam-and-Ball system is to stabilize the Ball position, from any initial position q_{20} , to any other desired position q_{2des} . Some works on the Beam-and-Ball system can be referred to [63–69].

For the dynamics of the Beam-and-Ball system in Eq. (3.11) we have:

$$\begin{aligned}
m_{11}(q_2) &= I_1 + m(q_2^2 + d^2) \\
m_{12}(q_2) &= -md \\
m_{21}(q_2) &= m_{12}(q_2) \\
m_{22}(q_2) &= m\left(1 + \frac{I_2}{mr^2}\right) \\
c_1(q, \dot{q}) &= 2m\dot{q}_1 q_2 \dot{q}_2 \\
c_2(q, \dot{q}) &= -mq_2 \dot{q}_1^2 \\
g_1(q_1, q_2) &= mg(q_2 \cos(q_1) - d \sin(q_1)) \\
g_2(q_1, q_2) &= mg \sin(q_1)
\end{aligned} \tag{3.16}$$

Remark 3.4. Setting $d = 0$ gives the well known model studied in the literature [63, 64].

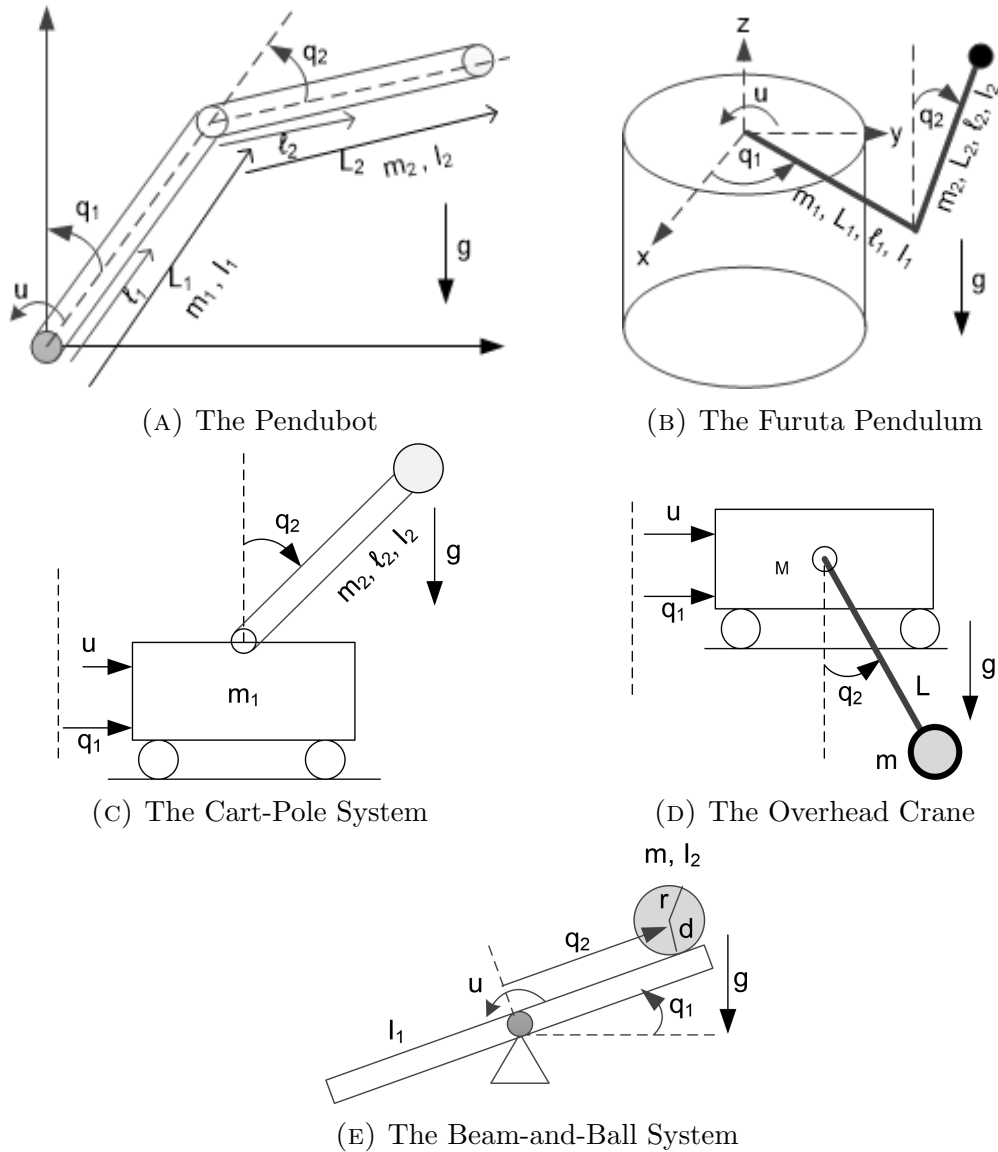


FIGURE 3.2: Schematics of Class-II Underactuated Mechanical Systems

C. The Magnetic Levitation System: The schematics of a Magnetic Levitation system are shown in Fig. 3.3. Although it is not an *all-mechanical* system but it is an underactuated system. The system consists of a electromagnet and a suspended object, shown as a ball. The control problem is to move the suspended object to a desired position by inducing a magnetic force via current in the coil.

The dynamical equations of motion of the system can be derived using the following

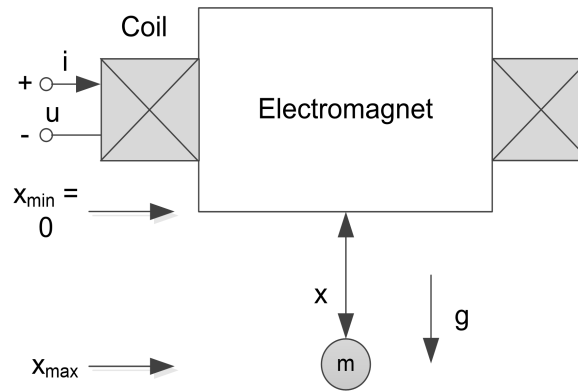


FIGURE 3.3: The Magnetic Levitation System

equations based on fundamental physical principles:

$$\begin{aligned} m\ddot{x} &= mg - F_m \\ Ri + \frac{d(L(x)i)}{dt} &= u \end{aligned} \quad (3.17)$$

where x is the ball position, m is the ball mass, g is acceleration due to gravity, F_m is the magnetic force, i is the current in the coil, R is the resistance of the coil, $L(x)$ is the inductance of the coil, and u is the voltage applied to the coil taken as the control input.

Note that the ball position x increases in the downward direction with $x_{min} = 0$ at the upper position and x_{max} at the ground position. The control task is to position the ball between x_{min} and x_{max} .

Remark 3.5. Similar to the well known Beam-and-Ball system, the Magnetic Levitation system is an underactuated electromechanical system. In the Beam-and-Ball system, the position of the ball is indirectly controlled by applying control torque to the beam. In the Magnetic Levitation system, the ball position is indirectly controlled by applying control voltage to the coil.

Remark 3.6. Defining the state variables $q_1 = i = \dot{q}$ and $q_2 = x$, Eq. (3.17) can be cast into the form of Eq. (3.11).

D. 3DOF Underactuated Mechanical Systems:

The VTOL aircraft and the Surface Vessel are examples of underactuated mechanical control systems with three degrees of freedom and two actuators.

1. *The Vertical Take Off and Landing (VTOL) Aircraft:*

The VTOL aircraft is shown in Fig. 3.4a. There are three degrees of freedom with configuration vector $[q_1, q_2, q_3]$ and two independent actuators u_1 and u_2 . Some works on the VTOL can be referred to [76, 115]. The dynamics of the VTOL aircraft are given by:

$$\begin{aligned}\ddot{q}_1 &= -u_1 \sin(q_3) + \epsilon u_2 \cos(q_3) \\ \ddot{q}_2 &= u_1 \cos(q_3) + \epsilon u_2 \sin(q_3) - g \\ \ddot{q}_3 &= u_2\end{aligned}\tag{3.18}$$

Remark 3.7. The inertia matrix $M(q)$ of the VTOL aircraft does not depend on the configuration vector q and hence is referred to as the *Flat* 3DOF underactuated mechanical system.

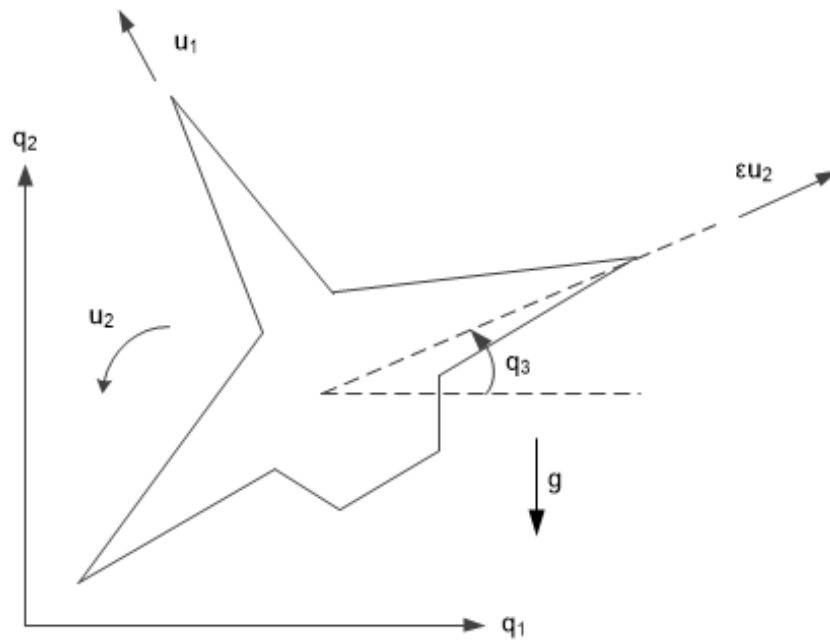
2. *The Surface Vessel:*

Figure 3.4b shows the Surface Vessel. There are three degrees of freedom with configuration vector $[q_1, q_2, q_3]$ and two independent actuators u_1 and u_2 . Some work can be referred to [109, 110, 134]. The dynamics of the Surface Vessel are given by:

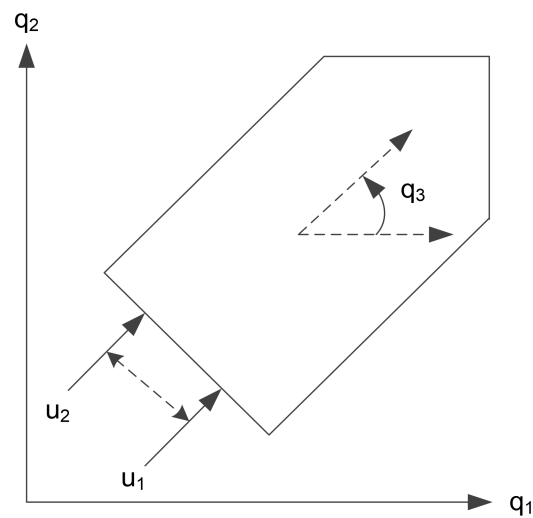
$$\begin{aligned}m \cos(q_3)\ddot{q}_1 + m \sin(q_3)\ddot{q}_2 + \nu_1 \cos(q_3)\dot{q}_1 + \nu_1 \sin(q_3)\dot{q}_2 &= u_1 + u_2 \\ -m \sin(q_3)\ddot{q}_1 + m \cos(q_3)\ddot{q}_2 + -\nu_2 \sin(q_3)\dot{q}_1 + \nu_2 \cos(q_3)\dot{q}_2 &= 0 \\ \ddot{q}_3 + \nu_3 \dot{q}_3 &= \frac{d}{2}u_1 - \frac{d}{2}u_2\end{aligned}\tag{3.19}$$

3.5 Sliding Mode Control and Observation

The design of control law is essentially based on the mathematical model of the plant to be controlled. There always exist discrepancies between the actual plant dynamics and its mathematical model. These discrepancies arise due to external disturbances, unmodeled/neglected dynamics and parametric uncertainties. To



(A) The VTOL Aircraft



(B) The Surface Vessel

FIGURE 3.4: 3DOF Underactuated Mechanical Systems

achieve the desired closed loop performance for plants operating in the presence of disturbances/uncertainties, the controller must be robust to external disturbances and model uncertainties and model uncertainties. However, designing robust controllers is a difficult task. Sliding Mode Control (SMC) is the most successful robust control approach for high order nonlinear complex plants operating in the presence of disturbances/uncertainties.

Historically, the discontinuous the relay on-off control of the 30's with its generalization in the 50's, and the theory of variable structure systems (VSS) provided the underlying key ideas for sliding mode control. SMC theory, as a unified and established control discipline in itself, was formally introduced in [81–83].

The following *two steps design procedure* is carried out in sliding mode control:

1. The design of a **sliding manifold** (also called sliding surface or sliding variable) such that, when system states belong to this manifold, desired closed loop performance for the system is achieved, and
2. The selection of a **control law** to enforce sliding mode, i.e., to drive the sliding manifold to zero, in the presence of external disturbances and model uncertainties.

System closed loop response in SMC has the following *two phases*:

1. **Reaching phase**: Motion in which the trajectories of the system are driven to the sliding manifold by the control, and
2. **Sliding phase**: Motion in which the trajectories of the system slide to the desired values after reaching the sliding manifold.

Motion of system trajectories on the sliding manifold is called **sliding mode**. This motion is on a reduced space and is characterized by the parameters of the sliding manifold that are user defined and not system dependent. User defined characterization ensures robustness to parametric variations. Robustness to external disturbance is ensured through a discontinuous term in the control law or through estimation by observer and then cancellation by the control law.

3.5.1 Standard Sliding Mode Control

In standard or conventional sliding mode control, only the sliding variable itself (not its derivatives) is driven to zero, in finite time, by the control law. Standard

SMC is also called First Order Sliding Mode (FOSM) in comparison to HOSM control. Standard SMC can control, with high accuracy, higher order nonlinear complex plant with external disturbances and parametric variations but, from practical point of view, has the following two main limitations:

1. The control action suffers from high frequency switching called **Chattering**. Chattering can cause wear and tear in the physical control loop and can also cause damage to the plant itself and hence is undesired, especially, for mechanical control systems.
2. Can be used for the control systems whose **relative degree** is 1 thus restricting its general use.

To overcome the above two main limitations, HOSM control techniques, briefly discussed in the next section, were developed.

3.5.2 Higher Order Sliding Mode (HOSM) Control

To mitigate the undesired chattering, present in standard SMC, different techniques [138–144] were introduced. To eliminate chattering and achieve the benefits of sliding mode at the same time, HOSM [11, 145–152] control techniques were introduced to the already mature and established conventional SMC theory. In HOSM, the sliding variable and its first $k - 1$ successive derivative (for k th order sliding mode) are driven to zero in finite time. The chattering phenomenon is significantly reduced in HOSM control and the limitation of system relative degree is also relaxed from 1 to arbitrary order.

A number of HOSM control schemes have been reported in the literature. The Super-Twisting Algorithm (STA) [147], the Smooth Super-Twisting Algorithm (SSTA) [153], the Real Twisting Algorithm (RTA) [148] and the Smooth Real Twisting Algorithm (SRTA) [154] are well known examples. All these control schemes ensure ideal 2-sliding mode, $\sigma = \dot{\sigma} = 0$, and significantly reduces chattering or completely smooths it, hiding it in the internal dynamics of the control.

3.5.3 Sliding Mode Observation

First, a failure of actuator in a fully actuated mechanical system will render that system underactuated and a failure of actuator in an already unactuated system will increase the degree of underactuation. Detecting and diagnosing such faults and switching to suitable control, which is designed for that specific underactuation case, is an important area of research. Also failure of sensor will lead to no or delayed feedback signals and hence causing poor performance. Treating this case also in an underactuated way will enhance system performance. To achieve this, we need observation and fault diagnostic techniques. Sliding mode control offers a rich set of such observation and diagnostic techniques.

Second, in practical scenarios of control applications, not always all the states of the plant are measurable. Uncertainty due to unmodeled dynamics, unknown parameters and unanticipated external disturbances degrade system performance. For the control scheme to be effective, system states may be needed to be observed, parameters to be estimated and disturbance to be reconstructed. In sliding mode control powerful tools for such observation have been developed over the years. Now sliding mode control and observation techniques provide a complete design framework for any practical control problem. The beauty of these techniques is that complete knowledge of the mathematical model of the plant is not necessary. Since sliding mode is robust to uncertainties due to unmodeled dynamics and external disturbances, observation through SMC techniques is robust giving a leverage to sliding mode over other techniques.

The fundamental concepts of the Luenberger linear observer were generalized in conventional sliding mode in [82, 155–157]. Then the latest powerful class of second and high order observers and differentiators [148, 158–160] were added to the classic sliding mode observers. The traditional state observation and parameter estimation needs went a step further when these techniques were started to find use in fault detection and isolation [161–164]. These powerful and robust sliding mode observation, estimation and differentiation techniques are also important in the analysis and control of underactuated mechanical systems.

3.5.4 The Benchmark Nonlinear Control Design Problem

Illustrative design example of the TORA system will show the level of difficulty arising in the control design for underactuated mechanical systems. Furthermore, the example will show how the application of SMC theory can help to solve this difficult control problem in a relatively simple way. The control problem of TORA system is a benchmark for nonlinear control design [16] and the whole issue 8 (1998) of the *International Journal of Robust and Nonlinear Control* is dedicated to this problem. The problem is also the focus of latest research as discussed below.

Example 3.1. *Figure 3.1b shows the TORA system [17]. The system has a translational oscillating platform of mass m_1 controlled via a rotational eccentric mass m_2 . Originally, the TORA system was studied, as a simplified model of a dual-spin spacecraft, to investigate the resonance capture phenomenon [165]. Later, the system was studied to investigate the practical usefulness of a rotational actuator for stabilizing translational motion [166]. The control problem, which is a benchmark for nonlinear control design [16], is to stabilize the oscillating platform translational displacement q_1 to zero via the rotational actuator. The TORA system is widely studied using different control techniques such as: backstepping [17, 94], passivity-based [18], output feedback stabilization and tracking [19–21], hybrid [22], sliding mode [76], dynamic surface control [167], output feedback stabilization and tracking [168], adaptive [169], Riccati equation method [23], LMI [24], and H_∞ [25]. In most works, for example, [17, 25, 76, 169], the gravity term, $g_2(q_1, q_2)$, is ignored that is retained in this work. Furthermore, in most works, nondimensionalized equations of motion [17, 165] are used that makes difficult the comparison of different control strategies, especially, due to normalization of time t .*

For the TORA system, choose the physical parameters as specified in [16] and used in [24]:

$$m_1 = 1.3608 \text{ (kg)}, m_2 = 0.096 \text{ (kg)}, I_2 = 0.0002175 \text{ (kg.m}^2\text{)}, r = 0.0592 \text{ (m)}, \\ k = 186.3 \text{ (N.m}^{-1}\text{)}, \varepsilon = 0.200.$$

According to Eqs. (3.7), (3.9), the dynamics of the TORA system are described

as:

$$\begin{aligned} (m_1 + m_2)\ddot{q}_1 + (m_2 r \cos(q_2))\ddot{q}_2 - m_2 r \sin(q_2)\dot{q}_2^2 + kq_1 &= 0 \\ (m_2 r \cos(q_2))\ddot{q}_1 + (I_2 + m_2 r^2)\ddot{q}_2 + m_2 r g \sin(q_2) &= u + d(t) \end{aligned} \quad (3.20)$$

where $d(t)$ is the matched uncertain term bounded as $|d(t)| \leq D_0$.

Denoting $x = [x_1, x_2, x_3, x_4]^T = q = [q_1, \dot{q}_1, q_2, \dot{q}_2]^T$, the nominal state space representation of (3.20) is:

$$\begin{aligned} \dot{x}_1 &= x_2 \\ \dot{x}_2 &= \frac{c_2 c_3 x_4^2 \sin(x_3) + c_2^2 g \sin(x_3) \cos(x_3) - k c_3 x_1}{c_1 c_3 - c_2^2 \cos^2(x_3)} - \frac{c_2 \cos(x_3)}{c_1 c_3 - c_2^2 \cos^2(x_3)} u \\ \dot{x}_3 &= x_4 \\ \dot{x}_4 &= \frac{-c_2^2 x_4^2 \sin(x_3) \cos(x_3) - c_1 c_2 g \sin(x_3) + k c_2 x_1 \cos(x_3)}{c_1 c_3 - c_2^2 \cos^2(x_3)} + \frac{c_1}{c_1 c_3 - c_2^2 \cos^2(x_3)} u \end{aligned} \quad (3.21)$$

where

$$\begin{aligned} c_1 &= m_1 + m_2 \\ c_2 &= m_2 r \\ c_3 &= I_2 + m_2 r^2 \end{aligned}$$

System (3.21) is highly nonlinear and coupled in the control and its control design is quite difficult with traditional nonlinear control design techniques. The presence of uncertainties makes it further challenging. The application of SMC makes this challenging problem much simple. Before proceeding to apply the proposed simple SMC solution, we discuss some existing interesting approaches specially the nondimensionalized equations of motion [17, 165].

Setting $g = 0$ and $d = 0$, and using the following dimensionless variables:

$$\begin{aligned} q_{1d} &= \sqrt{\frac{m_1 + m_2}{I_2 + m_2 r^2}} q_1 \\ u_d &= \frac{(m_1 + m_2)}{k(I_2 + m_2 r^2)} u \\ t_d &= \sqrt{\frac{k}{m_1 + m_2}} t \\ \epsilon &= \frac{m_1 r}{\sqrt{(m_1 + m_2)(I_2 + m_2 r^2)}} \end{aligned} \quad (3.22)$$

the dynamics in (3.20) become

$$\begin{aligned}\ddot{q}_{1d} + q_{1d} &= \epsilon(\dot{q}_2^2 \sin(q_2) - \ddot{q}_2 \cos(q_2)) \\ \ddot{q}_2 &= u_d - \epsilon \dot{q}_{1d} \cos(q_2)\end{aligned}\tag{3.23}$$

Now using $[x_1, x_2, x_3, x_4]^T = [q_{1d}, \dot{q}_{1d}, q_2, \dot{q}_2]^T$ as state variable, the state space representation of (3.23) is:

$$\begin{aligned}\dot{x}_1 &= x_2 \\ \dot{x}_2 &= \frac{\epsilon x_4^2 \sin(x_3) - x_1}{1 - \epsilon^2 \cos^2(x_3)} - \frac{\epsilon \cos(x_3)}{1 - \epsilon^2 \cos^2(x_3)} u_d \\ \dot{x}_3 &= x_4 \\ \dot{x}_4 &= \frac{\epsilon \cos(x_3)(x_1 - \epsilon x_4^2 \sin(x_3))}{1 - \epsilon^2 \cos^2(x_3)} + \frac{1}{1 - \epsilon^2 \cos^2(x_3)} u_d\end{aligned}\tag{3.24}$$

Further, using the following state and control transformation in (3.24)

$$\begin{aligned}z_1 &= x_1 + \epsilon \sin(x_3) \\ z_2 &= x_2 + \epsilon x_4 \cos(x_3) \\ \xi_1 &= x_3 \\ \xi_2 &= x_4 \\ v &= \frac{1}{1 - \epsilon^2 \cos^2(\xi_1)} (\epsilon \cos(\xi_1)(z_1 - (1 + \xi_2^2)\epsilon \sin(\xi_1)) + u_d)\end{aligned}\tag{3.25}$$

transform the dynamics in (3.24) to the following simple form:

$$\begin{aligned}\dot{z}_1 &= z_2 \\ \dot{z}_2 &= -z_1 + \epsilon \sin(\xi_1) \\ \dot{\xi}_1 &= \xi_2 \\ \dot{\xi}_2 &= v\end{aligned}\tag{3.26}$$

The above simple form is used in most of the above cited works.

We have arrived at the simple form (3.26) after:

- ignoring the gravity term

- two levels of coordinate transformation one of which is dimensionless
- two levels of control transformation one of which is dimensionless
- one level of time transformation that is dimensionless

These transformation make the control design and its comparison difficult especially due to dimensionless transformation of time [24]. Moreover the final form (3.26) depends on a single dimensionless parameter ϵ taken as $\epsilon = 0.1$ or 0.2 in most works This does not reelect the real dynamics. The system studied in [94, 167] and in [16] has the same ($\epsilon = .2$) but much differences in physical parameters and hence much difference in response, for example, in settling time.

Here, first, a standard SMC law based on linear sliding manifold is designed. Then to achieve smooth control action and global convergence, a smooth HOSM control based on the design of a nonlinear sliding manifold is applied.

A. Standard SMC law based on linear sliding manifold:

Since (3.21) is not in the canonical form the standard two steps SMC design procedure is directly not applicable. First, for (3.7) or (3.20) define the following

$$\begin{aligned}
 \bar{m}_{11}(q) &= m_{21} - m_{22}m_{12}^{-1}m_{11} \\
 \bar{c}_1(q, \dot{q}) &= c_2 - m_{22}m_{12}^{-1}c_1 \\
 \bar{g}_1(q) &= g_2 - m_{22}m_{12}^{-1}g_1 \\
 \bar{m}_{22}(q) &= m_{22} - m_{21}m_{11}^{-1}m_{12} \\
 \bar{c}_2(q, \dot{q}) &= c_2 - m_{21}m_{11}^{-1}c_1 \\
 \bar{g}_2(q) &= g_2 - m_{21}m_{11}^{-1}g_1
 \end{aligned} \tag{3.27}$$

Then define the sliding manifold as the linear combination of the actuated and unactuated configuration variables as below:

$$\sigma = \dot{q}_2 + \gamma_1 q_2 + \gamma_2 \dot{q}_1 + \gamma_3 q_1 \tag{3.28}$$

where γ_1 , γ_2 , and γ_3 are design parameters.

Theorem 3.8. *The following standard SMC law*

$$u = \frac{\bar{m}_{11}\bar{m}_{22}}{\bar{m}_{11} + \gamma_2\bar{m}_{22}} \left(\bar{m}_{22}^{-1}(\bar{c}_2 + \bar{g}_2) + \gamma_2\bar{m}_{11}^{-1}(\bar{c}_1 + \bar{g}_1) - (\gamma_3\dot{q}_1 + \gamma_1\dot{q}_2) - \left| \frac{\bar{m}_{11}\bar{m}_{22}}{\bar{m}_{11} + \gamma_2\bar{m}_{22}} \right| D_0 \text{sign}(\sigma) - \Gamma \text{sign}(\sigma) \right) \quad (3.29)$$

with positive design constant Γ , will enforce sliding mode in the manifold (3.28) along the dynamics (3.20).

Proof. The proof is given in Chapter 4. \square

Lyapunov stability analysis requires the following values for the sliding parameters.

Proposition 3.9. *Choosing the design parameters γ_1 , γ_2 , and γ_3 as below in Eq. (3.30), with a , b , c strictly positive, proves stability of the sliding mode dynamics locally.*

$$\gamma_1 = \frac{a(b^2 + c^2)}{b^2 + c^2 + 2ab} \quad (3.30a)$$

$$\gamma_2 = \frac{(b^2 + c^2 + 2ab)(m_1 + m_2) - k}{(b^2 + c^2 + 2ab)m_2r} \quad (3.30b)$$

$$\gamma_3 = \frac{a(b^2 + c^2)(m_1 + m_2) - (a + 2b)k}{(b^2 + c^2 + 2ab)m_2r} \quad (3.30c)$$

where $a > 0$, $b > 0$, $c > 0$ are design constants for desired performance.

Proof. The proof is given in Chapter 4. \square

Choose $a = 12$, $b = 1$, $c = 12$ and $\Gamma = 1$. Figure 3.5 shows open loop response that is unstable but bounded. Small disturbance $d(t) = 0.02 \sin\left(\sqrt{\frac{k}{m_1}}t\right)$ with natural frequency greatly disturbs system dynamics. Parameter variations have small effect on response. Figure 3.6 shows closed loop response SMC control (3.29) with $D_0 = 0$ that is less robust. Figure 3.6e shows the chattering and also the effects of parameter variations. Figure 3.7 shows closed loop response with $D_0 = 0.02$ and is robust but at the cost of increased control effort and chattering.

B. HOSM control law based on nonlinear sliding manifold:

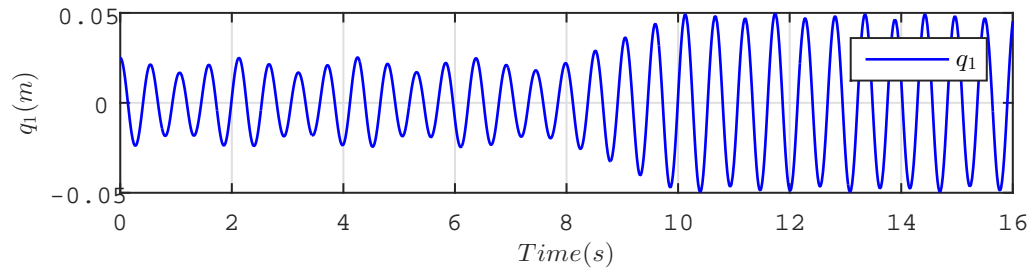
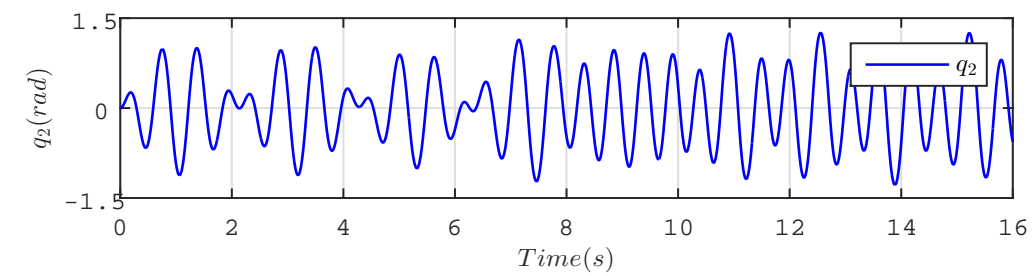
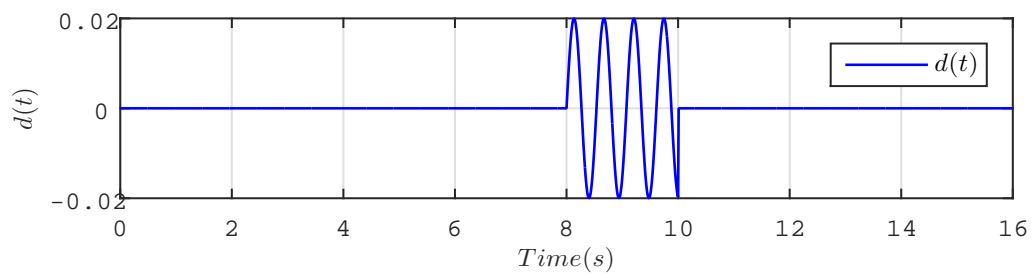
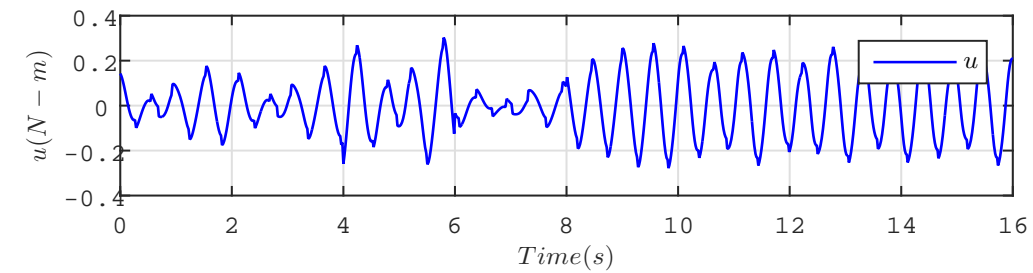
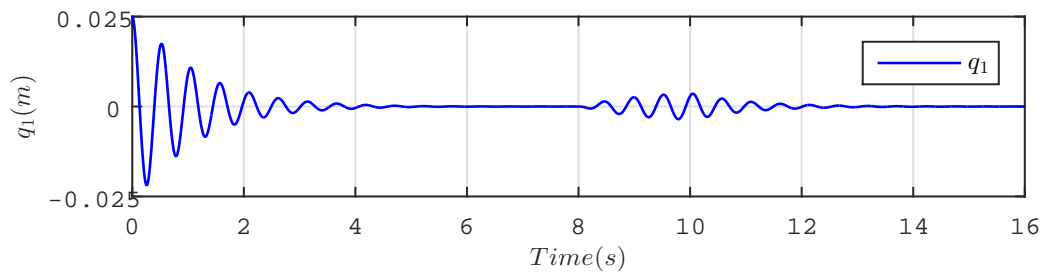
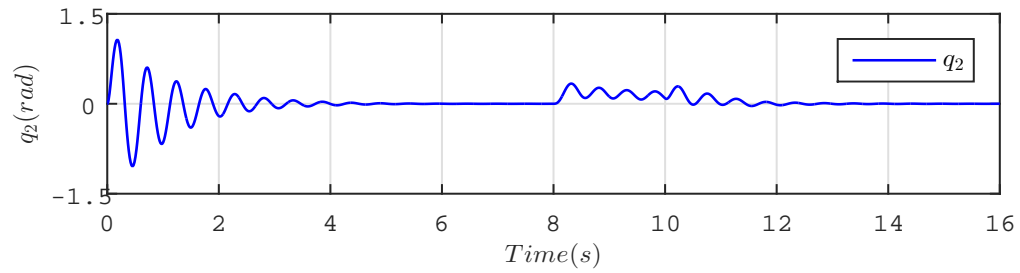
(A) Oscillator position q_1 (m)(B) Pendulum position q_2 (rad)(C) Disturbance $d(t) = 0.02 \sin\left(\sqrt{\frac{k}{m_1}}t\right)$ (D) Control effort u (N-m), shown but not applied

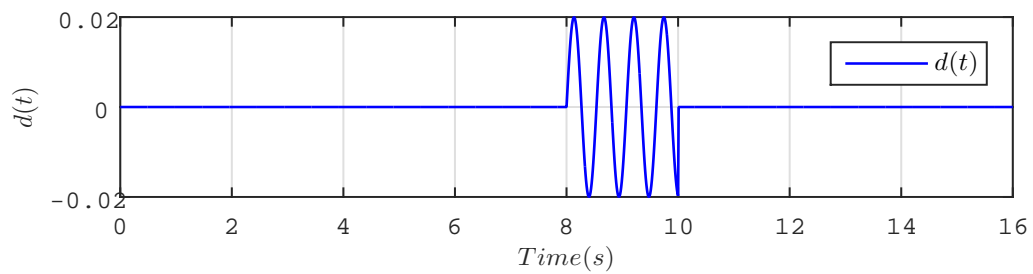
FIGURE 3.5: Open loop response of the TORA system to $q(0) = [0.025, 0, 0, 0]^T$ in the presence of disturbance and parametric variations.



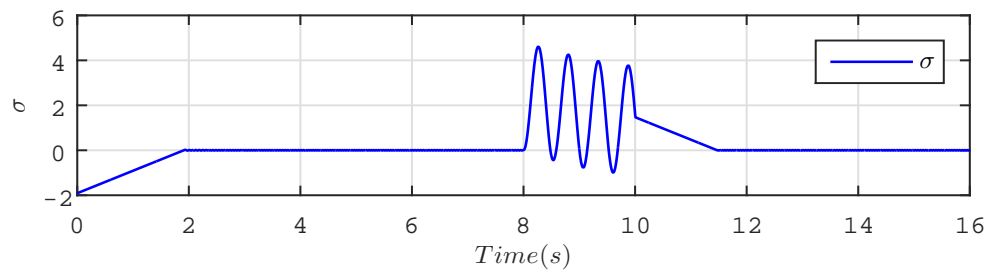
(A) Oscillator position q_1 (m)



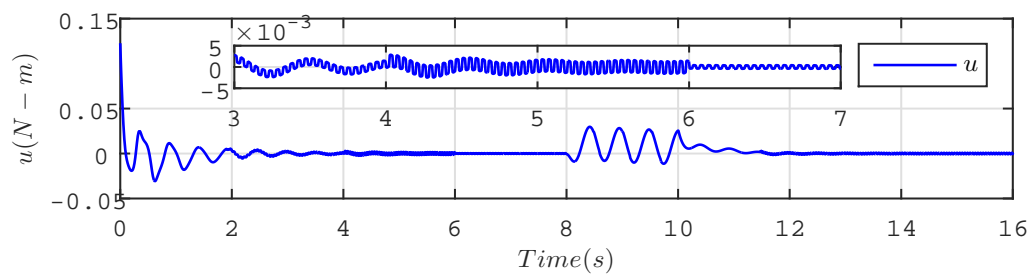
(B) Pendulum position q_2 (rad)



(C) Disturbance $d(t) = 0.02 \sin\left(\sqrt{\frac{k}{m_1}}t\right)$



(D) Sliding surface σ



(E) Control effort u (N-m)

FIGURE 3.6: Closed loop response of the TORA system with SMC law (3.29) with $D_0 = 0$, $q(0) = [0.025, 0, 0, 0]^T$

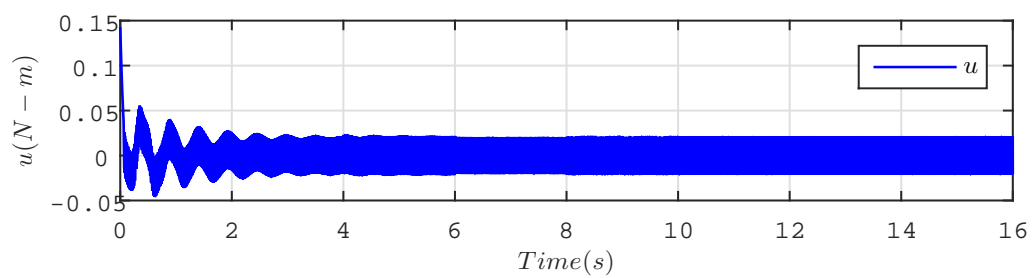
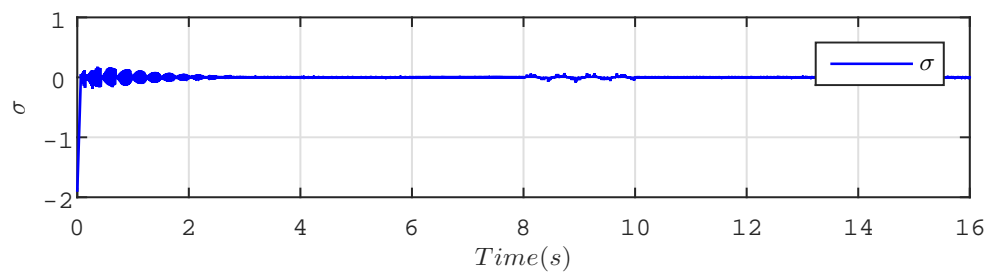
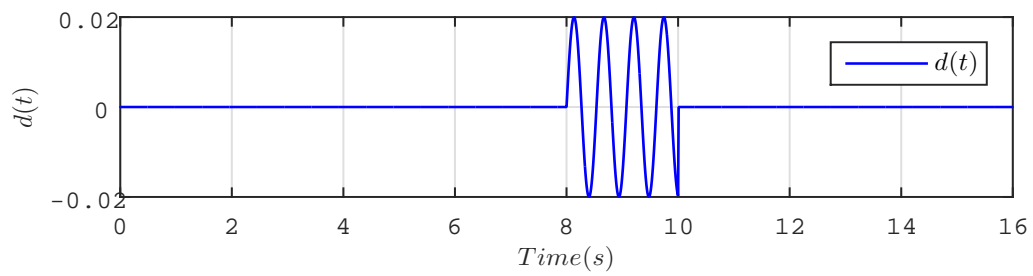
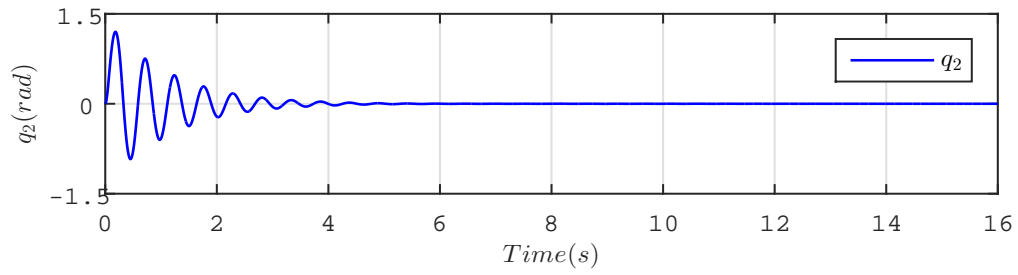
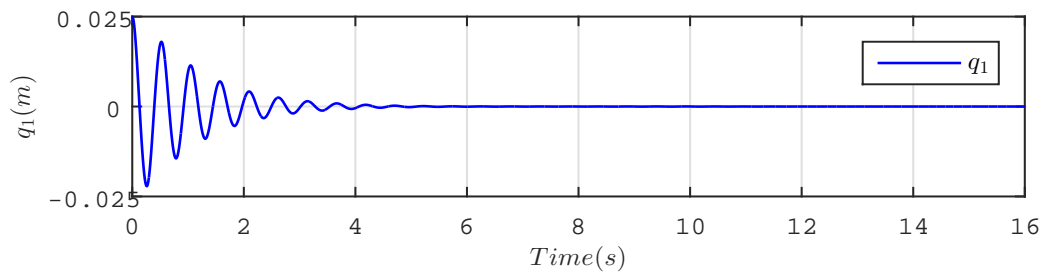


FIGURE 3.7: Closed loop response of the TORA system with SMC law (3.29) with $D_0 = 0.02$, $q(0) = [0.025, 0, 0, 0]^T$

Using the collocated partial feedback linearizing control:

$$u = (m_{22} - m_{21}m_{11}^{-1}m_{12})v + c_2 + g_2 - m_{21}m_{11}^{-1}(c_1 + g_1) \quad (3.31)$$

where v is a new control input, and the nonlinear coordinate transformation:

$$\begin{aligned} z_1 &= q_1 + \frac{m_2 r}{m_1 + m_2} \sin(q_2) \\ z_2 &= (m_1 + m_2)\dot{q}_1 + m_2 r \cos(q_2)\dot{q}_2 \\ \xi_1 &= q_2 \\ \xi_2 &= \dot{q}_2 \end{aligned} \quad (3.32)$$

transforms the dynamics of the TORA system (3.20) into the following form:

$$\ddot{z} = -k_1 z + k_2 \sin(\xi) \quad (3.33a)$$

$$\ddot{\xi} = v + D(t) \quad (3.33b)$$

where $k_1 = \frac{k}{m_1 + m_2}$, $k_2 = \frac{km_2 r}{(m_1 + m_2)^2}$, and $D(t)$ represents the transformed uncertain term, matched and bounded as $D(t) \leq |D_0|$.

Note that stabilization of ξ -subsystem (3.33b) does not imply stabilization of the z -subsystem (3.33a) but the reverse is true. To stabilize (3.33a), define the the following nonlinear sliding manifold:

$$\sigma = k_2 \sin(\xi) + \alpha \dot{z} \quad (3.34)$$

with $\alpha > 0$ as a design constant.

Since the relative degree of system (3.34) is two, take twice the time derivative of σ along the dynamics (3.33) to achieve:

$$\ddot{\sigma} = a(z, \dot{z}, \xi, \dot{\xi}) + w \quad (3.35)$$

where $a(z, \dot{z}, \xi, \dot{\xi})$ contains the uncertain term $D(t)$ along with system dynamics and

$$w = b(z, \dot{z}, \xi, \dot{\xi})v \quad (3.36)$$

Choose the following smooth HOSM control law [154] to enforce sliding mode in relative degree 2 system (3.35):

$$w = -s_2 - K_1|\sigma|^{(\rho-2)/\rho}\text{sign}(\sigma) - K_2|\dot{\sigma}|^{(\rho-2)/(\rho-1)}\text{sign}(\dot{\sigma}) \quad (3.37)$$

where $\rho \geq 2$ and $K_1 > 0$, $K_2 > 0$ are design constants.

The term s_2 in the control law (3.37) is used to cancel the the uncertain bounded term $a(z, \dot{z}, \xi, \dot{\xi})$ in (3.35) and is estimated via the observer [154] ($m = 2$):

$$\begin{aligned} \dot{s}_0 &= s_1 \\ \dot{s}_1 &= v_1 + w \\ v_1 &= -\lambda_2|\Lambda|^{1/3}|s_1 - \dot{\sigma}|^{2/3}\text{sign}(s_1 - \dot{\sigma}) + s_2 \\ \dot{s}_2 &= -\lambda_1|\Lambda|\text{sign}(s_2 - v_1) \end{aligned} \quad (3.38)$$

where λ_2 and λ_1 are design parameters and $\Lambda > 0$ is Lipshitz constant of $\ddot{a}(z, \dot{z}, \xi, \dot{\xi})$.

Theorem 3.10. *The closed loop system (3.35), (3.37), (3.38) is finite time stable and hence σ , $\dot{\sigma}$ converge to 0 in finite time.*

Proof. The proof can be found in [154]. □

Once sliding mode is established, $\sigma = 0$, system (3.33a) becomes stable and z , \dot{z} converge to zero. With $(z = 0, \dot{z} = 0)$ the ξ -dynamics are governed by:

$$\sin(\xi) = 0 \quad (3.39)$$

that is an algebraic equation. By assuming that the origin is the equilibrium point of the open loop system, the solution to this equation is $\xi = 0$, and hence, ξ tends to zero as well, and consequently, the overall system (3.33) becomes stable.

In terms of the actual states $(q_1, \dot{q}_1, q_2, \dot{q}_2)$ of the TORA (3.20) we have:

$$\sigma = k_2 \sin(q_2) + \alpha \left(\dot{q}_1 + \frac{m_2 r}{m_1 + m_2} \dot{q}_2 \cos(q_2) \right) \quad (3.40)$$

$$\dot{\sigma} = k_2 \dot{q}_2 \cos(q_2) + k_2 \alpha \sin(q_2) - k_1 \alpha \left(q_1 + \frac{m_2 r}{m_1 + m_2} \sin(q_2) \right) \quad (3.41)$$

$$b(z, \dot{z}, \xi, \dot{\xi}) = k_2 \cos(q_2) \quad (3.42)$$

Choose sliding parameter $\alpha = 1.5$, the controller parameters $\rho = 3$, $K_1 = 10$, $K_2 = 15$, and the observer parameters $\lambda_1 = 10$, $\lambda_2 = 15$. Figure 3.8 shows closed loop response SSOSM control (3.37). The control action is smooth. Robustness is not good but can be improved with parameter tuning.

Remark 3.11. The transformed system (3.33) is similar to (3.26) but uses one level of transformation with no time transformation, retain the gravity term, and captures all the physical parameters of the system in the transformation. Furthermore, the control laws use the actual system states and is applicable to the actual system directly.

Results:

Both the control laws successfully stabilize the TORA system in less than 5 seconds that is an improvement to most works. The nonlinear benchmark specifications [16] are met, i.e., the closed loop system is stable and the control effort is less than 0.05 N-m (specifications states less than 0.1 N-m continuous).

Conclusion:

A well known nonlinear benchmark control problem was solved using SMC theory in a novel and simple way. The closed loop performance is improved and meets the specifications. Furthermore, system response is robust to parameters variations, internal model uncertainties and unknown external disturbances. Simplicity of the design approach, excellent closed loop response, and remarkable robustness to uncertainties are highly desirable for complex systems operating in uncertain environments. In this work, the author investigates a comprehensive design framework, for underactuated mechanical systems, with these desirable features.

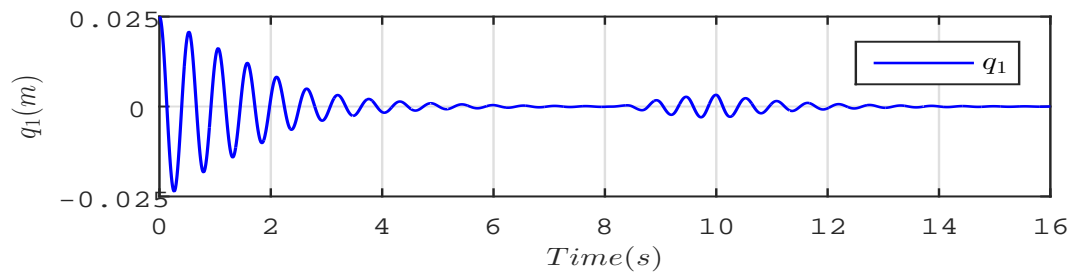
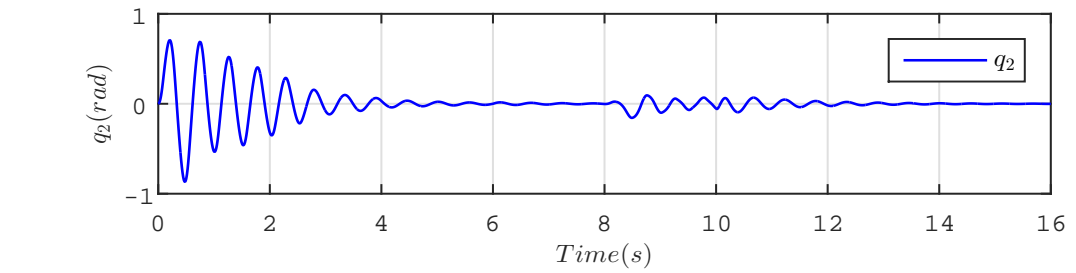
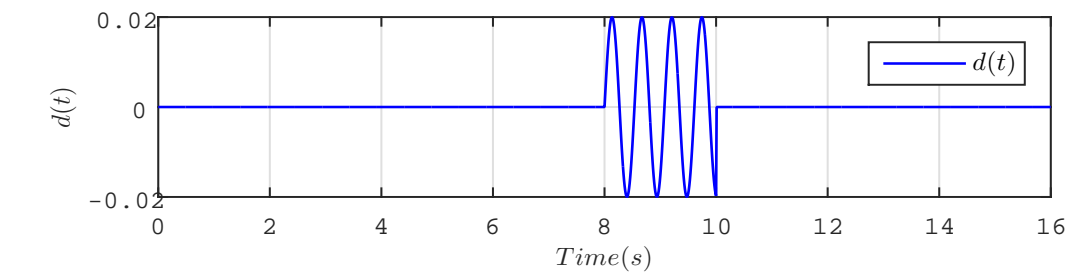
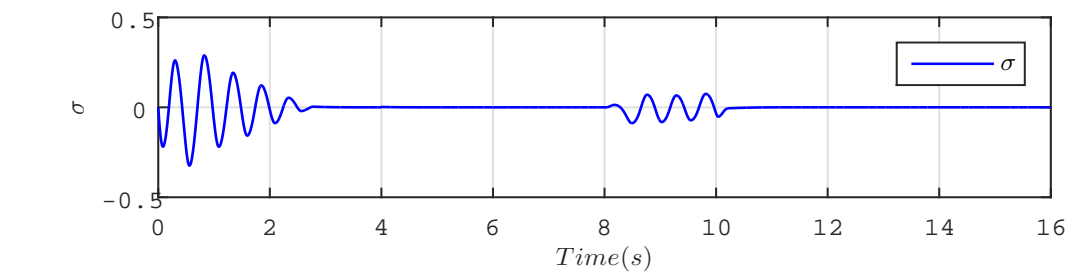
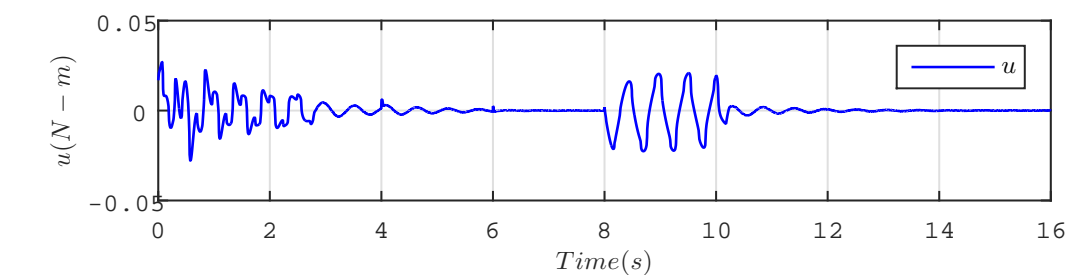
(A) Oscillator position q_1 (m)(B) Pendulum position q_2 (rad)(C) Disturbance $d(t) = 0.02 \sin\left(\sqrt{\frac{k}{m_1}}t\right)$ (D) Sliding surface σ (E) Control effort u (N-m)

FIGURE 3.8: Closed loop response of the TORA system with HOSM control law (3.29), $q(0) = [0.025, 0, 0, 0]^T$

Chapter 4

Standard SMC Design for Underactuated Mechanical Systems

In this chapter, author designs a standard SMC design framework for underactuated mechanical systems using the Euler-Lagrange equations of motion. The framework takes into account both the matched and unmatched disturbances explicitly in the design. The author derives expressions for the sliding mode dynamics and also for the parameters of the sliding surface. The main results in this chapter are based on [170]. The design procedure is validated for the following benchmark underactuated mechanical systems:

1. The Inertia-Wheel Pendulum
2. The TORA System
3. The Beam-and-Ball System
4. The Cart-Pole System
5. The Overhead Crane

4.1 Problem Formulation

The dynamical equations of motion of an n degrees of freedom mechanical control system are given by Euler-Lagrange equation as below [97]:

$$\frac{d}{dt} \frac{\partial \mathcal{L}}{\partial \dot{q}} - \frac{\partial \mathcal{L}}{\partial q} = F(q)u + D(q, \dot{q}, t) \quad (4.1)$$

where $q \in \mathfrak{R}^n$ is the configuration vector in generalized coordinates, $F(q) \in \mathfrak{R}^{n \times m}$ is the control input matrix, $u \in \mathfrak{R}^m$ is the control input vector, $D(q, \dot{q}, t) \in \mathfrak{R}^n$ represents the uncertainties, and $\mathcal{L}(q, \dot{q})$ is the *Lagrangian* of the system. The case, $m = \text{rank}(F) = n$, represents a fully actuated mechanical system, and, the case, $m = \text{rank}(F) < n$, characterizes an underactuated mechanical system.

The vector form of Eq. (4.1) is:

$$M(q)\ddot{q} + C(q, \dot{q})\dot{q} + G(q) = F(q)u + D(q, \dot{q}, t) \quad (4.2)$$

where $M(q) \in \mathfrak{R}^{n \times n}$ is the positive definite symmetric inertia matrix, $G(q)$ consists of gravitational terms and $C(q, \dot{q})\dot{q}$ consists of centrifugal and Coriolis terms.

: For the underactuation case, i.e., $n < m$, system (4.2) can be partitioned into actuated and unactuated subsystems and two classes can be defined as below:

A. Class-I Underactuated Mechanical Systems:

Partitioning the configuration vector $q \in \mathfrak{R}^n$ into unactuated $q_1 \in \mathfrak{R}^{n-m}$ and actuated $q_2 \in \mathfrak{R}^m$ configuration vectors and also partitioning the inertia matrix accordingly, and taking the special case $F(q) = [0, I_m]^T$, system (4.2) takes the form:

$$m_{11}(q_2)\ddot{q}_1 + m_{12}(q_2)\ddot{q}_2 + c_1(q, \dot{q}) + g_1(q_1, q_2) = d_1(q, \dot{q}, t) \quad (4.3a)$$

$$m_{21}(q_2)\ddot{q}_1 + m_{22}(q_2)\ddot{q}_2 + c_2(q, \dot{q}) + g_2(q_1, q_2) = u + d_2(q, \dot{q}, t) \quad (4.3b)$$

where $M(q_2) = \begin{bmatrix} m_{11}(q_2) & m_{12}(q_2) \\ m_{21}(q_2) & m_{22}(q_2) \end{bmatrix}$, $c_1(q, \dot{q}) \in \mathfrak{R}^{(n-m)}$ and $c_2(q, \dot{q}) \in \mathfrak{R}^m$ are the centrifugal and Coriolis terms, $g_1(q) \in \mathfrak{R}^{(n-m)}$ and $g_2(q) \in \mathfrak{R}^m$ are the gravitational terms, $d_1(q, \dot{q}, t) \in \mathfrak{R}^{(n-m)}$ and $d_2(q, \dot{q}, t) \in \mathfrak{R}^m$ are the uncertainties, and $u \in \mathfrak{R}^m$ is the vector of control inputs produced by m actuators. The special case, $n = 2$, $m = 1$, give 2DOF underactuated mechanical systems.

Remark 4.1. The IWP, TORA system, and the Acrobot are underactuated mechanical systems described by Eq. (4.3) with $n = 2$, $m = 1$.

Remark 4.2. In (4.3), $d_1(q, \dot{q}, t) \in \mathfrak{R}^{(n-m)}$ is unmatched, acts on the unactuated variable q_1 , and hence, can disturb system stability and dynamics to a greater extent. On the other hand, $d_2(q, \dot{q}, t) \in \mathfrak{R}^m$ is matched, acts on the actuated variable q_2 , and hence, system response can be made robust it.

B. Class-II Underactuated Mechanical Systems:

Partitioning the configuration vector $q \in \mathfrak{R}^n$ into actuated $q_1 \in \mathfrak{R}^m$ and unactuated $q_2 \in \mathfrak{R}^{n-m}$ configuration vectors and also the inertia matrix, and taking the special case $F(q) = [I_m, 0]^T$, system (4.2) takes the form:

$$m_{11}(q_2)\ddot{q}_1 + m_{12}(q_2)\ddot{q}_2 + c_1(q, \dot{q}) + g_1(q_1, q_2) = u + d_1(q, \dot{q}, t) \quad (4.4a)$$

$$m_{21}(q_2)\ddot{q}_1 + m_{22}(q_2)\ddot{q}_2 + c_2(q, \dot{q}) + g_2(q_1, q_2) = d_2(q, \dot{q}, t) \quad (4.4b)$$

where $M(q_2) = \begin{bmatrix} m_{11}(q_2) & m_{12}(q_2) \\ m_{21}(q_2) & m_{22}(q_2) \end{bmatrix}$, $c_1(q, \dot{q}) \in \mathfrak{R}^m$ and $c_2(q, \dot{q}) \in \mathfrak{R}^{(n-m)}$ are the centrifugal and Coriolis terms, $g_1(q) \in \mathfrak{R}^m$ and $g_2(q) \in \mathfrak{R}^{(n-m)}$ are the gravitational terms, $d_1(q, \dot{q}, t) \in \mathfrak{R}^m$ and $d_2(q, \dot{q}, t) \in \mathfrak{R}^{(n-m)}$ are the uncertainties, and $u \in \mathfrak{R}^m$ is the vector of control inputs produced by m actuators. The special case $n = 2$, $m = 1$ give 2DOF underactuated mechanical systems.

Remark 4.3. The Furuta Pendulum, the Overhead Crane, the Cart-Pole system, the Pendubot, and the Beam-and-Ball system are underactuated mechanical systems described by Eq. (4.4) with $n = 2$, $m = 1$.

Remark 4.4. In (4.4), $d_1(q, \dot{q}, t) \in \mathfrak{R}^m$ is matched, acts on the actuated variable q_1 , and hence, robustness can be achieved for it, On the other hand, $d_2(q, \dot{q}, t) \in$

$\mathfrak{R}^{(n-m)}$ is unmatched, acts on the unactuated variable q_2 , and hence, is expected to disturb system dynamics greatly.

For notational simplicity, henceforth, omit the dependence of $m_{11}(q_2)$, $m_{12}(q_2)$, $m_{21}(q_2)$, $m_{22}(q_2)$, $c_1(q, \dot{q})$, $c_2(q, \dot{q})$, $g_1(q_1, q_2)$ and $g_2(q_1, q_2)$ on states.

4.2 Standard SMC Design for Class-I Underactuated Mechanical Systems

Consider Class-I underactuated mechanical systems represented by Eq. (4.3) with $n = 2$, $m = 1$ as:

$$m_{11}\ddot{q}_1 + m_{12}\ddot{q}_2 + c_1 + g_1 = d_1 \quad (4.5a)$$

$$m_{21}\ddot{q}_1 + m_{22}\ddot{q}_2 + c_2 + g_2 = u + d_2 \quad (4.5b)$$

Write (4.5) as

$$\bar{m}_{11}\ddot{q}_1 + \bar{c}_1 + \bar{g}_1 = u + \bar{d}_1 \quad (4.6a)$$

$$\bar{m}_{22}\ddot{q}_2 + \bar{c}_2 + \bar{g}_2 = u + \bar{d}_2 \quad (4.6b)$$

with the following definitions:

$$\begin{aligned} \bar{m}_{11} &= m_{21} - m_{22}m_{12}^{-1}m_{11} \\ \bar{c}_1 &= c_2 - m_{22}m_{12}^{-1}c_1 \\ \bar{g}_1 &= g_2 - m_{22}m_{12}^{-1}g_1 \\ \bar{d}_1 &= d_2 - m_{22}m_{12}^{-1}d_1 \\ \bar{m}_{22} &= m_{22} - m_{21}m_{11}^{-1}m_{12} \\ \bar{c}_2 &= c_2 - m_{21}m_{11}^{-1}c_1 \\ \bar{g}_2 &= g_2 - m_{21}m_{11}^{-1}g_1 \\ \bar{d}_2 &= d_2 - m_{21}m_{11}^{-1}d_1 \end{aligned} \quad (4.7)$$

Using $x = [x_1, x_2, x_3, x_4]^T = q = [q_1, \dot{q}_1, q_2, \dot{q}_2]^T$, we achieve the state space representation of (4.5) as:

$$\dot{x}_1 = x_2 \quad (4.8a)$$

$$\dot{x}_2 = f_1(x) + b_1(x)(u + \bar{d}_1) \quad (4.8b)$$

$$\dot{x}_3 = x_4 \quad (4.8c)$$

$$\dot{x}_4 = f_2(x) + b_2(x)(u + \bar{d}_1) \quad (4.8d)$$

where

$$\begin{aligned} f_1(x) &= -\bar{m}_{11}^{-1}(\bar{c}_1 + \bar{g}_1) \\ b_1(x) &= \bar{m}_{11}^{-1} \\ \bar{d}_1 &= d_2 - m_{22}m_{12}^{-1}d_1 \\ f_2(x) &= -\bar{m}_{22}^{-1}(\bar{c}_2 + \bar{g}_2) \\ b_2(x) &= \bar{m}_{22}^{-1} \\ \bar{d}_2 &= d_2 - m_{21}m_{11}^{-1}d_1 \end{aligned} \quad (4.9)$$

are the nonlinear nominal functions.

It is important to note that in the state space representation (4.8) of the underactuated mechanical system (4.5), both the disturbances, d_2 and d_1 , appear in the same equation in which the control u appears. The appearance of (4.8) may tempt a designer to achieve robustness for both the disturbances by designing sliding mode control. But this not the case. Both the disturbances, d_2 and d_1 , affect both the unactuated (q_1) and actuated (q_2) dynamics through coupling similar to the control u . Disturbance d_2 appears as it for both the dynamics and d_1 is scaled to $m_{22}m_{12}^{-1}d_1$ for the unactuated dynamism and scaled to $m_{21}m_{11}^{-1}d_1$ for the actuated dynamics. Depending upon the value of this scaling, the effect of d_1 may be enhanced further or be reduced. If the scaling is 1, which is the case for IWP, then d_1 and d_2 may cancel the effect of each other if these are the same. This scenario is special characteristic of underactuated mechanical systems not analyzed or discussed before to best of our knowledge. This issue will be discussed at length for the application example later in this chapter.

4.2.1 Control Law Design

To design the standard SMC law for Class-I systems (4.5), define the unactuated and actuated control errors as follows:

$$e_1 = q_1 - q_{1des} \quad (4.10a)$$

$$e_2 = q_2 - q_{2des} \quad (4.10b)$$

Next define the sliding variable σ as below:

$$\sigma = \dot{e}_2 + \gamma_1 e_2 + \gamma_2 \dot{e}_1 + \gamma_3 e_1 \quad (4.11)$$

where γ_1 , γ_2 , and γ_3 are design parameters.

Consider the following assumptions holds.

Assumption 4.1. $(\bar{m}_{22}^{-1} + \gamma_2 \bar{m}_{11}^{-1}) \neq 0$.

Assumption 4.2. The uncertainties are bounded as $|d_1(q, \dot{q}, t)| \leq D_1$, $|d_2(q, \dot{q}, t)| \leq D_2$.

Now the standard SMC law for Class-I systems (4.5) is given by the following theorem.

Theorem 4.5. *The following standard SMC law*

$$\begin{aligned} u = \frac{1}{(\bar{m}_{22}^{-1} + \gamma_2 \bar{m}_{11}^{-1})} & \left(\bar{m}_{22}^{-1} (\bar{c}_2 + \bar{g}_2) + \gamma_2 \bar{m}_{11}^{-1} (\bar{c}_1 + \bar{g}_1) - (\gamma_3 \dot{q}_1 + \gamma_1 \dot{q}_2) \right. \\ & - \left| (\bar{m}_{22}^{-1} m_{21} m_{11}^{-1} + \gamma_2 \bar{m}_{11}^{-1} m_{22} m_{12}^{-1}) \right| D_1 \text{sign}(\sigma) \\ & \left. - \left| (\bar{m}_{22}^{-1} + \gamma_2 \bar{m}_{11}^{-1}) \right| D_2 \text{sign}(\sigma) - \Gamma \text{sign}(\sigma) \right) \end{aligned} \quad (4.12)$$

with positive design constant Γ , will enforce sliding mode in the manifold (4.11) along the dynamics (4.5).

Proof. To prove the theorem, take, for (4.11), the Lyapunov function as

$$V = \frac{1}{2} \sigma^2 \quad (4.13)$$

and take its time derivative along the dynamics (4.5) to obtain:

$$\dot{V} = \sigma \dot{\sigma} = \sigma (\ddot{e}_2 + \gamma_1 \dot{e}_2 + \gamma_2 \ddot{e}_1 + \gamma_3 \dot{e}_1) \quad (4.14)$$

Using the control error definitions in e_1 and e_2 in (4.10), the above derivative of the sliding variable can be written as:

$$\dot{V} = \sigma (\ddot{q}_2 + \gamma_1 \dot{q}_2 + \gamma_2 \ddot{q}_1 + \gamma_3 \dot{q}_1) \quad (4.15)$$

Using \ddot{q}_1 and \ddot{q}_2 from (4.6a) and (4.6b) respectively, the above derivative becomes:

$$\dot{V} = \sigma (\bar{m}_{22}^{-1} (u + \bar{d}_2 - \bar{c}_2 - \bar{g}_2) + \gamma_1 \dot{q}_2 + \gamma_2 \bar{m}_{11}^{-1} (u + \bar{d}_1 - \bar{c}_1 - \bar{g}_1) + \gamma_3 \dot{q}_1) \quad (4.16)$$

or

$$\begin{aligned} \dot{V} = \sigma & ((\bar{m}_{22}^{-1} + \gamma_2 \bar{m}_{11}^{-1})u + (\bar{m}_{22}^{-1} \bar{d}_2 + \gamma_2 \bar{m}_{11}^{-1} \bar{d}_1) - \bar{m}_{22}^{-1} (\bar{c}_2 + \bar{g}_2) \\ & - \gamma_2 \bar{m}_{11}^{-1} (\bar{c}_1 + \bar{g}_1) + \gamma_1 \dot{q}_2 + \gamma_3 \dot{q}_1) \end{aligned} \quad (4.17)$$

or

$$\begin{aligned} \dot{V} = \sigma & ((\bar{m}_{22}^{-1} + \gamma_2 \bar{m}_{11}^{-1})u + (\bar{m}_{22}^{-1} + \gamma_2 \bar{m}_{11}^{-1})d_2 - (\bar{m}_{22}^{-1} m_{21} m_{11}^{-1} + \gamma_2 \bar{m}_{11}^{-1} m_{22} m_{12}^{-1})d_1 \\ & - \bar{m}_{22}^{-1} (\bar{c}_2 + \bar{g}_2) - \gamma_2 \bar{m}_{11}^{-1} (\bar{c}_1 + \bar{g}_1) + \gamma_1 \dot{q}_2 + \gamma_3 \dot{q}_1) \end{aligned} \quad (4.18)$$

Substituting for u from the control law (4.12) we have:

$$\begin{aligned} \dot{V} = \sigma & (-(\bar{m}_{22}^{-1} m_{21} m_{11}^{-1} + \gamma_2 \bar{m}_{11}^{-1} m_{22} m_{12}^{-1})D_1 \text{sign}(\sigma) \\ & - (\bar{m}_{22}^{-1} m_{21} m_{11}^{-1} + \gamma_2 \bar{m}_{11}^{-1} m_{22} m_{12}^{-1})d_1 \\ & - (\bar{m}_{22}^{-1} + \gamma_2 \bar{m}_{11}^{-1})D_2 \text{sign}(\sigma) + (\bar{m}_{22}^{-1} + \gamma_2 \bar{m}_{11}^{-1})d_2 - \Gamma \text{sign}(\sigma)) \end{aligned} \quad (4.19)$$

or

$$\begin{aligned} \dot{V} = & -(\bar{m}_{22}^{-1} m_{21} m_{11}^{-1} + \gamma_2 \bar{m}_{11}^{-1} m_{22} m_{12}^{-1})D_1 \sigma \text{sign}(\sigma) \\ & - (\bar{m}_{22}^{-1} m_{21} m_{11}^{-1} + \gamma_2 \bar{m}_{11}^{-1} m_{22} m_{12}^{-1})d_1 \sigma \\ & - (\bar{m}_{22}^{-1} + \gamma_2 \bar{m}_{11}^{-1})D_2 \sigma \text{sign}(\sigma) + (\bar{m}_{22}^{-1} + \gamma_2 \bar{m}_{11}^{-1})d_2 \sigma - \Gamma \sigma \text{sign}(\sigma) \end{aligned} \quad (4.20)$$

Using the identity $\sigma \text{sign}(\sigma) = |\sigma|$, (4.19) can be written as:

$$\begin{aligned} \dot{V} = & -(\bar{m}_{22}^{-1}m_{21}m_{11}^{-1} + \gamma_2\bar{m}_{11}^{-1}m_{22}m_{12}^{-1})D_1|\sigma| - (\bar{m}_{22}^{-1}m_{21}m_{11}^{-1} + \gamma_2\bar{m}_{11}^{-1}m_{22}m_{12}^{-1})d_1\sigma \\ & - (\bar{m}_{22}^{-1} + \gamma_2\bar{m}_{11}^{-1})D_2|\sigma| + (\bar{m}_{22}^{-1} + \gamma_2\bar{m}_{11}^{-1})d_2\sigma - \Gamma|\sigma| \end{aligned} \quad (4.21)$$

that can be written as:

$$\dot{V} \leq -\Gamma|\sigma| \quad (4.22)$$

The reachability condition (4.22) ensures the existence of sliding modes in (4.11) and the convergence of σ to 0. This proves the theorem. \square

Lemma 4.6. *Upon the the establishment of sliding mode in system (4.11) along the dynamics of (4.5), in accordance with Theorem 4.5, the sliding mode dynamics of Class-I systems (4.5) are:*

$$\begin{aligned} \dot{\xi}_1 &= \xi_2 \\ \dot{\xi}_2 &= \frac{1}{m_{11} - m_{12}\gamma_2} (-m_{12}\gamma_1\gamma_3\xi_1 - m_{12}(\gamma_1\gamma_2 - \gamma_3)\xi_2 - m_{12}\gamma_1^2\xi_3 - c_1 - g_1 + d_1) \\ \dot{\xi}_3 &= -\gamma_3\xi_1 - \gamma_2\xi_2 - \gamma_1\xi_3 \end{aligned} \quad (4.23)$$

where

$$\xi_1 = q_1 - q_{1des} \quad (4.24a)$$

$$\xi_2 = \dot{q}_1 \quad (4.24b)$$

$$\xi_3 = q_2 - q_{2des} \quad (4.24c)$$

Proof. The condition $\sigma = 0$ governs the sliding mode dynamics, which by (4.10) and (4.11), implies that

$$\dot{e}_2 + \gamma_1 e_2 + \gamma_2 \dot{e}_1 + \gamma_3 e_1 = 0 \quad (4.25a)$$

$$\dot{q}_2 + \gamma_1 (q_2 - q_{2des}) + \gamma_2 \dot{q}_1 + \gamma_3 (q_1 - q_{1des}) = 0 \quad (4.25b)$$

$$\ddot{q}_2 + \gamma_1 \dot{q}_2 + \gamma_2 \ddot{q}_1 + \gamma_3 \dot{q}_1 = 0 \quad (4.25c)$$

Substituting $\ddot{q}_2 = -\gamma_2\ddot{q}_1 - \gamma_3\dot{q}_1 - \gamma_1\dot{q}_2$ from (4.25c) in (4.5a) we have:

$$m_{11}\ddot{q}_1 + m_{12}(-\gamma_2\ddot{q}_1 - \gamma_3\dot{q}_1 - \gamma_1\dot{q}_2) + c_1 + g_1 = d_1 \quad (4.26a)$$

$$m_{11}\dot{q}_1 - m_{12}\gamma_2\dot{q}_1 - m_{12}\gamma_3\dot{q}_1 - m_{12}\gamma_1\dot{q}_2 + c_1 + g_1 = d_1 \quad (4.26b)$$

$$(m_{11} - m_{12}\gamma_2)\ddot{q}_1 - m_{12}\gamma_3\dot{q}_1 - m_{12}\gamma_1\dot{q}_2 + c_1 + g_1 = d_1 \quad (4.26c)$$

Substituting $\dot{q}_2 = -\gamma_2\dot{q}_1 - \gamma_3(q_1 - q_{1des}) - \gamma_1(q_2 - q_{2des})$ from (4.25b) in (4.26c) we have:

$$\begin{aligned} (m_{11} - m_{12}\gamma_2)\ddot{q}_1 - m_{12}\gamma_3\dot{q}_1 - m_{12}\gamma_1(-\gamma_2\dot{q}_1 - \gamma_3(q_1 - q_{1des}) - \gamma_1(q_2 - q_{2des})) \\ + c_1 + g_1 = d_1 \end{aligned} \quad (4.27)$$

or

$$\begin{aligned} (m_{11} - m_{12}\gamma_2)\ddot{q}_1 + (m_{12}\gamma_1\gamma_2 - m_{12}\gamma_3)\dot{q}_1 + m_{12}\gamma_1\gamma_3(q_1 - q_{1des}) \\ + m_{12}\gamma_1^2(q_2 - q_{2des}) + c_1 + g_1 = d_1 \end{aligned} \quad (4.28)$$

Using $\xi_1 = q_1 - q_{1des}$, $\xi_2 = \dot{q}_1$, and $\xi_3 = q_2 - q_{2des}$ as state variables for (4.28), the expression for the sliding mode dynamics (4.23) follows, and hence, proves the lemma. \square

4.2.2 Application to Class-I Underactuated Mechanical Systems

The proposed control design framework is applied to Class-I underactuated mechanical systems of the Inertia-Wheel Pendulum, and the TORA system. Table 4.1 shows parameters for The Euler-Lagrange equations (4.5) of these systems.

TABLE 4.1: The Euler-Lagrange Equation (4.5) for IWP and TORA System

System	m_{11}	$m_{12} = m_{21}$	m_{22}	c_1	g_1	c_2	g_2
IWP	J	I_2	I_2	0	$-m_0 S_1$	0	0
TORA	$m_1 + m_2$	$m_2 r C_2$	$I_2 + m_2 r^2$	$-m_2 r S_2 \dot{q}_2^2$	$k q_1$	0	$m_2 r g S_2$

$C_i := \cos(q_i)$, $S_i := \sin(q_i)$, $i = 1, 2$, $J = I_1 + I_2 + m_1 l_1^2 + m_2 L_1^2$, $m_0 = (m_1 l_1 + m_2 L_1)g$

4.2.2.1 The Inertia-Wheel Pendulum (IWP)

Figure 3.1c shows the IWP [13]. The system is an inverted pendulum with a rotating inertia wheel at one end. The control objective is to swing up the pendulum, by rotating the wheel, from its stable downward equilibrium position ($q_1 = \pi$) to the upright unstable equilibrium position ($q_1 = 0$) and stabilize it thereafter. Excellent research works on IWP can be found as backstepping [14, 94], IDA-PBC [72], sliding mode [171], passivity [13], saturation [15], dynamic surface control [167], equivalent-input-disturbance approach [75], and output feedback stabilization [168].

Choose the physical parameters of the IWP according to [13, 94, 167] as:

$$m_{11} = I_1 + I_2 + m_1 l_1^2 + m_2 L_1^2 = 4.83 \times 10^{-3} \text{ (kg.m}^2 \text{)}, \quad m_{12} = m_{21} = m_{22} = I_2 = 32.0 \times 10^{-6} \text{ (kg.m}^2 \text{)},$$

$$m_1 l_1 + m_2 L_1 = 38.7 \times 10^{-3} \text{ (kg.m)}, \quad \text{and } g = 9.8 \text{ (m.sec}^{-2}\text{)}.$$

According to Lemma 4.6, the sliding mode dynamics in Eq. (4.23) for the IWP are:

$$\begin{aligned} \dot{\xi}_1 &= \xi_2 \\ \dot{\xi}_2 &= \frac{1}{m_{11} - m_{12}\gamma_2} \left(-m_{12}\gamma_1\gamma_3\xi_1 - m_{12}(\gamma_1\gamma_2 - \gamma_3)\xi_2 - m_{12}\gamma_1^2\xi_3 \right. \\ &\quad \left. + (m_1 l_1 + m_2 L_1)g \sin(\xi_1 + q_{1des}) + d_1 \right) \\ \dot{\xi}_3 &= -\gamma_3\xi_1 - \gamma_2\xi_2 - \gamma_1\xi_3 \end{aligned} \quad (4.29)$$

that can be written as:

$$\dot{\boldsymbol{\xi}}(t) = \mathbf{f}_{\text{IWP}}(\boldsymbol{\xi}(t)) \quad (4.30)$$

Take the Jacobian linearization of (4.30) around the equilibrium $\boldsymbol{\xi} = [0, 0, 0]^T$ as:

$$\dot{\boldsymbol{\xi}}(t) = \mathbf{A}_{\text{IWP}}\boldsymbol{\xi}(t) \quad (4.31)$$

with $\mathbf{A}_{\text{IWP}} = \left. \frac{\partial \mathbf{f}_{\text{IWP}}}{\partial \boldsymbol{\xi}} \right|_{\boldsymbol{\xi}=\mathbf{0}}$ representing the Jacobian matrix of \mathbf{f}_{IWP} w.r.t. $\boldsymbol{\xi}$ at $\boldsymbol{\xi} = \mathbf{0}$.

Proposition 4.7 below gives stability of the dynamics in Eq. (4.29).

Proposition 4.7. *Choosing the the design parameters γ_1 , γ_2 , and γ_3 as below in Eq. (4.32), with a , b , c strictly positive, proves stability of (4.31) and stability of (4.29) is implied by Lyapunov indirect method.*

$$\gamma_1 = \frac{a(b^2 + c^2)}{b^2 + c^2 + 2ab} \quad (4.32a)$$

$$\gamma_2 = \frac{(b^2 + c^2 + 2ab)m_{11} + (m_1 l_1 + m_2 L_1)g}{(b^2 + c^2 + 2ab)m_{12}} \quad (4.32b)$$

$$\gamma_3 = \frac{a(b^2 + c^2)m_{11} + (a + 2b)(m_1 l_1 + m_2 L_1)g}{(b^2 + c^2 + 2ab)m_{12}} \quad (4.32c)$$

Proof. Linearizing system (4.29) for the stabilization of IWP, $q_{1des} = 0$, we have:

$$\mathbf{A}_{IWP} = \begin{bmatrix} 0 & 1 & 0 \\ \frac{-m_{12}\gamma_1\gamma_3 + (m_1 l_1 + m_2 L_1)g}{m_{11} - m_{12}\gamma_2} & \frac{-m_{12}(\gamma_1\gamma_2 - \gamma_3)}{m_{11} - m_{12}\gamma_2} & \frac{-m_{12}\gamma_1^2}{m_{11} - m_{12}\gamma_2} \\ -\gamma_3 & -\gamma_2 & -\gamma_1 \end{bmatrix} \quad (4.33)$$

with the characteristic equation as:

$$(m_{11} - m_{12}\gamma_2)s^3 + (m_{11}\gamma_1 - m_{12}\gamma_3)s^2 - (m_1 l_1 + m_2 L_1)gs + \gamma_1(m_1 l_1 + m_2 L_1)g = 0 \quad (4.34)$$

Now the desired stable poles $s_1 = -a$, $s_2 = -b + jc$, and $s_3 = -b - jc$, has the characteristic equation as:

$$s^3 + (a + 2b)s^2 + (b^2 + c^2 + 2ab)s + a(b^2 + c^2) = 0 \quad (4.35)$$

Comparing the corresponding coefficients in Eqs. (4.34) and (4.35), the closed form expressions in Eq. (4.32) are achieved. The values in Eq. (4.32) will ensure stability of system (4.31) and system (4.29) will be stable as a result of Lyapunov indirect method, and hence, proves the proposition. \square

For the analysis of Assumption 4.1, we have:

$$(\bar{m}_{22}^{-1} + \gamma_2 \bar{m}_{11}^{-1}) = \frac{m_{11} - \gamma_2 m_{12}}{m_{11} m_{22} - m_{12}^2} \quad (4.36)$$

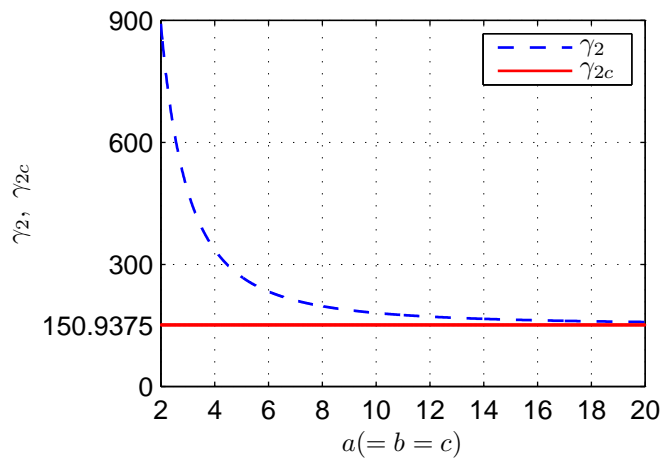


FIGURE 4.1: IWP - variation of γ_2 in Eq. (4.38) with design constants a , b , c , and its lower limit γ_{2c} , in Eq. (4.37).

It can assume value 0 at:

$$\gamma_{2c} = \frac{m_{11}}{m_{12}} = 150.9375 \quad (4.37)$$

To fulfill Assumption 4.1, using a combination of a , b , and c that results in $\gamma_2 = \gamma_{2c}$ must be avoided by the designer. In fact, γ_{2c} is the minimum value of γ_2 . Equation (4.32b) can be written as:

$$\gamma_2 = \gamma_{2c} + \frac{(m_1 l_1 + m_2 L_1)g}{(b^2 + c^2 + 2ab)I_2} \quad (4.38)$$

This shows that γ_2 can assume its minimum value γ_{2c} if and only if one of the design constants a , b , and c is infinite. Figure 4.1 graphically shows this fact. However, infinite values of a , b , and c are not allowed by the design. For the selected values of $a = 10$, $b = 5$, and $c = 5$, we have $\gamma_2 = 229.9500$, and hence Assumption 4.1 is valid.

Figures 4.2 and 4.3 show simulation results for the IWP with SMC law (4.12) in the presence of both matched and unmatched external disturbance, and parametric variations. Figure 4.4 shows how the unmatched and matched disturbances $d_1(t)$, $d_2(t)$ affect the unactuated configuration q_1 and actuated configuration q_2 through their contributions $\bar{d}_1(t)$, $\bar{d}_2(t)$. These results are discussed in the next section in detail.

4.2.2.2 Performance Analysis of The IWP

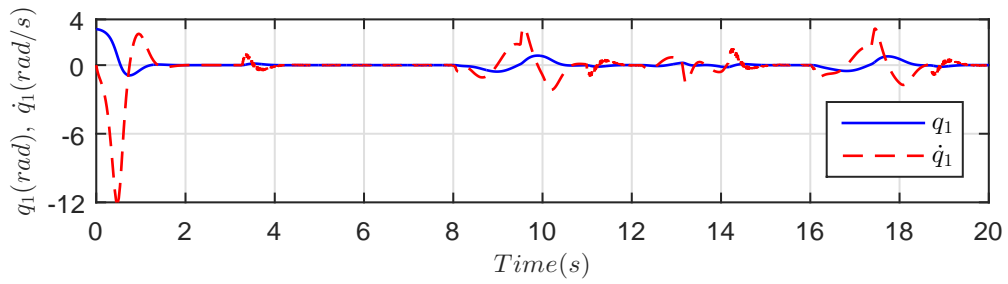
Figures 4.2 and 4.3 show closed loop response of the IWP with SMC law (4.12) in the presence of external disturbance and parametric variations. The controller gain are chosen as $\Gamma = 2000$ and the sliding parameters as $a = 10$, $b = 5$, $c = 5$. Parametric variations is chosen as 25% decrease from $t = 4$ (s) to $t = 6$ (s) and 25% increase from $t = 6$ (s) to $t = 8$ (s). The unmatched disturbance $d_1(t) = 0.2 \sin(\pi t)$ and the matched disturbance $d_2(t) = 0.2 \sin(\pi t)$ are applied to system at time intervals shown in Figures 4.2c and 4.3c.

The controller successfully stabilizes the IWP from its downward stable equilibrium position $q_1 = \pi$ to the upward unstable equilibrium position $q_1 = 0$ in 2 seconds. The Wheel comes to rest in less than 4 seconds. The results are in agreement with [14, 94, 167] with improved settling time. The overshoot in Wheel velocity is less than in [14, 94] but the peak control effort is high.

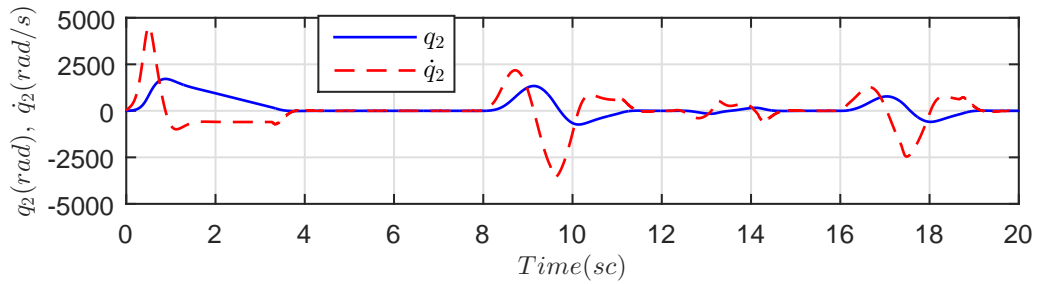
System response is robust to wide parametric variations. In Figure 4.2, $D_1 = D_2 = 0$ and hence both the disturbances, unmatched $d_1(t)$ and matched $d_2(t)$, affect system response. It is important to note that for IWP, in equilibrium, $\frac{1}{(\bar{m}_{22}^{-1} + \gamma_2 \bar{m}_{11}^{-1})} = -7.5906 \times 10^{-5}$, and hence the net effective discontinuous gain is $-7.5906 \times 10^{-5} * 2000 = 0.1518$. This is the reason that the controller attenuates the matched disturbance $d_2(t)$ with magnitude 0.2 but does not fully reject it. In Figure 4.3, $D_1 = D_2 = 0.2$ and hence the matched disturbance $d_2(t)$ is fully rejected but the unmatched disturbance $d_1(t)$ still affects system stability and dynamics inspite of the fact that the net effective discontinuous gain is now increased from 0.1518 to 0.9313, much higher than 0.2.

Equation (4.6) shows that both $d_1(t)$ and $d_2(t)$ affect the unactuated configuration variable q_1 and similarly both affect the actuated variable q_2 . Equation (4.7) shows that the contribution of matched disturbance $d_2(t)$ is the same and similar to the control u . On the other hand, the contribution of unmatched disturbance $d_1(t)$ is scaled to $-m_{22}m_{12}^{-1}d_1(t) = -1d_1(t)$ for the unactuated variable q_1 and scaled to $-m_{21}m_{11}^{-1}d_1(t) = -0.0066d_1(t)$ for the actuated variable q_2 . In Figure 4.2, $d_1(t)$ and $d_2(t)$ when combined, in the time interval $t = 16 - 18$ seconds, have less effect on dynamics, states and sliding variable, than $d_1(t)$ alone, in the time interval

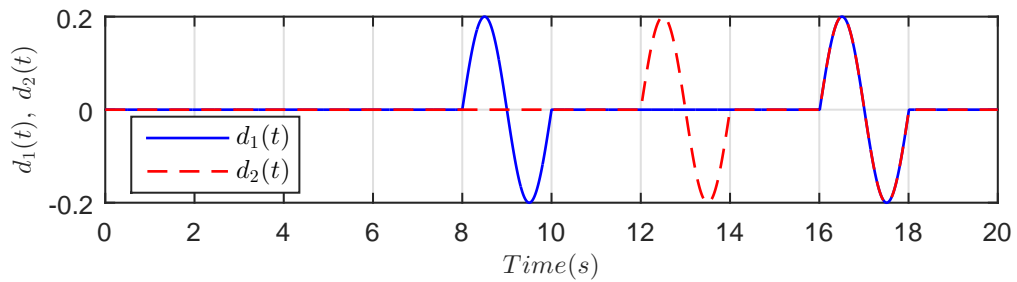
$t = 8 - 10$ seconds. This interesting and important observation is according to above mentioned reasoning i.e., $d_1(t)$ and $d_2(t)$ cancel each other ($\bar{d}_1 = 0$) for the unactuated variable q_1 . Figure 4.4 shows $d_1(t)$ and $d_2(t)$ and their effects $\bar{d}_1(t)$ and $\bar{d}_2(t)$ in accordance with the above observation.



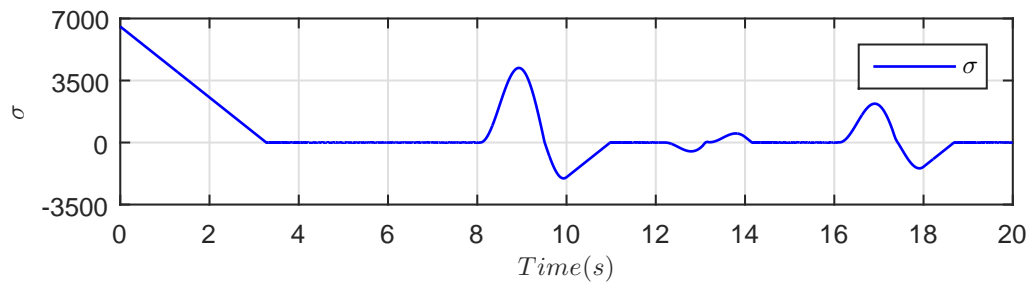
(A) Pendulum position q_1 (rad) and velocity \dot{q}_1 (rad/s)



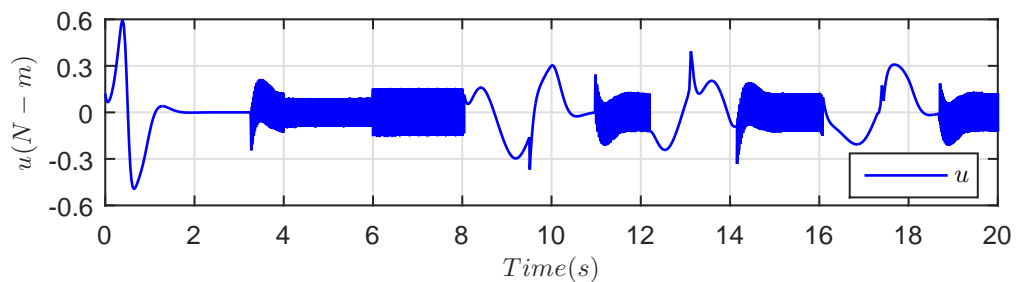
(B) Wheel position q_2 (rad) and velocity \dot{q}_2 (rad/s)



(C) Disturbance $d_1(t) = d_2(t) = 0.2 \sin(\pi t)$

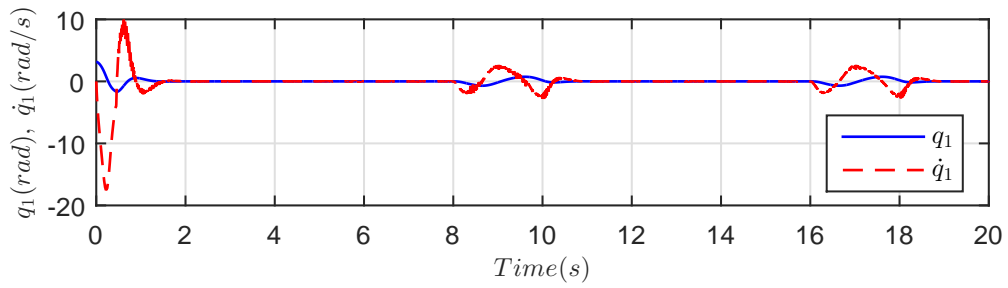


(D) Sliding surface σ

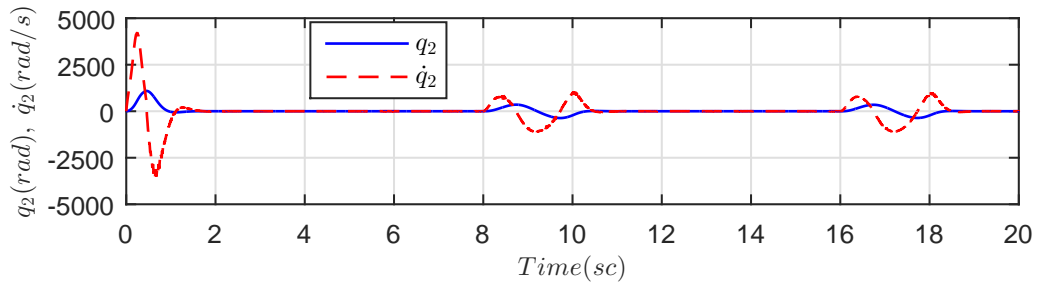


(E) Control effort u (N-m)

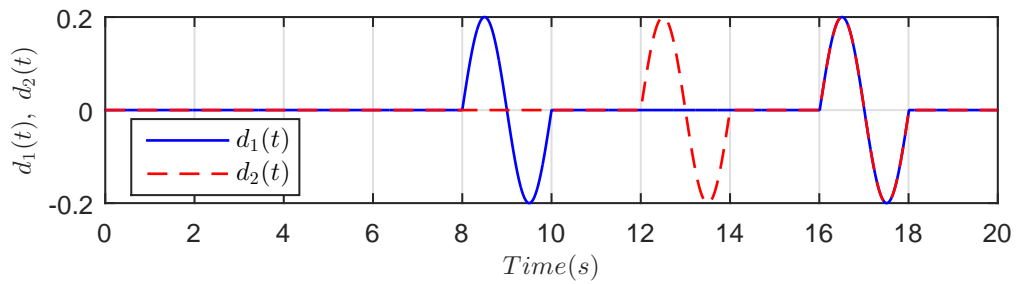
FIGURE 4.2: IWP - Closed loop response with SMC law (4.12) ($\Gamma = 2000.0$, $D_1 = 0$, $D_2 = 0$), $q(0) = [\pi, 0, 0, 0]^T$,



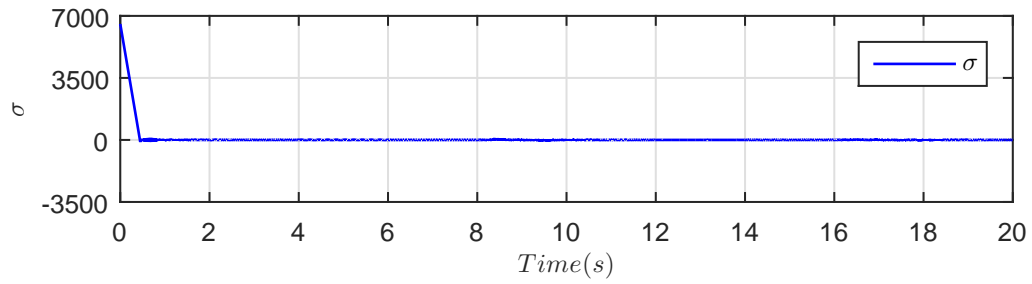
(A) Pendulum position q_1 (rad), velocity \dot{q}_1 (rad/s)



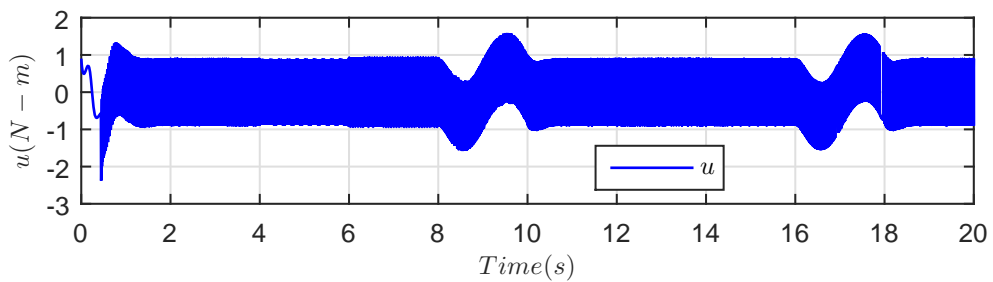
(B) Wheel position q_2 (rad) and velocity \dot{q}_2 (rad/s)



(C) Disturbance $d_1(t) = d_2(t) = 0.2 \sin(\pi t)$



(D) Sliding surface σ



(E) Control effort u (N-m)

FIGURE 4.3: IWP - Closed loop response with SMC law (4.12) ($\Gamma = 2000.0$, $D_1 = 0.2$, $D_2 = 0.2$), $q(0) = [\pi, 0, 0, 0]^T$,

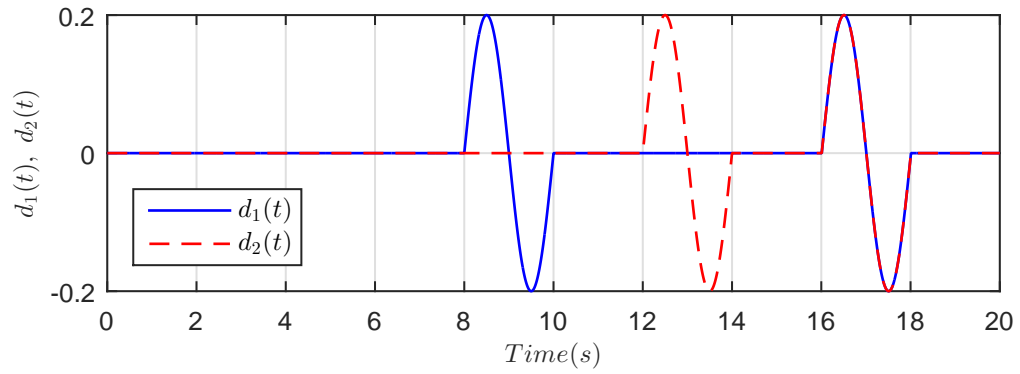
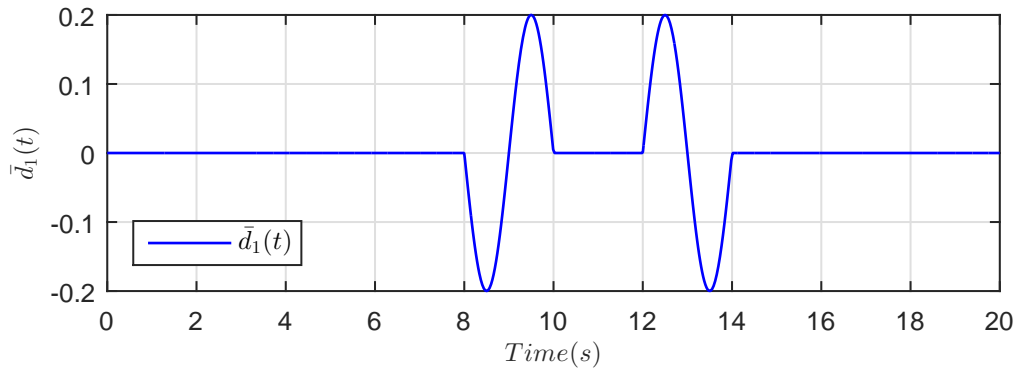
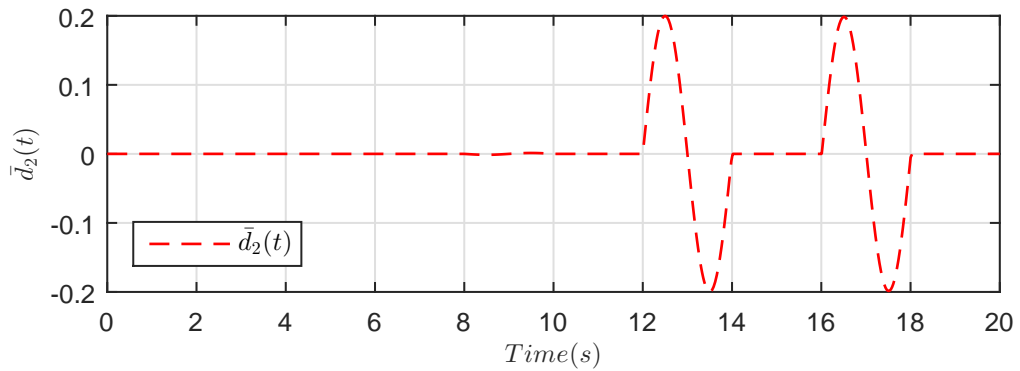
(A) Disturbances $d_1(t) = d_2(t) = 0.2 \sin(\pi t)$ (B) Effective disturbance $\bar{d}_1(t)$ as in (4.6)(C) Effective disturbance $\bar{d}_2(t)$ as in (4.6)

FIGURE 4.4: IWP - Unmatched and matched disturbances $d_1(t)$, $d_2(t)$ and effective disturbances $\bar{d}_1(t)$, $\bar{d}_2(t)$ on unactuated variable q_1 and actuated variable q_2 .

4.2.2.3 The TORA System

Figure 3.1b shows the TORA system [17]. The system has a translational oscillating platform of mass m_1 controlled via a rotational eccentric mass m_2 . The TORA system was originally studied as a simplified model of a dual-spin spacecraft to investigate the resonance capture phenomenon [165]. Later, the system was studied to investigate the practical usefulness of a rotational actuator for stabilizing translational motion [166]. The control problem, which is a benchmark for nonlinear control design [16], is to stabilize the oscillating platform translational displacement q_1 to zero via the rotational actuator. The TORA system is widely studied like backstepping [17, 94], passivity-based [18], output feedback stabilization and tracking [19–21], hybrid [22], sliding mode [76], dynamic surface control [167], output feedback stabilization and tracking [168], adaptive [169], Riccati equation method [23], LMI [24], and H_∞ [25]. In most works [17, 25, 76, 169], gravity term $g_2(q_1, q_2)$ is ignored that is retained in this work. Furthermore, in most works, non-dimensionalized equations of motion [17, 165] are used that, as pointed out in [24], makes difficult the comparison of different control strategies, especially, due to normalization of time t . For more discussion on this nonlinear benchmark problem, the interested reader can see Example 3.1 in Chapter 3 of this thesis.

Choose the physical parameters of the TORA system as specified in [16] and used in [24]:

$$m_1 = 1.3608 \text{ (kg)}, m_2 = 0.096 \text{ (kg)}, I_2 = 0.0002175 \text{ (kg.m}^2\text{)}, r = 0.0592 \text{ (m)}, \\ k = 186.3 \text{ (N.m}^{-1}\text{)}, \varepsilon = 0.200.$$

According to Lemma 4.6, the sliding mode dynamics in Eq. (4.23) for the TORA are:

$$\begin{aligned} \dot{\xi}_1 &= \xi_2 \\ \dot{\xi}_2 &= \frac{1}{m_{11} - m_{12}\gamma_2} \left(-m_{12}\gamma_1\gamma_3\xi_1 - m_{12}(\gamma_1\gamma_2 - \gamma_3)\xi_2 - m_{12}\gamma_1^2\xi_3 \right. \\ &\quad \left. + m_2r \sin(\xi_3 + q_{2des})(-\gamma_3\xi_1 - \gamma_2\xi_2 - \gamma_1\xi_3)^2 - k(\xi_1 + q_{1des}) + d_1 \right) \\ \dot{\xi}_3 &= -\gamma_3\xi_1 - \gamma_2\xi_2 - \gamma_1\xi_3 \end{aligned} \tag{4.39}$$

or

$$\dot{\boldsymbol{\xi}}(t) = \mathbf{f}_{\text{TORA}}(\boldsymbol{\xi}(t)) \quad (4.40)$$

Take the Jacobian linearization of (4.40) around the equilibrium $\boldsymbol{\xi} = [0, 0, 0]^T$ as:

$$\dot{\boldsymbol{\xi}}(t) = \mathbf{A}_{\text{TORA}}\boldsymbol{\xi}(t) \quad (4.41)$$

with $\mathbf{A}_{\text{TORA}} = \left. \frac{\partial \mathbf{f}_{\text{TORA}}}{\partial \boldsymbol{\xi}} \right|_{\boldsymbol{\xi}=\mathbf{0}}$ denoting the Jacobian matrix of \mathbf{f}_{TORA} w.r.t. $\boldsymbol{\xi}$ at $\boldsymbol{\xi} = \mathbf{0}$.

Proposition 4.8 below gives stability of the dynamics in Eq. (4.39).

Proposition 4.8. *Choosing the design parameters γ_1 , γ_2 , and γ_3 as below in Eq. (4.42), with a , b , c strictly positive, proves stability of (4.41) and stability of (4.39) is implied by Lyapunov indirect method.*

$$\gamma_1 = \frac{a(b^2 + c^2)}{b^2 + c^2 + 2ab} \quad (4.42a)$$

$$\gamma_2 = \frac{(b^2 + c^2 + 2ab)(m_1 + m_2) - k}{(b^2 + c^2 + 2ab)m_2r} \quad (4.42b)$$

$$\gamma_3 = \frac{a(b^2 + c^2)(m_1 + m_2) - (a + 2b)k}{(b^2 + c^2 + 2ab)m_2r} \quad (4.42c)$$

Proof. Linearizing system (4.39) for the stabilization of the TORA, $q_{1des} = 0$, $q_{2des} = 0$, we have:

$$\mathbf{A}_{\text{TORA}} = \begin{bmatrix} 0 & 1 & 0 \\ \frac{-m_2r\gamma_1\gamma_3 - k}{m_{11} - m_2r\gamma_2} & \frac{-m_2r(\gamma_1\gamma_2 - \gamma_3)}{m_{11} - m_2r\gamma_2} & \frac{-m_2r\gamma_1^2}{m_{11} - m_2r\gamma_2} \\ -\gamma_3 & -\gamma_2 & -\gamma_1 \end{bmatrix} \quad (4.43)$$

The rest of the proof is similar to Proposition 4.7 and is omitted here. \square

For the analysis of Assumption 4.1, we have:

$$(\bar{m}_{22}^{-1} + \gamma_2\bar{m}_{11}^{-1}) = \frac{m_1 + m_2 - \gamma_2m_2r \cos(q_2)}{(m_1 + m_2)(I_2 + m_2r^2) - (m_2r \cos(q_2))^2} \quad (4.44)$$

that assume the value 0 at:

$$q_{2c} = \cos^{-1} \left(\frac{m_1 + m_2}{\gamma_2 m_2 r} \right) = \cos^{-1} \left(\frac{256.3345}{\gamma_2} \right) \quad (4.45)$$

Eq. (4.45) shows that q_{2c} depends on the design constants a , b , c through the design parameter γ_2 in Eq. (4.42b). Equation (4.45) has no solution for $\gamma_2 < |256.3345|$ and the designer must use this range. γ_2 can have both positive and negative values, and, in fact, $\left(\frac{m_1 + m_2}{m_2 r} \right) = 256.3345$ is the maximum positive value of γ_2 . Equation (4.42b) can be written as:

$$\gamma_2 = \left(\frac{m_1 + m_2}{m_2 r} \right) - \frac{k}{(b^2 + c^2 + 2ab)m_2 e} \quad (4.46)$$

which shows that γ_2 can assume the value 256.3345 if and only if one of the constants a , b , c , is infinite, which is not allowed by design. Figure 4.5a graphically shows variation of γ_2 with constants a , c , taking $b = 1$. γ_2 cannot cross 256.3345 for finite value of a and c , it crosses -256.3345 at $a = c \approx 7$. For $a = c < 7$, $\gamma_2 > |256.3345|$ and Eq (4.45) has solution which is shown in Fig. 4.5b. For $a = c > 7$, $\gamma_2 < |256.3345|$ and Eq. (4.45) has no solution and Assumption 4.1 is satisfied. For the chosen constants $a = 12$, $b = 1$, and $c = 12$, $\gamma_2 = 62.3651$, and Eq. (4.45) has no solution and hence Assumption 4.1 is satisfied in this case. Figure 4.6 shows open loop response of the TORA. Figures 4.7 and 4.8 show closed loop response with SMC law (4.12) in the presence of parametric variations and disturbance. Figure 4.9 shows how the unmatched and matched disturbances $d_1(t)$, $d_2(t)$ affect the unactuated variable q_1 and actuated variable q_2 through their contributions $\bar{d}_1(t)$, $\bar{d}_2(t)$. These results are discussed in the next section in detail.

4.2.2.4 Performance Analysis of The TORA System

Figure 4.6 shows open loop response of the TORA system that is bounded but unstable. Figures 4.7 and 4.8 show closed loop response of the TORA system with SMC law (4.12) in the presence of external disturbance and parametric variations.

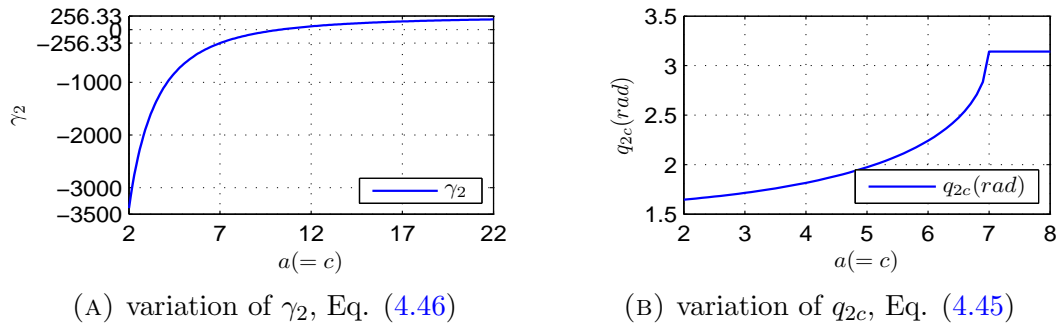


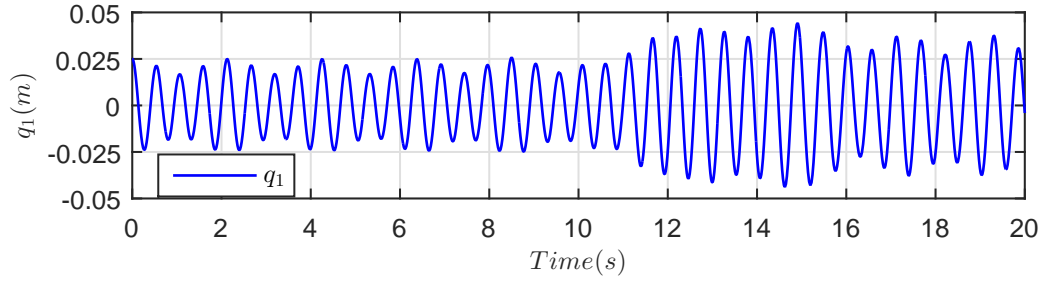
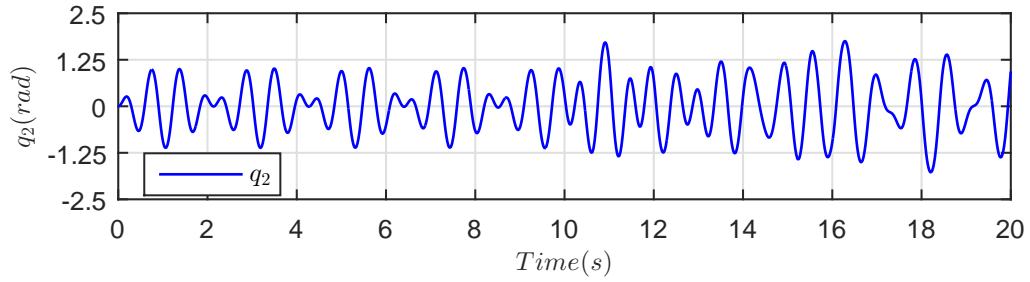
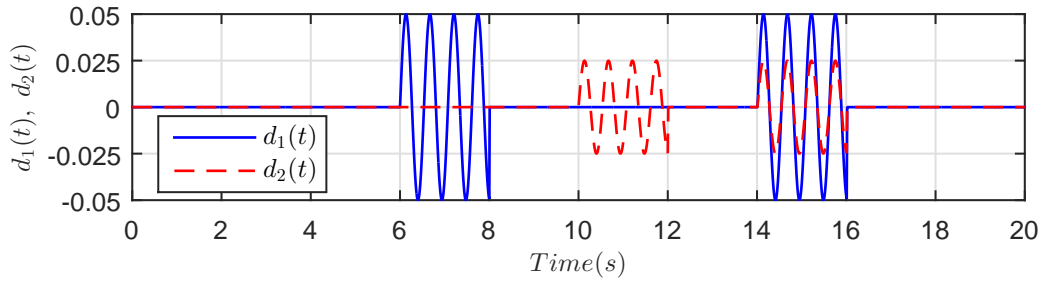
FIGURE 4.5: TORA - variation of γ_2 (a) and q_{2c} (b) with design constants a and c , taking $b = 1$.

The controller gain is chosen as $\Gamma = 1$ and the sliding parameters as $a = 12$, $b = 1$, $c = 12$. Parametric variations is chosen as 25% decrease from $t = 4$ (s) to $t = 5$ (s) and 25% increase from $t = 5$ (s) to $t = 6$ (s). The unmatched disturbance $d_1(t) = 0.05 \sin\left(\sqrt{\frac{k}{m_1}}t\right)$ and the matched disturbance $d_2(t) = 0.025 \sin\left(\sqrt{\frac{k}{m_1}}t\right)$ are applied to system at time intervals shown in Figures 4.7c and 4.8c.

The controller successfully stabilizes the TORA system in less than 5 seconds that is an improvement to most works such as [24]. The nonlinear benchmark specifications [16] are met, i.e., the closed loop system is stable and the control effort is less than 0.05 N-m (specifications states less than 0.1 N-m continuous).

System response is robust to wide parametric variations. In Figure 4.7, $D_1 = D_2 = 0$ and hence both the disturbances, unmatched $d_1(t)$ and matched $d_2(t)$, affect system response. It is important to note that for the TORA system, in equilibrium, $\frac{1}{(\bar{m}_{22}^{-1} + \gamma_2 \bar{m}_{11}^{-1})} = 7.0275 \times 10^{-4}$, and hence the net effective discontinuous gain is $7.0275 \times 10^{-4} * 1 = 7.0275 \times 10^{-4}$. This is the reason that the controller does not fully reject the matched disturbance $d_2(t)$ with magnitude 0.025. In Figure 4.7, $D_1 = 0.05$, $D_2 = 0.025$ and hence the matched disturbance $d_2(t)$ is fully rejected but the unmatched disturbance $d_1(t)$ still affects system stability and dynamics inspite of the fact that the net effective discontinuous gain is now increased from 7.0275×10^{-4} to 0.02701, higher than 0.025.

Equation (4.6) shows that both $d_1(t)$ and $d_2(t)$ affect the unactuated configuration variable q_1 and similarly both affect the actuated variable q_2 . Equation (4.7) shows that the contribution of matched disturbance $d_2(t)$ is the same and similar to the control u . On the other hand, the contribution of unmatched disturbance $d_1(t)$ is

(A) Oscillator position q_1 (m)(B) Pendulum position q_2 (rad)(C) Disturbance $d_1(t) = 0.05 \sin\left(\sqrt{\frac{k}{m_1}}t\right)$, $d_2(t) = 0.025 \sin\left(\sqrt{\frac{k}{m_1}}t\right)$ FIGURE 4.6: TORA - Open loop response to $q(0) = [0.025, 0, 0, 0]^T$ in the presence of disturbance.

scaled to $-m_{22}m_{12}^{-1}d_1(t) = -0.1016d_1(t)$ for the unactuated variable q_1 and scaled to $-m_{21}m_{11}^{-1}d_1(t) = -0.0037d_1(t)$ for the actuated variable q_2 . Figure 4.9 shows this scaling of $d_1(t)$ and $d_2(t)$ into $\bar{d}_1(t)$ and $\bar{d}_2(t)$. Figure 4.9b shows how $d_1(t)$, from $t = 6 - 8$ seconds, is scaled down from 0.05 to 0.005 in $\bar{d}_1(t)$ and to 0.000185 in $\bar{d}_2(t)$ in Figure 4.9c and hence have less effects on dynamics even if unmatched and also higher than $d_2(t)$.

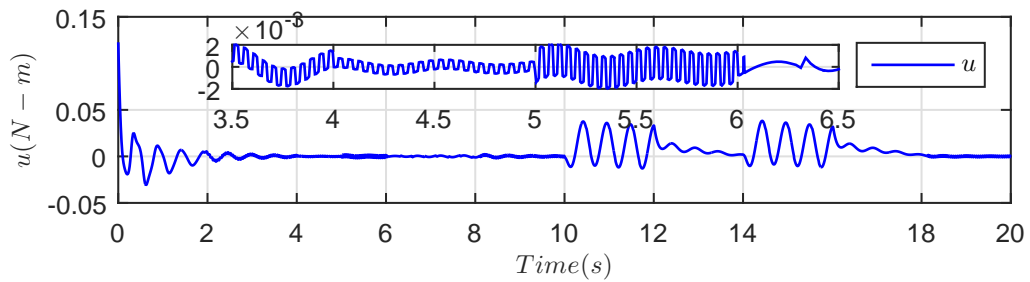
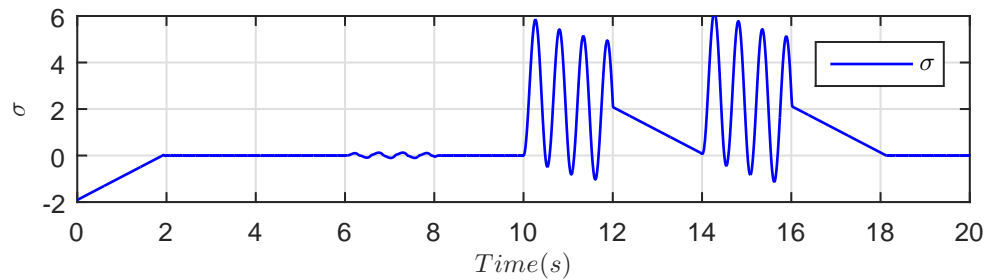
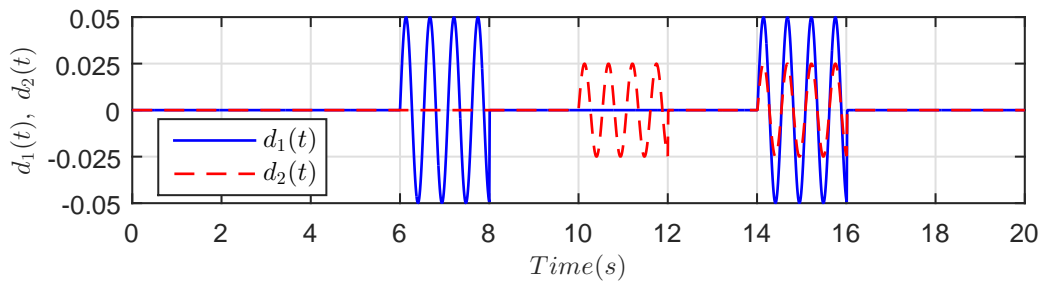
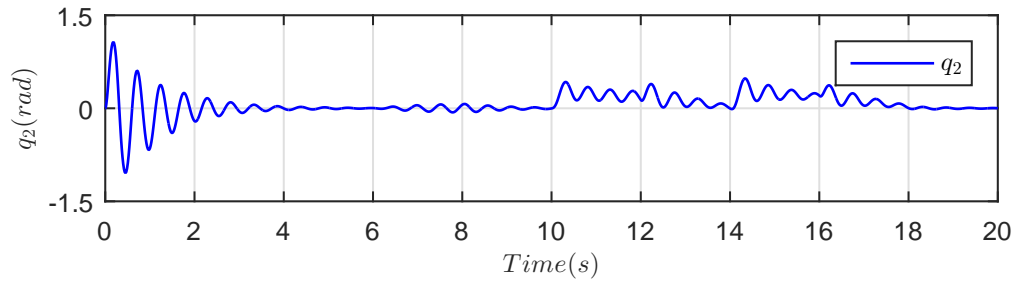
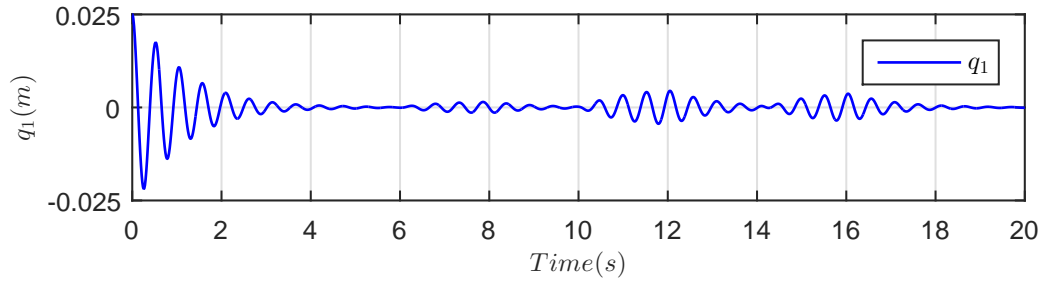
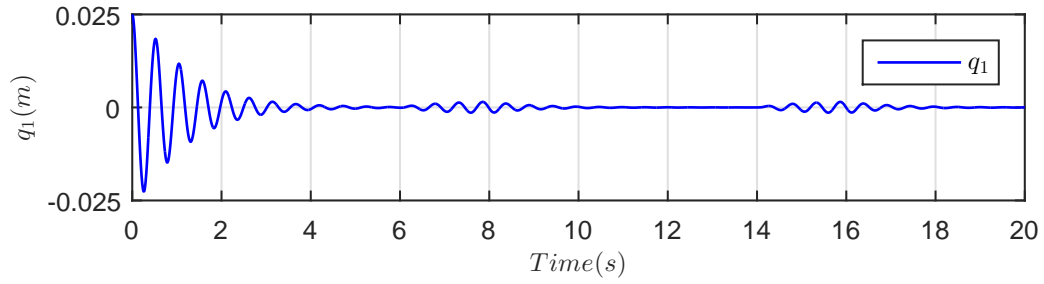
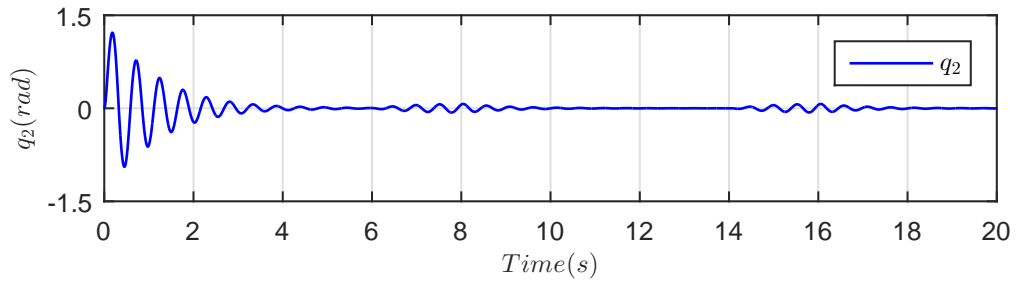


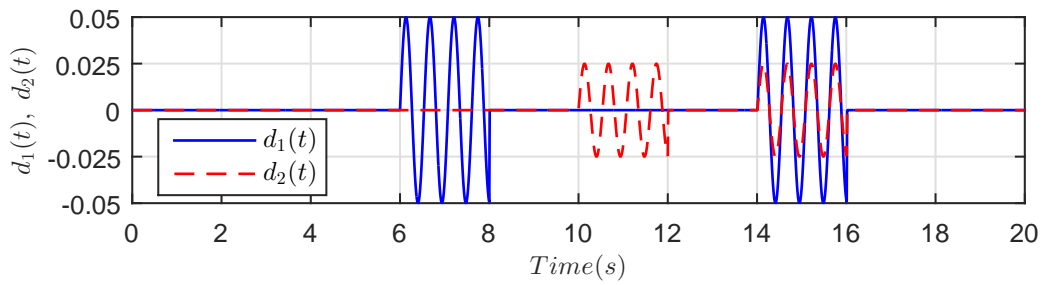
FIGURE 4.7: TORA - Closed loop response with SMC law (4.12) ($\Gamma = 1.0$, $D_1 = 0$, $D_2 = 0$), $q(0) = [0.025, 0, 0, 0]^T$



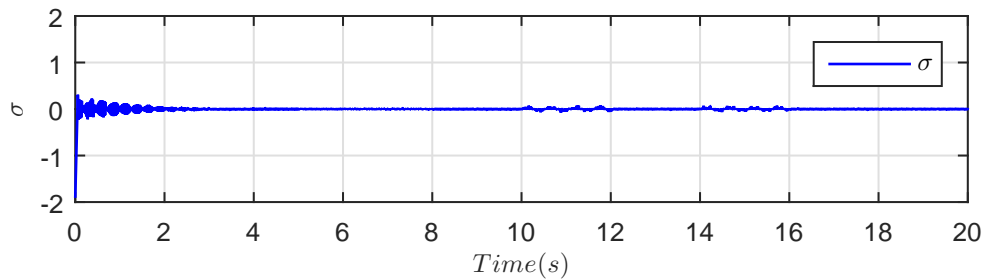
(A) Oscillator position q_1 (m)



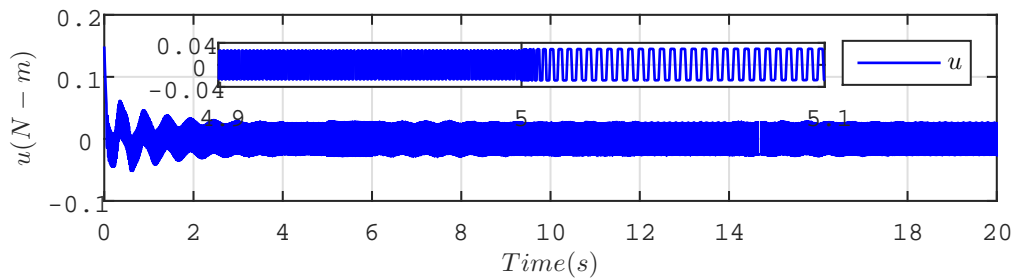
(B) Pendulum position q_2 (rad)



(C) Disturbance $d_1(t) = 0.05 \sin\left(\sqrt{\frac{k}{m_1}}t\right)$, $d_2(t) = 0.025 \sin\left(\sqrt{\frac{k}{m_1}}t\right)$

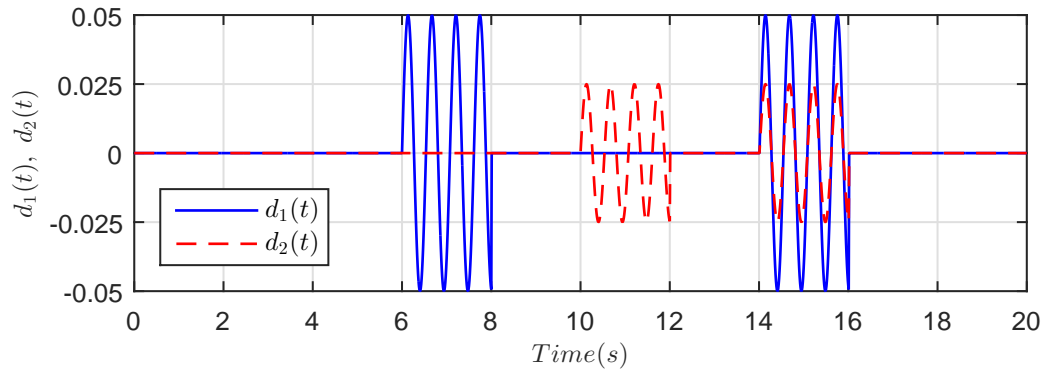


(D) Sliding surface σ

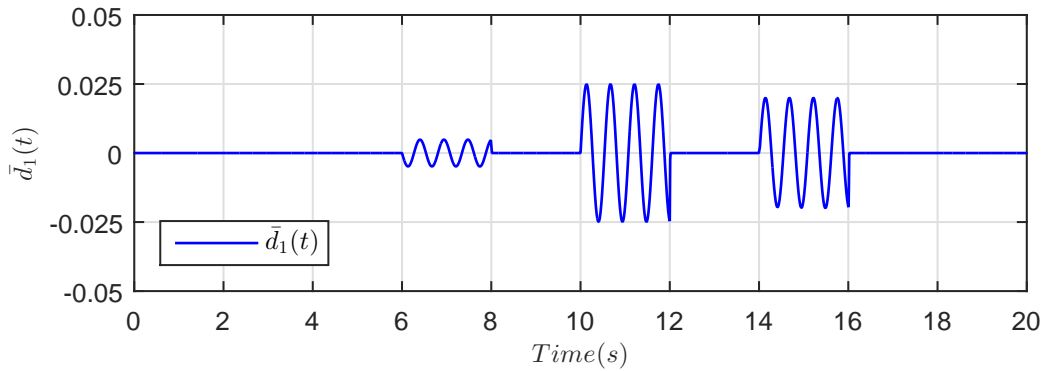


(E) Control effort u (N-m)

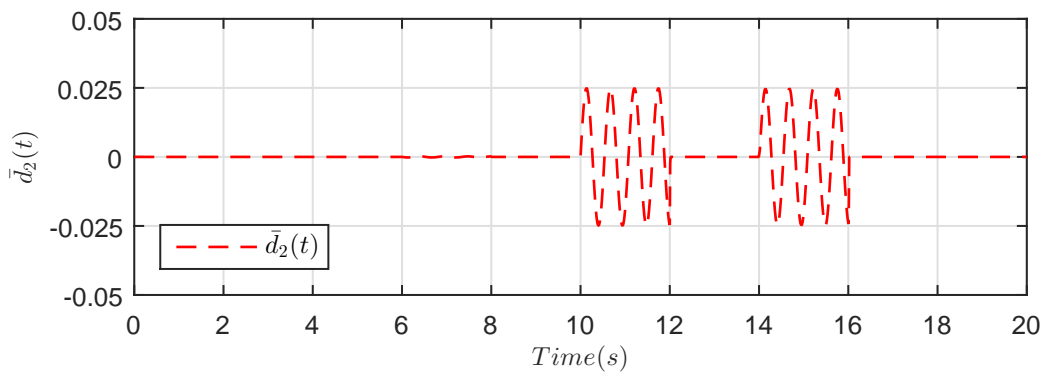
FIGURE 4.8: TORA - Closed loop response with SMC law (4.12) ($\Gamma = 1.0$, $D_1 = 0.05$, $D_2 = 0.025$), $q(0) = [0.025, 0, 0, 0]^T$



(A) Disturbances $d_1(t) = 0.05 \sin\left(\sqrt{\frac{k}{m_1}}t\right)$, $d_2(t) = 0.025 \sin\left(\sqrt{\frac{k}{m_1}}t\right)$



(B) Effective disturbance $\bar{d}_1(t)$ as in (4.6)



(C) Effective disturbance $\bar{d}_2(t)$ as in (4.6)

FIGURE 4.9: TORA - Unmatched and matched disturbances $d_1(t)$, $d_2(t)$ and the effective disturbances $\bar{d}_1(t)$, $\bar{d}_2(t)$ on unactuated variable q_1 and actuated variable q_2 .

4.3 Standard SMC Design for Class-II Underactuated Mechanical Systems

Consider Class-II underactuated mechanical systems represented by Eq. (4.4) with $n = 2$, $m = 1$. as:

$$m_{11}\ddot{q}_1 + m_{12}\ddot{q}_2 + c_1 + g_1 = u + d_1 \quad (4.47a)$$

$$m_{21}\ddot{q}_1 + m_{22}\ddot{q}_2 + c_2 + g_2 = d_2 \quad (4.47b)$$

Write (4.47) as

$$\bar{m}_{11}\ddot{q}_1 + \bar{c}_1 + \bar{g}_1 = u + \bar{d}_1 \quad (4.48a)$$

$$\bar{m}_{22}\ddot{q}_2 + \bar{c}_2 + \bar{g}_2 = u + \bar{d}_2 \quad (4.48b)$$

with the following definitions:

$$\begin{aligned} \bar{m}_{11}(q) &= m_{11} - m_{12}m_{22}^{-1}m_{21} \\ \bar{c}_1(q, \dot{q}) &= c_1 - m_{12}m_{22}^{-1}c_2 \\ \bar{g}_1(q) &= g_1 - m_{12}m_{22}^{-1}g_2 \\ \bar{d}_1(q) &= d_1 - m_{12}m_{22}^{-1}d_2 \\ \bar{m}_{22}(q) &= m_{12} - m_{11}m_{21}^{-1}m_{22} \\ \bar{c}_2(q, \dot{q}) &= c_1 - m_{11}m_{21}^{-1}c_2 \\ \bar{g}_2(q) &= g_1 - m_{11}m_{21}^{-1}g_2 \\ \bar{d}_2(q) &= d_1 - m_{11}m_{21}^{-1}d_2 \end{aligned} \quad (4.49)$$

Using $x = [x_1, x_2, x_3, x_4]^T = q = [q_1, \dot{q}_1, q_2, \dot{q}_2]^T$, we achieve the state space representation of (4.47) as:

$$\dot{x}_1 = x_2 \quad (4.50a)$$

$$\dot{x}_2 = f_1(x) + b_1(x)(u + \bar{d}_1) \quad (4.50b)$$

$$\dot{x}_3 = x_4 \quad (4.50c)$$

$$\dot{x}_4 = f_2(x) + b_2(x)(u + \bar{d}_1) \quad (4.50d)$$

where

$$\begin{aligned} f_1(x) &= -\bar{m}_{11}^{-1}(\bar{c}_1 + \bar{g}_1) \\ b_1(x) &= \bar{m}_{11}^{-1} \\ \bar{d}_1(q) &= d_1 - m_{12}m_{22}^{-1}d_2 \\ f_2(x) &= -\bar{m}_{22}^{-1}(\bar{c}_2 + \bar{g}_2) \\ b_2(x) &= \bar{m}_{22}^{-1} \\ \bar{d}_2(q) &= d_1 - m_{11}m_{21}^{-1}d_2 \end{aligned} \quad (4.51)$$

are the nonlinear nominal functions.

It is important to note that in the state space representation (4.50) of the underactuated mechanical system (4.47), both the disturbances, d_2 and d_1 , appear in the same equation in which the control u appears. The appearance of (4.8) may tempt a designer to achieve robustness for both the disturbances by designing sliding mode control. But this not the case. Both the disturbances, d_2 and d_1 , affect both the actuated (q_1) and unactuated (q_2) dynamics through coupling similar to the control u . Disturbance d_1 appears as it for both the dynamics and d_2 is scaled to $m_{12}m_{22}^{-1}d_2$ for the actuated dynamism and scaled to $m_{11}m_{21}^{-1}d_2$ for the unactuated dynamics. Depending upon the value of this scaling the bad effects of d_2 may made further bad, may be reduced or d_1 and d_2 may cancel each other. This is scenario is special characteristic of underactuated mechanical systems not analyzed or discussed before to best of our knowledge. This issue will be discussed at length for the application examples later in this chapter.

4.3.1 Control Law Design

To design the standard SMC law for Class-II systems (4.47), define the actuated and unactuated control errors as follows:

$$e_1 = q_1 - q_{1des} \quad (4.52a)$$

$$e_2 = q_2 - q_{2des} \quad (4.52b)$$

Next define the sliding variable σ as below:

$$\sigma = \dot{e}_2 + \gamma_1 e_2 + \gamma_2 \dot{e}_1 + \gamma_3 e_1 \quad (4.53)$$

where γ_1 , γ_2 , and γ_3 are design parameters.

Consider the following assumptions holds.

Assumption 4.3. $(\bar{m}_{22}^{-1} + \gamma_2 \bar{m}_{11}^{-1}) \neq 0$.

Assumption 4.4. The uncertainties are bounded as $|d_1(q, \dot{q}, t)| \leq D_1$, $|d_2(q, \dot{q}, t)| \leq D_2$.

Now the standard SMC law for Class-II systems (4.47) is given by the following theorem.

Theorem 4.9. *The following standard SMC law*

$$\begin{aligned} u = & \frac{1}{(\bar{m}_{22}^{-1} + \gamma_2 \bar{m}_{11}^{-1})} \left(\bar{m}_{22}^{-1} (\bar{c}_2 + \bar{g}_2) + \gamma_2 \bar{m}_{11}^{-1} (\bar{c}_1 + \bar{g}_1) - (\gamma_3 \dot{q}_1 + \gamma_1 \dot{q}_2) \right. \\ & - |(\bar{m}_{22}^{-1} + \gamma_2 \bar{m}_{11}^{-1})| D_1 \text{sign}(\sigma) \\ & \left. - |(\bar{m}_{22}^{-1} m_{21} m_{11}^{-1} + \gamma_2 \bar{m}_{11}^{-1} m_{22} m_{12}^{-1})| D_2 \text{sign}(\sigma) - \Gamma \text{sign}(\sigma) \right) \end{aligned} \quad (4.54)$$

with positive design constant Γ , will enforce sliding mode in the manifold in (4.53) along the dynamics (4.47).

Proof. The proof is similar to the proof of Theorem 4.5 and is omitted here. \square

Lemma 4.10. *Upon the the establishment of sliding mode in system (4.53) along the dynamics of (4.47), accordance with Theorem 4.9, the sliding mode dynamics*

of Class-II systems (4.47) are:

$$\begin{aligned}\dot{\xi}_1 &= \xi_2 \\ \dot{\xi}_2 &= \frac{1}{m_{21} - m_{22}\gamma_2} (-m_{22}\gamma_1\gamma_3\xi_1 - m_{22}(\gamma_1\gamma_2 - \gamma_3)\xi_2 - m_{22}\gamma_1^2\xi_3 - c_2 - g_2) \\ \dot{\xi}_3 &= -\gamma_3\xi_1 - \gamma_2\xi_2 - \gamma_1\xi_3\end{aligned}\tag{4.55}$$

where

$$\xi_1 = q_1 - q_{1des}\tag{4.56a}$$

$$\xi_2 = \dot{q}_1\tag{4.56b}$$

$$\xi_3 = q_2 - q_{2des}\tag{4.56c}$$

Proof. The proof is similar to the proof of Lemma 4.10 and is omitted here. \square

4.3.2 Application to Class-II Underactuated Mechanical Systems

The proposed control design framework is applied to Class-II underactuated mechanical systems of the Beam-and-Ball system, the Cart-Pole system, and the Overhead Crane.

4.3.2.1 The Beam-and-Ball System

Fig. 3.2e shows the Beam-and-Ball system. The actuator is at the Beam. The control problem for this system is to stabilize the Ball from any initial position q_{20} to any desired position, q_{2des} . The Beam-and-Ball system has been studied in numerous excellent research works, for example, [63–69, 72, 94, 172, 173].

For the Beam-and-Ball, chose the physical parameters according to [63, 64] as:

$$m = 0.05 \text{ (kg)}, I_1 = 0.02 \text{ (kg.m}^2\text{)}, I_2 = 2 \times 10^{-6} \text{ (kg.m}^2\text{)}, r = 0.01 \text{ (m)}, g = 9.8 \text{ (m.s}^{-2}\text{)}.$$

For the Euler-Lagrange equation of the Beam-and-Ball system in Eq. (4.47) we have:

$$\begin{aligned}
m_{11}(q_2) &= I_1 + m(q_2^2 + d^2) \\
m_{12}(q_2) &= -md \\
m_{21}(q_2) &= m_{12}(q_2) \\
m_{22}(q_2) &= m\left(1 + \frac{I_2}{mr^2}\right) \\
c_1(q, \dot{q}) &= 2m\dot{q}_1 q_2 \dot{q}_2 \\
c_2(q, \dot{q}) &= -mq_2 \dot{q}_1^2 \\
g_1(q_1, q_2) &= mg(q_2 \cos(q_1) - d \sin(q_1)) \\
g_2(q_1, q_2) &= mg \sin(q_1)
\end{aligned} \tag{4.57}$$

According to Lemma 4.10, the sliding mode dynamics in Eq. (4.55) for the Beam-and-Ball system are:

$$\begin{aligned}
\dot{\xi}_1 &= \xi_2 \\
\dot{\xi}_2 &= \frac{1}{m_{21} - m_{22}\gamma_2} \left(-m_{22}\gamma_1\gamma_3\xi_1 - m_{22}(\gamma_1\gamma_2 - \gamma_3)\xi_2 - m_{22}\gamma_1^2\xi_3 + m(\xi_3 + q_{2des})\xi_2^2 \right. \\
&\quad \left. - mg \sin(\xi_1 + q_{1des})\xi_2^2 \right) \\
\dot{\xi}_3 &= -\gamma_3\xi_1 - \gamma_2\xi_2 - \gamma_1\xi_3
\end{aligned} \tag{4.58}$$

or

$$\dot{\boldsymbol{\xi}}(t) = \mathbf{f}_{\text{BB}}(\boldsymbol{\xi}(t)) \tag{4.59}$$

Take the Jacobian linearization of (4.59) around the equilibrium $\boldsymbol{\xi} = [0, 0, 0]^T$ as:

$$\dot{\boldsymbol{\xi}}(t) = \mathbf{A}_{\text{BB}}\boldsymbol{\xi}(t) \tag{4.60}$$

with $\mathbf{A}_{\text{BB}} = \left. \frac{\partial \mathbf{f}_{\text{BB}}}{\partial \boldsymbol{\xi}} \right|_{\boldsymbol{\xi}=\mathbf{0}}$ denoting the Jacobian matrix of \mathbf{f}_{BB} w.r.t. $\boldsymbol{\xi}$ at $\boldsymbol{\xi} = \mathbf{0}$.

Proposition 4.11 below gives stability of the dynamics (4.58).

Proposition 4.11. *Choosing the the design parameters γ_1 , γ_2 , and γ_3 as below in Eq. (4.61), with a , b , c strictly positive, proves stability of Eq. (4.60) and stability*

of (4.58) is implied by Lyapunov indirect method.

$$\gamma_1 = \frac{a(b^2 + c^2)}{b^2 + c^2 + 2ab} \quad (4.61a)$$

$$\gamma_2 = \frac{-(b^2 + c^2 + 2ab)md - mg}{(b^2 + c^2 + 2ab)(m + I_2/r^2)} \quad (4.61b)$$

$$\gamma_3 = \frac{-a(b^2 + c^2)md - (a + 2b)mg}{(b^2 + c^2 + 2ab)(m + I_2/r^2)} \quad (4.61c)$$

Proof. Linearizing system (4.58) for the stabilization of the Beam-and-Ball, $q_{1des} = 0$, $q_{2des} = 0$, we have:

$$\mathbf{A}_{BB} = \begin{bmatrix} 0 & 1 & 0 \\ \frac{-m_{22}\gamma_1\gamma_3 - mg}{m_{21} - m_{22}\gamma_2} & \frac{-m_{22}(\gamma_1\gamma_2 - \gamma_3)}{m_{21} - m_{22}\gamma_2} & \frac{-m_{22}\gamma_1^2}{m_{21} - m_{22}\gamma_2} \\ -\gamma_3 & -\gamma_2 & -\gamma_1 \end{bmatrix} \quad (4.62)$$

The rest of the proof is similar to Proposition 4.7 and is omitted here. \square

To check Assumption 4.3, we have:

$$(\bar{m}_{22}^{-1} + \gamma_2\bar{m}_{11}^{-1}) = \frac{d + \gamma_2 \left(1 + \frac{I_2}{mr^2}\right)}{(I_1 + m(q_2^2 + d^2)) \left(1 + \frac{I_2}{mr^2}\right) - md^2} \quad (4.63)$$

that becomes 0 at:

$$\gamma_{2c} = -\frac{d}{1 + \frac{I_2}{mr^2}} = -0.0071 \quad (4.64)$$

and hence, this value of γ_2 must be avoided by the designer. We can write Eq. (4.61b) as below:

$$\gamma_2 = \gamma_{2c} - \frac{g}{(b^2 + c^2 + 2ab)\left(1 + \frac{I_2}{mr^2}\right)} \quad (4.65)$$

that shows γ_2 achieves its maximum value γ_{2c} only when at least one of the design constants a , b , c is infinite, a choice not allowed by design. For the selected constants $a = b = 1, c = 0.5$, we have $\gamma_2 = -2.1610$, and hence Assumption 4.3 is also satisfied. Figures 4.10 and 4.11 show closed loop response of the Beam-and-Ball system with SMC law (4.54) for comparison with [63, 64]. Figures 4.12 and 4.14 show closed loop response in the presence of parametric variations and disturbance. Figure 4.15 shows how the matched and unmatched disturbances

$d_1(t)$, $d_2(t)$ affect the actuated variable q_1 and the unactuated variable q_2 through their contributions $\bar{d}_1(t)$, $\bar{d}_2(t)$. Figure 4.16 shows tracking response of the Beam-and-Ball system for a desired signal with SMC law (4.54). These results are discussed in the next section in detail.

4.3.2.2 Performance Analysis of The Beam-and-Ball System

Figures 4.10 and 4.16 show closed loop response of the Beam-and-Ball system with SMC law (4.54). The sliding parameters are chosen as $a = 1$, $b = 1$, $c = 0.5$. The controller gain is $\Gamma = 5.0$ in Figures 4.10 and 4.11 and $\Gamma = 2.5$ in Figures 4.12 - 4.16. Parametric variations is chosen as 35% decrease from $t = 5(\text{s})$ to $t = 7(\text{s})$ and 35% increase from $t = 7(\text{s})$ to $t = 9(\text{s})$. The matched disturbance $d_1(t) = 0.5 \sin(\pi t)$ and the unmatched disturbance $d_2(t) = 0.25 \sin(\pi t)$ are applied to system at time intervals shown in Figures 4.12c-4.14c.

The initial conditions in Figures 4.10 and 4.11 are the same as in HOCSMC [64]. Comparing to [64], the settling time, the overshoots/undershoots in the Ball position are considerable improved. As shown in [64], for these initial conditions, the HOCSMC law based on [63] becomes unstable.

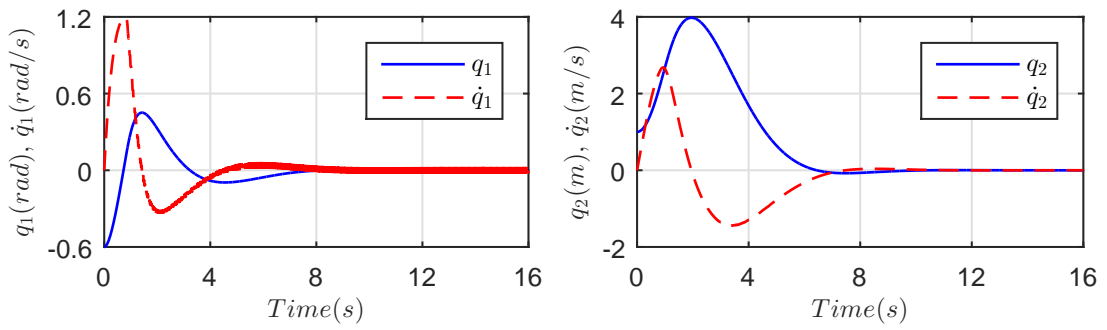
Figures 4.12-4.14 show closed loop response of the Beam-and-Ball system with SMC law (4.54) in the presence of parameter variations and external disturbance. The controller successfully stabilizes the Beam-and-Ball system in 10 seconds.

System response is robust to wide parametric variations. In Figure 4.12, $D_1 = D_2 = 0$ and hence both the disturbances, matched $d_1(t)$ and unmatched $d_2(t)$, affect system response. It is important to note that for Beam-and-Ball system, in equilibrium, $\frac{1}{(\bar{m}_{22}^{-1} + \gamma_2 \bar{m}_{11}^{-1})} = -0.0929$, and hence the net effective discontinuous gain is $-0.0929 * 2.5 = 0.02322$. This is the reason that the controller attenuates the matched disturbance $d_1(t)$ with magnitude 0.5 but does not fully reject it. In Figure 4.13, $D_1 = 0.5$, $D_2 = 0$, increasing the gain to 0.52322, and hence, the matched disturbance $d_1(t)$ is fully rejected but the unmatched disturbance $d_2(t)$ affects system stability and dynamics. In Figure 4.14, $D_1 = 0.5$, $D_2 = 0.025$ but still the unmatched disturbance $d_2(t)$ affects system stability and dynamics inspite

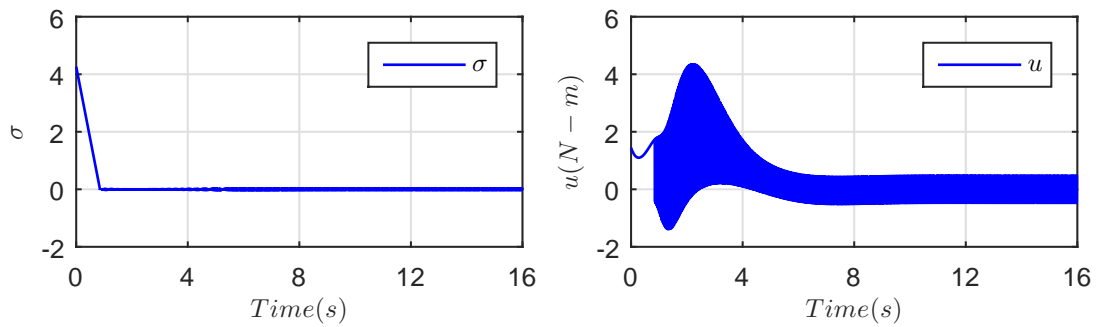
of the fact that the net effective discontinuous gain is now increased from 0.52322 to 4.03669, much higher than 0.25.

Equation (4.48) shows that both $d_1(t)$ and $d_2(t)$ affect the actuated configuration variable q_1 and similarly both affect the unactuated variable q_2 . Equation (4.49) shows that the contribution of matched disturbance $d_1(t)$ is the same and similar to the control u . On the other hand, the contribution of unmatched disturbance $d_2(t)$ is scaled to $-m_{12}m_{22}^{-1}d_2(t) = -0.0071d_2(t)$ for the actuated variable q_1 and scaled to $-m_{11}m_{21}^{-1}d_2(t) = -400.3837d_2(t)$ (0.25 to 100.1 in steady state) for the unactuated variable q_2 !. Since m_{11} depends on the square of the Ball position q_2 , ($m_{11}(q_2) = I_1 + m(q_2^2 + d^2)$), the contribution of $d_2(t)$ goes high and high when the disturbance affects the Ball position. Figure 4.15 shows $d_1(t)$ and $d_2(t)$ and their effects $\bar{d}_1(t)$ and $\bar{d}_2(t)$ in accordance with the above observation. Figure 4.15c shows how the negative peak of $\bar{d}_2(t)$ goes to -154.58 (instead of 100.1) due disturbed Ball position.

Figure 4.16 shows tracking response of the Beam-and-Ball system with SMC law (4.54). The Ball perfectly tracks the desired square wave signal of amplitude 5(m). The settling time is 6 seconds and the control effort is within range. The important and interesting observation here is that the system is more sensitive to matched disturbance when the Ball is at the center than when it is far away from the center.

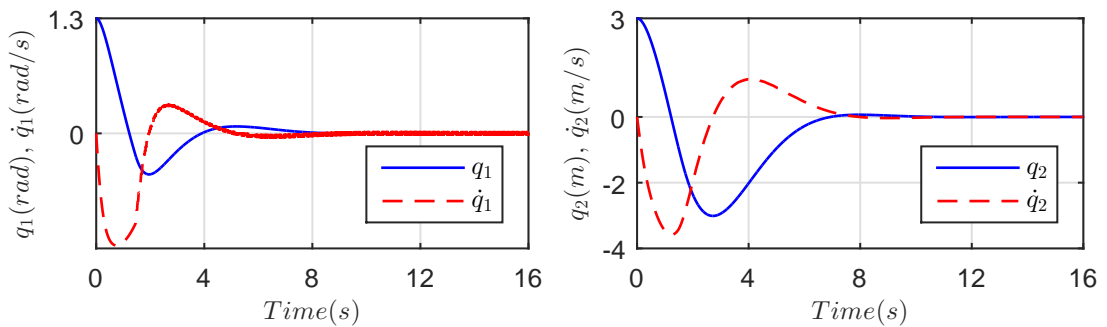


(A) Beam angle q_1 (rad), velocity \dot{q}_1 (rad/s) (B) Ball position q_2 (m), velocity \dot{q}_2 (m/s)

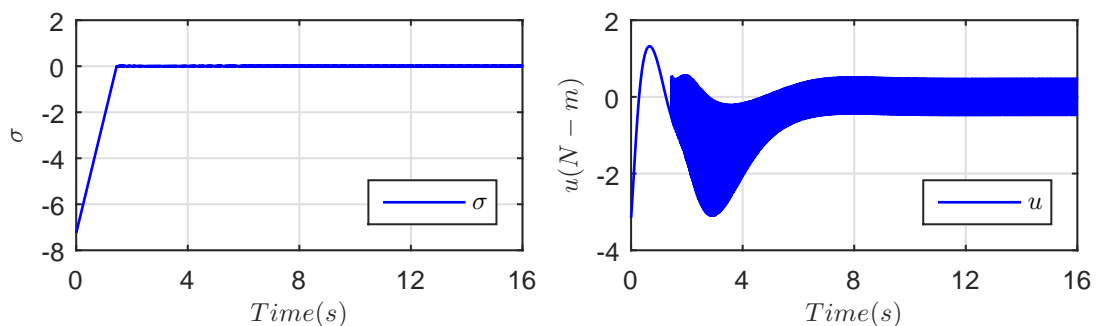


(C) Sliding surface σ (D) Control effort u (N-m)

FIGURE 4.10: The Beam-and-Ball - Closed loop response with SMC law (4.54) ($\Gamma = 5.0, D_1 = 0, D_2 = 0$), $q(0) = [-0.6, 0, 1.0, 0]^T$.



(A) Beam angle q_1 (rad), velocity \dot{q}_1 (rad/s) (B) Ball position q_2 (m), velocity \dot{q}_2 (m/s)



(C) Sliding surface σ (D) Control effort u (N-m)

FIGURE 4.11: The Beam-and-Ball - Closed loop response with SMC law (4.54) ($\Gamma = 5.0, D_1 = 0, D_2 = 0$), $q(0) = [1.3, 0, 3.0, 0]^T$.

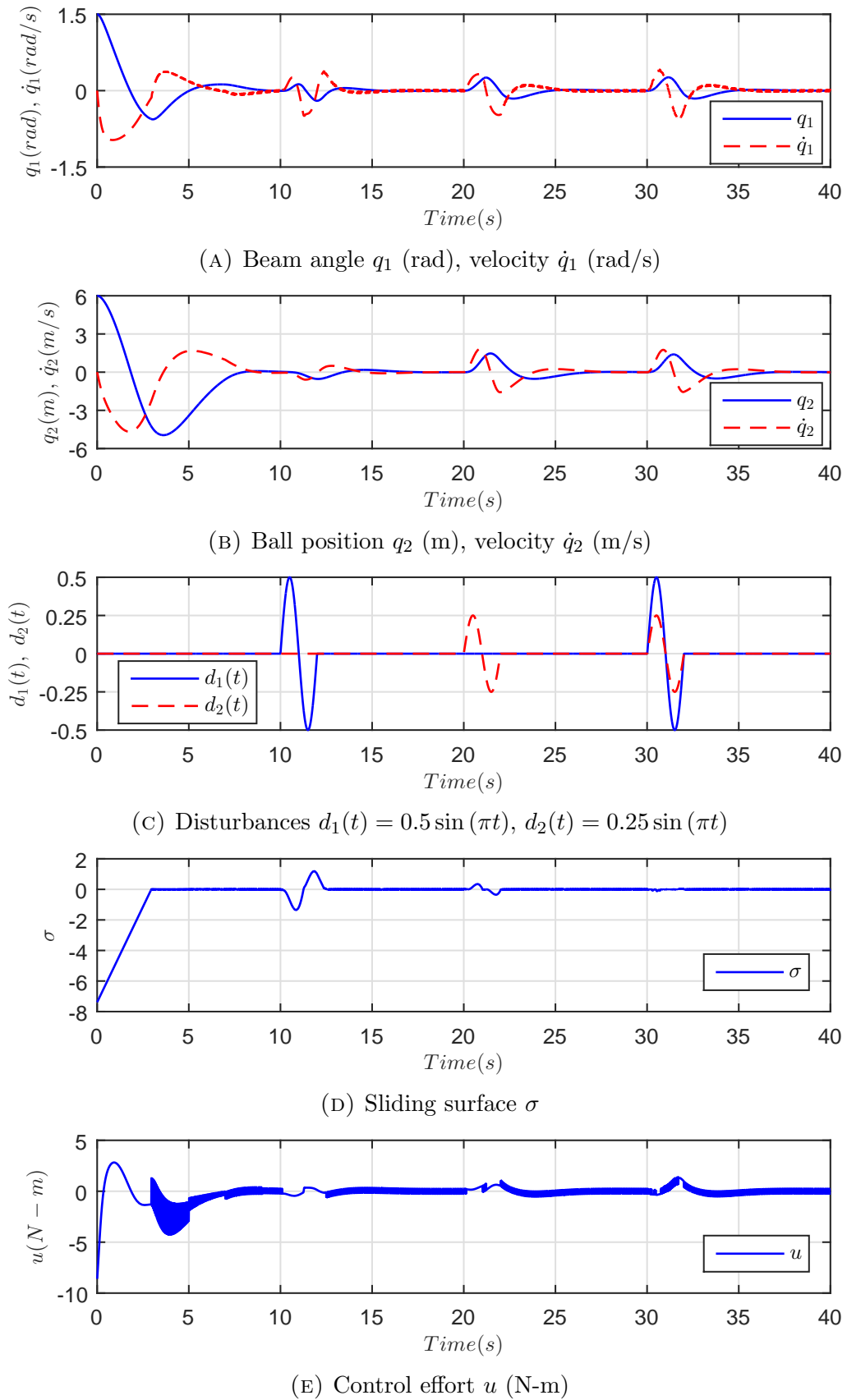
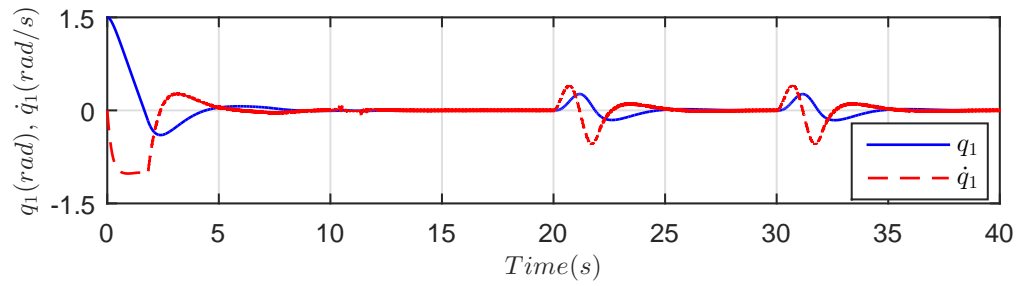
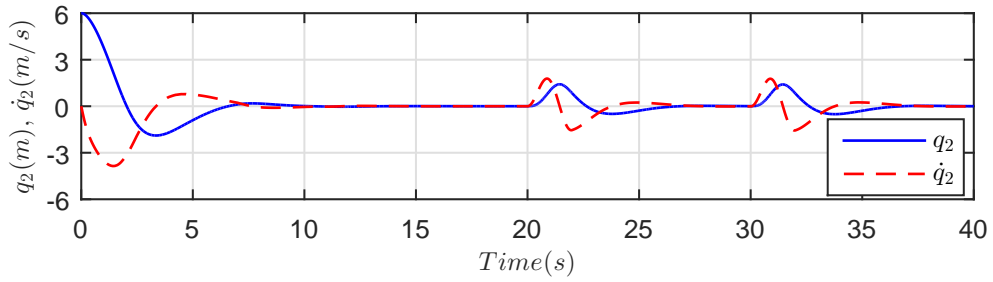


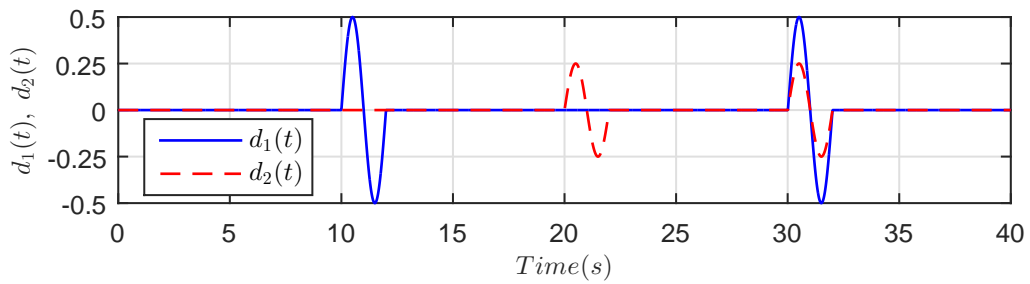
FIGURE 4.12: The Beam-and-Ball - Closed loop response with SMC law (4.54) ($\Gamma = 2.5.0$, $D_1 = 0$, $D_2 = 0$), $q(0) = [1.5, 0, 6.0, 0]^T$.



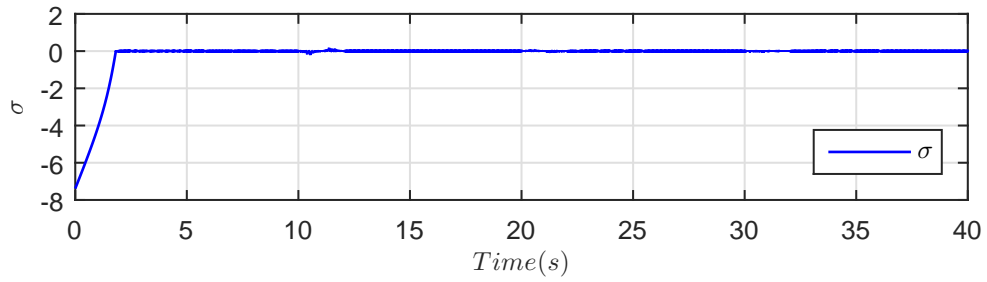
(A) Beam angle q_1 (rad), velocity \dot{q}_1 (rad/s)



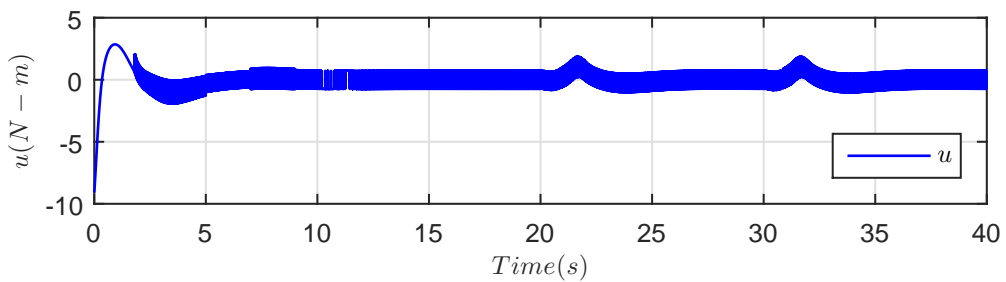
(B) Ball position q_2 (m), velocity \dot{q}_2 (m/s)



(C) Disturbances $d_1(t) = 0.5 \sin(\pi t)$, $d_2(t) = 0.25 \sin(\pi t)$

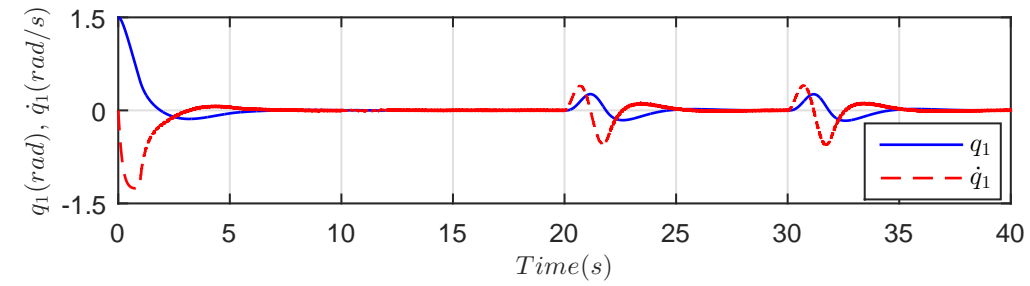


(D) Sliding surface σ

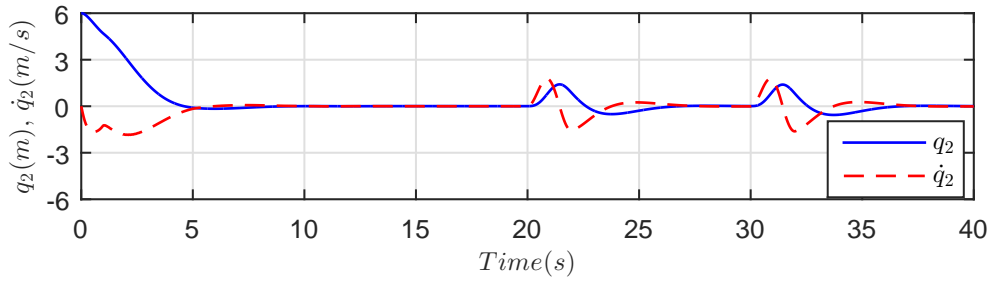


(E) Control effort u (N-m)

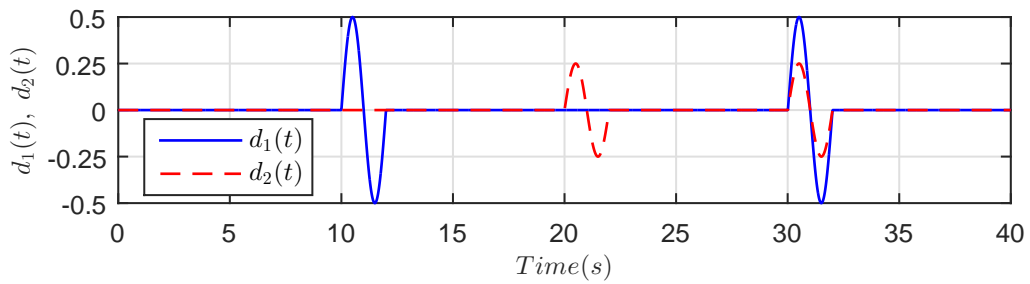
FIGURE 4.13: The Beam-and-Ball - Closed loop response with SMC law (4.54) ($\Gamma = 2.5.0$, $D_1 = 0.5$, $D_2 = 0$), $q(0) = [1.5, 0, 6.0, 0]^T$.



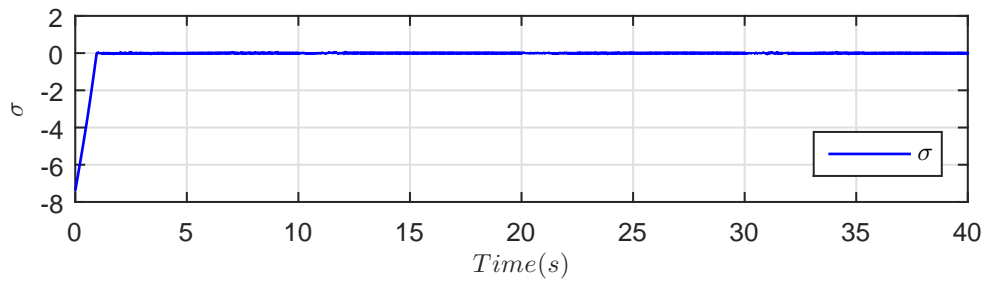
(A) Beam angle q_1 (rad), velocity \dot{q}_1 (rad/s)



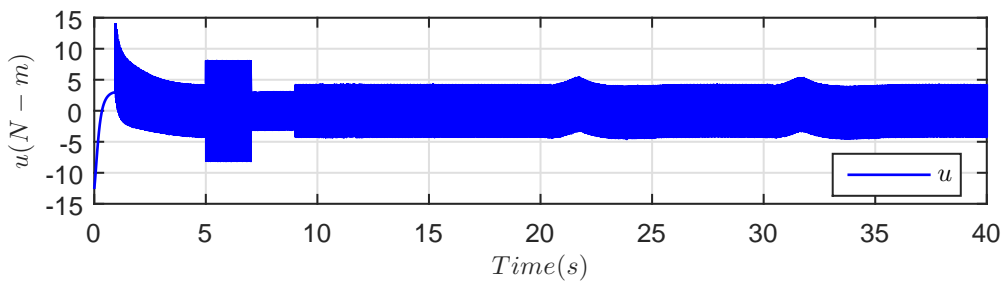
(B) Ball position q_2 (m), velocity \dot{q}_2 (m/s)



(C) Disturbances $d_1(t) = 0.5 \sin(\pi t)$, $d_2(t) = 0.25 \sin(\pi t)$

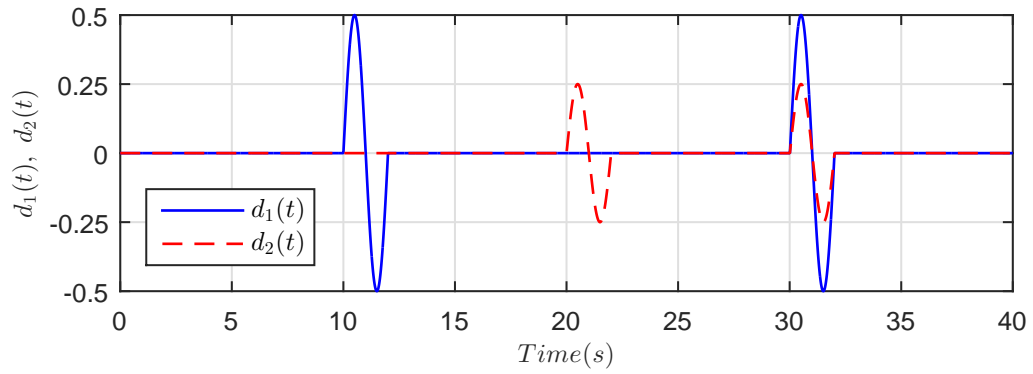


(D) Sliding surface σ

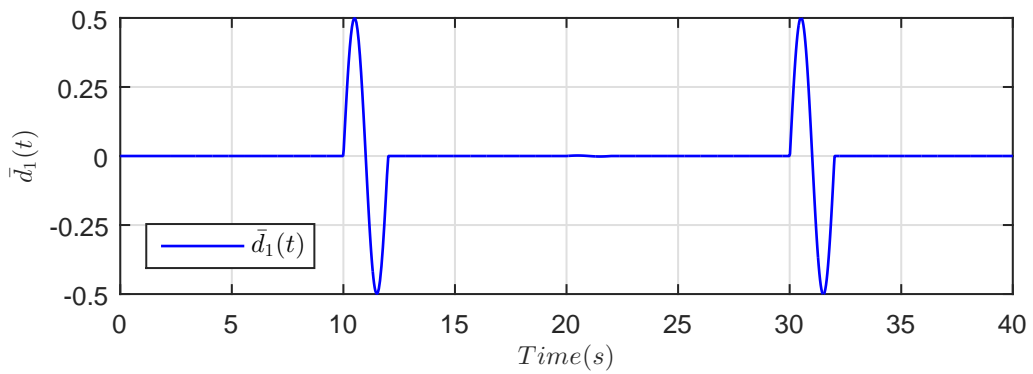


(E) Control effort u (N-m)

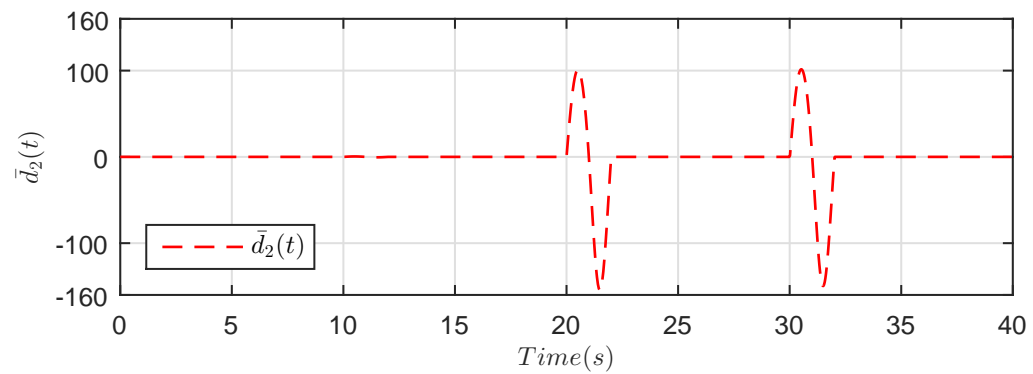
FIGURE 4.14: The Beam-and-Ball - Closed loop response with SMC law (4.54) ($\Gamma = 2.5.0$, $D_1 = 0.5$, $D_2 = 0.025$), $q(0) = [1.5, 0, 6.0, 0]^T$.



(A) Disturbances $d_1(t) = 0.5 \sin(\pi t)$, $d_2(t) = 0.25 \sin(\pi t)$

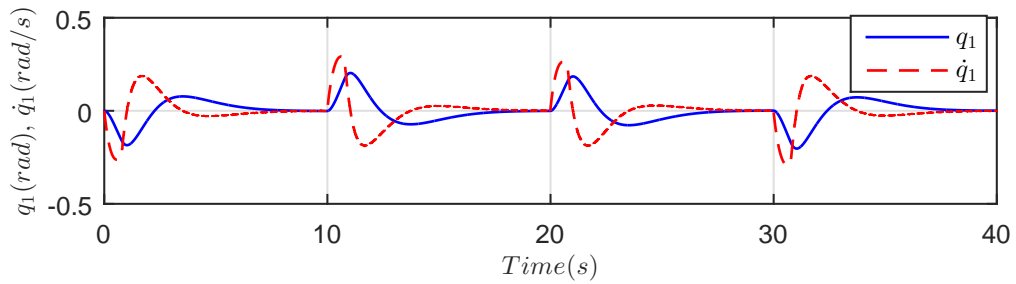


(B) Effective disturbance $\bar{d}_1(t)$ as in (4.48)

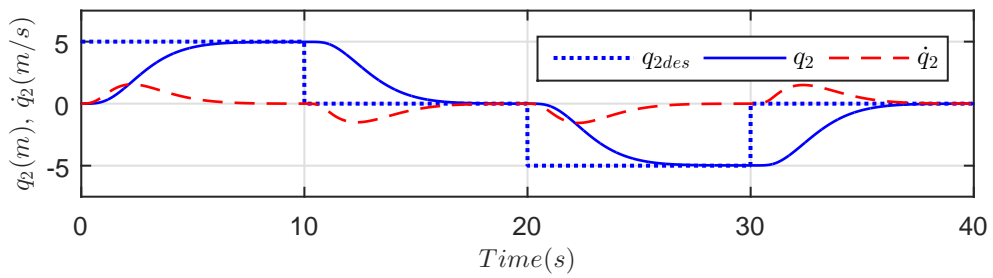


(C) Effective disturbance $\bar{d}_2(t)$ as in (4.48)

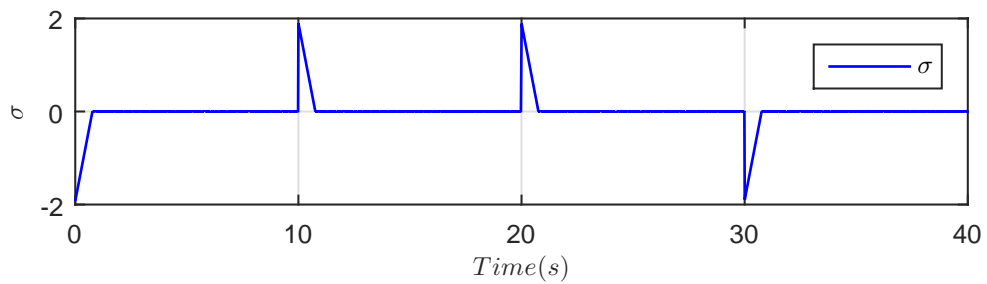
FIGURE 4.15: The Beam-and-Ball - Matched and unmatched disturbances $d_1(t)$, $d_2(t)$ and the effective disturbances $\bar{d}_1(t)$, $\bar{d}_2(t)$ on actuated variable q_1 and unactuated variable q_2 .



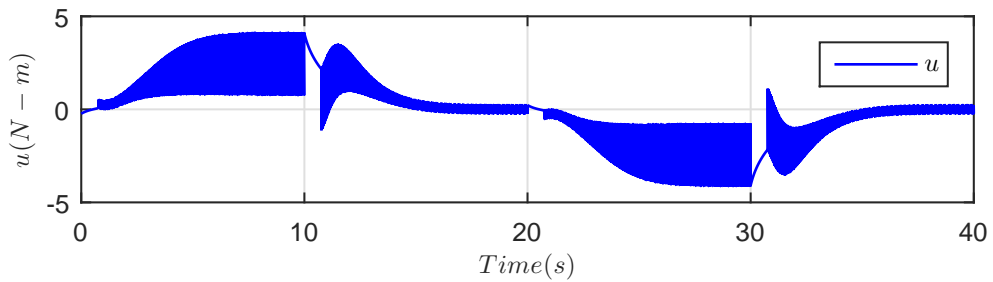
(A) Beam angle q_1 (rad), velocity \dot{q}_1 (rad/s)



(B) Ball position q_2 (m), velocity \dot{q}_2 (m/s)



(C) Sliding surface σ



(D) Control effort u (N-m)

FIGURE 4.16: The Beam-and-Ball - Closed loop tracking response with SMC law (4.54) ($\Gamma = 2.5.0$, $D_1 = 0$, $D_2 = 0$), $q(0) = [0, 0, 0, 0]^T$.

4.3.2.3 The Cart-Pole System

Figure 3.2c shows the Cart-Pole system. The actuator is at the Cart. The control task of this system is to stabilize the Pole (pendulum) from the stable downward equilibrium position $q_2 = \pi$ to the unstable upward equilibrium position $q_2 = 0$ and tracking the position of the Cart from any initial position q_{10} to any other desired position q_{1des} . Some work can be referred to [9, 44–51, 75, 79, 94, 169, 171, 174].

For the Cart-Pole system, the physical parameters are chosen according to [94] as: $m_1 = 1.0$ (kg), $m_2 = 1.0$ (kg), $\ell_2 = 0.75$ (m), and $g = 9.8$ (m.sec⁻²).

In the Euler-Lagrange equation (4.47) for the Cart-Pole system we have:

$$\begin{aligned}
 m_{11}(q_2) &= m_1 + m_2 \\
 m_{12}(q_2) &= m_2 \ell_2 \cos(q_2) \\
 m_{21}(q_2) &= m_{12}(q_2) \\
 m_{22}(q_2) &= I_2 + m_2 \ell_2^2 \\
 c_1(q, \dot{q}) &= -m_2 \ell_2 \sin(q_2) \dot{q}_2^2 \\
 c_2(q, \dot{q}) &= 0 \\
 g_1(q_1, q_2) &= 0 \\
 g_2(q_1, q_2) &= -m_2 \ell_2 g \sin(q_2)
 \end{aligned} \tag{4.66}$$

According to Lemma 4.10, the sliding mode dynamics in Eq. (4.55) for the Cart-Pole system are:

$$\begin{aligned}
 \dot{\xi}_1 &= \xi_2 \\
 \dot{\xi}_2 &= \frac{1}{m_{21} - m_{22}\gamma_2} \left(-m_{22}\gamma_1\gamma_3\xi_1 - m_{22}(\gamma_1\gamma_2 - \gamma_3)\xi_2 - m_{22}\gamma_1^2\xi_3 + m_2\ell_2g \sin(\xi_3 + q_{2des}) \right) \\
 \dot{\xi}_3 &= -\gamma_3\xi_1 - \gamma_2\xi_2 - \gamma_1\xi_3
 \end{aligned} \tag{4.67}$$

or

$$\dot{\boldsymbol{\xi}}(t) = \mathbf{f}_{CP}(\boldsymbol{\xi}(t)) \tag{4.68}$$

Take the Jacobian linearization of (4.68) around the equilibrium $\boldsymbol{\xi} = [0, 0, 0]^T$ as:

$$\dot{\boldsymbol{\xi}}(t) = \mathbf{A}_{\text{CP}}\boldsymbol{\xi}(t) \quad (4.69)$$

with $\mathbf{A}_{\text{CP}} = \left. \frac{\partial \mathbf{f}_{\text{CP}}}{\partial \boldsymbol{\xi}} \right|_{\boldsymbol{\xi}=\mathbf{0}}$ denoting the Jacobian matrix of \mathbf{f}_{CP} w.r.t. $\boldsymbol{\xi}$ at $\boldsymbol{\xi} = \mathbf{0}$.

Proposition 4.12 below gives stability of the dynamics in Eq. (4.67).

Proposition 4.12. *Choosing the the design parameters γ_1 , γ_2 , and γ_3 as below in Eq. (4.70), with a , b , c strictly positive, proves stability of Eq. (4.69) and stability of (4.67) is implied by Lyapunov indirect method.*

$$\gamma_1 = \frac{a(b^2 + c^2)(I_2 + m_2\ell_2^2) + (a + 2b)m_2\ell_2g}{(b^2 + c^2 + 2ab)(I_2 + m_2\ell_2^2) + m_2\ell_2g} \quad (4.70a)$$

$$\gamma_2 = \frac{(b^2 + c^2 + 2ab)m_2\ell_2}{(b^2 + c^2 + 2ab)(I_2 + m_2\ell_2^2) + m_2\ell_2g} \quad (4.70b)$$

$$\gamma_3 = \frac{a(b^2 + c^2)m_2\ell_2}{(b^2 + c^2 + 2ab)(I_2 + m_2\ell_2^2) + m_2\ell_2g} \quad (4.70c)$$

Proof. Linearizing system (4.67) for the stabilization of the Cart-Pole, $q_{1des} = 0$, $q_{2des} = 0$, we have:

$$\mathbf{A}_{\text{CP}} = \begin{bmatrix} 0 & 1 & 0 \\ \frac{-m_{22}\gamma_1\gamma_3}{m_2\ell_2 - m_{22}\gamma_2} & \frac{-m_{22}(\gamma_1\gamma_2 - \gamma_3)}{m_2\ell_2 - m_{22}\gamma_2} & \frac{-m_{22}\gamma_1^2 + m_2\ell_2g}{m_2\ell_2 - m_{22}\gamma_2} \\ -\gamma_3 & -\gamma_2 & -\gamma_1 \end{bmatrix} \quad (4.71)$$

The rest of the proof is similar to Proposition 4.7 and is omitted here. \square

For Assumption 4.3, we have:

$$(\bar{m}_{22}^{-1} + \gamma_2\bar{m}_{11}^{-1}) = \frac{-m_2\ell_2 \cos(q_2) + \gamma_2 (I_2 + m_2\ell_2^2)}{(m_1 + m_2) (I_2 + m_2\ell_2^2) - (m_2\ell_2 \cos(q_2))^2} \quad (4.72)$$

which is nonzero at $q_{2des} = q_2 = 0$, but becomes 0 at:

$$q_{2c} = \cos^{-1} \left(\frac{\gamma_2 (I_2 + m_2\ell_2^2)}{m_2\ell_2} \right) \quad (4.73)$$

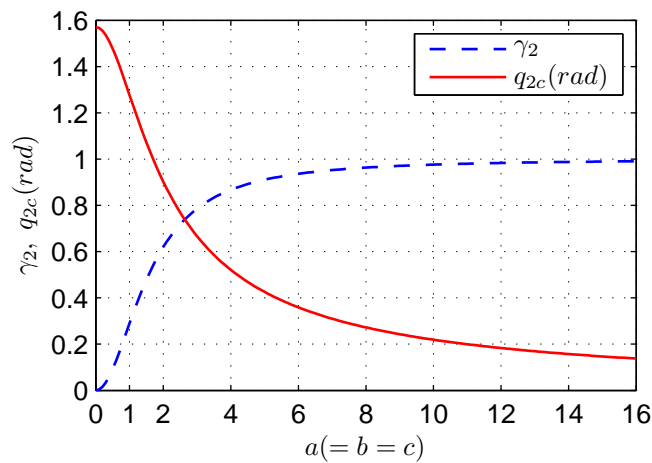


FIGURE 4.17: The Cart-Pole - variation of q_{2c} Eq. (4.73) with design constants a , b , and c through the design parameter γ_2 , Eq. (4.70b).

This shows that q_{2c} depends on the design constants a , b , and c through the design parameter γ_2 in Eq. (4.70b). γ_2 is strictly positive. Figure 4.17 shows this dependence graphically. The horizontal axis, $q_2 = \pi/2$, is the upper limit set at $a = b = c = 0$ ($\gamma_2 = 0$) and the design does not allow this choice. Figures 4.18 and 4.19 show closed loop response of the Cart-Pole system with SMC law (4.54) in the presence of parametric variations and disturbance. Figure 4.20 shows how the matched and unmatched disturbances $d_1(t)$, $d_2(t)$ affect the actuated variable q_1 and the unactuated variable q_2 through their contributions $\bar{d}_1(t)$, $\bar{d}_2(t)$. These results are discussed in the next section in detail.

4.3.2.4 Performance Analysis of The Cart-Pole System

Figures 4.18 and 4.19 show closed loop response of the Cart-Pole system with SMC law (4.54). The sliding parameters are chosen as $a = 1$, $b = .5$, $c = 0.5$. The controller gain is set to $\Gamma = 0.75$. Parametric variations is chosen as 35% decrease from $t = 5$ (s) to $t = 7$ (s) and 35% increase from $t = 7$ (s) to $t = 9$ (s). The matched disturbance $d_1(t) = 2 \sin(\pi t)$ and the unmatched disturbance $d_2(t) = 2 \sin(\pi t)$ are applied to system at time intervals shown in Figures 4.18c and 4.19c.

Figures 4.18-4.19 show closed loop response of the Cart-Pole system with SMC law (4.54) in the presence of parameter variations and external disturbance. The

controller successfully stabilizes the Cart-Pole system in 10 seconds.

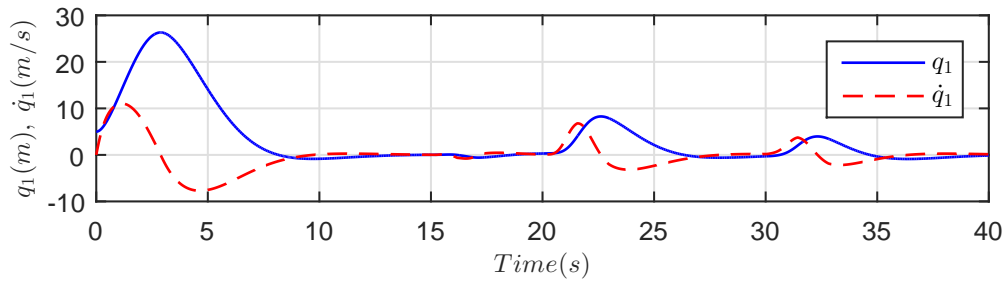
The initial conditions in Figures 4.18 and 4.19 are the same as in [94]. Comparing to [94], the overshoots/undershoots in the Cart position and the Pole angle are considerably improved with the settling time almost the same. Similarly the undershoot in the control effort is improved.

System response is robust to wide parametric variations. In Figure 4.18, $D_1 = D_2 = 0$ and hence both the disturbances, matched $d_1(t)$ and unmatched $d_2(t)$, affect system response. It is important to note that for the Cart-Pole system, in equilibrium, $\frac{1}{(\bar{m}_{22}^{-1} + \gamma_2 \bar{m}_{11}^{-1})} = -1.4413$, and hence the net effective discontinuous gain is $1.4413 * 0.75 = 1.080975$. This is the reason that the controller attenuates the matched disturbance $d_1(t)$ with magnitude 2 but does not fully reject it. In Figure 4.19, $D_1 = 2$, $D_2 = 2$ increasing the gain to 3.639571 and hence the matched disturbance $d_1(t)$ is fully rejected but the unmatched disturbance $d_2(t)$ still affects system stability and dynamics inspite of the fact that the net effective discontinuous gain is now increased from 1.080975 to 3.639571, much higher than 2.

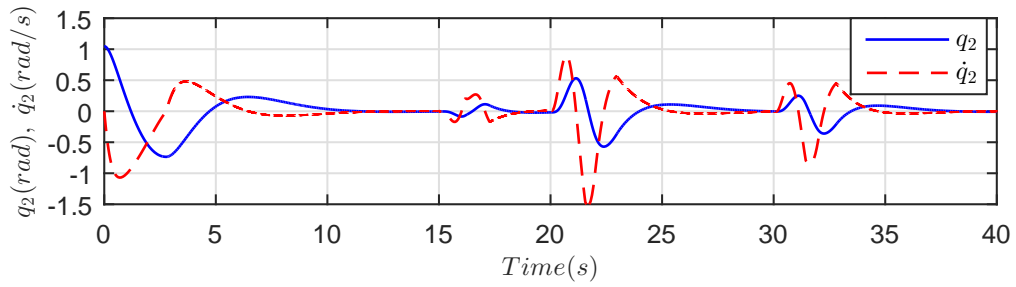
Equation (4.48) shows that both $d_1(t)$ and $d_2(t)$ affect the actuated configuration variable q_1 and similarly both affect the unactuated variable q_2 . Equation (4.49) shows that the contribution of matched disturbance $d_1(t)$ is the same and similar to the control u . On the other hand, the contribution of unmatched disturbance $d_2(t)$ is scaled to $-m_{12}m_{22}^{-1}d_2(t) = -1d_2(t)$ for the actuated variable q_1 and scaled to $-m_{11}m_{21}^{-1}d_2(t) = -2.6667d_2(t)$ for the unactuated variable q_2 . Figure 4.20 shows $d_1(t)$ and $d_2(t)$ and their effects $\bar{d}_1(t)$ and $\bar{d}_2(t)$ in accordance with the above observation.

In Figure 4.18, $d_1(t)$ and $d_2(t)$ when combined, in time interval $t = 30 - 32$ seconds, have less effect on dynamics, states and sliding variable, than $d_2(t)$ alone, in time interval $t = 20 - 22$ seconds. This interesting and important observation is according to above mentioned facts, i.e., $d_1(t)$ and $d_2(t)$ cancel each other ($\bar{d}_1 = 0$) for the actuated variable q_1 and remains 3.3334 for the unactuated variable q_2 . On the other hand, $d_2(t)$ alone affects the actuated variable q_1 with magnitude 2 and

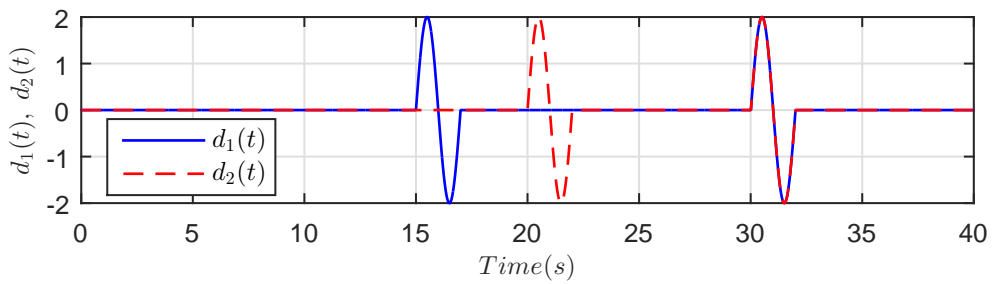
the unactuated variable q_2 with magnitude 5.3334. These interesting observations are shown in Figure [4.20](#).



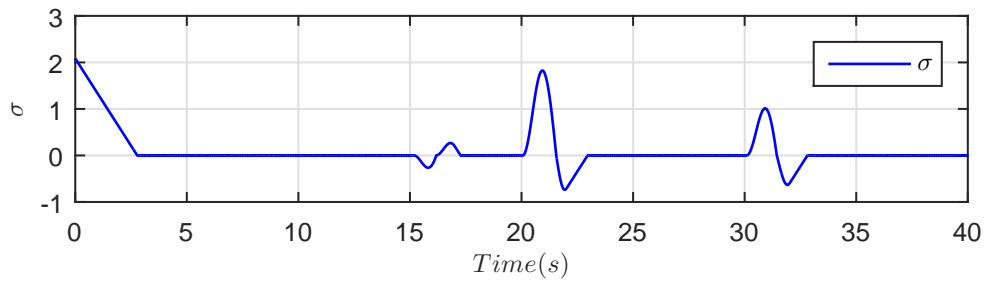
(A) Cart position q_1 (m), velocity \dot{q}_1 (m/s)



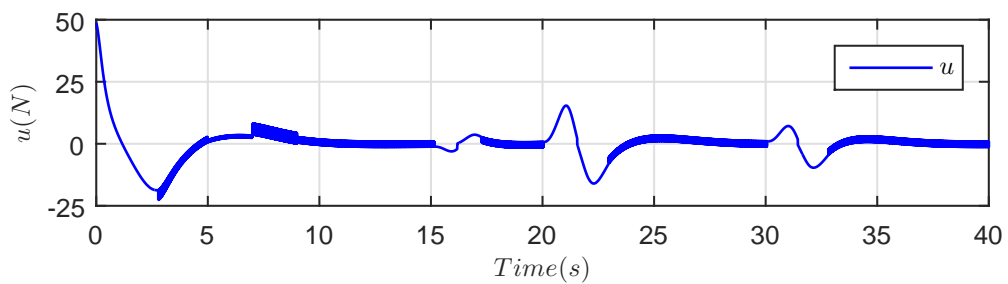
(B) Pole angle q_2 (rad), velocity \dot{q}_2 (rad/s)



(C) Disturbances $d_1(t) = 2 \sin(\pi t)$, $d_2(t) = 2 \sin(\pi t)$

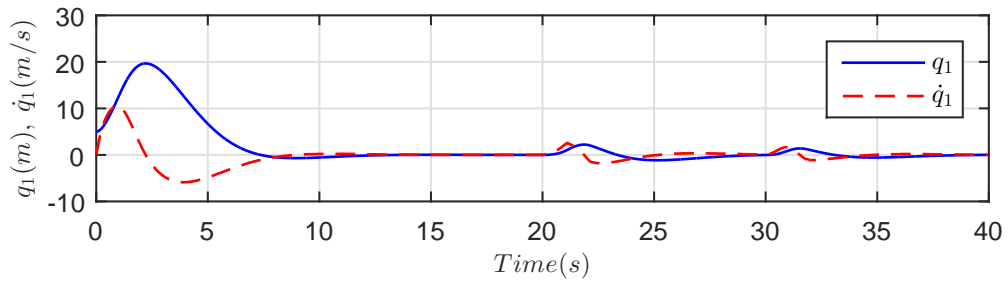


(D) Sliding surface σ

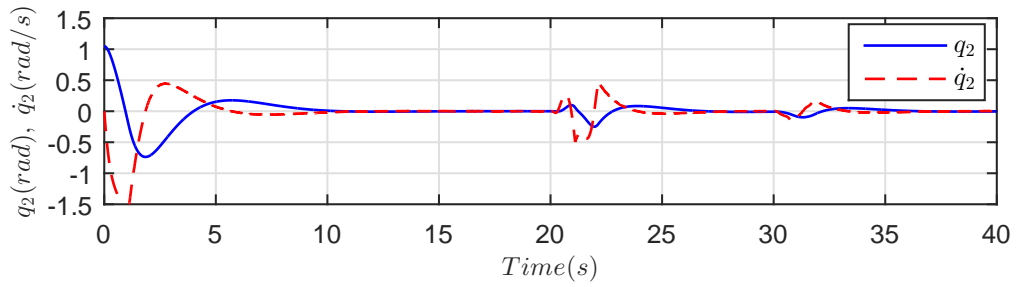


(E) Control effort u (N)

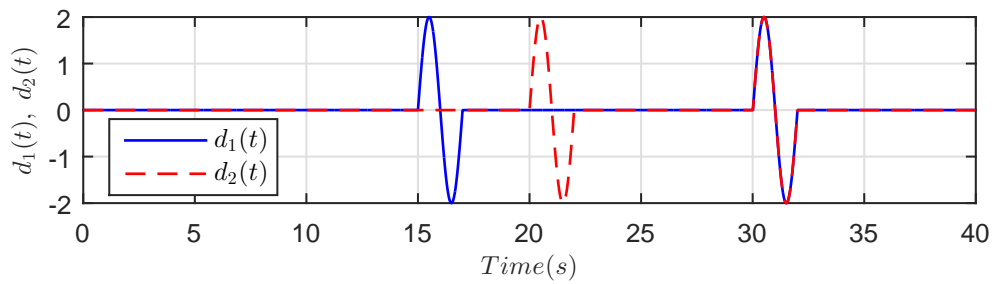
FIGURE 4.18: The Cart-Pole - Closed loop response with SMC law (4.54) ($\Gamma = 0.75.0$, $D_1 = 0$, $D_2 = 0$), $q(0) = [5, 0, \pi/3, 0]^T$.



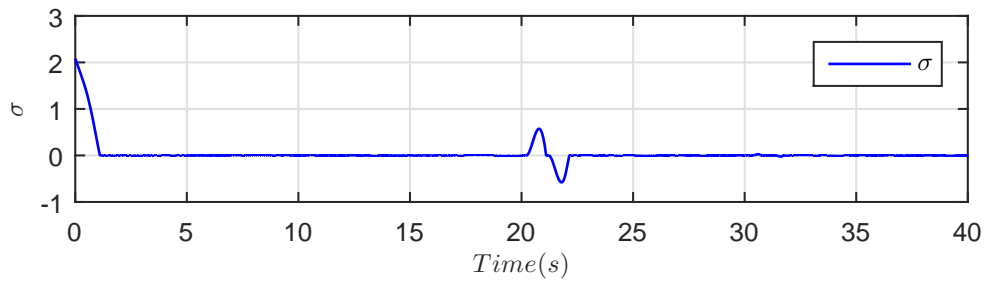
(A) Cart position q_1 (m), velocity \dot{q}_1 (m/s)



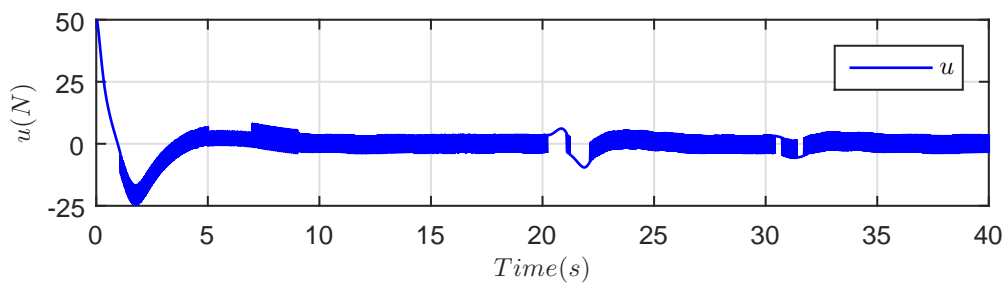
(B) Pole angle q_2 (rad), velocity \dot{q}_2 (rad/s)



(C) Disturbances $d_1(t) = 2 \sin(\pi t)$, $d_2(t) = 2 \sin(\pi t)$



(D) Sliding surface σ



(E) Control effort u (N)

FIGURE 4.19: The Cart-Pole - Closed loop response with SMC law (4.54) ($\Gamma = 0.75.0$, $D_1 = 2$, $D_2 = 2$), $q(0) = [5, 0, \pi/3, 0]^T$.

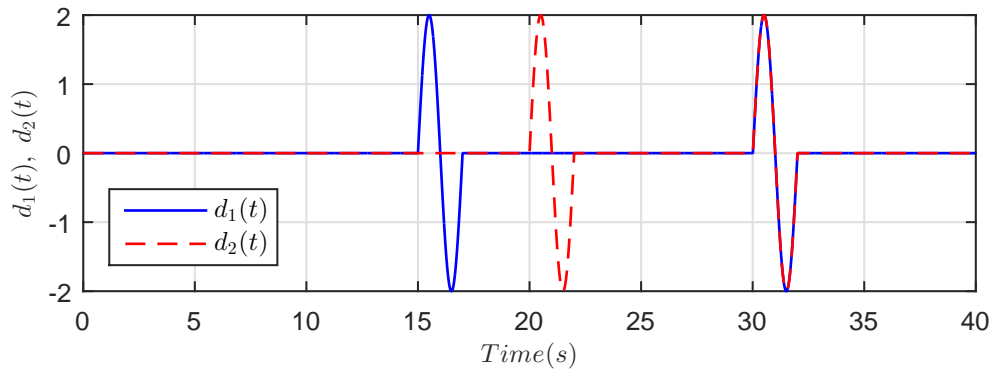
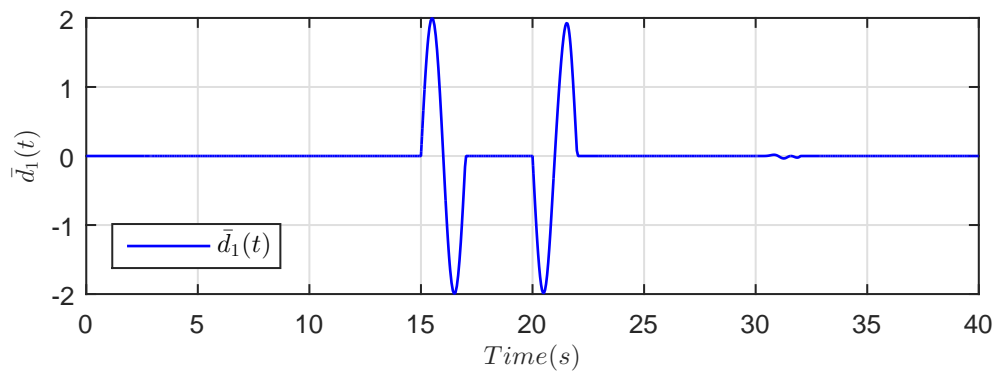
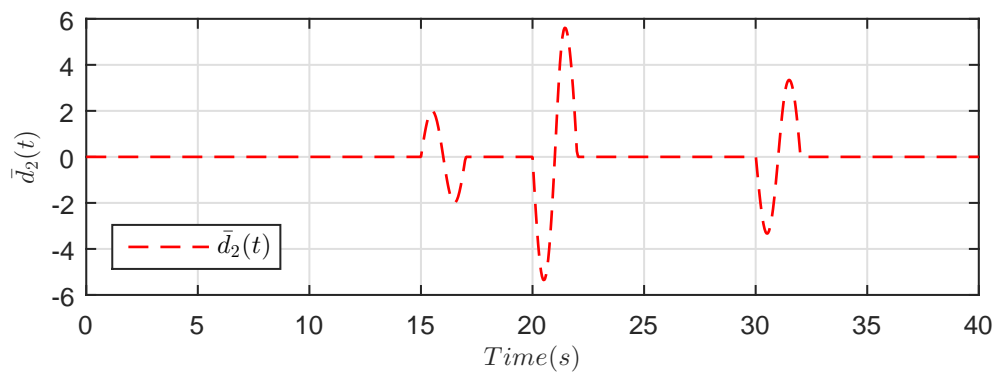
(A) Disturbances $d_1(t) = 2 \sin(\pi t)$, $d_2(t) = 2 \sin(\pi t)$ (B) Effective disturbance $\bar{d}_1(t)$ as in (4.48)(C) Effective disturbance $\bar{d}_2(t)$ as in (4.48)

FIGURE 4.20: The Cart-Pole - Matched and unmatched disturbances $d_1(t)$, $d_2(t)$ and the effective disturbances $\bar{d}_1(t)$, $\bar{d}_2(t)$ on actuated variable q_1 and unactuated variable q_2 .

4.3.2.5 The Overhead Crane

The Overhead Crane is shown in Fig. 3.2d. The actuator is at the Crane trolley. The control problem for the Overhead Crane is to track, as quickly as possible, the position of the Crane trolley from any initial position q_{10} to any other desired position q_{1des} and keeping the free swings of the Load angle q_2 as minimum as possible, i.e., the fast and precise transportation of the payload with minimum swing. Some work can be referred to [37–43].

Choose the physical parameters of the Overhead Crane according to [37] as:

$$M = 30.0 \text{ (kg)}, L = 2.0 \text{ (m)}, m = 20.0 \text{ (kg)}, \text{ and } g = 9.8 \text{ (m.s}^{-2}\text{)}.$$

For the Euler-Lagrange equation of the Overhead Crane in Eq. (4.47) we have:

$$\begin{aligned} m_{11}(q_2) &= M + m \\ m_{12}(q_2) &= mL \cos(q_2) \\ m_{21}(q_2) &= m_{12}(q_2) \\ m_{22}(q_2) &= I_2 + mL^2 \\ c_1(q, \dot{q}) &= -mL \sin(q_2) \dot{q}_2^2 \\ c_2(q, \dot{q}) &= 0 \\ g_1(q_1, q_2) &= 0 \\ g_2(q_1, q_2) &= mLg \sin(q_2) \end{aligned} \tag{4.74}$$

Note that the dynamics of the Overhead Crane (4.74) and the Cart-Pole system (4.66) are the same except for the term $g_2(q_1, q_2)$ that is positive for the Overhead Crane and negative for the Cart-Pole System. So instead of going into detail stability analysis for the Overhead Crane make use of the following corollary:

Corollary 4.13. *Sign inversion of g in Eq. (4.70) gives the following design parameters γ_1 , γ_2 , and γ_3 that will ensure stability of the sliding mode dynamics*

(4.55) for the Overhead Crane.

$$\gamma_1 = \frac{a(b^2 + c^2)(I_2 + mL^2) - (a + 2b)mLg}{(b^2 + c^2 + 2ab)(I_2 + mL^2) - mLg} \quad (4.75a)$$

$$\gamma_2 = \frac{(b^2 + c^2 + 2ab)mL}{(b^2 + c^2 + 2ab)(I_2 + mL^2) - mLg} \quad (4.75b)$$

$$\gamma_3 = \frac{a(b^2 + c^2)mL}{(b^2 + c^2 + 2ab)(I_2 + mL^2) - mLg} \quad (4.75c)$$

Figure 4.21 shows closed loop response of the Overhead Crane with SMC law (4.54) in the presence of disturbance. Figure 4.22 shows how the matched and unmatched disturbances $d_1(t)$, $d_2(t)$ affect the actuated variable q_1 and the unactuated variable q_2 through their contributions $\bar{d}_1(t)$, $\bar{d}_2(t)$. These results are discussed in the next section in detail.

4.3.2.6 Performance Analysis of The Overhead Crane

Figure 4.21 shows closed loop response of the Overhead Crane with SMC law (4.54). The sliding parameters are chosen as $a = 1$, $b = .5$, $c = 0.5$. The controller gain is set to $\Gamma = 0.45$. Parametric variations is chosen as 10% decrease from $t = 5(s)$ to $t = 7(s)$ and 10% increase from $t = 7(s)$ to $t = 9(s)$. The matched disturbance $d_1(t) = 10 \sin(\pi t)$ and the unmatched disturbance $d_2(t) = 10 \sin(\pi t)$ are applied to system at time intervals shown in Figures 4.21c.

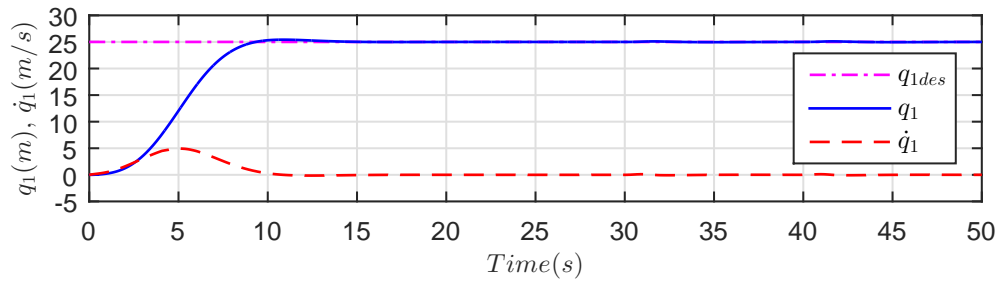
Figures 4.21 show closed loop response of the Overhead Crane with SMC law (4.54) in the presence of parameter variations and external disturbance. The Crane successfully transports the payload to the desired position $q_{1des} = 25(m)$ in less than 12 seconds while the payload swing angle q_2 remains within the desired range of $|q_2| < \frac{\pi}{18} = 0.1745$ radians, i.e., within 10 degrees. Comparing to [37], the results are considerably improved. An almost double, 25(m) instead of 14(m), desired position is achieved with the payload swing angle less than 10 degree instead of greater than 10 degree. The peak control force is less than 100(N) instead of greater than 200(N) and the peak velocity of the Crane is less than 5(m/s).

System response is robust to wide parametric variations. In Figure 4.21, $D_1 =$

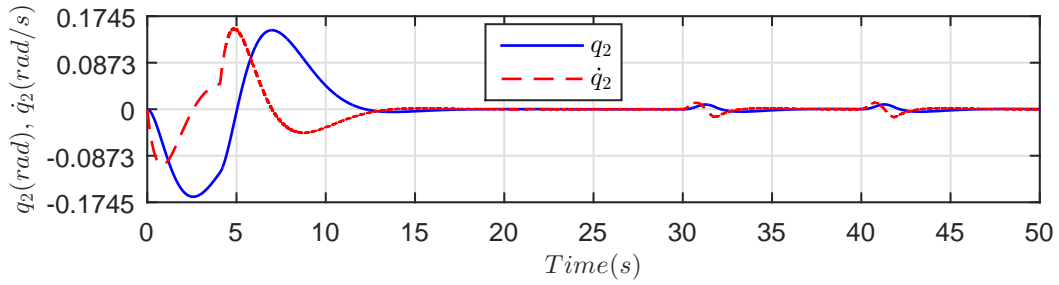
$D_2 = 0$, the matched disturbances $d_1(t)$ is fully rejected and the unmatched disturbances $d_2(t)$ affects system response. It is important to note that for the Overhead Crane, in equilibrium, $\frac{1}{(\bar{m}_{22}^{-1} + \gamma_2 \bar{m}_{11}^{-1})} = -41.632$, and hence the net effective discontinuous gain is $-41.632 * 0.45 = 18.7344$. This is the reason that the controller fully rejects the matched disturbance $d_1(t)$ with magnitude 10. The unmatched disturbance $d_2(t)$ still affects system stability and dynamics inspite of the fact that the net effective discontinuous gain is 18.7344, much higher than 10.

Equation (4.48) shows that both $d_1(t)$ and $d_2(t)$ affect the actuated configuration variable q_1 and similarly both affect the unactuated variable q_2 . Equation (4.49) shows that the contribution of matched disturbance $d_1(t)$ is the same and similar to the control u . On the other hand, the contribution of unmatched disturbance $d_2(t)$ is scaled to $-m_{12}m_{22}^{-1}d_2(t) = 0.5d_2(t)$ for the actuated variable q_1 and scaled to $-m_{11}m_{21}^{-1}d_2(t) = 1.25d_2(t)$ for the unactuated variable q_2 . Figure 4.22 shows $d_1(t)$ and $d_2(t)$ and their effects $\bar{d}_1(t)$ and $\bar{d}_2(t)$ in accordance with the above observation. The effect of unmatched disturbance $d_2(t)$ is reduced from 10 to 5 for actuated variable q_1 and increased to 12.5 for the unactuated variable q_2 . When applied both at the same time, time interval $t = 40 - 42$ seconds, the effect is reduced from 10 to 5 for actuated variable q_1 and reduced to 2.5 for the unactuated variable q_2 and hence have less effects than $d_2(t)$ alone.

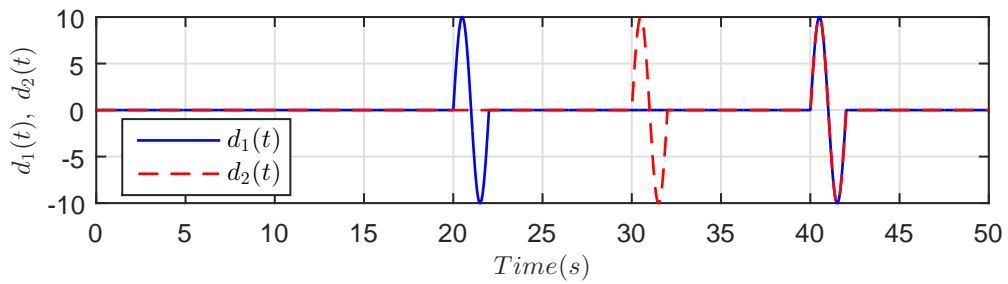
It is important that disturbance with amplitude 10 and time period 2 seconds is applied. On the hand, the disturbance applied in [37] has amplitude 0.5373 and time period 0.5 seconds. Disturbance with such small amplitude and high frequency are meaningless for a mechanical system with large physical parameters. Such systems absorb these disturbances due to slow response.



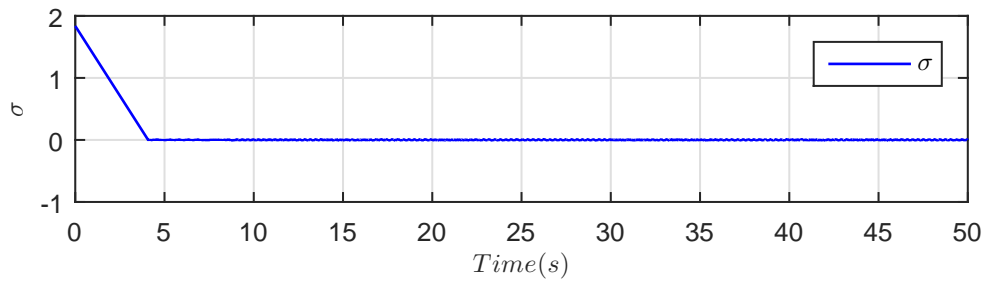
(A) Trolley position q_1 (m), velocity \dot{q}_1 (m/s)



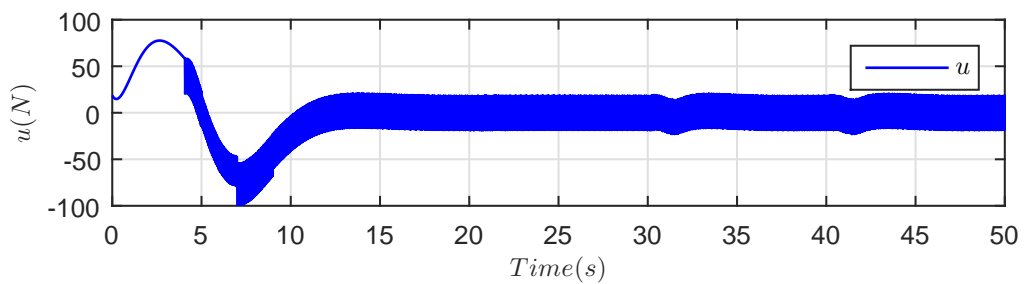
(B) Load angle q_2 (rad), velocity \dot{q}_2 (rad/s)



(C) Disturbances $d_1(t) = d_2(t) = 10 \sin(\pi t)$

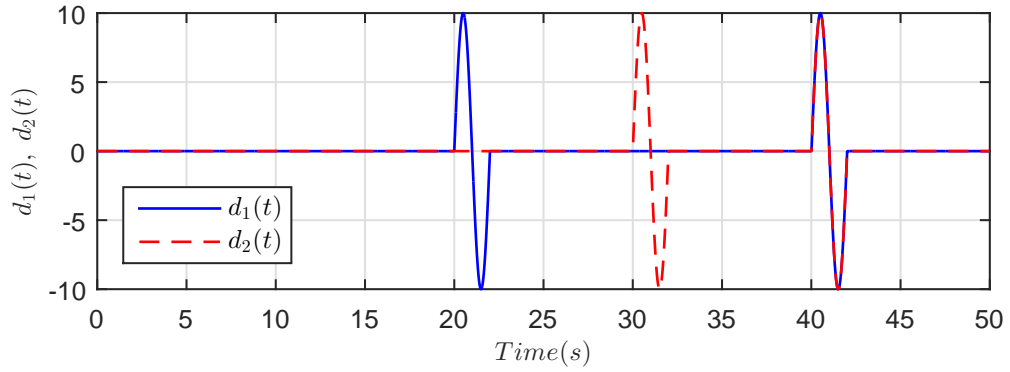


(D) Sliding surface σ

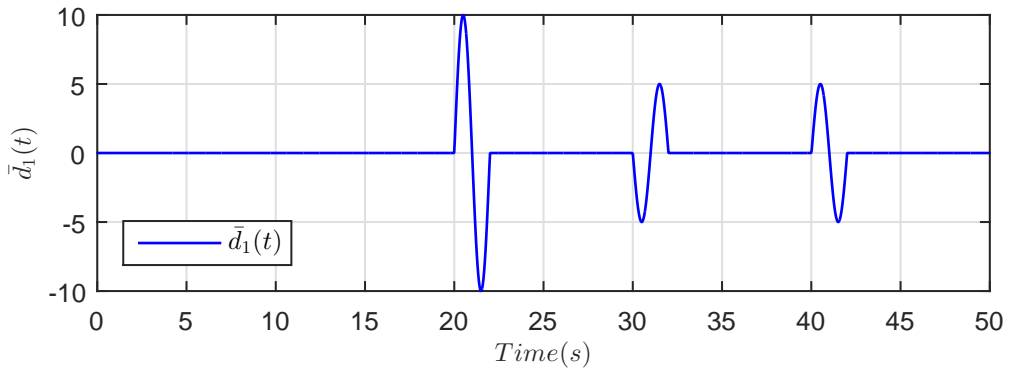


(E) Control effort u (N)

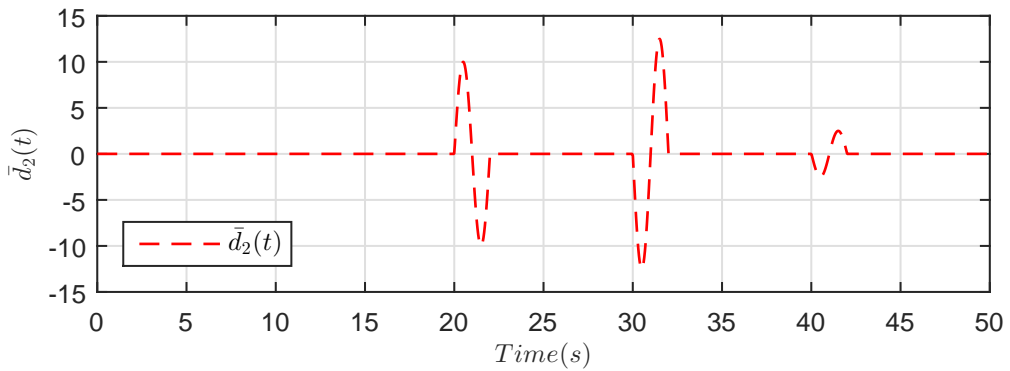
FIGURE 4.21: The Overhead Crane - Closed loop response with SMC law (4.54) ($\Gamma = 0.75$, $D_1 = 2$, $D_2 = 2$), $q(0) = [0, 0, 0, 0]^T$.



(A) Disturbances $d_1(t) = 10 \sin(\pi t)$, $d_2(t) = 10 \sin(\pi t)$



(B) Effective disturbance $\bar{d}_1(t)$ as in (4.48)



(C) Effective disturbance $\bar{d}_2(t)$ as in (4.48)

FIGURE 4.22: The Overhead Crane - Matched and unmatched disturbances $d_1(t)$, $d_2(t)$ and the effective disturbances $\bar{d}_1(t)$, $\bar{d}_2(t)$ on actuated variable q_1 and unactuated variable q_2 .

4.4 Chapter Summary and Conclusions

A standard SMC framework for underactuated mechanical systems was designed using the Euler-Lagrange representation. The framework takes into account both the matched and unmatched disturbances explicitly in the design. Expressions for the sliding mode dynamics were derived. Expressions for the parameters of the sliding surface in terms of system physical parameters were also derived. The design procedure was illustrated and the results compared to standard ones for the following benchmark underactuated mechanical systems:

1. The Inertia-Wheel Pendulum
2. The TORA System
3. The Beam-and-Ball System
4. The Cart-Pole System
5. The Overhead Crane

Based on the results, the following conclusion are drawn.

1. The proposed framework addresses the control problem of underactuated mechanical systems in a comprehensive way.
2. The designed control laws have enhanced stabilization and tracking (set-point regulation) response for the above benchmark underactuated mechanical systems.
3. The results are in agreement with and improved to standard results reported in the literature.
4. Being sliding mode, the framework is robust to parametric variations and disturbance in contrast to other works mentioned in the comparisons.
5. The design procedure is simple compared to other approaches the results were compared to.

Underactuated mechanical systems are more vulnerable to disturbances due to absence of actuators for some of the configuration variables and the effects of disturbances are more complex due to coupling. Both the matched and unmatched disturbances are taken care of explicitly in the design procedure. A detailed analysis of the results supports the following findings.

1. Both the matched and unmatched disturbances affect both the actuated and unactuated configuration variables.
2. The effect of the matched disturbance remains the same and can be fully rejected by the controller by utilizing the discontinuous gain of the controller embodied explicitly in the control law.
3. The effect of the unmatched disturbance is scaled to a lower or a higher value depending on the elements of the inertia matrix of the system.
4. The unmatched disturbance cannot be rejected by the controller by utilizing the discontinuous gain of the controller embodied explicitly in the control law.
5. When both matched and unmatched disturbances are applied at the same time, they may cancel their effects depending on the nature of the disturbances and the the elements of the inertia matrix of the system.

The proposed framework have the following limitations.

1. The control action suffers from chattering. Chattering is undesirable and, in mechanical control systems especially, even practically not applicable.
2. Stability proof of the sling mode dynamics is based on Lyapunov indirect method, and hence, the results are not global.

In Chapter 5, the application of HOSM control based on the Super-Twisting Algorithm (STA) is proposed to reduce the chattering. In Chapter 6, nonlinear sliding manifolds for underactuated mechanical systems and the application of smooth HOSM control is proposed to achieve both smooth control and global results.

Chapter 5

HOSM Design for Underactuated Mechanical Systems

This chapter investigates, the application of Higher Order Sliding Mode (HOSM) control based on the Super-Twisting Algorithm (STA) for underactuated mechanical systems to reduce the undesired chattering present in standard SMC design in the Chapter 4. The main results in this chapter are supported by [170]. The STA based HOSM control is applied to the following benchmark underactuated mechanical systems:

1. The Inertia-Wheel Pendulum
2. The TORA System
3. The Beam-and-Ball System
4. The Cart-Pole System
5. The Overhead Crane

5.1 HOSM Design for Class-I Underactuated Mechanical Systems

For the application of STA based HOSM control, consider Class-I underactuated mechanical systems represented by

$$m_{11}\ddot{q}_1 + m_{12}\ddot{q}_2 + c_1 + g_1 = d_1 \quad (5.1a)$$

$$m_{21}\ddot{q}_1 + m_{22}\ddot{q}_2 + c_2 + g_2 = u + d_2 \quad (5.1b)$$

Write (5.1) as

$$\bar{m}_{11}\ddot{q}_1 + \bar{c}_1 + \bar{g}_1 = u + \bar{d}_1 \quad (5.2a)$$

$$\bar{m}_{22}\ddot{q}_2 + \bar{c}_2 + \bar{g}_2 = u + \bar{d}_2 \quad (5.2b)$$

with the following definitions:

$$\begin{aligned} \bar{m}_{11}(q) &= m_{21} - m_{22}m_{12}^{-1}m_{11} \\ \bar{c}_1(q, \dot{q}) &= c_2 - m_{22}m_{12}^{-1}c_1 \\ \bar{g}_1(q) &= g_2 - m_{22}m_{12}^{-1}g_1 \\ \bar{d}_1(q) &= d_2 - m_{22}m_{12}^{-1}d_1 \\ \bar{m}_{22}(q) &= m_{22} - m_{21}m_{11}^{-1}m_{12} \\ \bar{c}_2(q, \dot{q}) &= c_2 - m_{21}m_{11}^{-1}c_1 \\ \bar{g}_2(q) &= g_2 - m_{21}m_{11}^{-1}g_1 \\ \bar{d}_2(q) &= d_2 - m_{21}m_{11}^{-1}d_1 \end{aligned} \quad (5.3)$$

Furthermore, consider the state space representation 4.8 with definition 4.9.

5.1.1 Control Law Design

For Class-I underactuated mechanical systems (4.5), define the following unactuated and actuated control errors as before:

$$e_1 = q_1 - q_{1des} \quad (5.4a)$$

$$e_2 = q_2 - q_{2des} \quad (5.4b)$$

Next define the sliding variable σ as below:

$$\sigma = \dot{e}_2 + \gamma_1 e_2 + \gamma_2 \dot{e}_1 + \gamma_3 e_1 \quad (5.5)$$

where γ_1 , γ_2 , and γ_3 are design parameters.

Take the time derivative (5.5) along the dynamics (4.5) to obtain:

$$\dot{\sigma} = \ddot{q}_2 + \gamma_1 \dot{q}_2 + \gamma_2 \ddot{q}_1 + \gamma_3 \dot{q}_1 \quad (5.6)$$

Using for \ddot{q}_1 and \ddot{q}_2 from (5.2a) and (5.2b) respectively, the above derivative becomes:

$$\dot{\sigma} = \bar{m}_{22}^{-1} (u + \bar{d}_2 - \bar{c}_2 - \bar{g}_2) + \gamma_1 \dot{q}_2 + \gamma_2 \bar{m}_{11}^{-1} (u + \bar{d}_1 - \bar{c}_1 - \bar{g}_1) + \gamma_3 \dot{q}_1 \quad (5.7)$$

or

$$\begin{aligned} \dot{\sigma} = & -\bar{m}_{22}^{-1} (\bar{c}_2 + \bar{g}_2) - \gamma_2 \bar{m}_{11}^{-1} (\bar{c}_1 + \bar{g}_1) + \gamma_1 \dot{q}_2 + \gamma_3 \dot{q}_1 + (\bar{m}_{22}^{-1} \bar{d}_2 + \gamma_2 \bar{m}_{11}^{-1} \bar{d}_1) \\ & + (\bar{m}_{22}^{-1} + \gamma_2 \bar{m}_{11}^{-1}) u \end{aligned} \quad (5.8)$$

or

$$\begin{aligned} \dot{\sigma} = & -\bar{m}_{22}^{-1} (\bar{c}_2 + \bar{g}_2) - \gamma_2 \bar{m}_{11}^{-1} (\bar{c}_1 + \bar{g}_1) + \gamma_1 \dot{q}_2 + \gamma_3 \dot{q}_1 + (\bar{m}_{22}^{-1} + \gamma_2 \bar{m}_{11}^{-1}) d_2 \\ & - (\bar{m}_{22}^{-1} m_{21} m_{11}^{-1} + \gamma_2 \bar{m}_{11}^{-1} m_{22} m_{12}^{-1}) d_1 + (\bar{m}_{22}^{-1} + \gamma_2 \bar{m}_{11}^{-1}) u \end{aligned} \quad (5.9)$$

or

$$\dot{\sigma} = a(q) + b(q)u \quad (5.10)$$

where

$$\begin{aligned} a(q) = & -\bar{m}_{22}^{-1}(\bar{c}_2 + \bar{g}_2) - \gamma_2 \bar{m}_{11}^{-1}(\bar{c}_1 + \bar{g}_1) + \gamma_1 \dot{q}_2 + \gamma_3 \dot{q}_1 \\ & + (\bar{m}_{22}^{-1} + \gamma_2 \bar{m}_{11}^{-1})d_2 - (\bar{m}_{22}^{-1}m_{21}m_{11}^{-1} + \gamma_2 \bar{m}_{11}^{-1}m_{22}m_{12}^{-1})d_1 \end{aligned} \quad (5.11)$$

and

$$b(q) = (\bar{m}_{22}^{-1}\gamma_2\bar{m}_{11}^{-1})u \quad (5.12)$$

Consider the following assumptions.

Assumption 5.1. The function $a(q)$ is assumed to be bounded.

Assumption 5.2. Relative degree requires, $b(q)|_{q=q_{des}} \neq 0$

Further, assume the existence of positive constants C , K_M , K_m , U_M , and p , such that:

$$\begin{aligned} \left| \dot{b}(q) \right| + U_M |\dot{a}(q)| & \leq C \\ 0 \leq K_m \leq b(q) & \leq K_M \\ \left| \frac{a(q)}{b(q)} \right| & < pU_M \\ 0 < p & < 1 \end{aligned} \quad (5.13)$$

Theorem 5.1. [147] *The following sliding mode control law based on the Super-Twisting Algorithm*

$$\begin{aligned} u & = -\lambda_1 |\sigma|^{1/2} \text{sign}(\sigma) + w \\ \dot{w} & = -\lambda_2 \text{sign}(\sigma) \end{aligned} \quad (5.14)$$

with $K_m \lambda_2 > C$ and λ_1 sufficiently large, guarantee the appearance of a 2-sliding mode $\sigma = \dot{\sigma} = 0$ in system (5.10), which attracts the trajectories in finite time. The control u enters in finite time the segment $[-U_M, U_m]$ and stays there. It never leaves the segment, if the initial value is inside at the beginning.

Proof. The proof of the theorem can be found in [147], and, elsewhere, in [175]. \square

Once sliding mode is established in system (5.10) along the dynamics of (5.1) according to Theorem 5.1, the sliding mode dynamics of Class-I underactuated mechanical systems (5.1) are given by Lemma 4.6.

5.1.2 Application to Class-I Underactuated Mechanical Systems

The STA based control law (5.14) is applied to the Inertia-Wheel Pendulum and the TORA system. The Euler-Lagrange equations (5.1) of these systems are shown in Table 4.1.

5.1.2.1 The Inertia-Wheel Pendulum

The sliding mode dynamics are given by Lemma 4.6 and their stability proof is given by Proposition 4.7. We use the results of Lemma 4.6 and Proposition 4.7 and apply the STA control law (5.14) to IWP. The analysis of Assumption 5.2 is similar to that in Section 4.2.2.1. The physical parameters are the same as in Section 4.2.2.1. Figure 5.1 shows simulation results for the IWP with STA law (5.14) in the presence of matched and unmatched external disturbances and parametric variations. These results are discussed in detail in the next section.

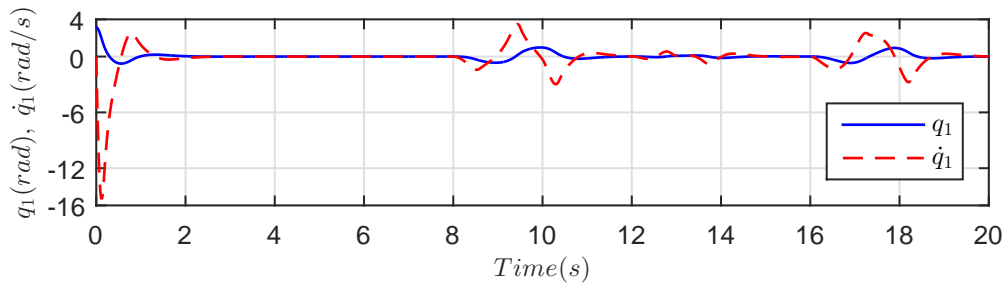
5.1.2.2 Performance Analysis of The IWP

Figure 5.1 shows closed loop response of the IWP with STA law (5.14) in the presence of matched and unmatched external disturbances and parametric variations. The controller gains are chosen as $\lambda_1 = -0.01$, $\lambda_2 = -0.02$ and the sliding parameters as $a = 4$, $b = 2$, $c = 2$. Parametric variations is chosen as 25% decrease from $t = 4$ (s) to $t = 6$ (s) and 25% increase from $t = 6$ (s) to $t = 8$ (s). The unmatched disturbance $d_1(t) = 0.2 \sin(\pi t)$ and the matched disturbance $d_2(t) = 0.2 \sin(\pi t)$ are applied to system at time intervals shown in Figures 5.1c.

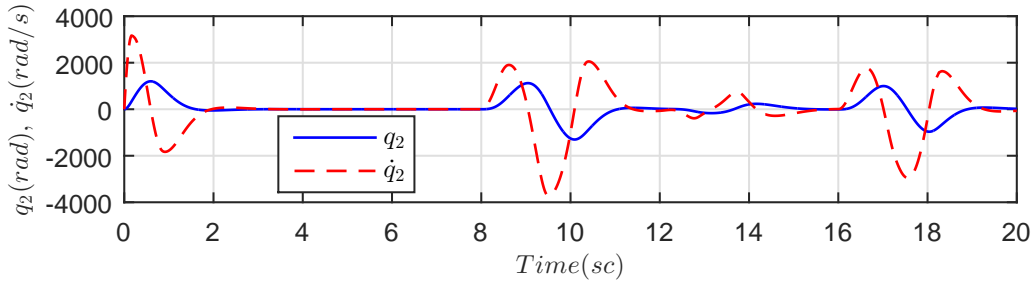
The same stabilization results are achieved as were achieved with SMC law 4.12 in Figure 4.2. The settling time is reduced from 4 seconds to 2 seconds now. The overshoot in Wheel velocity is reduced but the undershoot is increased. The main striking difference is that chattering in the control action is now reduced.

There is no built-in mechanism in the control law for handling the disturbances.

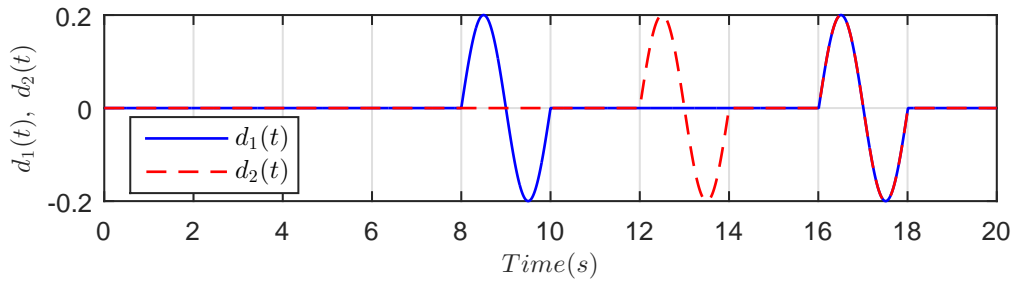
The adverse effects of the unmatched $d_1(t)$ and matched $d_2(t)$ disturbances on system stability is shown in the Figure 5.1. The role of disturbances on the unactuated variable q_1 and actuated variable q_2 is the same as analyzed and discussed in Section 4.2.2.2 and shown in Figure 4.4.



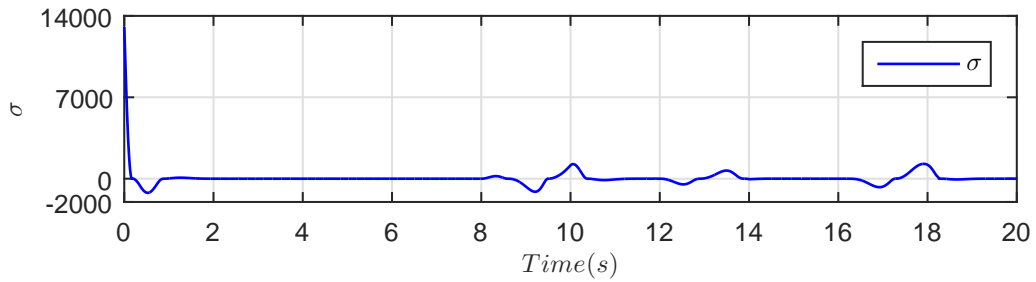
(A) Pendulum position q_1 (rad) and velocity \dot{q}_1 (rad/s)



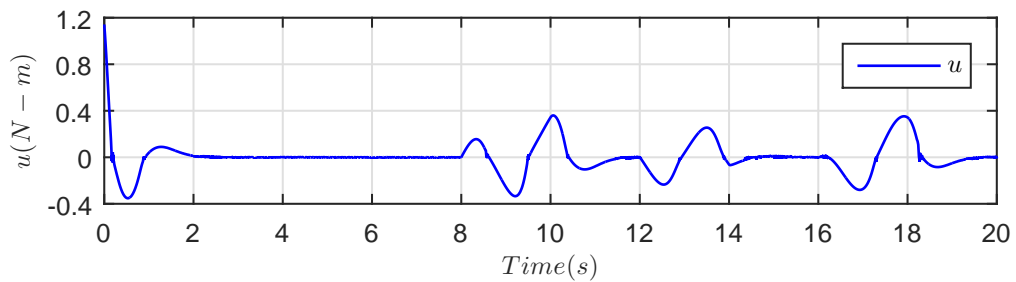
(B) Wheel position q_2 (rad) and velocity \dot{q}_2 (rad/s)



(C) Disturbances $d_1(t) = d_2(t) = 0.2 \sin(\pi t)$



(D) Sliding surface σ



(E) Control effort u (N-m)

FIGURE 5.1: IWP - Closed loop response with STA control law (5.14) ($\lambda_1 = -0.01$, $\lambda_2 = -0.02$), $q(0) = [\pi, 0, 0, 0]^T$,

5.1.2.3 The TORA System

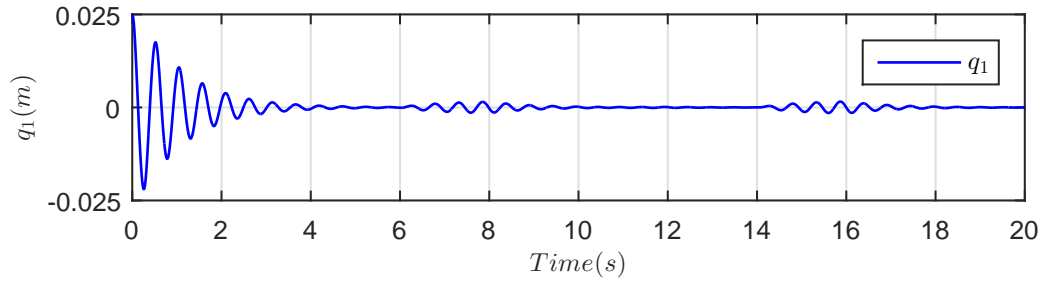
The sliding mode dynamics are given by Lemma 4.6 and their stability proof is given by Proposition 4.8. We use the results of Lemma 4.6 and Proposition 4.8 and apply the STA control law (5.14) to the TORA system. The analysis of Assumption 5.2 is similar to that in Section 4.2.2.3. The physical parameters are the same as in Section 4.2.2.3. Figure 5.2 shows simulation results for the TORA system with STA law (5.14) in the presence of matched and unmatched external disturbances and parametric variations. These results are discussed in detail in the next section.

5.1.2.4 Performance Analysis of The TORA System

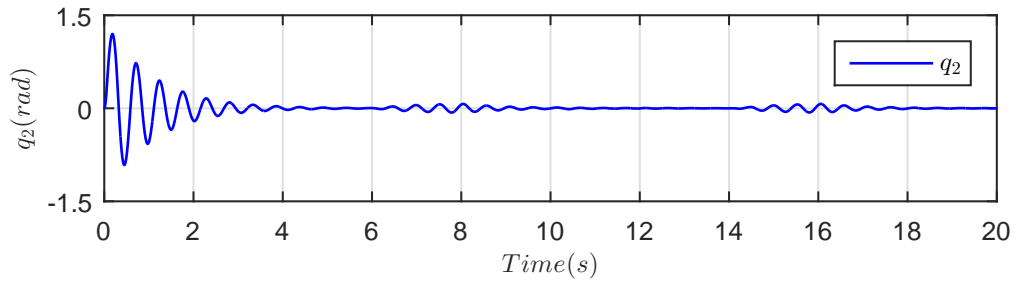
Figure 5.2 shows closed loop response of the TORA system with STA law (5.14) in the presence of matched and unmatched external disturbances and parametric variations. The controller gains are chosen as $\lambda_1 = 0.075$, $\lambda_2 = 0.050$, and the sliding parameters as $a = 12$, $b = 1$, $c = 12$. Parametric variations is chosen as 25% decrease from $t = 4$ (s) to $t = 5$ (s) and 25% increase from $t = 5$ (s) to $t = 6$ (s). The unmatched disturbance $d_1(t) = 0.05 \sin\left(\sqrt{\frac{k}{m_1}}t\right)$ and the matched disturbance $d_2(t) = 0.025 \sin\left(\sqrt{\frac{k}{m_1}}t\right)$ are applied to system at time intervals shown in Figures 5.2c.

The same stabilization results are achieved as were achieved with SMC law 4.12 in Figure 4.7. The controller successfully stabilizes the TORA system in less than 5 seconds with the nonlinear benchmark specifications [16] are met, i.e., the closed loop system is stable and the control effort is less than 0.05 N-m (specifications states less than 0.1 N-m continuous). Furthermore, chattering in the control action is now reduced.

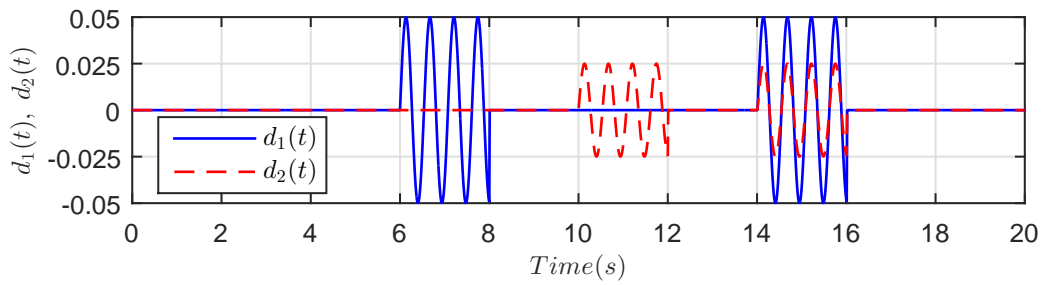
The adverse effects of the unmatched $d_1(t)$ and matched $d_2(t)$ disturbances on system stability is shown in the Figure 5.2. The role of disturbances on the unactuated variable q_1 and actuated variable q_2 is the same as analyzed and discussed in Section 4.2.2.3 and shown in Figure 4.9.



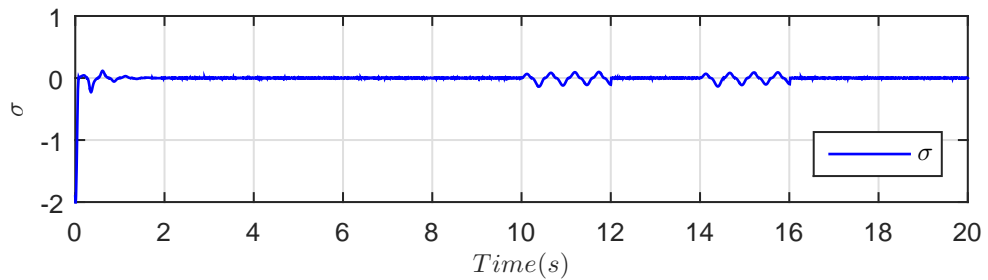
(A) Oscillator position q_1 (m)



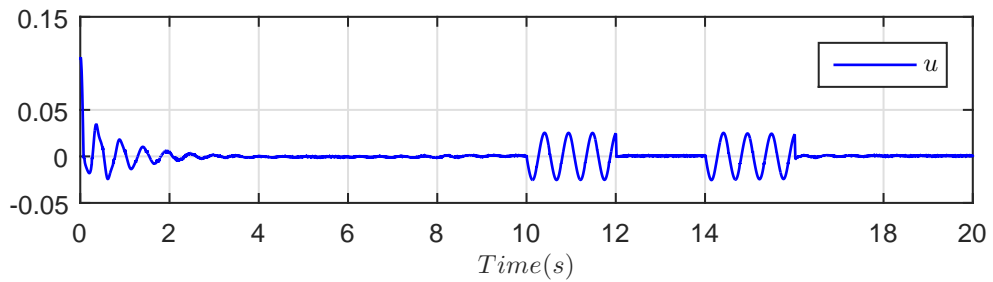
(B) Pendulum position q_2 (rad)



(C) Disturbances $d_1(t) = 0.05 \sin\left(\sqrt{\frac{k}{m_1}}t\right)$, $d_2(t) = 0.025 \sin\left(\sqrt{\frac{k}{m_1}}t\right)$



(D) Sliding surface σ



(E) Control effort u (N-m)

FIGURE 5.2: TORA - Closed loop response with STA control law (5.14) ($\lambda_1 = 0.075$, $\lambda_2 = 0.050$), $q(0) = [0.025, 0, 0, 0]^T$

5.2 HOSM Design for Class-II Underactuated Mechanical Systems

Consider Class-II underactuated mechanical systems represented by:

$$m_{11}\ddot{q}_1 + m_{12}\ddot{q}_2 + c_1 + g_1 = u + d_1 \quad (5.15a)$$

$$m_{21}\ddot{q}_1 + m_{22}\ddot{q}_2 + c_2 + g_2 = d_2 \quad (5.15b)$$

Write (5.15) as

$$\bar{m}_{11}\ddot{q}_1 + \bar{c}_1 + \bar{g}_1 = u + \bar{d}_1 \quad (5.16a)$$

$$\bar{m}_{22}\ddot{q}_2 + \bar{c}_2 + \bar{g}_2 = u + \bar{d}_2 \quad (5.16b)$$

with the following definitions:

$$\begin{aligned} \bar{m}_{11}(q) &= m_{11} - m_{12}m_{22}^{-1}m_{21} \\ \bar{c}_1(q, \dot{q}) &= c_1 - m_{12}m_{22}^{-1}c_2 \\ \bar{g}_1(q) &= g_1 - m_{12}m_{22}^{-1}g_2 \\ \bar{d}_1(q) &= d_1 - m_{12}m_{22}^{-1}d_2 \\ \bar{m}_{22}(q) &= m_{12} - m_{11}m_{21}^{-1}m_{22} \\ \bar{c}_2(q, \dot{q}) &= c_1 - m_{11}m_{21}^{-1}c_2 \\ \bar{g}_2(q) &= g_1 - m_{11}m_{21}^{-1}g_2 \\ \bar{d}_2(q) &= d_1 - m_{11}m_{21}^{-1}d_2 \end{aligned} \quad (5.17)$$

Furthermore, consider the state space representation 4.50 with definition 4.51.

5.2.1 Control Law Design

For Class-II systems (5.15), define the following actuated and unactuated control errors as before:

$$e_1 = q_1 - q_{1des} \quad (5.18a)$$

$$e_2 = q_2 - q_{2des} \quad (5.18b)$$

Next define the sliding variable σ as below:

$$\sigma = \dot{e}_2 + \gamma_1 e_2 + \gamma_2 \dot{e}_1 + \gamma_3 e_1 \quad (5.19)$$

where γ_1 , γ_2 , and γ_3 are design parameters.

Take the time derivative (5.19) along the dynamics (5.15) to obtain:

$$\dot{\sigma} = \ddot{q}_2 + \gamma_1 \dot{q}_2 + \gamma_2 \ddot{q}_1 + \gamma_3 \dot{q}_1 \quad (5.20)$$

Using for \ddot{q}_1 and \ddot{q}_2 from (5.16a) and (5.16b) respectively, the above derivative becomes, after some manipulation,:

$$\dot{\sigma} = a(q) + b(q)u \quad (5.21)$$

where

$$\begin{aligned} a(q) = & -\bar{m}_{22}^{-1} (\bar{c}_2 + \bar{g}_2) - \gamma_2 \bar{m}_{11}^{-1} (\bar{c}_1 + \bar{g}_1) + \gamma_1 \dot{q}_2 + \gamma_3 \dot{q}_1 \\ & + (\bar{m}_{22}^{-1} + \gamma_2 \bar{m}_{11}^{-1}) d_1 - (\bar{m}_{22}^{-1} m_{21} m_{11}^{-1} + \gamma_2 \bar{m}_{11}^{-1} m_{22} m_{12}^{-1}) d_2 \end{aligned} \quad (5.22)$$

and

$$b(q) = (\bar{m}_{22}^{-1} \gamma_2 \bar{m}_{11}^{-1}) u \quad (5.23)$$

Consider the following assumptions.

Assumption 5.3. The function $a(q)$ is assumed to be bounded.

Assumption 5.4. Relative degree requires, $b(q)|_{q=q_{des}} \neq 0$

Assume the existence of positive constants C , K_M , K_m , U_M , and p , such that:

$$\begin{aligned} \left| \dot{b}(q) \right| + U_M |\dot{a}(q)| &\leq C \\ 0 \leq K_m \leq b(q) &\leq K_M \\ \left| \frac{a(q)}{b(q)} \right| &< pU_M \\ 0 < p &< 1 \end{aligned} \tag{5.24}$$

Now this case becomes as the case for Class-I underactuated mechanical systems discussed previously and we can apply the STA control law in 5.1. Once sliding mode is established in system (5.21) along the dynamics of (5.15), according to Theorem 5.1, the sliding mode dynamics of Class-II underactuated mechanical systems (5.15) are given by Lemma 4.10.

5.2.2 Application to Class-II Underactuated Mechanical Systems

The STA based control law (5.14) is applied to the Beam-and-Ball system, the Cart-Pole system, and the Overhead Crane.

5.2.2.1 The Beam-and-Ball System

The sliding mode dynamics are given by Lemma 4.10 and their stability proof is given by Proposition 4.11. We use the results Lemma 4.10 and Proposition 4.11 and apply the STA control law (5.14) to the Beam-and-Ball system. The analysis of Assumption 5.4 is similar to that in Section 4.3.2.1. The physical parameters are the same as in Section 4.3.2.1. Figures 5.3-5.5 shows simulation results for the Beam-and-Ball system with STA control law (5.14) in the presence of matched and unmatched external disturbances and parametric variations. These results are discussed in detail in the next section.

5.2.2.2 Performance Analysis of The Beam-and-Ball System

Figures 5.3-5.5 show closed loop response of the Beam-and-Ball system with STA control law (5.14). The sliding parameters are chosen as $a = 1$, $b = 1$, $c = 0.5$. The controller gains are $\lambda_1 = -4.0$, $\lambda_2 = -0.5$. Parametric variations is chosen as 35% decrease from $t = 5(\text{s})$ to $t = 7(\text{s})$ and 35% increase from $t = 7(\text{s})$ to $t = 9(\text{s})$. The matched disturbance $d_1(t) = 0.5 \sin(\pi t)$ and the unmatched disturbance $d_2(t) = 0.25 \sin(\pi t)$ are applied to system at time intervals shown in Figure 5.5c.

The initial conditions in Figures 5.3 and 5.4 are the same as in HOCSMC [64]. Comparing to [64] the settling time, the overshoots/undershoots in the Ball position are considerable improved. Shown in [64], for these initial conditions, the HOCSMC based on [63] becomes unstable. Furthermore, chattering in the control action is now reduced.

Figures 5.5 shows closed loop response of the Beam-and-Ball system with STA control law (5.14) in the presence of parametric variations and external disturbance. The adverse effects of the unmatched $d_2(t)$ disturbances on system stability are prominent shown in the Figure 5.5. The role of disturbances on the actuated variable q_1 and unactuated variable q_2 is the same as analyzed and discussed in Section 4.3.2.2 and shown in Figure 4.15.

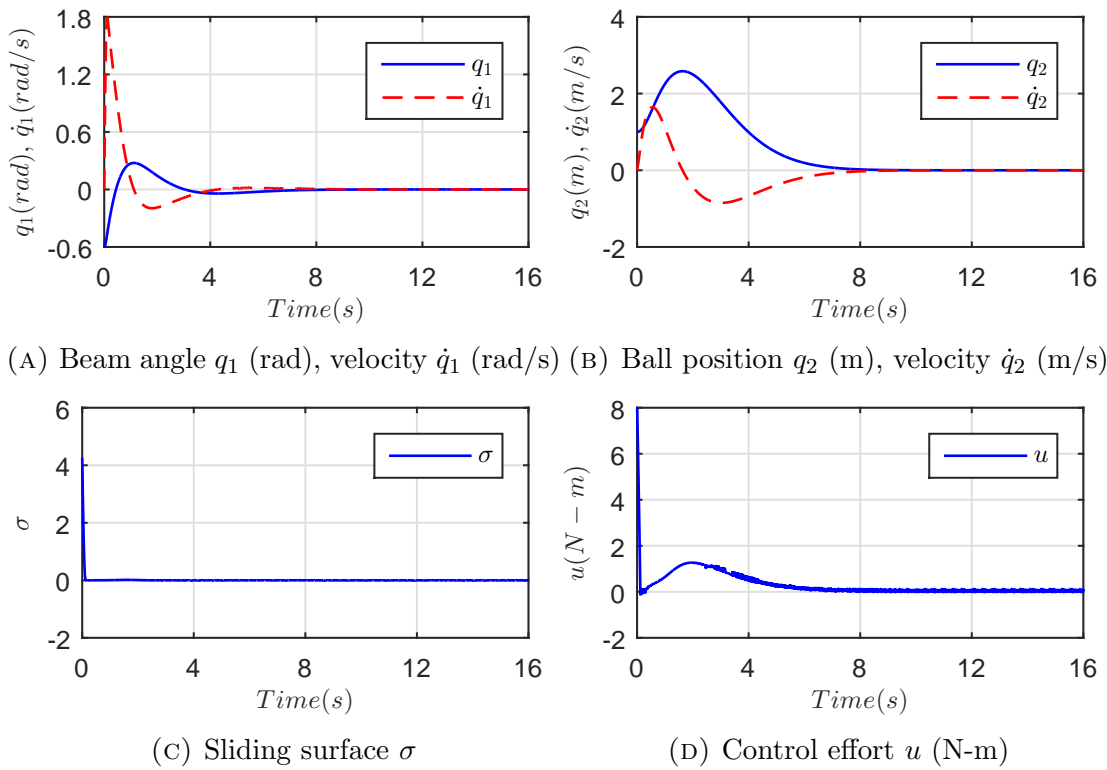


FIGURE 5.3: The Beam-and-Ball - Closed loop response with STA control law (5.14) ($\lambda_1 = -4.0, \lambda_2 = -0.5$), $q(0) = [-0.6, 0, 1.0, 0]^T$.

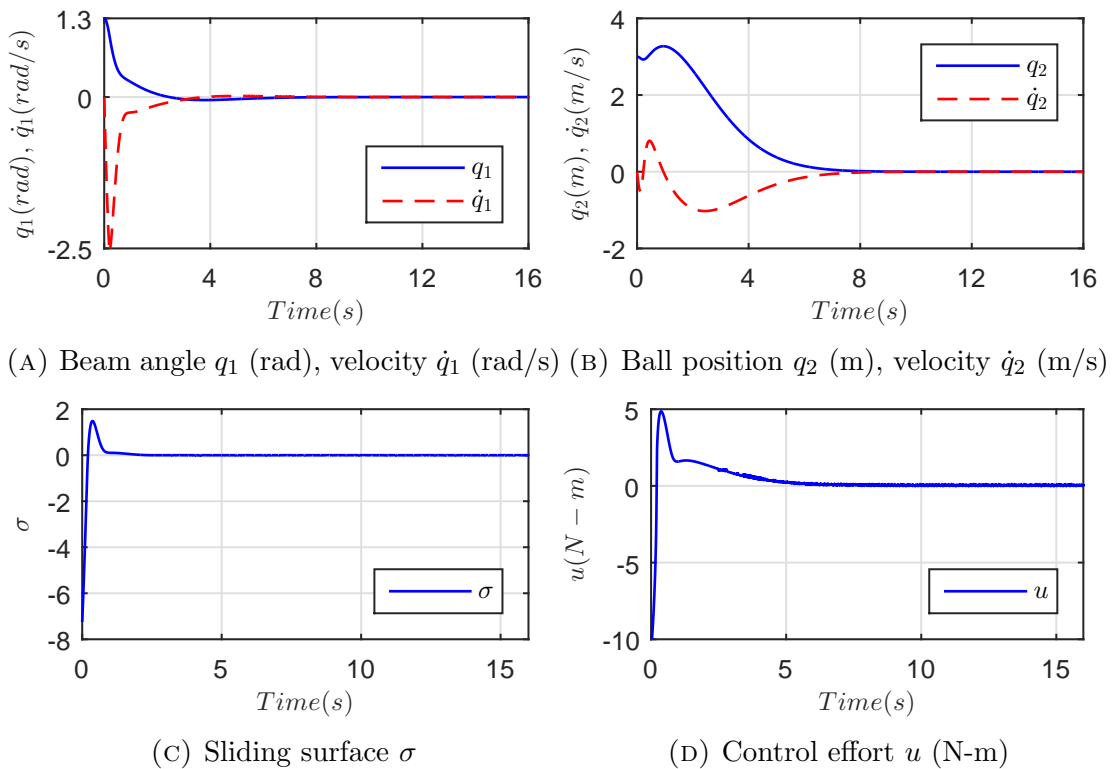


FIGURE 5.4: The Beam-and-Ball - Closed loop response with STA control law (5.14) ($\lambda_1 = -4.0, \lambda_2 = -0.5$), $q(0) = [1.3, 0, 3.0, 0]^T$.

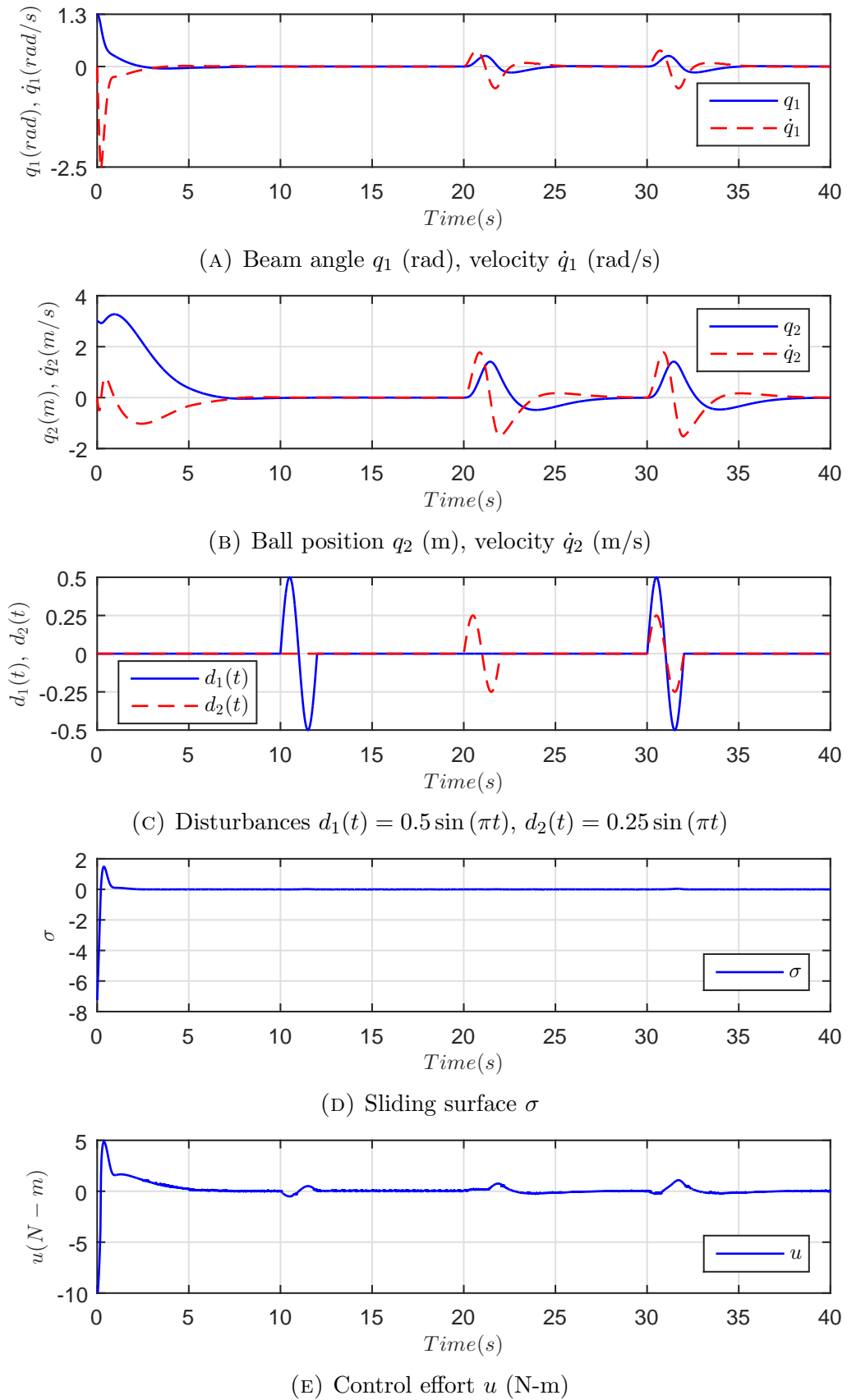


FIGURE 5.5: The Beam-and-Ball - Closed loop response with STA control law (5.14) ($\lambda_1 = -4.0$, $\lambda_2 = -0.5$), $q(0) = [1.3, 0, 3.0, 0]^T$.

5.2.2.3 The Cart-Pole System

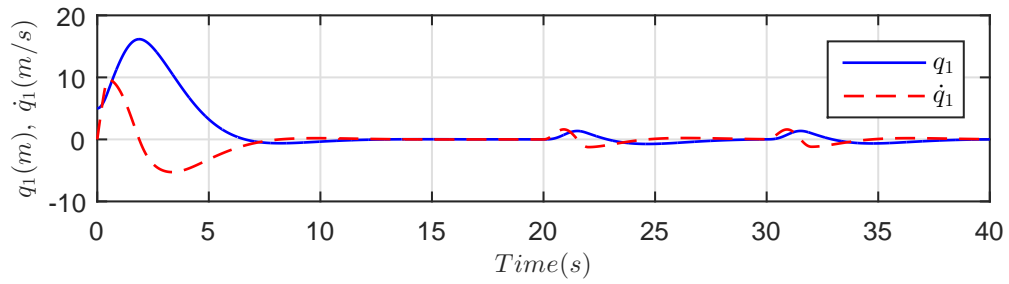
The sliding mode dynamics are given by Lemma 4.10 and their stability proof is given by Proposition 4.12. We use the results Lemma 4.10 and Proposition 4.12 and apply the STA control law (5.14) to the Cart-Pole system. The analysis of Assumption 5.4 is similar to that in Section 4.3.2.3. The physical parameters are the same as in Section 4.3.2.3. Figure 5.6 shows simulation results for the Cart-Pole system with STA control law (5.14) in the presence of matched and unmatched external disturbances and parametric variations. These results are discussed in detail in the next section.

5.2.2.4 Performance Analysis of The Cart-Pole System

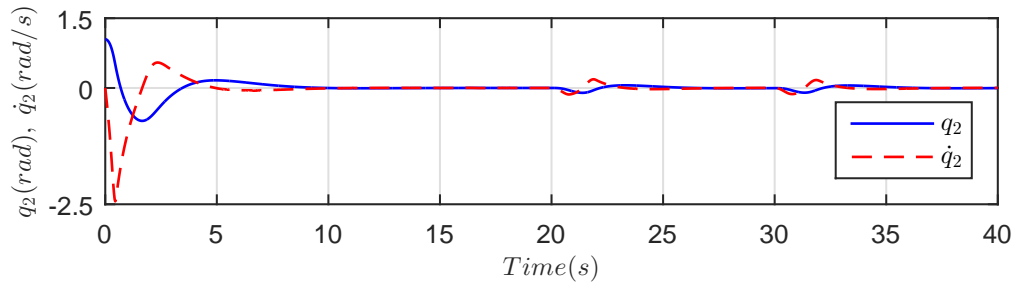
Figure 5.6 shows closed loop response of the Cart-Pole system with STA control law (5.14). The sliding parameters are chosen as $a = 1$, $b = .5$, $c = 0.5$. The controller gains are set to $\lambda_1 = -35.0$, $\lambda_2 = -2.5$. Parametric variations is chosen as 35% decrease from $t = 5(s)$ to $t = 7(s)$ and 35% increase from $t = 7(s)$ to $t = 9(s)$. The matched disturbance $d_1(t) = 2 \sin(\pi t)$ and the unmatched disturbance $d_2(t) = 2 \sin(\pi t)$ are applied to system at time intervals shown in Figure 5.6c.

Figure 5.6 shows closed loop response of the Cart-Pole system with STA control law (5.14) in the presence of parametric variations and external disturbance. The controller successfully stabilizes the Cart-Pole system in less than 10 seconds. The initial conditions in Figure 5.6 is the same as in [94]. Comparing to [94] the overshoot/undershoot in the Cart position and the Pole angle are considerably improved. Similarly the undershoot in the control effort and the settling time are improved. Furthermore, chattering in the control action is now reduced.

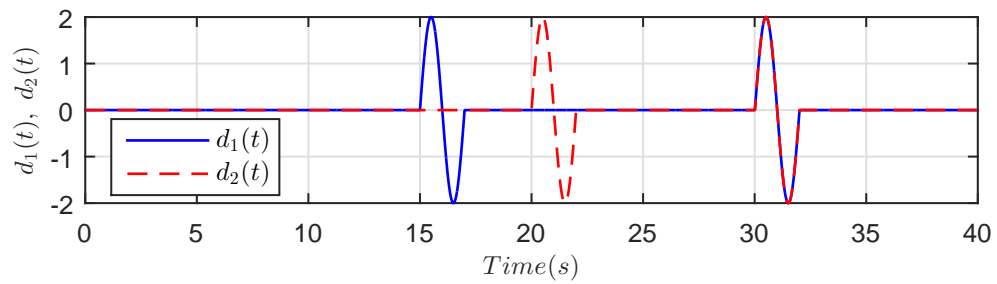
The effects of the unmatched $d_2(t)$ disturbance on system stability are prominent shown in the Figure 5.6. The role of disturbances on the actuated variable q_1 and unactuated variable q_2 is the same as analyzed and discussed in Section 4.3.2.4 and shown in Figure 4.20.



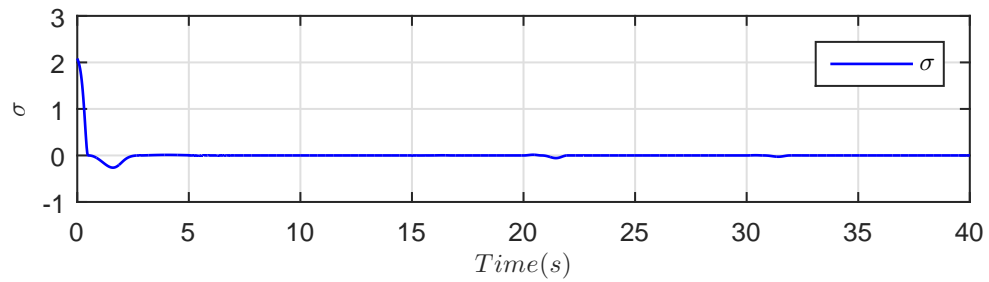
(A) Cart position q_1 (m), velocity \dot{q}_1 (m/s)



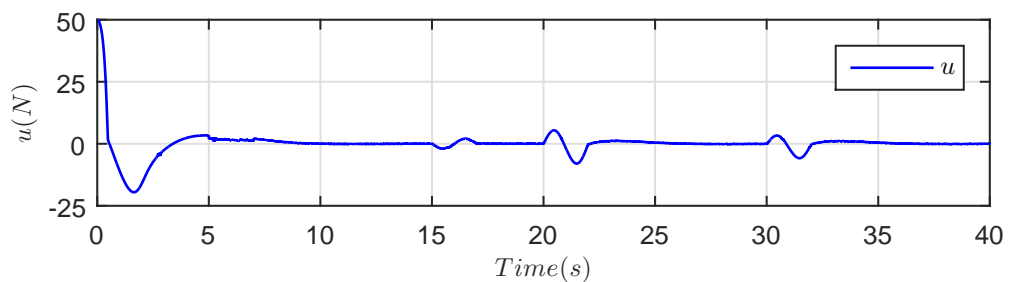
(B) Pole angle q_2 (rad), velocity \dot{q}_2 (rad/s)



(C) Disturbances $d_1(t) = 2 \sin(\pi t)$, $d_2(t) = 2 \sin(\pi t)$



(D) Sliding surface σ



(E) Control effort u (N)

FIGURE 5.6: The Cart-Pole - Closed loop response with STA control law (5.14) ($\lambda_1 = -35.0$, $\lambda_2 = -2.5$), $q(0) = [5, 0, \pi/3, 0]^T$.

5.2.2.5 The Overhead Crane

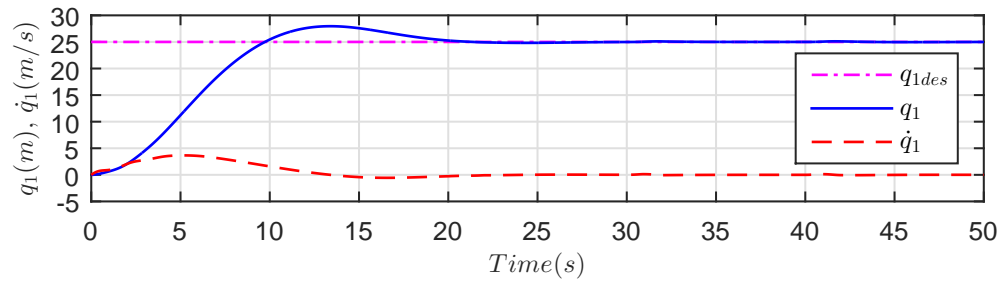
The sliding mode dynamics are given by Lemma 4.10 and their stability proof is given by Corollary 4.13. We use the results Lemma 4.10 and Corollary 4.13 and apply the STA control law (5.14) to the Overhead Crane. The analysis of Assumption 5.4 is similar to that in Section 4.3.2.5. The physical parameters are the same as in Section 4.3.2.5. Figure 5.7 shows simulation results for the Overhead Crane with STA control law (5.14) in the presence of matched and unmatched external disturbances and parametric variations. These results are discussed in detail in the next section.

5.2.2.6 Performance Analysis of The Overhead Crane

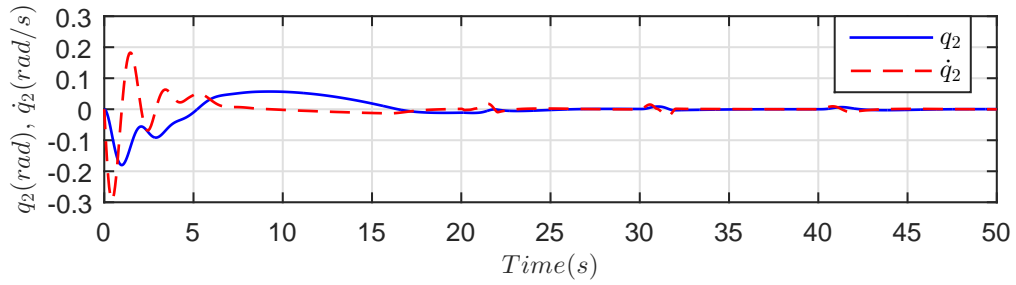
Figure 5.7 shows closed loop response of the Overhead Crane with STA control law (5.14). The sliding parameters are chosen as $a = 0.5$, $b = 0.5$, $c = 0.5$. The controller gains are set to $\lambda_1 = -100.0$, $\lambda_2 = -0.5$. Parametric variations is chosen as 10% decrease from $t = 5(s)$ to $t = 7(s)$ and 10% increase from $t = 7(s)$ to $t = 9(s)$. The matched disturbance $d_1(t) = 10 \sin(\pi t)$ and the unmatched disturbance $d_2(t) = 10 \sin(\pi t)$ are applied to system at time intervals shown in Figures 5.7c.

Figure 5.7 shows closed loop response of the Overhead Crane with STA law (5.14) in the presence of parameter variations and external disturbance. The results are not as good as achieved with SMC law (4.54) shown in Figure Figure 4.21. But the improvement is reduction in the chattering.

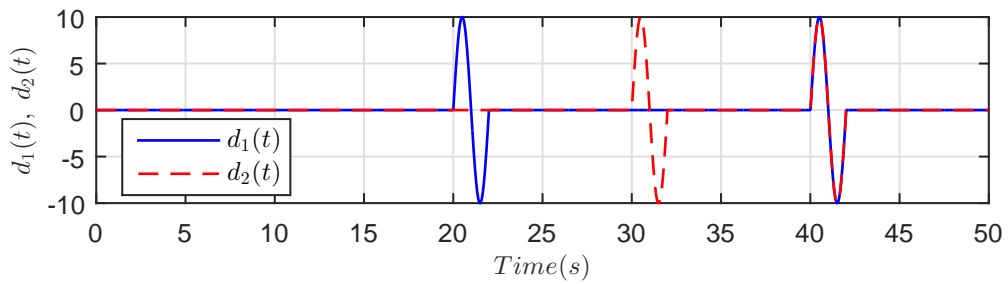
The role of disturbances on the actuated variable q_1 and unactuated variable q_2 is the same as analyzed and discussed in Section 4.3.2.6 and shown in Figure 4.22. It is important that we have applied disturbance with amplitude 10 and time period 2 seconds. On the hand, the disturbance applied in [37] has amplitude 0.5373 and time period 0.5 seconds. Disturbance with such small amplitude and high frequency are meaningless for a mechanical system with large physical parameters. Such systems absorb these disturbances.



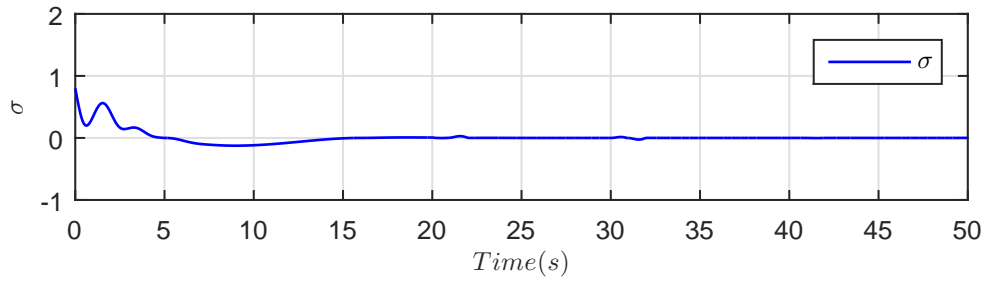
(A) Trolley position q_1 (m), velocity \dot{q}_1 (m/s)



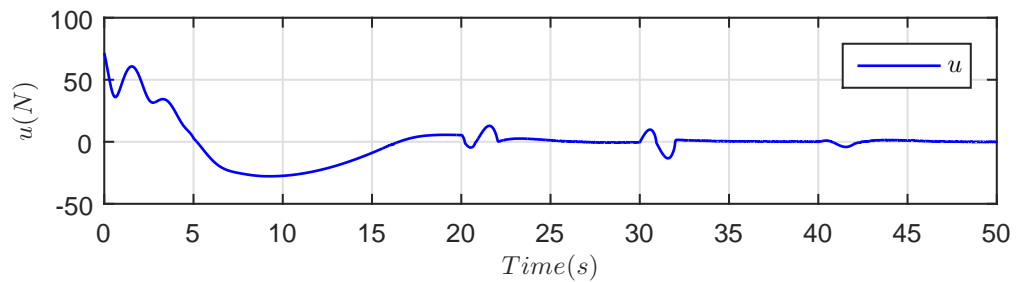
(B) Load angle q_2 (rad), velocity \dot{q}_2 (rad/s)



(C) Disturbances $d_1(t) = d_2(t) = 10 \sin(\pi t)$



(D) Sliding surface σ



(E) Control effort u (N)

FIGURE 5.7: The Overhead Crane - Closed loop response with STA control law (5.14) ($\lambda_1 = -100.0$, $\lambda_2 = -0.5$), $q(0) = [0, 0, 0, 0]^T$.

5.3 Chapter Summary and Conclusions

The application of Higher Order Sliding Mode (HOSM) control based on the Super-Twisting Algorithm (STA) was investigated for underactuated mechanical systems to reduce the undesired chattering present in standard SMC designed in the Chapter 4. The STA based HOSM control was applied to the following benchmark underactuated mechanical systems:

1. The Inertia-Wheel Pendulum
2. The TORA System
3. The Beam-and-Ball System
4. The Cart-Pole System
5. The Overhead Crane

Stabilization results similar to those achieved with SMC design were achieved with the extra advantage that chattering is now reduced. But the following limitations are still present.

1. Chattering is reduced but the control action is still not smooth.
2. Robustness is compromised as there is not built in mechanism for it in the control law.
3. Stability proof of the sling mode dynamics is based on Lyapunov indirect method and hence the results are not global.

In Chapter 6, novel nonlinear sliding manifolds are proposed for underactuated mechanical systems with the application of smooth HOSM control to achieve both smooth control and global results.

Chapter 6

Smooth HOSM Design for Underactuated Mechanical Systems

In this chapter, novel nonlinear sliding manifolds are proposed to achieve global convergence of underactuated mechanical systems. Furthermore, to achieve chattering free smooth control action, demanded for mechanical control systems, the application of Smooth Higher Order Sliding Mode (HOSM) control is proposed. Robustness is achieved using the well known disturbance observers. The main results in this chapter are supported by [176]. The design procedure is applied to the following benchmark underactuated mechanical systems:

A. Class-I Underactuated Mechanical Systems:

1. The Inertia-Wheel Pendulum
2. The TORA System
3. The Acrobot

B. Class-II Underactuated Mechanical Systems:

1. The Furuta Pendulum

2. The Overhead Crane
3. The Cart-Pole System
4. The Pendubot
5. The Beam-and-Ball System

6.1 Problem Formulation

The dynamical equations of an n degrees of freedom mechanical control system are as under:

$$M(q)\ddot{q} + C(q, \dot{q})\dot{q} + G(q) = F(q)u + d(q, \dot{q}, t) \quad (6.1)$$

where $q \in \mathfrak{R}^n$ is the generalized configuration vector, $M(q) \in \mathfrak{R}^{n \times n}$ is the positive definite symmetric inertia matrix, $C(q, \dot{q}) \in \mathfrak{R}^{n \times n}$ contains Coriolis and centrifugal terms, $G(q) \in \mathfrak{R}^{n \times 1}$ contains the gravitational terms, $F(q) \in \mathfrak{R}^{n \times m}$ is the control input matrix, $u \in \mathfrak{R}^m$ is the control input vector and $d(q, \dot{q}, t) \in \mathfrak{R}^n$ is the uncertainties term. The case, $m = \text{rank}(F) = n$, represents a fully actuated mechanical system, and, the case, $m = \text{rank}(F) < n$, characterizes an underactuated mechanical system.

We consider two classes of systems described by Eq. (6.1) with $M(q_2)$, first with $F(q) = [0, I_m]^T$ and second with $F(q) = [I_m, 0]^T$. For the first case, partitioning the configuration vector $q \in \mathfrak{R}^n$ into unactuated $q_1 \in \mathfrak{R}^{n-m}$ and actuated $q_2 \in \mathfrak{R}^m$ configuration vectors, the nominal dynamics in Eq.(6.1) take the form:

$$m_{11}(q_2)\ddot{q}_1 + m_{12}(q_2)\ddot{q}_2 + c_1(q, \dot{q}) + g_1(q_1, q_2) = 0 \quad (6.2a)$$

$$m_{21}(q_2)\ddot{q}_1 + m_{22}(q_2)\ddot{q}_2 + c_2(q, \dot{q}) + g_2(q_1, q_2) = u \quad (6.2b)$$

For the second case, partitioning the configuration vector $q \in \mathfrak{R}^n$ into actuated $q_1 \in \mathfrak{R}^m$ and unactuated $q_2 \in \mathfrak{R}^{n-m}$ configuration vectors, the nominal dynamics

in Eq. (6.1) take the form:

$$m_{11}(q_2)\ddot{q}_1 + m_{12}(q_2)\ddot{q}_2 + c_1(q, \dot{q}) + g_1(q_1, q_2) = u \quad (6.3a)$$

$$m_{21}(q_2)\ddot{q}_1 + m_{22}(q_2)\ddot{q}_2 + c_2(q, \dot{q}) + g_2(q_1, q_2) = 0 \quad (6.3b)$$

Remark 6.1. Systems described by Equation (6.2) in which the the Inertia Matrix is independent of the unactuated configuration variable q_1 were classified as Class-I underactuated mechanical systems in [94].

Remark 6.2. The Inertia-Wheel Pendulum, the TORA system, and the Acrobot are examples of underactuated mechanical systems described by Eq. (6.2) with $n = 2$, $m = 1$.

Remark 6.3. Systems described by Equation (6.3) in which the the Inertia Matrix depends on the unactuated configuration variable q_2 were classified as Class-II underactuated mechanical systems in [94].

Remark 6.4. The Furuta Pendulum, the Overhead Crane, the Cart-Pole system, the Pendubot, and the Beam-and-Ball system are examples of underactuated mechanical systems described by Eq. (6.3) with $n = 2$, $m = 1$.

Remark 6.5. In general, the dynamics in Eq. (6.2) and Eq. (6.3) are a set of n interconnected second order nonlinear subsystems and it is well known that the direct state space representations of Eq. (6.2) and Eq. (6.3) are not suitable for control design purposes even in the absence of uncertainties.

For notational simplicity, henceforth, omit the dependence of $m_{11}(q_2)$, $m_{12}(q_2)$, $m_{21}(q_2)$, $m_{22}(q_2)$, $c_1(q, \dot{q})$, $c_2(q, \dot{q})$, $g_1(q_1, q_2)$ and $g_2(q_1, q_2)$ on states. The functional dependence of these paramteres are shown in Chapter 3 for the application examples.

6.2 Smooth HOSM Design for Class-I Underactuated Mechanical Systems

Consider Class-I underactuated mechanical systems described by:

$$m_{11}(q_2)\ddot{q}_1 + m_{12}(q_2)\ddot{q}_2 + c_1(q, \dot{q}) + g_1(q_1, q_2) = 0 \quad (6.4a)$$

$$m_{21}(q_2)\ddot{q}_1 + m_{22}(q_2)\ddot{q}_2 + c_2(q, \dot{q}) + g_2(q_1, q_2) = u \quad (6.4b)$$

Using the following collocated partial feedback linearizing control:

$$u = (m_{22} - m_{21}m_{11}^{-1}m_{12})v + c_2 + g_2 - m_{21}m_{11}^{-1}(c_1 + g_1) \quad (6.5)$$

where v is a new control input, and the nonlinear coordinate transformation [96]:

$$\begin{aligned} z_1 &= q_1 + \psi(q_2) \\ z_2 &= m_{11}(q_2)\dot{q}_1 + m_{12}(q_2)\dot{q}_2 \\ \xi_1 &= q_2 \\ \xi_2 &= \dot{q}_2 \\ \psi(q_2) &= \int_0^{q_2} m_{11}^{-1}(\theta)m_{12}(\theta)d\theta \end{aligned} \quad (6.6)$$

transforms the dynamics in Eq. (6.4) into the following *strict feedback normal form*:

$$\begin{aligned} \dot{z}_1 &= m_{11}^{-1}(\xi_1)z_2 \\ \dot{z}_2 &= -g_1(z_1 - \psi(\xi_1), \xi_1) \\ \dot{\xi}_1 &= \xi_2 \\ \dot{\xi}_2 &= v \end{aligned} \quad (6.7)$$

which can be written, alternatively, as

$$\begin{aligned} \ddot{z} &= -m_{11}^{-1}(\xi)g_1(z - \psi(\xi), \xi) - m_{11}^{-1}(\xi)\dot{m}_{11}(\xi)\dot{z}\dot{\xi} \\ \ddot{\xi} &= v \end{aligned} \quad (6.8)$$

where \prime denotes d/dq_2 .

In general, the normal form (6.8) comprises a block of $(n - m)$ second order *nonlinear unactuated z -subsystems* and a block of m second order *linear actuated ξ -subsystems*. The beauty of the normal form is that, with ξ as output with global uniform relative degree two, the first block represents the *Lagrangian zero dynamics* for the second block. Treating ξ as control input for the first block, the form reduces the control of the original underactuated nonlinear system (6.4) to the control of the reduced order z -subsystem in (6.8).

Remark 6.6. The explicit transformation (6.6) applies to two degrees of freedom underactuated mechanical systems. Higher order systems can be reduced to form (6.8) through the procedure outlined in [94].

To stabilize the nonlinear underactuated dynamics in Eq. (6.4), we design sliding manifold and sliding mode control to stabilize its transformed normal form in Eq. (6.8) rewritten as:

$$\ddot{z} = f(z, \dot{z}, \xi, \dot{\xi}) \quad (6.9a)$$

$$\ddot{\xi} = v + D(z, \dot{z}, \xi, \dot{\xi}, t) \quad (6.9b)$$

where $z \in \mathfrak{R}^{(n-m)}$, $\xi \in \mathfrak{R}^m$, and $D(z, \dot{z}, \xi, \dot{\xi}, t)$ represents the lumped effect of all uncertainties after transformation.

The following assumptions are taken into account in the design of sliding manifold and sliding mode control.

Assumption 6.1. The origin in the system state space is an equilibrium point of the open loop Lagrangian zero dynamics subsystem (6.9a), i.e., $f(0, 0, 0, 0) = 0$.

The existence of well defined relative degree requires

$$\text{Assumption 6.2. } \frac{\partial f}{\partial \xi} \neq 0.$$

$$\text{Assumption 6.3. } \frac{\partial f}{\partial \xi} \neq 0.$$

In addition, we have,

Assumption 6.4. The transformed uncertainties $D(z, \dot{z}, \xi, \dot{\xi}, t)$ is bounded as $\left|D(z, \dot{z}, \xi, \dot{\xi}, t)\right| \leq D_0$.

Remark 6.7. Most underactuated mechanical systems have natural (open loop) equilibrium points including the origin and it is reasonable to expect that Assumption 6.1 will hold for these system. Assumptions 6.2, 6.3 are related to system dynamics and must be checked for the system in case. The loss of well defined relative degree at the origin for the Beam-and-Ball system is well known. This is discussed in Section 6.3.2.9 for the Beam-and-Ball system. Assumption 6.4 is reasonable to hold in any practical scenario.

The next section presents the design of sliding manifold and sliding mode control for the stabilization of system (6.9).

6.2.1 Nonlinear Sliding Manifolds and Control Law Design

Here assume that stabilization of (6.9b) does not imply stabilization of the overall system (6.9). This is true in general and for underactuated mechanical systems in specific. Hence, stabilization of (6.9) through stabilization of (6.9a) is investigated. To make the z -subsystem (6.9a) stable, the following condition is needed to be satisfied

$$f(z, \dot{z}, \xi, \dot{\xi}) = -\alpha\dot{z} - \beta z \quad (6.10)$$

with $\alpha > 0$, $\beta > 0$ as design constants. To meet condition (6.10) design the sliding manifold as:

$$\sigma = f(z, \dot{z}, \xi, \dot{\xi}) + \alpha\dot{z} + \beta z \quad (6.11)$$

When sliding mode is established, $\sigma = 0$, in (6.11), condition (6.10) is met and the dynamics in (6.9a) become

$$\ddot{z} + \alpha\dot{z} + \beta z = 0 \quad (6.12)$$

which is a stable linear system for $\alpha > 0$, $\beta > 0$ and hence z , \dot{z} converge to zero with convergence rate determined by the choice of design constants α , β .

To achieve the desired dynamics (6.12) for the z -subsystem a sliding mode control law is needed to enforce sliding mode in the manifold (6.11). The design of sliding mode control law depends on the relative degree of system (6.11). The relative degree is determined whether sliding variable σ or the function f explicitly depends on $\dot{\xi}$ or not as investigated below.

Case A. The sliding variable σ explicitly depends on $\dot{\xi}$:

In this case, the relative degree of system (6.11) is 1. Take the time derivative of σ in (6.11) along the dynamics (6.9) to get:

$$\dot{\sigma} = a(z, \dot{z}, \xi, \dot{\xi}) + w \quad (6.13)$$

where

$$a(z, \dot{z}, \xi, \dot{\xi}) = \left(\frac{\partial f}{\partial z} + \beta \right) \dot{z} + \left(\frac{\partial f}{\partial \dot{z}} + \alpha \right) f(z, \dot{z}, \xi, \dot{\xi}) + \frac{\partial f}{\partial \xi} \dot{\xi} + \frac{\partial f}{\partial \dot{\xi}} D(z, \dot{z}, \xi, \dot{\xi}, t) \quad (6.14)$$

$$w = b(z, \dot{z}, \xi, \dot{\xi})v \quad (6.15)$$

$$b(z, \dot{z}, \xi, \dot{\xi}) = \frac{\partial f}{\partial \dot{\xi}} \quad (6.16)$$

One choice for the control law to enforce sliding mode in relative degree 1 system (6.13) is the following standard SMC law

$$w = - \left(\left(\frac{\partial f}{\partial z} + \beta \right) \dot{z} + \left(\frac{\partial f}{\partial \dot{z}} + \alpha \right) f(z, \dot{z}, \xi, \dot{\xi}) + \frac{\partial f}{\partial \xi} \dot{\xi} + \left| \frac{\partial f}{\partial \dot{\xi}} \right| D_0 \text{sign}(\sigma) + K \text{sign}(\sigma) \right) \quad (6.17)$$

where K is a strictly positive design constant.

The above standard SMC law, which consists of an equivalent control term and a discontinuous term, can be proved by taking the Lyapunov function candidate $V = \frac{1}{2}\sigma^2$ for (6.13) and taking its time derivative along the dynamics (6.9). However the standard SMC law (6.17) suffers from chattering which is undesired especially for mechanical control systems. Furthermore, the above standard SMC law can not be applied if the relative degree of the system is not 1.

To avoid chattering a control law is needed that is smooth and, furthermore, to deal with internal uncertainties and external disturbances the control law must be robust. The following well known Smooth Super-Twisting Algorithm (SSTA) based sliding mode control law [153] is chosen to enforce sliding mode in relative degree 1 system (6.13):

$$\begin{aligned} w &= -s_1 - K_1|\sigma|^{m/(m+1)}\text{sign}(\sigma) + w_0 \\ \dot{w}_0 &= -K_2|\sigma|^{(m-1)/(m+1)}\text{sign}(\sigma) \end{aligned} \quad (6.18)$$

where $m \geq 1$ and $K_1 > 0$, $K_2 > 0$ are design constants.

The term $s_1 = \hat{a}(z, \dot{z}, \xi, \dot{\xi})$ in (6.18) is used to cancel the the uncertain bounded term $a(z, \dot{z}, \xi, \dot{\xi})$ in (6.13) and is estimated via the following observer [153] ($m = 2$):

$$\begin{aligned} \dot{s}_0 &= v_0 + w \\ v_0 &= -\lambda_0|\Lambda|^{1/3}|s_0 - \sigma|^{2/3}\text{sign}(s_0 - \sigma) + s_1 \\ \dot{s}_1 &= v_1 \\ v_1 &= -\lambda_1|\Lambda|^{1/2}|s_1 - v_0|^{1/2}\text{sign}(s_1 - v_0) + s_2 \\ \dot{s}_2 &= -\lambda_2|\Lambda|\text{sign}(s_2 - v_1) \end{aligned} \quad (6.19)$$

where $\lambda_0, \lambda_1, \lambda_2$ are design parameters and $\Lambda > 0$ is Lipshitz constant of $\hat{a}(z, \dot{z}, \xi, \dot{\xi})$.

Lemma 6.8. *The closed loop system (6.13), (6.18), (6.19) is finite time stable and hence $\sigma, \dot{\sigma}$ converge to 0 in finite time.*

Proof. The proof can be found in [153]. □

Once sliding mode is established, $\sigma = 0$, condition (6.10) is met and z, \dot{z} converge to zero in accordance with (6.12). With $(z = 0, \dot{z} = 0)$ the Lagrangian zero dynamics are given by (6.9a):

$$f(0, 0, \xi, \dot{\xi}) = 0 \quad (6.20)$$

If the *first order zero dynamics* in (6.20) are stable (see Assumption 4.1) then stabilization of the z -subsystem (6.9a) will render the overall system (6.9) stable.

Remark 6.9. Eqs. (6.13), (6.15) and (6.16) and hence the control laws (6.17) and (6.18) needs the validity of Assumption 4.2.

Case B. The sliding variable σ does not explicitly depend on $\dot{\xi}$

In this case the relative degree of system (6.11) is 2. Take twice the time derivative of σ in (6.11) along the dynamics (6.9) to achieve:

$$\ddot{\sigma} = a(z, \dot{z}, \xi, \dot{\xi}) + w \quad (6.21)$$

where

$$\begin{aligned} a(z, \dot{z}, \xi, \dot{\xi}) = & \frac{\partial^2 f}{\partial z^2} \dot{z}^2 + \frac{\partial^2 f}{\partial z^2} f^2 + \frac{\partial^2 f}{\partial \xi^2} \dot{\xi}^2 + 2 \frac{\partial^2 f}{\partial z \partial \dot{z}} f \dot{z} + 2 \frac{\partial^2 f}{\partial z \partial \xi} \dot{z} \dot{\xi} + 2 \frac{\partial^2 f}{\partial z \partial \xi} f \dot{\xi} \\ & + \left(\frac{\partial f}{\partial z} + \beta \right) f + \left(\frac{\partial f}{\partial \dot{z}} + \alpha \right) \left(\frac{\partial f}{\partial z} \dot{z} + \frac{\partial f}{\partial \dot{z}} f + \frac{\partial f}{\partial \xi} \dot{\xi} \right) \\ & + \frac{\partial f}{\partial \xi} D(z, \dot{z}, \xi, \dot{\xi}, t) \end{aligned} \quad (6.22)$$

$$w = b(z, \dot{z}, \xi, \dot{\xi})v \quad (6.23)$$

$$b(z, \dot{z}, \xi, \dot{\xi}) = \frac{\partial f}{\partial \xi} \quad (6.24)$$

The following Smooth Second Order Sliding Mode (SSOSM) control law [154] is chosen to enforce sliding mode in relative degree 2 system (6.21):

$$w = -s_2 - K_1 |\sigma|^{(\rho-2)/\rho} \text{sign}(\sigma) - K_2 |\dot{\sigma}|^{(\rho-2)/(\rho-1)} \text{sign}(\dot{\sigma}) \quad (6.25)$$

where $\rho \geq 2$ and $K_1 > 0$, $K_2 > 0$ are design constants.

The term $s_2 = \hat{a}(z, \dot{z}, \xi, \dot{\xi})$ in the control law (6.25) is used to cancel the the uncertain bounded term $a(z, \dot{z}, \xi, \dot{\xi})$ in (6.21) and is estimated via the observer [154] ($m = 2$):

$$\begin{aligned} \dot{s}_0 &= s_1 \\ \dot{s}_1 &= v_1 + w \\ v_1 &= -\lambda_2 |\Lambda|^{1/3} |s_1 - \dot{\sigma}|^{2/3} \text{sign}(s_1 - \dot{\sigma}) + s_2 \\ \dot{s}_2 &= -\lambda_1 |\Lambda| \text{sign}(s_2 - v_1) \end{aligned} \quad (6.26)$$

where λ_2 and λ_1 are design parameters and $\Lambda > 0$ is Lipschitz constant of $\ddot{a}(z, \dot{z}, \xi, \dot{\xi})$. Further the observer also estimate $\dot{\sigma}$ as $s_1 = \hat{\dot{\sigma}}$.

Lemma 6.10. *The closed loop system (6.21), (6.25), (6.26) is finite time stable and hence $\sigma, \dot{\sigma}$ converge to 0 in finite time.*

Proof. The proof can be found in [154]. □

Once sliding mode is established, $\sigma = 0$, condition (6.10) is met and z, \dot{z} converge to zero in accordance with (6.12). With $(z = 0, \dot{z} = 0)$ the Lagrangian zero dynamics are given by (6.9a):

$$f(0, 0, \xi) = 0 \tag{6.27}$$

which is an *algebraic equation*. By Assumption 4.1 $f(0, 0, 0) = 0$ and the solution to this equation is $\xi = 0$ and hence ξ tends to zero as well and, consequently, the overall system (6.9) becomes stable.

Remark 6.11. Eqs. (6.21), (6.23) and (6.24) and hence the control law (6.25) needs the validity of Assumption 4.3.

The next section presents illustrative design examples.

6.2.2 Application to Class-I Underactuated Mechanical Systems

We apply the results to the Inertia-Wheel Pendulum, the TORA system, and the Acrobot.

6.2.2.1 The Inertia-Wheel Pendulum (IWP)

Figure 3.1c shows the schematics of IWP. Choose the physical parameters of IWP according to [13, 94, 167] as:

$$m_{11} = I_1 + I_2 + m_1 l_1^2 + m_2 L_1^2 = 4.83 \times 10^{-3} \text{ (kg.m}^2 \text{)}, m_{12} = m_{21} = m_{22} = I_2 =$$

32.0×10^{-6} (kg.m²), $m_1 l_1 + m_2 L_1 = 38.7 \times 10^{-3}$ (kg.m), and $g = 9.8$ (m.sec⁻²).

According to Eqs. (3.10) and (6.4), the nominal dynamics of the IWP are:

$$m_{11}(q_2)\ddot{q}_1 + m_{12}(q_2)\ddot{q}_2 - (m_1 l_1 + m_2 L_1)g \sin(q_1) = 0 \quad (6.28a)$$

$$m_{21}(q_2)\ddot{q}_1 + m_{22}(q_2)\ddot{q}_2 = u \quad (6.28b)$$

Using the input and state transformations in (6.5) and (6.6), the normal form in Eq. (6.9) for the IWP is:

$$\ddot{z} = k_1 \sin(z - k_2 \xi) \quad (6.29a)$$

$$\ddot{\xi} = v \quad (6.29b)$$

where $k_1 = m_{11}^{-1}(m_1 l_1 + m_2 L_1)g$, $k_2 = m_{11}^{-1}m_{12}$.

Choose the nonlinear sliding manifold, in accordance with Eq. (6.11) as the following

$$\sigma = k_1 \sin(z - k_2 \xi) + \alpha \dot{z} + \beta z \quad (6.30)$$

Note that σ does not explicitly depends on $\dot{\xi}$, the relative degree of system (6.30) is 2 and the design Case B is applicable.

In terms of coordinates $(q_1, \dot{q}_1, q_2, \dot{q}_2)$ of the IWP (6.28) we have

$$\sigma = \alpha (\dot{q}_1 + k_2 \dot{q}_2) + k_1 \sin(q_1) + \beta (q_1 + k_2 q_2) \quad (6.31)$$

$$\dot{\sigma} = (k_1 \cos(q_1) + \beta) (\dot{q}_1 + k_2 \dot{q}_2) + k_1 \alpha \sin(q_1) - k_1 k_2 \dot{q}_2 \cos(q_1) \quad (6.32)$$

In Eq. (6.23), $b(z, \dot{z}, \xi, \dot{\xi})$ in terms of $(q_1, \dot{q}_1, q_2, \dot{q}_2)$ is:

$$b(q_1, \dot{q}_1, q_2, \dot{q}_2) = k_1 k_2 \cos(q_1) \quad (6.33)$$

The final real control u for the IWP (6.28) is given by (6.5) with v given by (6.23) and w given by (6.25) and (6.26). Fig. 6.1 shows simulation results for the IWP further discussed in the next section.

6.2.2.2 Performance Analysis of The IWP

Figure 6.1 shows closed loop response of the IWP with control law (6.25) in the presence of external disturbance and parametric variations. The controller gains are chosen as $K_1 = 500$, $K_2 = 400$, observer gain as $\lambda_1 = 2$, $\lambda_2 = 3$ and the sliding parameters as $\alpha = 3$, $\beta = 2$. Parametric variations is chosen as 25% decrease from $t = 4$ (s) to $t = 6$ (s) and 25% increase from $t = 6$ (s) to $t = 8$ (s). The matched disturbance $d(t) = 0.1 \sin(\pi t)$ is applied to system at time intervals shown in Figure 6.1c.

The controller successfully stabilizes the IWP from its downward position $q_1 = \pi/3$ to the upward unstable equilibrium position $q_1 = 0$ in 4 seconds. The Wheel comes to rest in less than 7 seconds. The results are similar to those obtained with SMC law 4.12 and STA (5.14) but the attractive region is limited to $q_1 = \pi/2$ due to singularity at $q_1 = \pi/2$ in the control law Eq. (6.33). The controller is able to keep the system stable at its unstable equilibrium position in the presence of wide parametric variations. Disturbance rejection is also good and reflected by a similar opposite corrective action in the control in the Figure 6.1e. Moreover, the control action is smooth that is necessary for mechanical control systems, and hence, is an obvious great advantage over standard SMC and STA control laws.

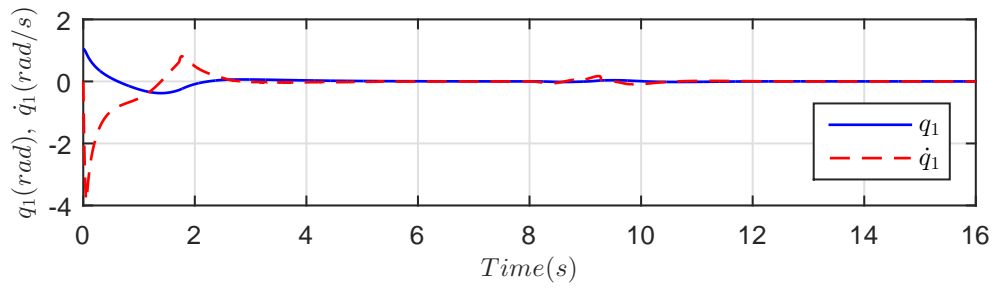
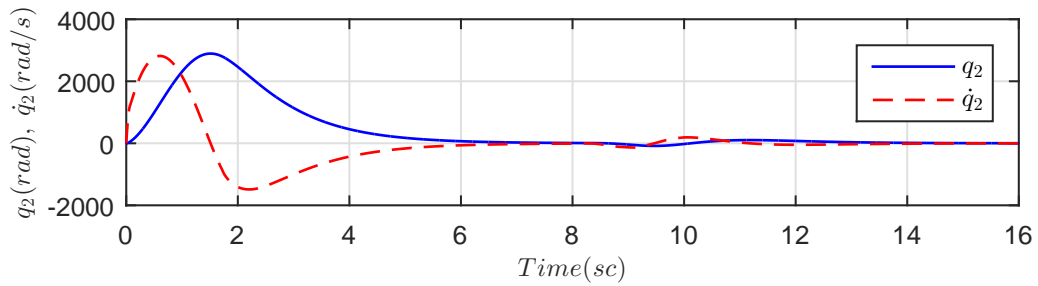
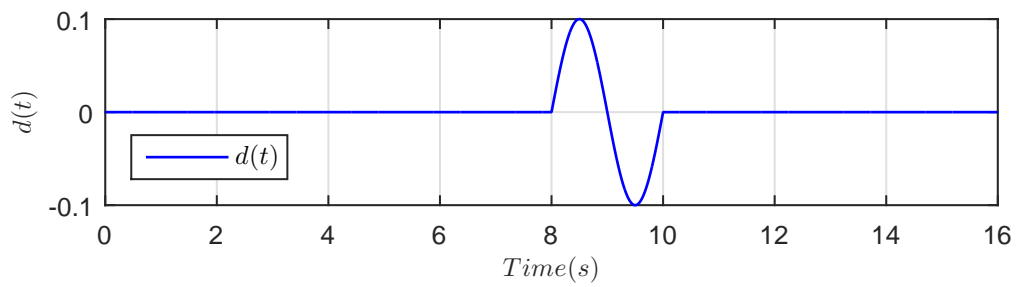
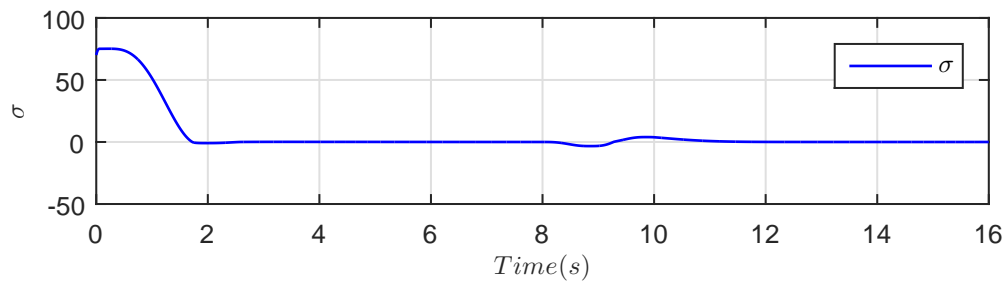
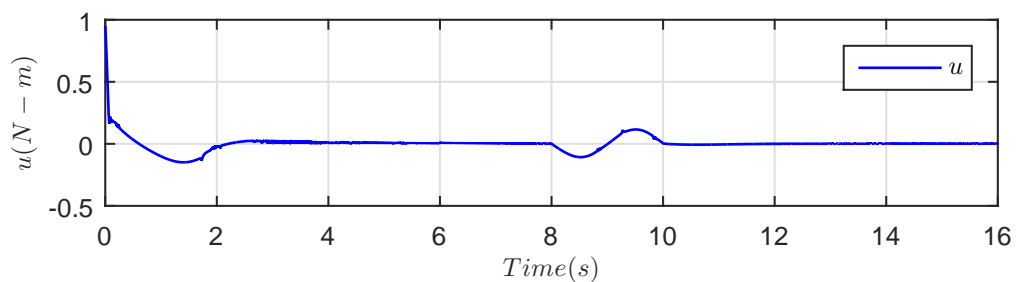
(A) Pendulum position q_1 (rad) and velocity \dot{q}_1 (rad/s)(B) Wheel position q_2 (rad) and velocity \dot{q}_2 (rad/s)(C) Disturbance $d(t) = 0.1 \sin(\pi t)$ (D) Sliding surface σ (E) Control effort u (N-m)

FIGURE 6.1: IWP - Closed loop response with control law (6.25) ($K_1 = 500$, $K_2 = 400$) and observer (6.26) ($\lambda_1 = 2$, $\lambda_2 = 3$), sliding parameters ($\alpha = 3$, $\beta = 2$), $q(0) = [\pi()/3, 0, 0, 0]^T$

6.2.2.3 The TORA System

Figure 3.1b shows the schematics of the TORA system. Choose the physical parameters of TORA as specified in [16] and used in [24]:

$$m_1 = 1.3608 \text{ (kg)}, m_2 = 0.096 \text{ (kg)}, I_2 = 0.0002175 \text{ (kg.m}^2\text{)}, r = 0.0592 \text{ (m)}, \\ k = 186.3 \text{ (N.m}^{-1}\text{)}, \varepsilon = 0.200.$$

According to Eqs. (3.9) and (6.4), the nominal dynamics of the TORA are:

$$(m_1 + m_2)\ddot{q}_1 + m_2 r \cos(q_2)\ddot{q}_2 - m_2 r \sin(q_2)\dot{q}_2^2 + kq_1 = 0 \quad (6.34a)$$

$$m_2 r \cos(q_2)\ddot{q}_1 + (I_2 + m_2 r^2)\ddot{q}_2 + m_2 r g \sin(q_2) = u \quad (6.34b)$$

Using the input and state transformations in (6.5) and (6.6), the normal form in Eq. (6.9) for the TORA is:

$$\ddot{z} = -k_1 z + k_2 \sin(\xi) \quad (6.35a)$$

$$\ddot{\xi} = v \quad (6.35b)$$

where $k_1 = \frac{k}{m_1 + m_2}$, $k_2 = \frac{km_2 r}{(m_1 + m_2)^2}$.

Note that in Eq. (6.35a), $k_1 > 0$, and hence the first term $-k_1 z$ on the right hand side is naturally helpful in the stabilization of the system. Therefore leave this term and choose the sliding manifold in accordance with Eq. (6.11) as the following:

$$\sigma = k_2 \sin(\xi) + \alpha \dot{z} \quad (6.36)$$

Note that σ does not explicitly depends on $\dot{\xi}$, the relative degree of system (6.36) is 2, and the design Case B is applicable.

In terms of coordinates $(q_1, \dot{q}_1, q_2, \dot{q}_2)$ of the TORA (6.34) we have

$$\sigma = k_2 \sin(q_2) + \alpha \left(\dot{q}_1 + \frac{m_2 r}{m_1 + m_2} \dot{q}_2 \cos(q_2) \right) \quad (6.37)$$

$$\dot{\sigma} = k_2 \dot{q}_2 \cos(q_2) + k_2 \alpha \sin(q_2) - k_1 \alpha \left(q_1 + \frac{m_2 r}{m_1 + m_2} \sin(q_2) \right) \quad (6.38)$$

In Eq. (6.23), $b(z, \dot{z}, \xi, \dot{\xi})$ in terms of $(q_1, \dot{q}_1, q_2, \dot{q}_2)$ is:

$$b(q_1, \dot{q}_1, q_2, \dot{q}_2) = k_2 \cos(q_2) \quad (6.39)$$

The final real control u for the TORA (6.34) is given by (6.5) with v given by (6.23) and w given by (6.25) and (6.26). Fig. 6.2 shows simulation results for the TORA further discussed in the next section.

6.2.2.4 Performance Analysis of The TORA System

Figure 6.2 shows closed loop response of the TORA system with control law (6.25) in the presence of parameter variations and external disturbance. The controller gains are chosen as $K_1 = 20$, $K_2 = 25$, observer gain as $\lambda_1 = 1.5$, $\lambda_2 = 2$ and the sliding parameters as $\alpha = 1.5$, $\beta = 0$. Parametric variations is chosen as 25% decrease from $t = 4$ (s) to $t = 6$ (s) and 25% increase from $t = 6$ (s) to $t = 8$ (s). The matched disturbance $d(t) = 0.025 \sin\left(\sqrt{\frac{k}{m_1}}t\right)$ is applied to system at time intervals shown in Figure 6.2c.

Stabilization is achieved similar to that achieved with SMC law 4.12 and STA (5.14). The controller successfully stabilizes the TORA system in less than 5 seconds with the nonlinear benchmark specifications [16] are met, i.e., the closed loop system is stable and the control effort is less than 0.05 N-m (specifications states less than 0.1 N-m continuous). The controller is able to withstand wide parametric variations. The effects of the disturbance on system stability are less compared to STA but greater than SMC. The great advantage is the smooth control action.

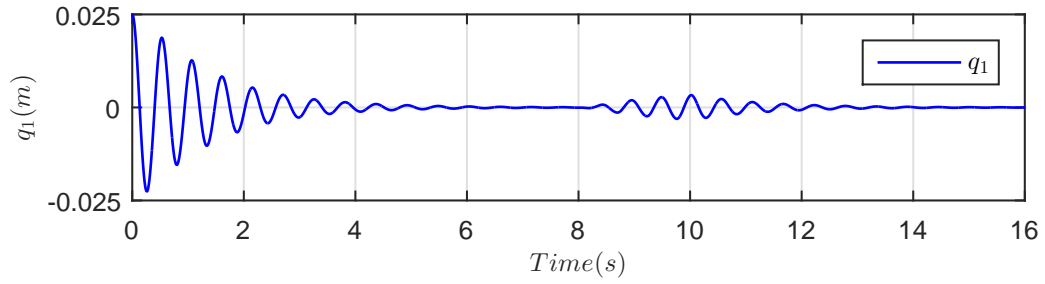
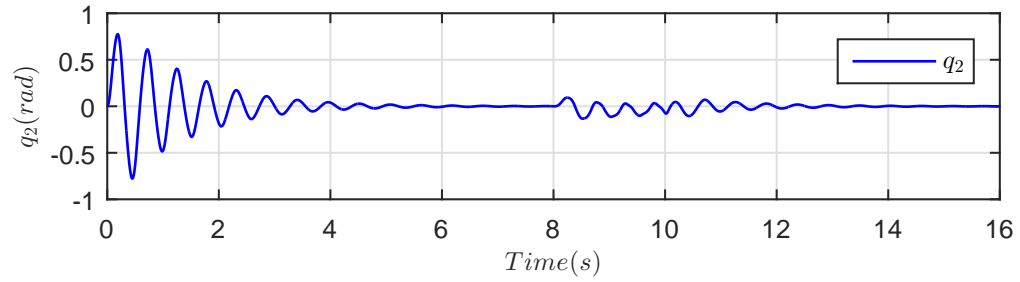
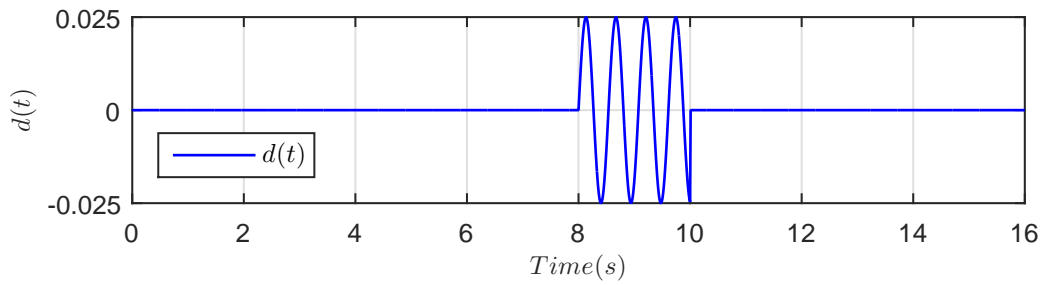
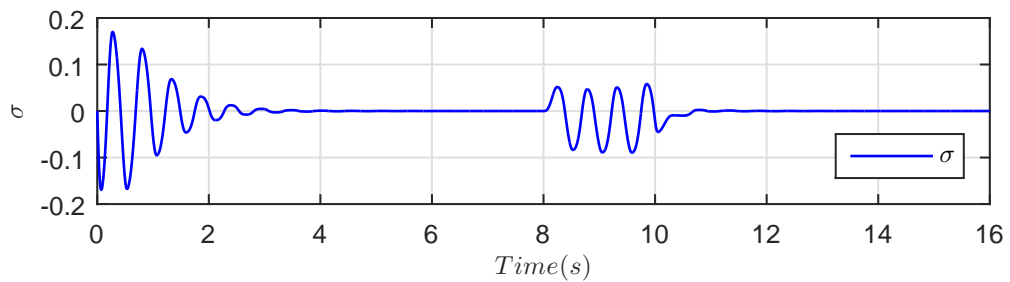
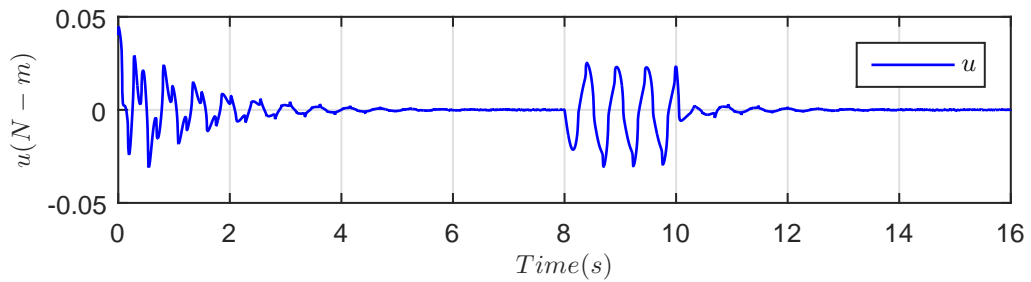
(A) Oscillator position q_1 (m)(B) Pendulum position q_2 (rad)(C) Disturbance $d(t) = 0.025 \sin\left(\sqrt{\frac{k}{m_1}}t\right)$ (D) Sliding surface σ (E) Control effort u (N-m)

FIGURE 6.2: TORA - Closed loop response with control law (6.25) ($K_1 = 20$, $K_2 = 25$) and observer (6.26) ($\lambda_1 = 1.5$, $\lambda_2 = 2$), sliding parameters ($\alpha = 1.5$, $\beta = 0$), $q(0) = [0.025, 0, 0, 0]^T$

6.2.2.5 The Acrobot

Figure 3.1a shows the schematics of Acrobot. Choose the physical parameters of Acrobot according to [27] as:

$$m_1 = 1 \text{ (kg)}, m_2 = 1 \text{ (kg)}, L_1 = 1 \text{ (m)}, L_2 = 2 \text{ (m)}, \ell_1 = 0.5 \text{ (m)}, \ell_2 = 1 \text{ (m)}, \\ I_1 = 0.083 \text{ (kg.m}^2\text{)}, I_2 = 0.33 \text{ (kg.m}^2\text{)}.$$

Expression for the nominal dynamics of the Acrobot are achieved by putting the following in Eq. (6.4):

$$\begin{aligned} m_{11}(q_2) &= m_1 \ell_1^2 + m_2(L_1^2 + \ell_2^2) + I_1 + I_2 + 2m_2 L_1 \ell_2 \cos(q_2) \\ m_{12}(q_2) &= m_2 \ell_2^2 + I_2 + m_2 L_1 \ell_2 \cos(q_2) \\ m_{21}(q_2) &= m_{12} \\ m_{22}(q_2) &= m_2 \ell_2^2 + I_2 \\ c_1(q_1, \dot{q}_1, q_2, \dot{q}_2) &= -m_2 L_1 \ell_2 \sin(q_2)(2\dot{q}_1 \dot{q}_2 + \dot{q}_2^2) \\ c_2(q_1, \dot{q}_1, q_2, \dot{q}_2) &= m_2 L_1 \ell_2 \sin(q_2) \dot{q}_1^2 \\ g_1(q_1, q_2) &= -(m_1 \ell_1 + m_2 L_1)g \sin(q_1) - m_2 \ell_2 g \sin(q_1 + q_2) \\ g_2(q_1, q_2) &= -m_2 \ell_2 g \sin(q_1 + q_2) \end{aligned} \tag{6.40}$$

Using the input and state transformations in (6.5) and (6.6), the normal form in Eq. (6.9) for the Acrobot is:

$$\ddot{z} = \frac{1}{a + b \cos(\xi)} \left(k_1 \sin(\varphi_1(z, \xi)) + k_2 \sin(\varphi_2(z, \xi)) + b \sin(\xi) \dot{\xi} \dot{z} \right) \tag{6.41a}$$

$$\ddot{\xi} = v \tag{6.41b}$$

where

$$\begin{aligned}
\varphi_1(z, \xi) &= z - \frac{\xi}{2} - w_1 \tan^{-1} \left(w_2 \tan \left(\frac{\xi}{2} \right) \right) \\
\varphi_2(z, \xi) &= z + \frac{\xi}{2} - w_1 \tan^{-1} \left(w_2 \tan \left(\frac{\xi}{2} \right) \right) \\
w_1 &= \frac{2c - a}{\sqrt{a^2 - b^2}} \\
w_2 &= \sqrt{\frac{a - b}{a + b}} \\
a &= m_1 \ell_1^2 + m_2 (L_1^2 + \ell_2^2) + I_1 + I_2 \\
b &= 2m_2 L_1 \ell_2 \\
c &= m_2 \ell_2^2 + I_2 \\
k_1 &= (m_1 \ell_1 + m_2 L_1)g \\
k_2 &= m_2 \ell_2 g
\end{aligned} \tag{6.42}$$

Note that in Eq. (6.41a), the denominator term $(a + b \cos(\xi))$ is strictly positive for $-\frac{\pi}{2} < \xi < \frac{\pi}{2}$ (always positive for the physical parameters used to avoid singularities in the transformations!), and hence, to achieve the stable system in Eq. (6.12), choose the sliding manifold in accordance with Eq. (6.11) as the following:

$$\sigma = k_1 \sin(\varphi_1(z, \xi)) + k_2 \sin(\varphi_2(z, \xi)) + \alpha \dot{z} + \beta z \tag{6.43}$$

The last term $b \sin(\xi) \dot{\xi} \dot{z}$ in Eq. (6.41a) is taken into account in controller synthesis but excluded in the design of sliding manifold in Eq. (6.43) for the following reasons:

1. including this term in the sliding manifold makes Assumption 6.3 invalid.
2. being a third order, is small near the origin.
3. the coefficient α of \dot{z} in the sliding manifold (6.43) can be chosen sufficiently large to dominate the state dependent coefficient $b \sin(\xi) \dot{\xi}$ of \dot{z} in this term.

Reasons (ii) and (iii) are crude assumptions but simulation results justify their validity.

Note that σ does not explicitly depends on $\dot{\xi}$, the relative degree of system (6.43) is 2, and the design Case B is applicable.

In terms of coordinates $(q_1, \dot{q}_1, q_2, \dot{q}_2)$ of the Acrobot (6.40) we have

$$\begin{aligned} \sigma = k_1 \sin(q_1) + k_2 \sin(q_1 + q_2) + \alpha \dot{q}_1 + \frac{\alpha \dot{q}_2 (1 + h_0)}{2} \\ + \beta \left(q_1 + \frac{q_2}{2} + w_1 \tan^{-1} (w_2 \tan (q_2/2)) \right) \end{aligned} \quad (6.44)$$

$$\dot{\sigma} = k_1 \dot{q}_1 \cos(q_1) + k_2 (\dot{q}_1 + \dot{q}_2) \cos(q_1 + q_2) + \beta \dot{q}_1 + \frac{\beta \dot{q}_2 (1 + h_0)}{2} + \alpha h_1 \quad (6.45)$$

In Eq. (6.23), $b(z, \dot{z}, \xi, \dot{\xi})$ in terms of $(q_1, \dot{q}_1, q_2, \dot{q}_2)$ is:

$$\begin{aligned} b(z, \dot{z}, \xi, \dot{\xi}) = \frac{1}{2} k_1 (-1 - h_0) \cos(q_1) + \frac{1}{2} k_2 (+1 - h_0) \cos(q_1 + q_2) \\ + \frac{\alpha b (2\dot{q}_1 + \dot{q}_2 (1 + h_0)) \sin(q_2)}{2a + 2b \cos(q_2)} \end{aligned} \quad (6.46)$$

where

$$h_0 = \frac{w_1 w_2 \sec^2 (q_2/2)}{1 + w_2^2 \tan^2 (q_2/2)}$$

$$h_1 = \frac{b \sin(q_2) \dot{q}_2 (2\dot{q}_1 + \dot{q}_2 (1 + h_0)) h_2 + 2k_1 \sin(q_1) + 2k_2 \sin(q_1 + q_2)}{2a + 2b \cos(q_2)}$$

The final real control u for the Acrobot (6.40) is given by (6.5) with v given by (6.23) and w given by (6.25) and (6.26). Fig. 6.3 shows simulation results for the Acrobot further discussed in the next section.

6.2.2.6 Performance Analysis of The Acrobot

Figure 6.3 shows closed loop response of the Acrobot with control law (6.25) in the presence of external disturbance and parameter variations. The controller gains are chosen as $K_1 = 75$, $K_2 = 50$, observer gain as $\lambda_1 = 1$, $\lambda_2 = 3$ and the sliding parameters as $\alpha = 8$, $\beta = 16$. Parametric variations is chosen as 25% decrease from $t = 4$ (s) to $t = 6$ (s) and 25% increase from $t = 6$ (s) to $t = 8$ (s). A large magnitude disturbance $d(t) = 4 \sin (\pi t)$ is applied to system at time intervals shown in Figure 6.3c.

The controller successfully stabilizes the Acrobot from the the initial position $q(0) = [-\frac{\pi}{6}, 0, \frac{\pi}{3}, 0]^T$ to the upward unstable equilibrium position $q_1 = 0$ in 5 seconds. The controller keep the system stable at its unstable position even in the presence of wide parametric variations and large external disturbance. The control action is smooth.

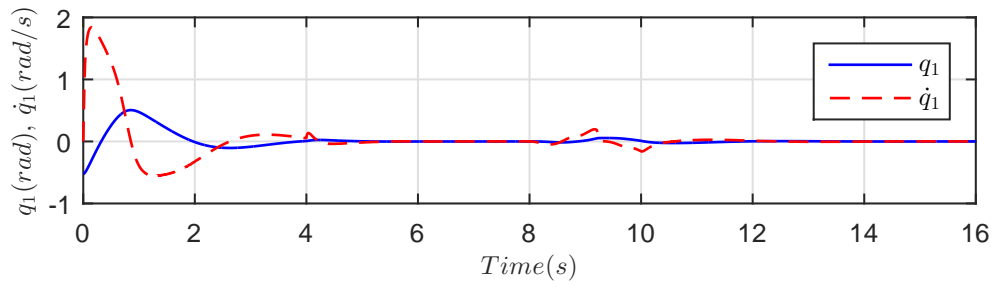
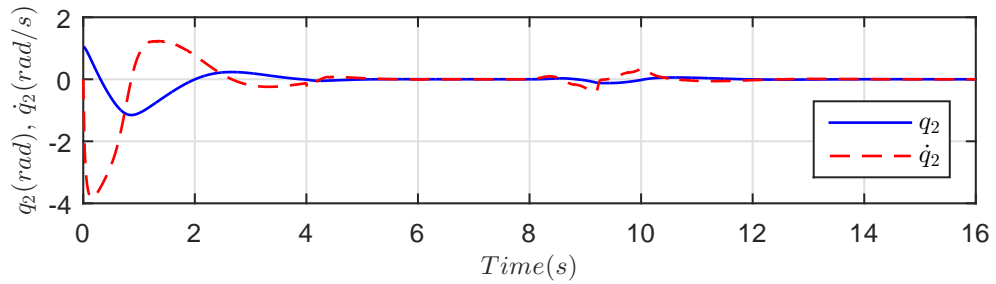
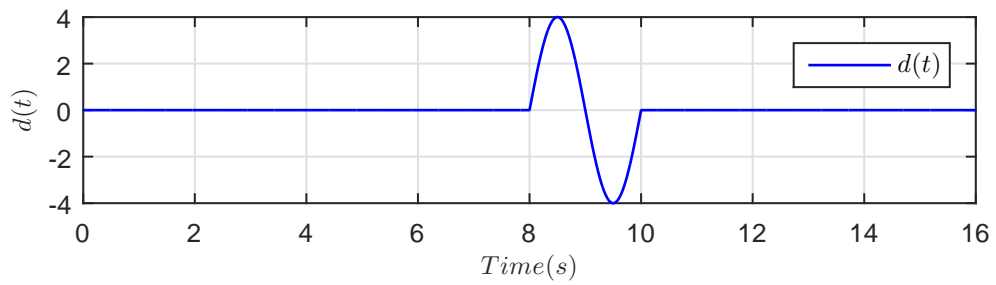
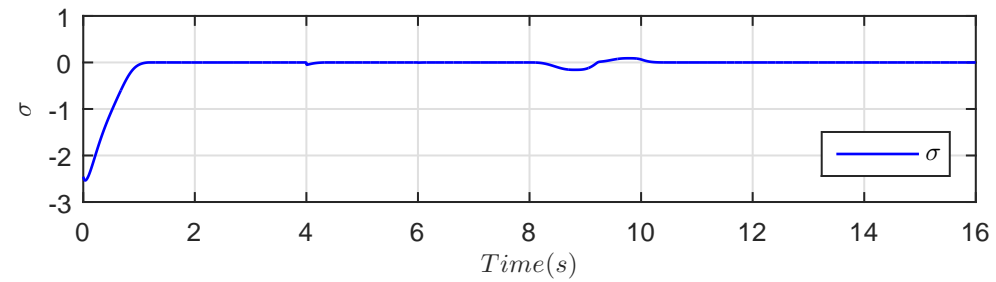
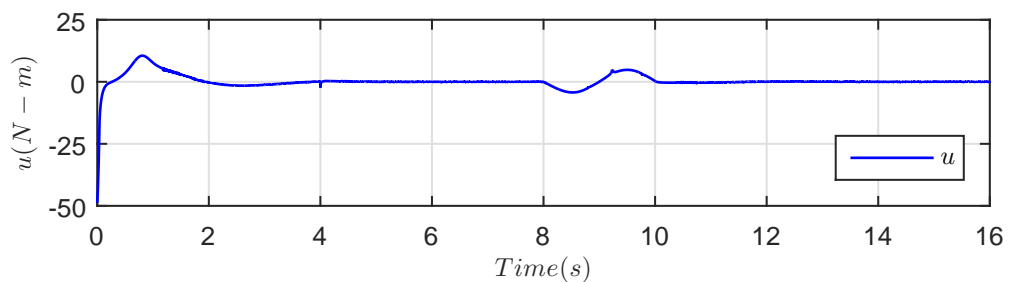
(A) Link 1 position q_1 (rad) and velocity \dot{q}_1 (rad/s)(B) Link 2 position q_2 (rad) and velocity \dot{q}_2 (rad/s)(C) Disturbance $d(t) = 4 \sin(\pi t)$ (D) Sliding surface σ (E) Control effort u (N-m)

FIGURE 6.3: Acrobot - Closed loop response with control law (6.25) ($K_1 = 75$, $K_2 = 50$) and observer (6.26) ($\lambda_1 = 1$, $\lambda_2 = 3$), sliding parameters ($\alpha = 8$, $\beta = 16$), $q(0) = [-\frac{\pi}{6}, 0, \frac{\pi}{3}, 0]^T$

6.3 Smooth HOSM Design for Class-II Underactuated Mechanical Systems

Consider Class-II underactuated mechanical systems described by:

$$m_{11}(q_2)\ddot{q}_1 + m_{12}(q_2)\ddot{q}_2 + c_1(q, \dot{q}) + g_1(q_1, q_2) = u \quad (6.47a)$$

$$m_{21}(q_2)\ddot{q}_1 + m_{22}(q_2)\ddot{q}_2 + c_2(q, \dot{q}) + g_2(q_1, q_2) = 0 \quad (6.47b)$$

Using the following collocated partial feedback linearizing control:

$$u = (m_{12} - m_{11}m_{21}^{-1}m_{22})v + c_1 + g_1 - m_{11}m_{21}^{-1}(c_2 + g_2) \quad (6.48)$$

where v is a new control input, and the nonlinear coordinate transformation [96]:

$$\begin{aligned} z_1 &= q_1 + \psi(q_2) \\ z_2 &= m_{21}(q_2)\dot{q}_1 + m_{22}(q_2)\dot{q}_2 \\ \xi_1 &= q_2 \\ \xi_2 &= \dot{q}_2 \\ \psi(q_2) &= \int_0^{q_2} m_{21}^{-1}(\theta)m_{22}(\theta)d\theta \end{aligned} \quad (6.49)$$

transforms the dynamics in Eq. (6.47) into the following *nontriangular quadratic normal form*:

$$\begin{aligned} \dot{z}_1 &= m_{21}^{-1}(\xi_1)z_2 \\ \dot{z}_2 &= -g_2(z_1 - \psi(\xi_1), \xi_1) + \frac{\dot{m}_{11}(\xi_1)}{2m_{21}^2(\xi_1)}z_2^2 + \left(\frac{\dot{m}_{21}(\xi_1)}{m_{21}(\xi_1)} - \frac{m_{22}(\xi_1)\dot{m}_{11}(\xi_1)}{m_{21}^2(\xi_1)} \right) z_2\xi_2 \\ &\quad + \left(\frac{m_{22}^2(\xi_1)}{2m_{21}^2(\xi_1)}\dot{m}_{11}(\xi_1) - \frac{m_{22}(\xi_1)}{m_{21}(\xi_1)}\dot{m}_{21}(\xi_1) + \frac{1}{2}\dot{m}_{22}(\xi_1) \right) \xi_2^2 \\ \dot{\xi}_1 &= \xi_2 \\ \dot{\xi}_2 &= v \end{aligned} \quad (6.50)$$

which can be written, alternatively, as

$$\begin{aligned}\ddot{z} &= -m_{21}^{-1}(\xi)g_2(z - \psi(\xi), \xi) + \frac{1}{2}\dot{m}_{11}(\xi)m_{21}^{-1}(\xi) \left(\dot{z} - m_{21}^{-1}(\xi)m_{22}(\xi)\dot{\xi} \right)^2 \\ &\quad - m_{21}^{-2}(\xi)\dot{m}_{21}(\xi)m_{22}(\xi)\dot{\xi}^2 + \frac{1}{2}m_{21}^{-1}(\xi)\dot{m}_{21}(\xi)\dot{\xi}^2 \\ \ddot{\xi} &= v\end{aligned}\tag{6.51}$$

where \prime denotes d/dq_2 .

In general, the normal form (6.51) comprises a block of (m) second order *nonlinear actuated z -subsystems* and a block of $n - m$ second order *linear unactuated ξ -subsystems*. The beauty of the normal form is that, with ξ as output with global uniform relative degree two, the first block represents the *Lagrangian zero dynamics* for the second block. Treating ξ as control input for the first block, the form reduces the control of the original underactuated nonlinear system (6.47) to the control of the reduced order z -subsystem in (6.51).

Remark 6.12. The explicit transformation (6.49) applies to two degrees of freedom underactuated mechanical systems. Higher order systems can be reduced to form (6.51) through the procedure outlined in [94].

To stabilize the nonlinear underactuated dynamics in Eq. (6.47), design sliding manifold and sliding mode control to stabilize its transformed normal form in Eq. (6.51) rewritten as:

$$\ddot{z} = f(z, \dot{z}, \xi, \dot{\xi})\tag{6.52a}$$

$$\ddot{\xi} = v + D(z, \dot{z}, \xi, \dot{\xi}, t)\tag{6.52b}$$

where $z \in \mathfrak{R}^{(m)}$, $\xi \in \mathfrak{R}^{(n - m)}$, and $D(z, \dot{z}, \xi, \dot{\xi}, t)$ represents the lumped effect of all uncertainties after transformation.

The normal form (6.52) is the same as (6.9) and consider here the same Assumptions 6.1-6.4. Remark 6.7 is applicable here too.

6.3.1 Nonlinear Sliding Manifold and Control Law Design

Since the general normal form (6.52) is the same as in (6.9), we apply the design procedure in Section 6.2.1.

6.3.2 Application to Class-II Underactuated Mechanical Systems

We apply the results the Furuta Pendulum, the Overhead Crane, the Cart-Pole system, the Pendubot, and the Beam-and-Ball system.

6.3.2.1 The Furuta Pendulum

Figure 3.2b shows the schematics of Furuta Pendulum. Choose the physical parameters of Furuta Pendulum according to [94] as:

$m_1 = 1.0$ (kg), $L_1 = 1.0$ (m), $\ell_1 = 0.5$ (m), $m_2 = 1.0$ (kg), $L_2 = 1.5$ (m), $\ell_2 = 0.75$ (m) and $g = 9.8$ (m.s⁻²).

According to Eqs. (3.13) and (6.47), the nominal dynamics of the Furuta Pendulum are:

$$\begin{aligned} (I_1 + m_1\ell_1^2 + m_2(L_1^2 + \ell_2^2 \sin^2(q_2))) \ddot{q}_1 + m_2L_1\ell_2 \cos(q_2)\ddot{q}_2 \\ + 2m_2\ell_2^2 \sin(q_2) \cos(q_2)\dot{q}_1\dot{q}_2 - m_2\ell_2L_1 \sin(q_2)\dot{q}_2^2 = u \end{aligned} \quad (6.53a)$$

$$\begin{aligned} m_2L_1\ell_2 \cos(q_2)\ddot{q}_1 + (I_2 + m_2\ell_2^2) \ddot{q}_2 \\ - m_2\ell_2^2 \sin(q_2) \cos(q_2)\dot{q}_1^2 - m_2\ell_2g \sin(q_2) = 0 \end{aligned} \quad (6.53b)$$

Using the input and state transformations in (6.48) and (6.49), the normal form in Eq. (6.52) for the Furuta Pendulum is:

$$\ddot{z} = \left(k_1 + k_2 \frac{(\dot{z} - k_3 \dot{\xi})^2}{\cos(\xi)} + k_4 \frac{\dot{\xi}^2}{\cos(\xi)} \right) \tan(\xi) \quad (6.54a)$$

$$\ddot{\xi} = v \quad (6.54b)$$

where $k_1 = \frac{g}{L_1}$, $k_2 = \frac{1}{m_2^2 L_1^3 \ell_2}$, $k_3 = (I_2 + m_2 \ell_2^2)$ and $k_4 = \frac{(I_2 + m_2 \ell_2^2)}{m_2 L_1 \ell_2}$.

Note that in (6.54a), the term in the parenthesis in front of $\tan(\xi)$ is strictly positive for $-\frac{\pi}{2} < \xi < \frac{\pi}{2}$, and hence to achieve the stable system in (6.12), Choose the nonlinear sliding manifold, in accordance with Eq. (6.11) as the following:

$$\sigma = \tan(\xi) + \alpha \dot{z} + \beta z \quad (6.55)$$

Note that σ does not explicitly depends on $\dot{\xi}$, the relative degree of system (6.55) is 2 and the design Case B is applicable.

In terms of coordinates $(q_1, \dot{q}_1, q_2, \dot{q}_2)$ of the Furuta Pendulum (6.53) we have

$$\sigma = \alpha \dot{q}_1 + \alpha k_4 \dot{q}_2 \sec(q_2) + \beta q_1 + \beta k_4 \ln(\sec(q_2) + \tan(q_2)) + \tan(q_2) \quad (6.56)$$

$$\begin{aligned} \dot{\sigma} = & \alpha k_2 (\alpha \dot{q}_1 + \alpha k_4 \dot{q}_2 \sec(q_2) - k_3 \dot{q}_2)^2 \sec(q_2) \tan(q_2) + \alpha k_1 \tan(q_2) \\ & + \alpha k_4 \dot{q}_2^2 \sec(q_2) \tan(q_2) + \dot{q}_2 \sec^2(q_2) + \alpha \beta \dot{q}_1 + \alpha \beta k_4 \dot{q}_2 \sec(q_2) \end{aligned} \quad (6.57)$$

In Eq. (6.23), $b(z, \dot{z}, \xi, \dot{\xi})$ in terms of $(q_1, \dot{q}_1, q_2, \dot{q}_2)$ is:

$$\begin{aligned} b(q_1, \dot{q}_1, q_2, \dot{q}_2) = & \sec^2(q_2) + 2\alpha \dot{q}_2 (k_4 + k_2 k_3^2) \sec(q_2) \tan(q_2) \\ & - 2\alpha k_2 k_3 (\dot{q}_1 + k_4 \dot{q}_2 \sec(q_2)) \sec(q_2) \tan(q_2) \end{aligned} \quad (6.58)$$

The final real control u for the Furuta Pendulum (6.53) is given by (6.48) with v given by (6.23) and w given by (6.25) and (6.26). Fig. 6.4 shows simulation results for the Furuta Pendulum further discussed in the next section.

6.3.2.2 Performance Analysis of The Furuta Pendulum

Figure 6.4 shows closed loop response of the Furuta Pendulum with control law (6.25) in the presence of external disturbance parametric variations. The controller gains are chosen as $K_1 = 25$, $K_2 = 20$, observer gain as $\lambda_1 = 1$, $\lambda_2 = 3$ and the sliding parameters as $\alpha = 0.3061$, $\beta = 0.2041$. Parametric variations is chosen as 25% decrease from $t = 4(\text{s})$ to $t = 6(\text{s})$ and 25% increase from $t = 6(\text{s})$ to $t = 8(\text{s})$. The matched disturbance $d(t) = 1 \sin(\pi t)$ is applied to system at time intervals shown in Figure 6.4c.

The controller successfully stabilizes the Furuta Pendulum to the upward unstable equilibrium position $q_1 = 0$ in 5 seconds. The controller is able to keep the system stable at its unstable equilibrium position in the presence of wide parametric variations. Disturbance rejection is also good and reflected by a similar opposite corrective action in the control in the Figure 6.4e. The control action is smooth that is necessary for mechanical control systems, and hence, is an obvious great advantage compared to SMC and STA design.

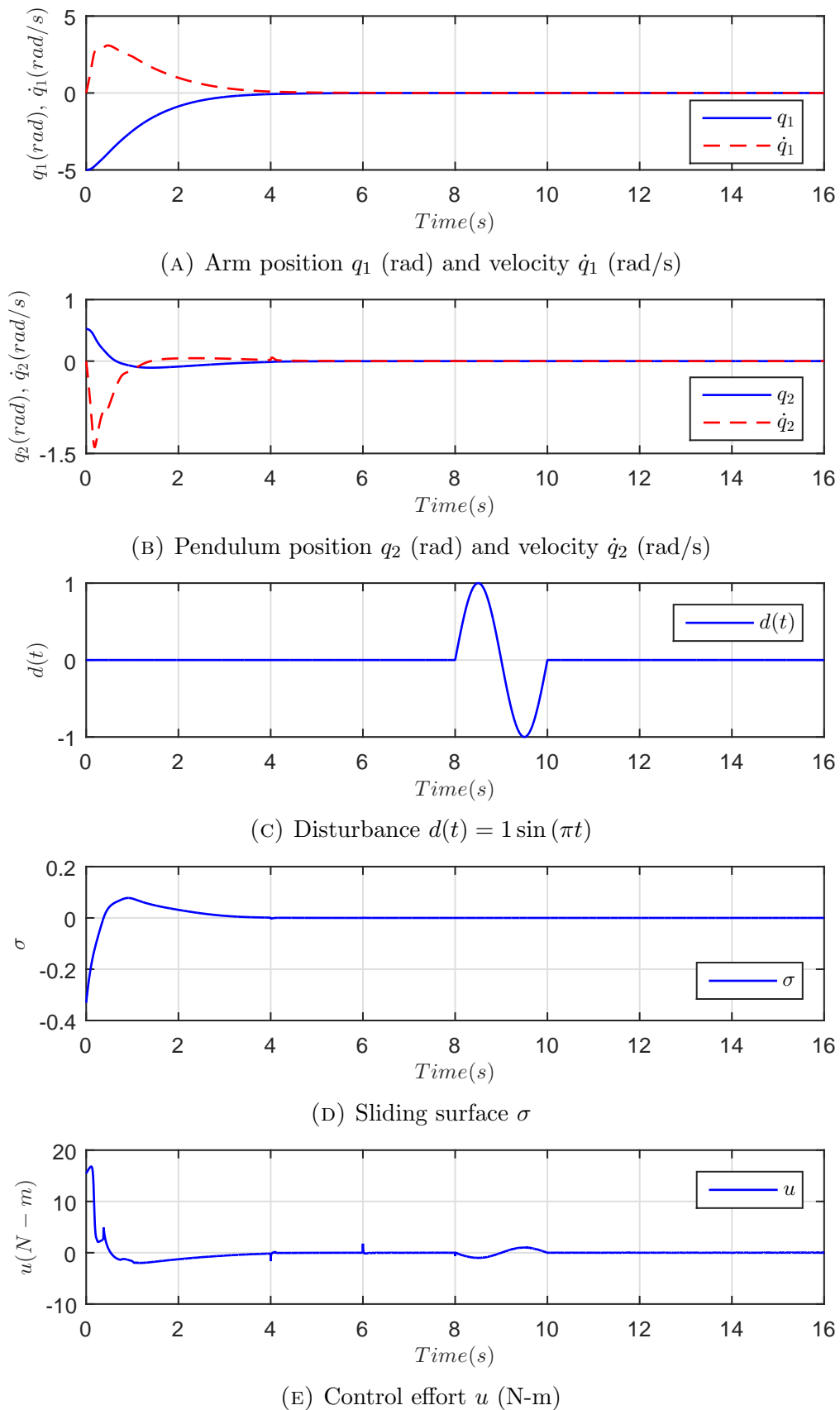


FIGURE 6.4: Furuta Pendulum - Closed loop response with control law (6.25) ($K_1 = 25$, $K_2 = 20$) and observer (6.26) ($\lambda_1 = 1$, $\lambda_2 = 3$), sliding parameters ($\alpha = 0.3061$, $\beta = 0.2041$), $q(0) = [-5, 0, \frac{\pi}{6}, 0]^T$

6.3.2.3 The Overhead Crane

Figure 3.2d shows the schematics of Overhead Crane. Choose the physical parameters of Overhead Crane according to [37] as:

$$M = 30.0 \text{ (kg)}, L = 2.0 \text{ (m)}, m = 20.0 \text{ (kg)}, \text{ and } g = 9.8 \text{ (m.s}^{-2}\text{)}.$$

According to Eqs. (3.15) and (6.47), the nominal dynamics of the Overhead Crane are:

$$(M + m)\ddot{q}_1 + mL \cos(q_2)\ddot{q}_2 - mL \sin(q_2)\dot{q}_2^2 = u \quad (6.59a)$$

$$mL \cos(q_2)\ddot{q}_1 + mL^2\ddot{q}_2 + mLg \sin(q_2) = 0 \quad (6.59b)$$

Using the input and state transformations in (6.48) and (6.49), the normal form in Eq. (6.52) for the Overhead Crane is:

$$\ddot{z} = \left(-g + L \frac{\dot{\xi}^2}{\cos(\xi)} \right) \tan(\xi) \quad (6.60a)$$

$$\ddot{\xi} = v \quad (6.60b)$$

Note that in (6.60a), the term $\left(-g + L \frac{\dot{\xi}^2}{\cos(\xi)} \right)$ is not strictly positive or negative. To solve this problem the following assumptions and explanation are presented.

First, for practical crane systems, the payload swing angle $q_2 = \xi$ is usually less than $\frac{\pi}{18}$ radians and the payload swing velocity $|\dot{q}_2| = |\dot{\xi}| < 1$ radians/second and hence $\frac{\dot{\xi}^2}{\cos(\xi)} \ll 1$. Second, assume $L < g$. Therefore $\left(-g + L \frac{\dot{\xi}^2}{\cos(\xi)} \right)$ can be assumed to be strictly negative.

With the above assumptions and explanation in hand, to achieve the stable system in (6.12), choose the nonlinear sliding manifold, in accordance with Eq. (6.11) as the following:

$$\sigma = \tan(\xi) - \alpha \dot{z} - \beta z \quad (6.61)$$

Note that σ does not explicitly depends on $\dot{\xi}$, the relative degree of system (6.61) is 2 and the design Case B is applicable.

In terms of coordinates $(q_1, \dot{q}_1, q_2, \dot{q}_2)$ of the Overhead Crane (6.59) we have

$$\sigma = -\alpha\dot{q}_1 - \alpha L\dot{q}_2 \sec(q_2) - \beta q_1 - \beta L \ln(\sec(q_2) + \tan(q_2)) + \tan(q_2) \quad (6.62)$$

$$\dot{\sigma} = \sec^2(q_2)\dot{q}_2 - \alpha(-g + L\dot{q}_2^2 \sec(q_2)) \tan(q_2) - \beta\dot{q}_1 - \beta L\dot{q}_2 \sec(q_2) \quad (6.63)$$

In Eq. (6.23), $b(z, \dot{z}, \xi, \dot{\xi})$ in terms of $(q_1, \dot{q}_1, q_2, \dot{q}_2)$ is:

$$b(q_1, \dot{q}_1, q_2, \dot{q}_2) = \sec^2(q_2) - 2\alpha L\dot{q}_2 \sec(q_2) \tan(q_2) \quad (6.64)$$

The final real control u for the Overhead Crane (6.59) is given by (6.48) with v given by (6.23) and w given by (6.25) and (6.26). Fig. 6.5 shows simulation results for the Overhead Crane further discussed in the next section.

6.3.2.4 Performance Analysis of The Overhead Crane

Figure 6.5 shows closed loop response of the Overhead Crane with control law (6.25) in the presence of external disturbance parametric variations. The controller gains are chosen as $K_1 = 1$, $K_2 = 1.6$, observer gain as $\lambda_1 = 1$, $\lambda_2 = 3$ and the sliding parameters as $\alpha = 0.2041$, $\beta = 0.1020$. Parametric variations is chosen as 10% decrease from $t = 4$ (s) to $t = 6$ (s) and 10% increase from $t = 6$ (s) to $t = 8$ (s). A large matched disturbance $d(t) = 10 \sin(\pi t)$ is applied to system at time intervals shown in Figure 6.5c.

The Crane successfully transports the payload to the desired position $q_{1des} = 20$ (m) in less than 12 seconds while the payload swing angle q_2 remains within the desired range of $|q_2| < \frac{\pi}{18} = 0.1745$ radians, i.e., within 10 degrees. Comparing to [37] the results are considerably improved. A desired position of 20(m) instead of 14(m) is achieved with the payload swing angle less than 10 degree instead of greater than 10 degree. The peak control force is less than 100(N) instead of greater than 200(N) and the peak velocity of the Crane is less than 5(m/s). The controller

withstands wide parametric variations and response is robust to large external disturbance. Moreover, the control action is smooth.

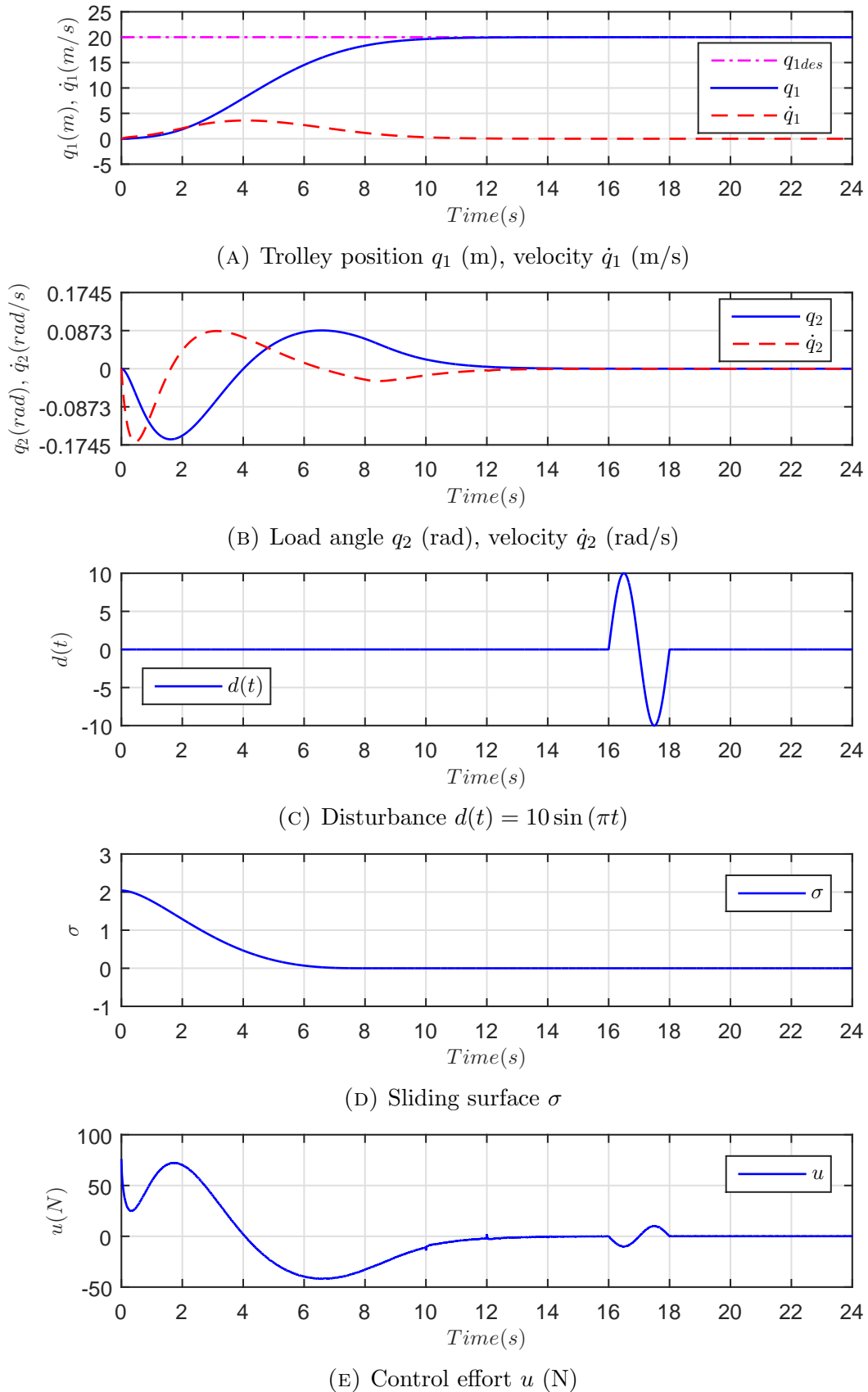


FIGURE 6.5: The Overhead Crane - Closed loop response with control law (6.25) ($K_1 = 1$, $K_2 = 1.6$) and observer (6.26) ($\lambda_1 = 1$, $\lambda_2 = 3$), sliding parameters ($\alpha = 0.2041$, $\beta = 0.1020$), $q(0) = [0, 0, 0, 0]^T$

6.3.2.5 The Cart-Pole System

Figure 3.2c shows the schematics of Cart-Pole system. Choose the physical parameters of Cart-Pole system according to [94] as:

$$m_1 = 1.0 \text{ (kg)}, m_2 = 1.0 \text{ (kg)}, \ell_2 = 0.75 \text{ (m)}, \text{ and } g = 9.8 \text{ (m.sec}^{-2}\text{)}.$$

According to Eqs. (3.14) and (6.47), the nominal dynamics of the Cart-Pole system are:

$$(m_1 + m_2)\ddot{q}_1 + m_2\ell_2 \cos(q_2)\ddot{q}_2 - m_2\ell_2 \sin(q_2)\dot{q}_2^2 = u \quad (6.65a)$$

$$m_2\ell_2 \cos(q_2)\ddot{q}_1 + (I_2 + m_2\ell_2^2)\ddot{q}_2 - m_2\ell_2g \sin(q_2) = 0 \quad (6.65b)$$

Using the input and state transformations in (6.48) and (6.49), the normal form in Eq. (6.52) for the Cart-Pole is:

$$\ddot{z} = \left(g + k_1 \frac{\dot{\xi}^2}{\cos(\xi)} \right) \tan(\xi) \quad (6.66a)$$

$$\ddot{\xi} = v \quad (6.66b)$$

where $k_1 = \frac{(I_2 + m_2\ell_2^2)}{m_2\ell_2}$.

Note that in (6.66a), the term $\left(g + k_1 \frac{\dot{\xi}^2}{\cos(\xi)} \right)$ is strictly positive for $-\frac{\pi}{2} < \xi < \frac{\pi}{2}$, and hence to achieve the stable system in (6.12), choose the nonlinear sliding manifold, in accordance with Eq. (6.11) as the following:

$$\sigma = \tan(\xi) + \alpha\dot{z} + \beta z \quad (6.67)$$

Note that σ does not explicitly depends on $\dot{\xi}$, the relative degree of system (6.67) is 2 and the design Case B is applicable.

In terms of coordinates $(q_1, \dot{q}_1, q_2, \dot{q}_2)$ of the Cart-Pole (6.65) we have

$$\sigma = \alpha\dot{q}_1 + \alpha k_1 \dot{q}_2 \sec(q_2) + \beta q_1 + \beta k_1 \ln(\sec(q_2) + \tan(q_2)) + \tan(q_2) \quad (6.68)$$

$$\dot{\sigma} = \sec^2(q_2)\dot{q}_2 + \alpha (g + k_1\dot{q}_2^2 \sec(q_2)) \tan(q_2) + \beta\dot{q}_1 + \beta k_1\dot{q}_2 \sec(q_2) \quad (6.69)$$

In Eq. (6.23), $b(z, \dot{z}, \xi, \dot{\xi})$ in terms of $(q_1, \dot{q}_1, q_2, \dot{q}_2)$ is:

$$b(q_1, \dot{q}_1, q_2, \dot{q}_2) = \sec^2(q_2) + 2\alpha k_1\dot{q}_2 \sec(q_2) \tan(q_2) \quad (6.70)$$

The final real control u for the Cart-Pole (6.65) is given by (6.48) with v given by (6.23) and w given by (6.25) and (6.26). Fig. 6.6 shows simulation results for the Cart-Pole further discussed in the next section.

6.3.2.6 Performance Analysis of The Cart-Pole System

Figure 6.6 shows closed loop response of the Cart-Pole with control law (6.25) in the presence of external disturbance parametric variations. The controller gains are chosen as $K_1 = 20$, $K_2 = 15$, observer gain as $\lambda_1 = 3$, $\lambda_2 = 5$ and the sliding parameters as $\alpha = 0.1531$, $\beta = 0.0510$. Parametric variations is chosen as 25% decrease from $t = 4$ (s) to $t = 6$ (s) and 25% increase from $t = 6$ (s) to $t = 8$ (s). The matched disturbance $d(t) = 5 \sin(\pi t)$ is applied to system at time intervals shown in Figure 6.6c.

The controller successfully stabilizes the Cart-Pole system in 12 seconds. The initial conditions in Figure 6.6 is the same as in [94]. Comparing to [94] the overshoot/undershoot in the Cart position and the Pole angle are considerably improved. Similarly the settling time and the undershoot in the control effort is improved. The controller is able to keep the system stable at its unstable equilibrium position in the presence of wide parametric variations. Disturbance rejection is also good and reflected by a similar opposite corrective action in the control in the Figure 6.6e. Moreover, control action is smooth as needed for mechanical control systems.

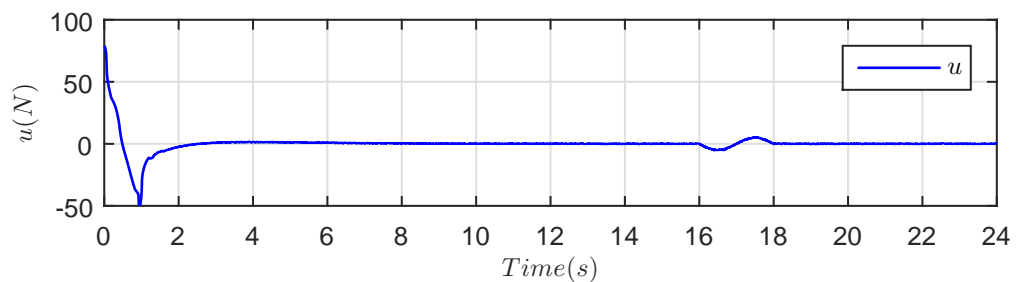
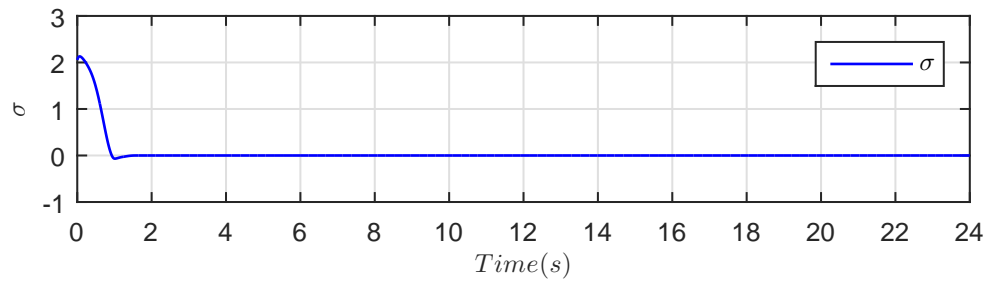
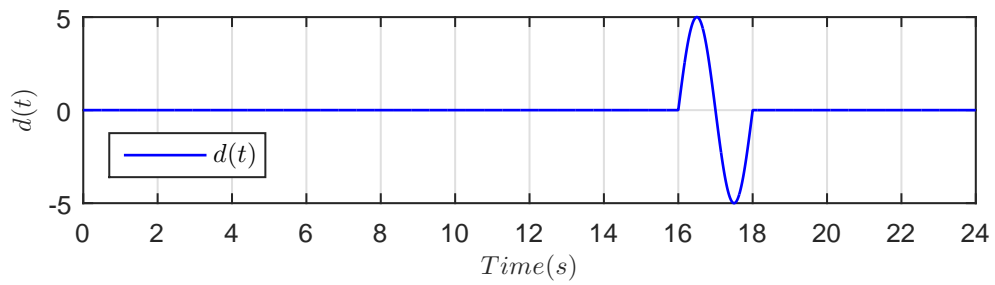
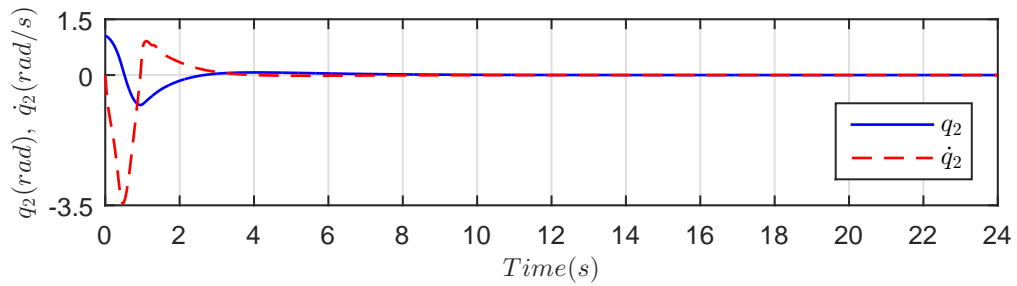
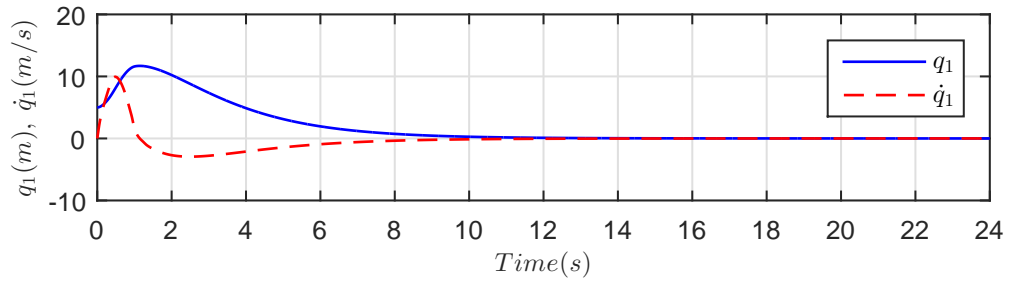


FIGURE 6.6: The Cart-Pole - Closed loop response with control law (6.25) ($K_1 = 20$, $K_2 = 15$) and observer (6.26) ($\lambda_1 = 3$, $\lambda_2 = 5$), sliding parameters ($\alpha = 0.1531$, $\beta = 0.0510$), $q(0) = [5, 0, \pi/3, 0]^T$.

6.3.2.7 The Pendubot

Figure 3.2a shows the schematics of Pendubot. Choose the physical parameters of Pendubot similar to the Acrobot as:

$$m_1 = 1 \text{ (kg)}, m_2 = 1 \text{ (kg)}, L_1 = 1 \text{ (m)}, L_2 = 2 \text{ (m)}, \ell_1 = 0.5 \text{ (m)}, \ell_2 = 1 \text{ (m)}, \\ I_1 = 0.083 \text{ (kg.m}^2\text{)}, I_2 = 0.33 \text{ (kg.m}^2\text{)}.$$

Expression for the nominal dynamics of the Pendubot is achieved by putting the following in Eq. (6.47):

$$\begin{aligned} m_{11}(q_2) &= m_1 \ell_1^2 + m_2(L_1^2 + \ell_2^2) + I_1 + I_2 + 2m_2 L_1 \ell_2 \cos(q_2) \\ m_{12}(q_2) &= m_2 \ell_2^2 + I_2 + m_2 L_1 \ell_2 \cos(q_2) \\ m_{21}(q_2) &= m_{12} \\ m_{22}(q_2) &= m_2 \ell_2^2 + I_2 \\ c_1(q_1, \dot{q}_1, q_2, \dot{q}_2) &= -m_2 L_1 \ell_2 \sin(q_2)(2\dot{q}_1 \dot{q}_2 + \dot{q}_2^2) \\ c_2(q_1, \dot{q}_1, q_2, \dot{q}_2) &= m_2 L_1 \ell_2 \sin(q_2) \dot{q}_1^2 \\ g_1(q_1, q_2) &= -(m_1 \ell_1 + m_2 L_1)g \sin(q_1) - m_2 \ell_2 g \sin(q_1 + q_2) \\ g_2(q_1, q_2) &= -m_2 \ell_2 g \sin(q_1 + q_2) \end{aligned} \tag{6.71}$$

Using the input and state transformations in (6.48) and (6.49), the normal form in Eq. (6.52) for the Pendubot is:

$$\ddot{z} = \frac{1}{c + b \cos(\xi)} \left(k \sin(\varphi(z, \xi)) - b \sin(\xi) \left(\left(\dot{z} - \frac{c \dot{\xi}}{c + b \cos(\xi)} \right)^2 - \frac{c \dot{\xi}^2}{c + b \cos(\xi)} \right) \right) \tag{6.72a}$$

$$\ddot{\xi} = v \tag{6.72b}$$

where

$$\begin{aligned}
\varphi(z, \xi) &= z + \xi - w_1 \tan^{-1} \left(w_2 \tan \left(\frac{\xi}{2} \right) \right) \\
w_1 &= \frac{2c}{\sqrt{c^2 - b^2}} \\
w_2 &= \sqrt{\frac{c-b}{c+b}} \\
a &= m_1 \ell_1^2 + m_2 (L_1^2 + \ell_2^2) + I_1 + I_2 \\
b &= m_2 L_1 \ell_2 \\
c &= m_2 \ell_2^2 + I_2 \\
k &= m_2 \ell_2 g
\end{aligned} \tag{6.73}$$

Note that in Eq. (6.72a), the denominator term $(c + b \cos(\xi))$ is strictly positive for $-\frac{\pi}{2} < \xi < \frac{\pi}{2}$ (always positive for the physical parameters used to avoid singularities in the transformations!), and hence to achieve the stable system in (6.12), choose the nonlinear sliding manifold, in accordance with Eq. (6.11) as the following:

$$\sigma = k \sin(\varphi(z, \xi)) + \alpha \dot{z} + \beta z \tag{6.74}$$

The last term in Eq. (6.72a) is taken into account in controller synthesis but excluded in the design of sliding manifold in Eq. (6.74) for the following reasons:

1. including this term in the sliding manifold makes Assumption 6.3 invalid.
2. being higher order, is small near the origin.

Reason (ii) is a crude assumption but simulation results justify its validity.

Note that σ does not explicitly depends on $\dot{\xi}$, the relative degree of system (6.74) is 2 and the design Case B is applicable.

In terms of coordinates $(q_1, \dot{q}_1, q_2, \dot{q}_2)$ of the Pendubot (6.71) we have

$$\sigma = k \sin(q_1 + q_2) + \alpha(\dot{q}_1 + h_0 \dot{q}_2) + \beta (q_1 + w_1 \tan^{-1} (w_2 \tan (q_2/2))) \tag{6.75}$$

$$\dot{\sigma} = k(\dot{q}_1 + \dot{q}_2) \cos(q_1 + q_2) + \beta(\dot{q}_1 + h_0 \dot{q}_2) + \alpha h_1 \tag{6.76}$$

In Eq. (6.23), $b(z, \dot{z}, \xi, \dot{\xi})$ in terms of $(q_1, \dot{q}_1, q_2, \dot{q}_2)$ is:

$$b(q_1, \dot{q}_1, q_2, \dot{q}_2) = \frac{2\alpha bc \sin(q_2) ((\dot{q}_1 + h_0 \dot{q}_2) (a + 2b \cos(q_2)) - c\dot{q}_2 + (a + 2b \cos(q_2))\dot{q}_2)}{(a + 2b \cos(q_2))^3} + k(1 - h_0) \cos(q_1 + q_2) \quad (6.77)$$

where

$$h_0 = \frac{1}{2} \frac{w_1 w_2 \sec^2(q_2/2)}{1 + w_2^2 \tan^2(q_2/2)}$$

$$h_1 = \frac{-b \sin(q_2) (((\dot{q}_1 + h_0 \dot{q}_2) (a + 2b \cos(q_2)) - c\dot{q}_2)^2 - c(a + 2b \cos(q_2))\dot{q}_2^2)}{(a + 2b \cos(q_2))^3} + \frac{k(a + 2b \cos(q_2))^2 \sin(q_1 + q_2)}{(a + 2b \cos(q_2))^3}$$

The final real control u for the Pendubot (6.71) is given by (6.48) with v given by (6.23) and w given by (6.25) and (6.26). Fig. 6.7 shows simulation results for the Pendubot further discussed in the next section.

6.3.2.8 Performance Analysis of The Pendubot

Figure 6.7 shows closed loop response of the Pendubot with control law (6.25) in the presence of external disturbance parametric variations. The controller gains are chosen as $K_1 = 125$, $K_2 = 100$, observer gain as $\lambda_1 = 3$, $\lambda_2 = 5$ and the sliding parameters as $\alpha = 8$, $\beta = 16$. Parametric variations is chosen as 25% decrease from $t = 4$ (s) to $t = 6$ (s) and 25% increase from $t = 6$ (s) to $t = 8$ (s). The matched disturbance $d(t) = 5 \sin(\pi t)$ is applied to system at time intervals shown in Figure 6.7c.

The controller successfully stabilizes the Pendubot in less than 4 seconds. The controller is able to keep the system stable at its unstable equilibrium position in the presence of wide parametric variations. System response is robust to a large disturbance. Moreover, control action is smooth.

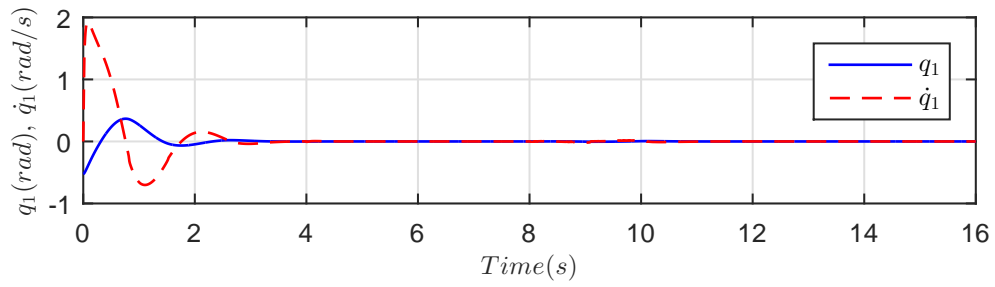
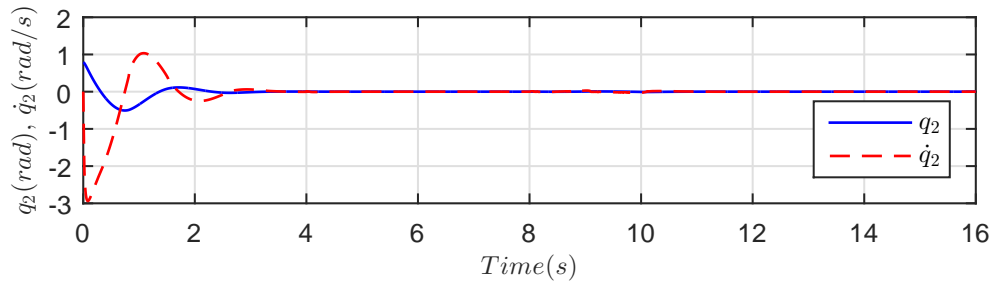
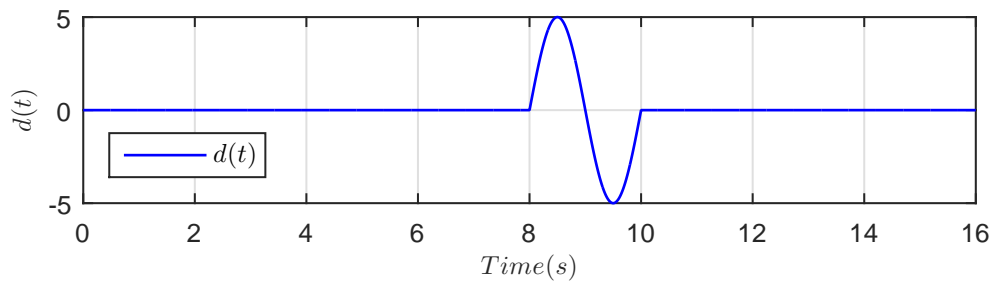
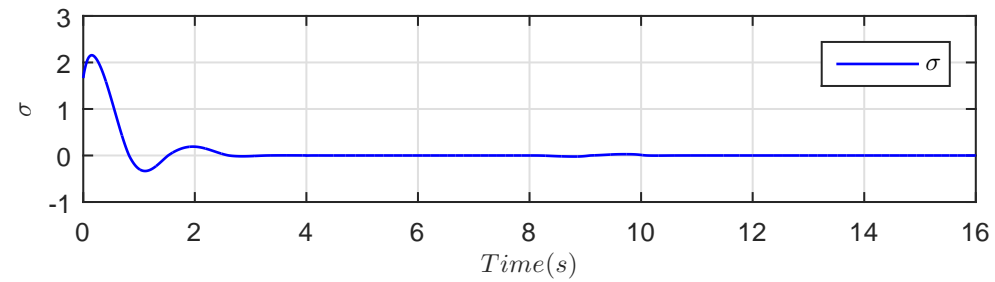
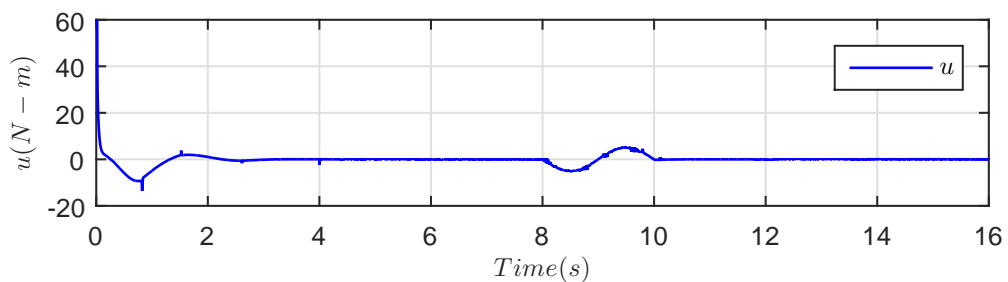
(A) Link 1 position q_1 (rad) and velocity \dot{q}_1 (rad/s)(B) Link 2 position q_2 (rad) and velocity \dot{q}_2 (rad/s)(C) Disturbance $d(t) = 5 \sin(\pi t)$ (D) Sliding surface σ (E) Control effort u (N-m)

FIGURE 6.7: Pendubot - Closed loop response with control law (6.25) ($K_1 = 125$, $K_2 = 100$) and observer (6.26) ($\lambda_1 = 3$, $\lambda_2 = 5$), sliding parameters ($\alpha = 8$, $\beta = 16$), $q(0) = [-\frac{\pi}{6}, 0, \frac{\pi}{4}, 0]^T$

6.3.2.9 The Beam-and-Ball System

Figure 3.2e shows the schematics of Beam-and-Ball system. Choose the physical parameters of Beam-and-Ball system according to [63, 64] as the following:

$m = 0.05$ (kg), $I_1 = 0.02$ (kg.m²), $I_2 = 2 \times 10^{-6}$ (kg.m²), $r = 0.01$ (m), $g = 9.8$ (m.s⁻²).

Using Eq. (3.16) with $d = 0$ in Eq. (6.47) gives the nominal dynamics of the Beam-and-Ball system, as in [63, 64]:

$$(I_1 + mq_2^2) \ddot{q}_1 + 2m\dot{q}_1 q_2 \dot{q}_2 + mgq_2 \cos(q_1) = u \quad (6.78a)$$

$$\left(m + \frac{I_2}{r^2}\right) \ddot{q}_2 - mq_2 \dot{q}_1^2 + mg \sin(q_1) = 0 \quad (6.78b)$$

Using the control input transformation

$$u = (I_1 + mq_2^2) v + 2m\dot{q}_1 q_2 \dot{q}_2 + mgq_2 \cos(q_1) \quad (6.79)$$

where v is a new control input and writing $[z_1, z_2, \xi_1, \xi_2]^T = [q_2, \dot{q}_2, q_1, \dot{q}_1]^T$, the normal form in Eq. (6.52) for the Beam-and-Ball system is:

$$\ddot{z} = k_0 \dot{\xi}^2 z - k_0 g \sin(\xi) \quad (6.80a)$$

$$\ddot{\xi} = v \quad (6.80b)$$

where $k_0 = \frac{1}{1 + \frac{I_2}{mr^2}} = 0.7143$.

Choose the nonlinear sliding manifold, in accordance with Eq. (6.11) as the following:

$$\sigma = -k_0 g \sin(\xi) + \alpha \dot{z} + \beta z \quad (6.81)$$

The first term $k_0 \dot{\xi}^2 z$ in (6.80a) is taken into account in controller synthesis but excluded in the design of sliding manifold in (6.81) for the following reasons:

1. including this term in the sliding manifold results in undefined relative degree at the origin and Assumption 6.3 becomes invalid.

2. being third order, is small near the origin.
3. To achieve the stable system in (6.12), the coefficient β of z in the sliding manifold (6.81) can be chosen sufficiently large to dominate the strictly positive state dependent coefficient $k_0\dot{\xi}^2$ of z in (6.80a). The Beam velocity $\dot{q}_1 = \dot{\xi}$ is usually less than 2 radians/second, and hence, $k_0\dot{\xi}^2 < 2$ and choosing $\beta \geq 2$ is sufficient.

Reasons (ii) and (iii) are crude assumptions but simulation results justify their validity.

Note that σ does not explicitly depends on $\dot{\xi}$, the relative degree of system (6.81) is 2 and the design Case B is applicable.

In terms of coordinates $(q_1, \dot{q}_1, q_2, \dot{q}_2)$ of the Beam-and-Ball (6.78) we have

$$\sigma = -k_0g \sin(q_1) + \alpha\dot{q}_2 + \beta q_2 \quad (6.82)$$

$$\dot{\sigma} = -k_0g\dot{q}_1 \cos(q_1) + \alpha k_0\dot{q}_1^2 q_2 - \alpha k_0g \sin(q_1) + \beta\dot{q}_2 \quad (6.83)$$

In Eq. (6.23), $b(z, \dot{z}, \xi, \dot{\xi})$ in terms of $(q_1, \dot{q}_1, q_2, \dot{q}_2)$ is:

$$b(q_1, \dot{q}_1, q_2, \dot{q}_2) = 2k_0\alpha q_2\dot{q}_2 - k_0g \cos(q_1) \quad (6.84)$$

The final real control u for the Beam-and-Ball system (6.78) is given by (6.79) with v given by (6.23) and w given by (6.25) and (6.26). Figures 6.8-6.10 shows simulation results for the Beam-and-Ball further discussed in the next section.

6.3.2.10 Performance Analysis of The Beam-and-Ball System

Figures 6.8 and 6.9 show closed loop response of the Beam-and-Ball system with control law (6.25) in the presence of external disturbance parametric variations. The controller gains are chosen as $K_1 = 5$, $K_2 = 6$, observer gain as $\lambda_1 = 4$, $\lambda_2 = 5$ and the sliding parameters as $\alpha = 1.5$, $\beta = 1.5$. Parametric variations is chosen as 25% decrease from $t = 4$ (s) to $t = 6$ (s) and 25% increase from $t = 6$ (s) to $t = 8$ (s).

The matched disturbance $d(t) = 0.25 \sin(\pi t)$ is applied to system at time intervals shown in Figures 6.8c-6.9c.

The initial condition, in Figure 5.3, is the same as in HOCSMC [64]. Comparing to [64], the settling time and the overshoots/undershoots in the Ball position are considerable improved. Shown in [64], for this initial condition, the HOCSMC based on [63] becomes unstable. Figure 5.4 shows repose for a larger initial condition.

System response is robust to wide parametric variations but is sensitive to small disturbance. The effects of applied disturbance on stability are made visible in simulation. Small variations in Beam angle due to disturbance cause large variation in Ball position, which is unactuated, and then the control takes action by changing the Beam angle to bring the Ball back to desired position.. Furthermore, the control action is smooth.

Figure 5.5 shows tracking response of the Beam-and-Ball system with control law (6.25). The Ball perfectly tracks the desired square wave signal of amplitude 5(m). The settling time is 6 seconds and the control effort is within range. Comparing to SMC tracking in Figure 4.16, the results are improved with the extra advantage of that the control action is now smooth.

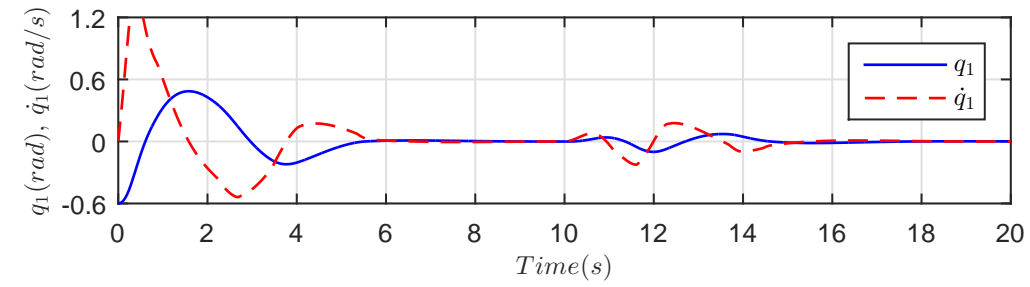
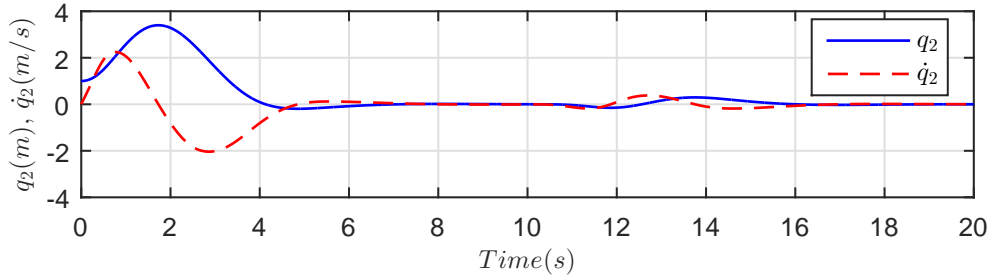
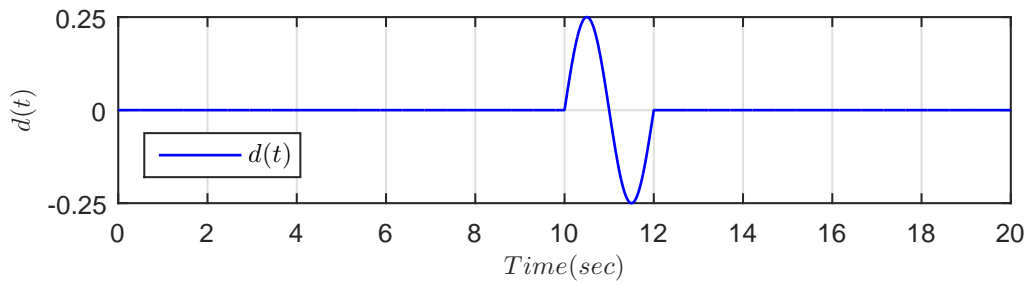
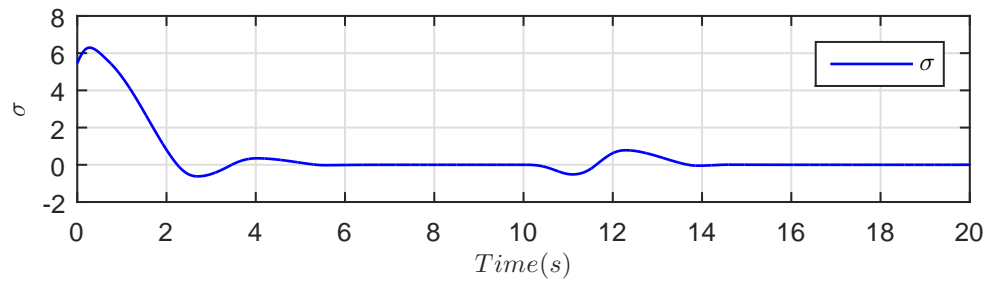
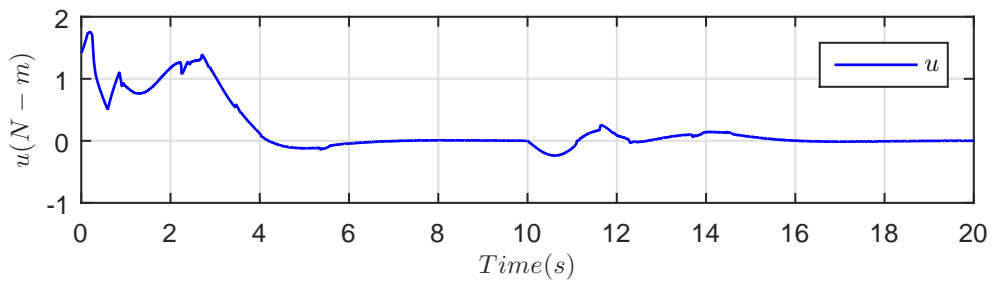
(A) Beam angle q_1 (rad), velocity \dot{q}_1 (rad/s)(B) Ball position q_2 (m), velocity \dot{q}_2 (m/s)(C) Disturbance $d(t) = 0.25 \sin(\pi t)$ (D) Sliding surface σ (E) Control effort u (N-m)

FIGURE 6.8: The Beam-and-Ball - Closed loop response with control law (6.25) ($K_1 = 5$, $K_2 = 6$) and observer (6.26) ($\lambda_1 = 4$, $\lambda_2 = 5$), sliding parameters ($\alpha = 1.5$, $\beta = 1.5$), $q(0) = [-0.6, 0, 1.0, 0]^T$.

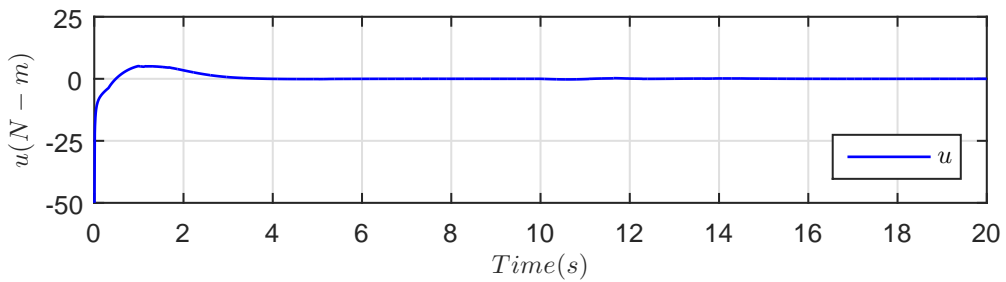
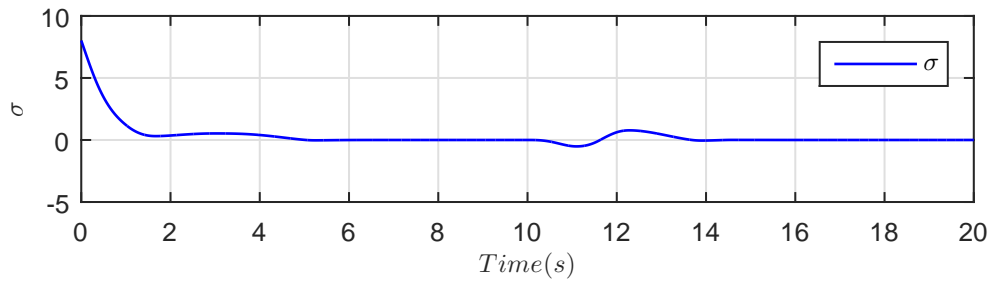
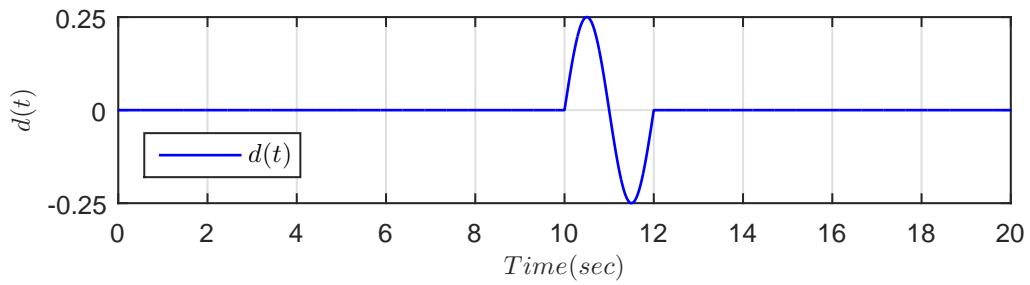
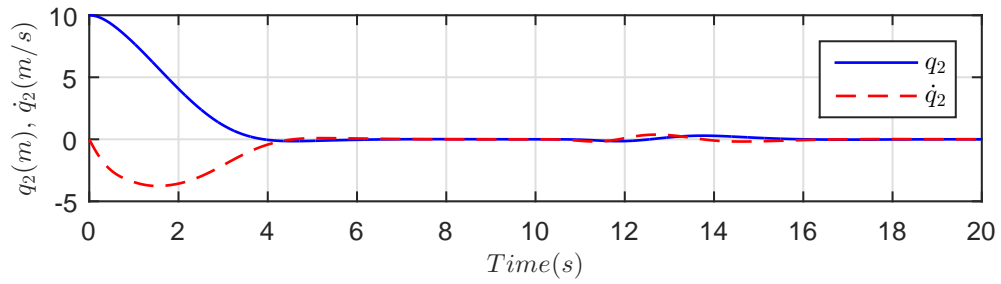
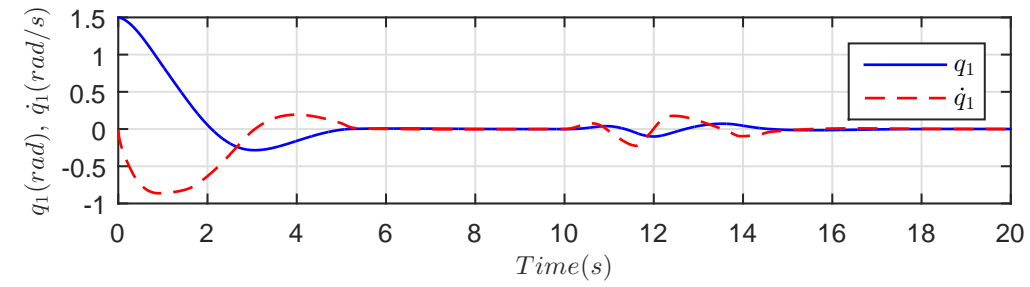


FIGURE 6.9: The Beam-and-Ball - Closed loop response with control law (6.25) ($K_1 = 5$, $K_2 = 6$) and observer (6.26) ($\lambda_1 = 4$, $\lambda_2 = 5$), sliding parameters ($\alpha = 1.5$, $\beta = 1.5$), $q(0) = [1.5, 0, 10.0, 0]^T$.

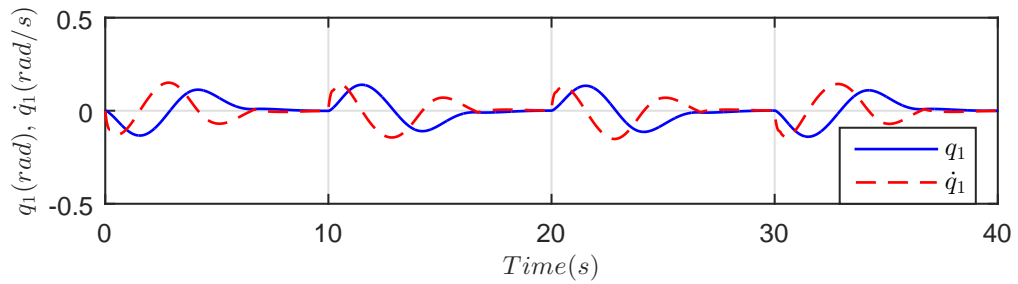
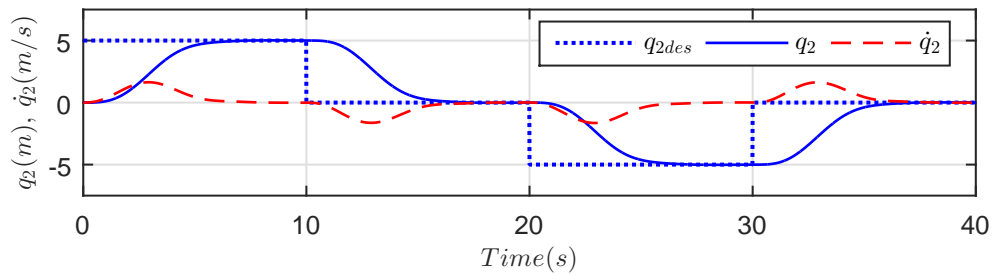
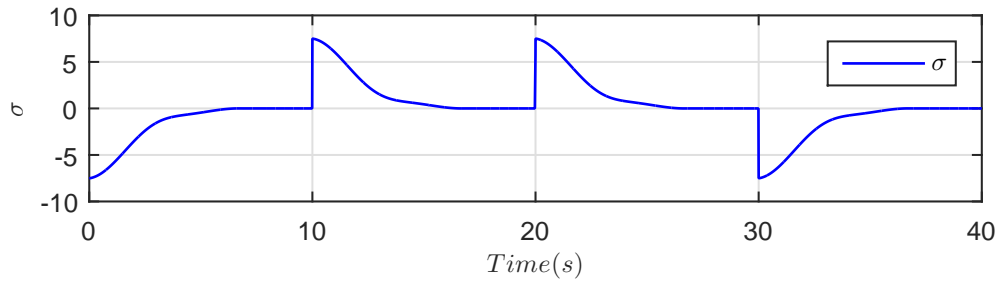
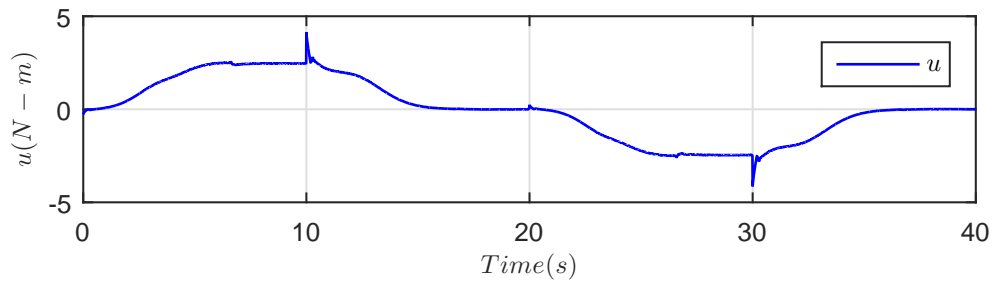
(A) Beam angle q_1 (rad), velocity \dot{q}_1 (rad/s)(B) Ball position q_2 (m), velocity \dot{q}_2 (m/s)(C) Sliding surface σ (D) Control effort u (N-m)

FIGURE 6.10: The Beam-and-Ball - Closed loop tracking response with control law (6.25) ($K_1 = 5$, $K_2 = 6$) and observer (6.26) ($\lambda_1 = 4$, $\lambda_2 = 5$), sliding parameters ($\alpha = 1.5$, $\beta = 1.5$), $q(0) = [0, 0, 0, 0]^T$.

6.4 Comparison of Proposed Control Design Strategies

This section provides a comparison the proposed control design strategies. Figures 6.11-6.15 show and compare the responses of the standard sliding mode control (SMC), the Super-Twisting Algorithm (STA), and Smooth Second Order Sliding Mode (SSOSM) controls for the Inertia-Wheel Pendulum, TORA, the Beam-and-Ball, the Cart-Pole, and the Overhead Crane.

The simulation results show satisfactory response for the all the three control strategies. However, the SMC has excessive chattering in the control action which is not suitable for mechanical control systems. The chattering is significantly reduced in the STA and further smoothed by the SSOSM. The SMC has the advantage of finite time convergence of the sliding variable which is asymptotic for the STA and SSOSM. Furthermore, the system response is robust to matched disturbance.

For the IWP the overshoot in the wheel position is high for the SSOSM. For the TORA the three responses are almost the same. For the Beam-and-Ball the undershoots are high for the SMC. For the Cart-Pole the overshoot is high for the SMC. For the Overhead Crane the overshoot is high for the STA.

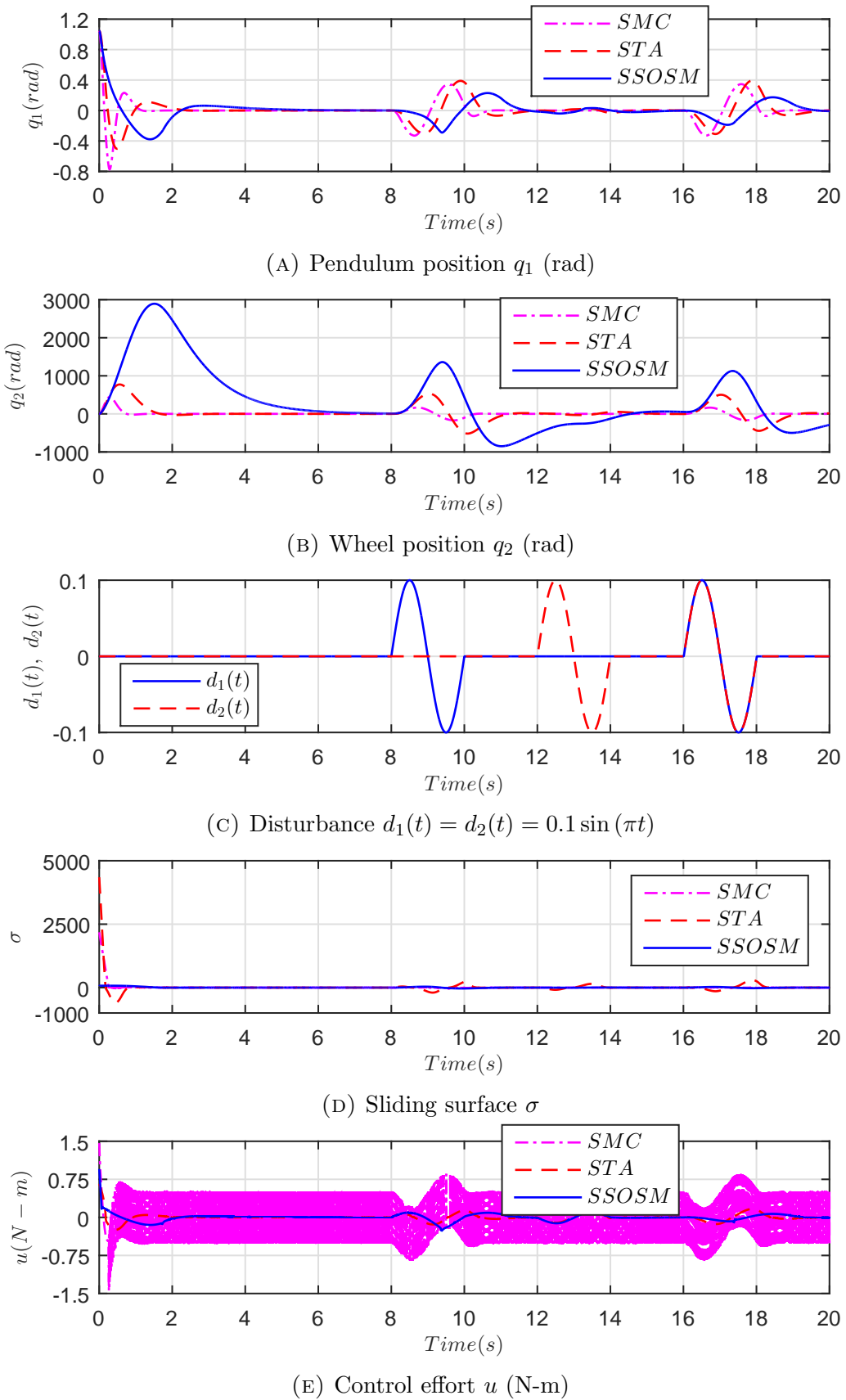


FIGURE 6.11: IWP - Comparison of SMC law (4.12) ($\Gamma = 2000.0$), STA law (5.14) ($\lambda_1 = -0.01$, $\lambda_2 = -0.02$) and SSOSM law (6.25) ($K_1 = 500$, $K_2 = 400$), $q(0) = [\pi/3, 0, 0, 0]^T$.

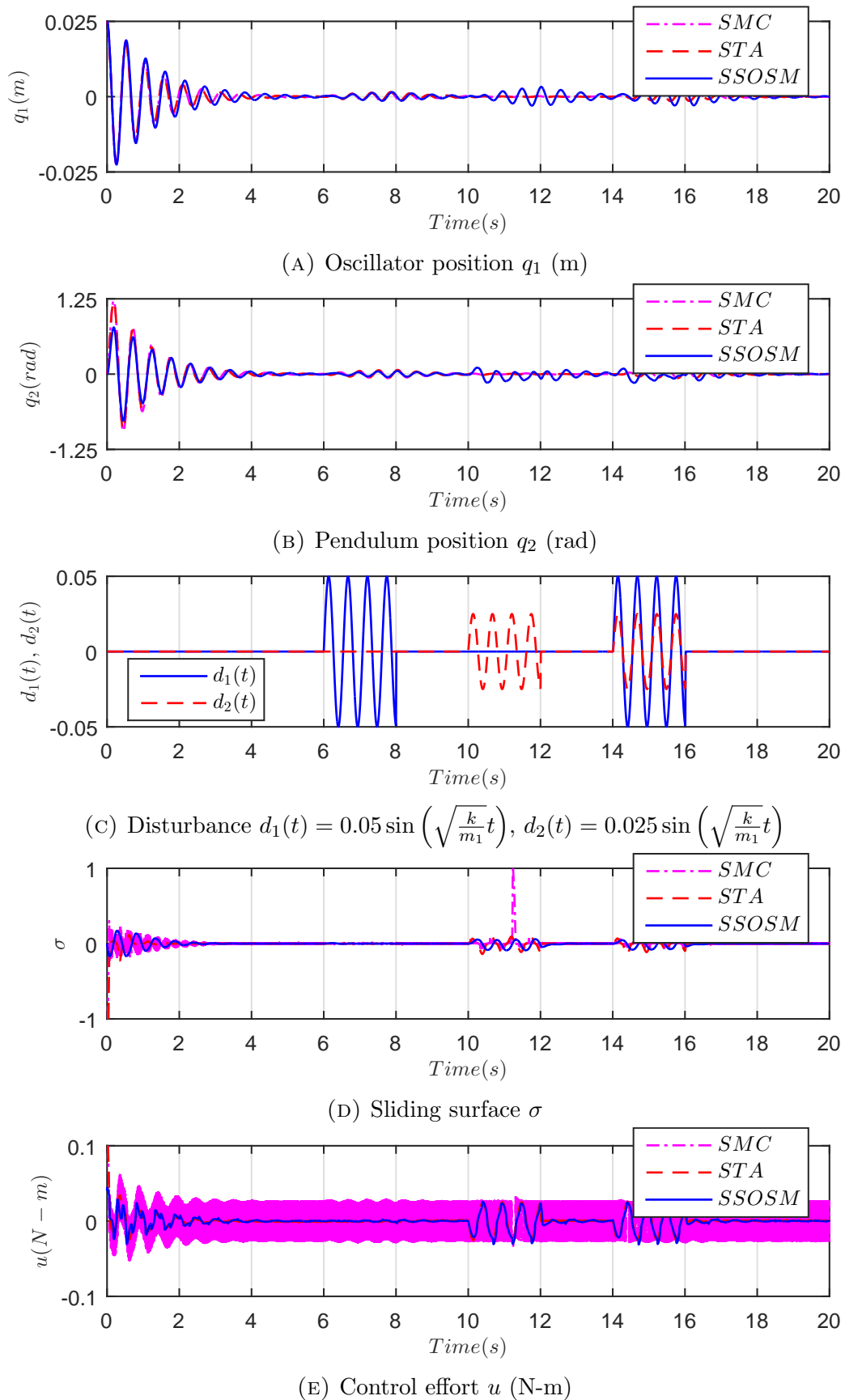


FIGURE 6.12: TORA - Comparison of SMC law (4.12) ($\Gamma = 1$), STA law (5.14) ($\lambda_1 = 0.075$, $\lambda_2 = 0.050$) and SSOSM law (6.25) ($K_1 = 500$, $K_2 = 400$), $q(0) = [0.025, 0, 0, 0]^T$

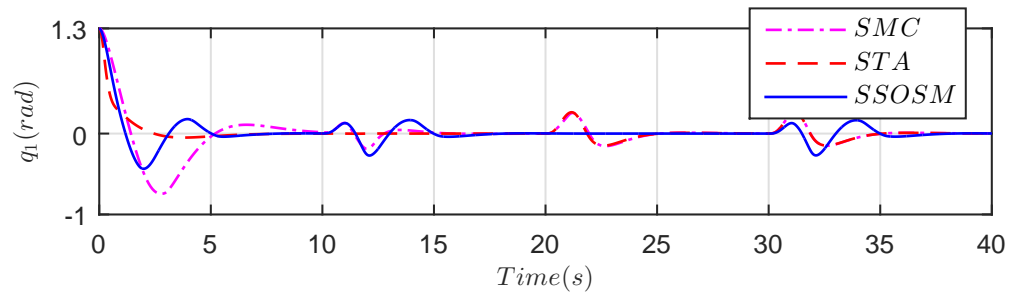
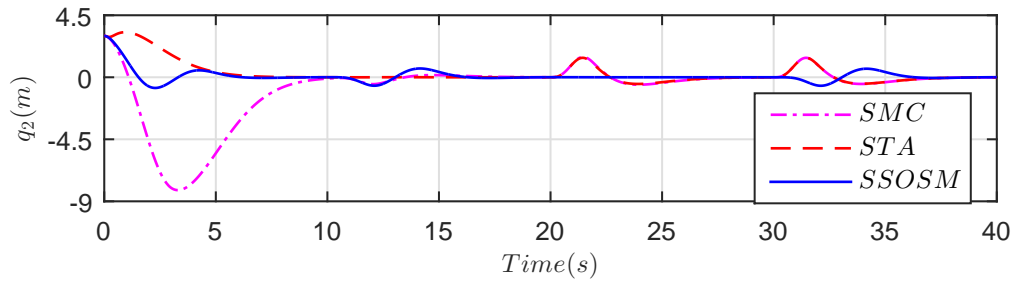
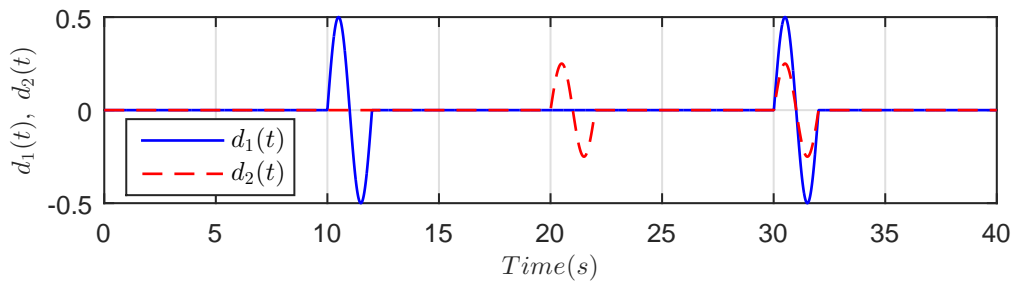
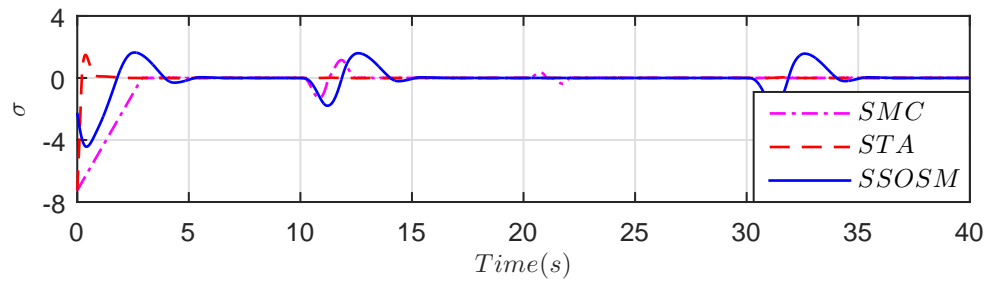
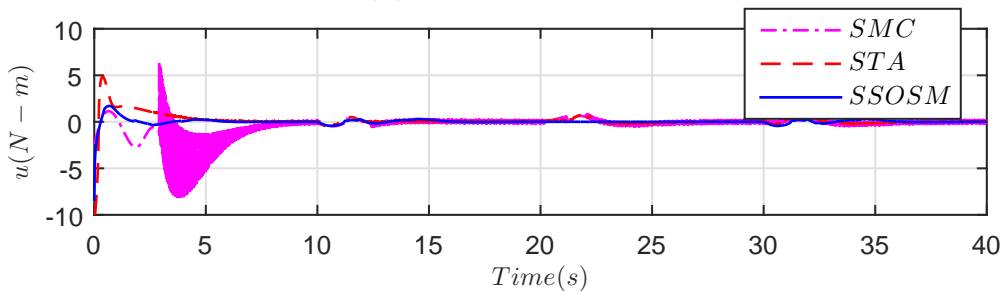
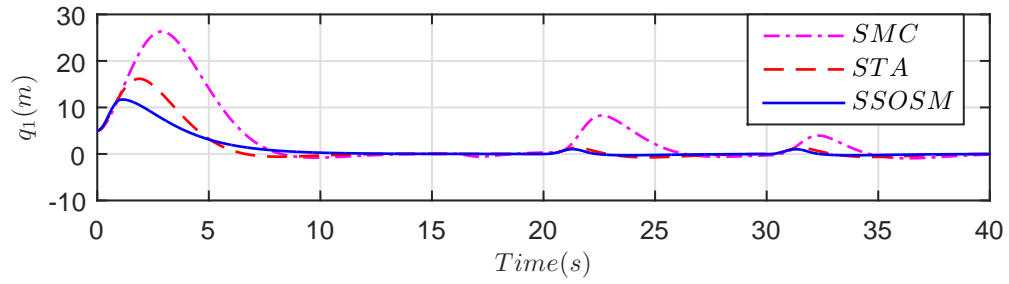
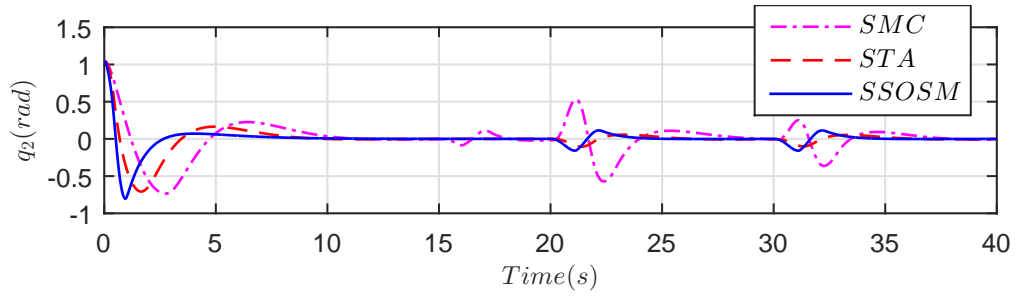
(A) Beam angle q_1 (rad)(B) Ball position q_2 (m)(C) Disturbance $d_1(t) = 0.5 \sin(\pi t)$, $d_2(t) = 0.25 \sin(\pi t)$ (D) Sliding surface σ (E) Control effort u (N-m)

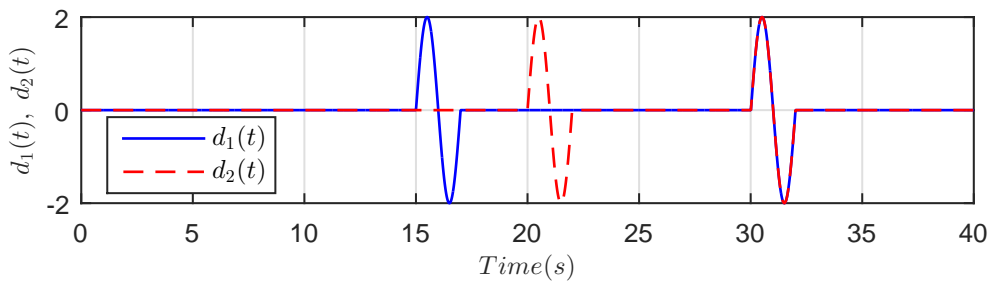
FIGURE 6.13: The Beam-and-Ball - Comparison of SMC law (4.12) ($\Gamma = 2.5$), STA law (5.14) ($\lambda_1 = -4.0$, $\lambda_2 = -0.5$) and SSOSM law (6.25) ($K_1 = 5$, $K_2 = 6$), $q(0) = [1.3, 0, 3.0, 0]^T$.



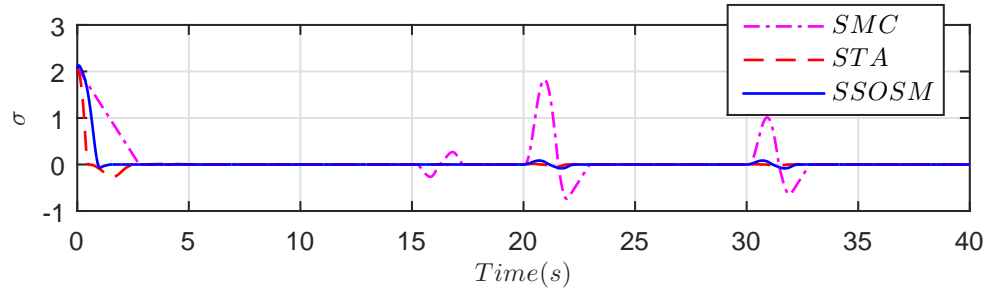
(A) Cart position q_1 (m)



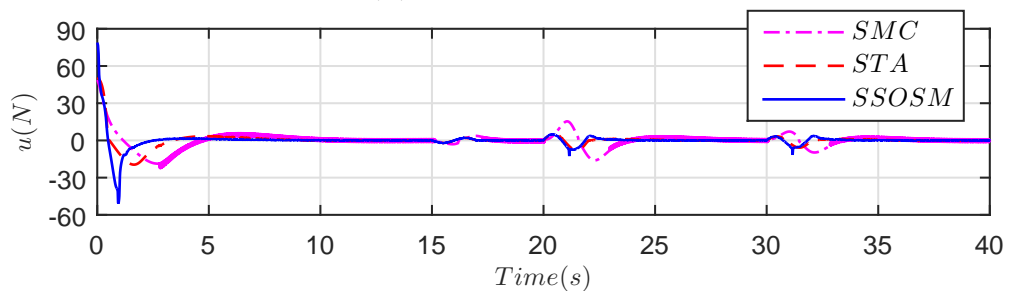
(B) Pole angle q_2 (rad)



(C) Disturbance $d_1(t) = d_2(t) = 2 \sin(\pi t)$



(D) Sliding surface σ



(E) Control effort u (N)

FIGURE 6.14: The Cart-Pole - Comparison of SMC law (4.12) ($\Gamma = 0.75$), STA law (5.14) ($\lambda_1 = -35.0$, $\lambda_2 = -2.5$) and SSOSM law (6.25) ($K_1 = 20$, $K_2 = 15$), $q(0) = [5, 0, \pi/3, 0]^T$.

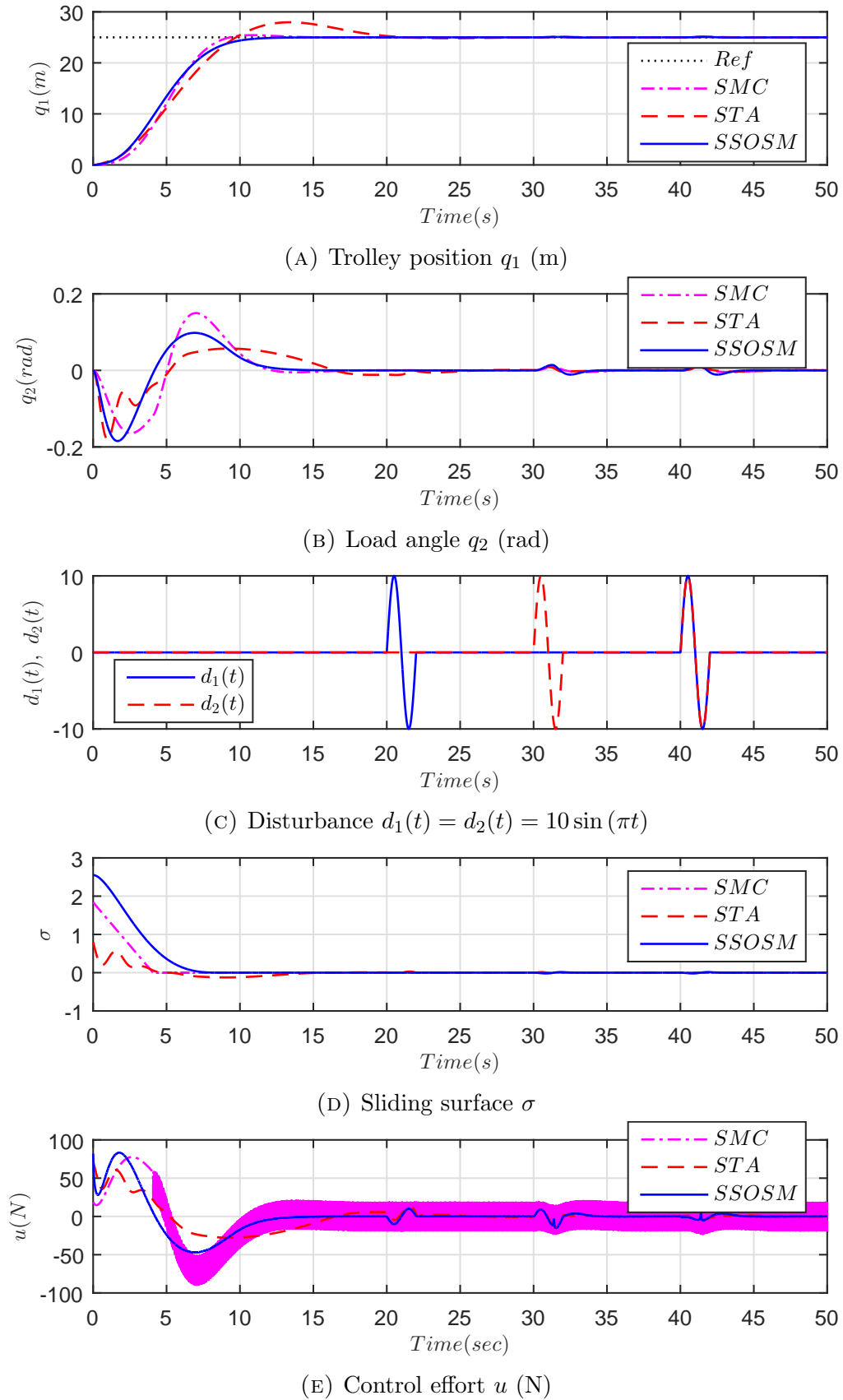


FIGURE 6.15: The Overhead Crane - Comparison of SMC law (4.12) ($\Gamma = 0.45$), STA law (5.14) ($\lambda_1 = -80.0$, $\lambda_2 = -0.5$) and SSOSM law (6.25) ($K_1 = 1$, $K_2 = 1.6$), $q(0) = [0, 0, 0, 0]^T$

6.5 Novelty Highlights

TABLE 6.1: Lagrangian Zero Dynamic Function $f(z, \dot{z}, \xi, \dot{\xi})$ in Eqs. (6.9), (6.52)

System	$f(z, \dot{z}, \xi, \dot{\xi})$
IWP	$k_1 \sin(z - k_2 \xi)$
TORA	$-k_1 z + k_2 \sin(\xi)$
Acrobot	$\frac{1}{a+b \cos(\xi)} \left(k_1 \sin(\varphi_1(z, \xi)) + k_2 \sin(\varphi_2(z, \xi)) + b \sin(\xi) \dot{\xi} \dot{z} \right)$
Beam-and-Ball	$k_0 \dot{\xi}^2 z - k_0 g \sin(\xi)$
Cart-Pole	$\left(g + k_1 \frac{\dot{\xi}^2}{\cos(\xi)} \right) \tan(\xi)$
Overhead Crane	$\left(-g + L \frac{\dot{\xi}^2}{\cos(\xi)} \right) \tan(\xi)$
Furuta Pendulum	$\left(k_1 + k_2 \frac{(z - k_3 \xi)^2}{\cos(\xi)} + k_4 \frac{\dot{\xi}^2}{\cos(\xi)} \right) \tan(\xi)$
Pendubot	$\frac{1}{c+b \cos(\xi)} \left(k \sin(\varphi(z, \xi)) - b \sin(\xi) \left(\left(\dot{z} - \frac{c \dot{\xi}}{c+b \cos(\xi)} \right)^2 - \frac{c \dot{\xi}^2}{c+b \cos(\xi)} \right) \right)$

TABLE 6.2: Nonlinear Sliding Manifolds in Transformed Coordinates $(z, \dot{z}, \xi, \dot{\xi})$

System	$\sigma(z, \dot{z}, \xi, \dot{\xi})$
IWP	$k_1 \sin(z - k_2 \xi) + \alpha \dot{z} + \beta z$
TORA	$k_2 \sin(\xi) + \alpha \dot{z}$
Acrobot	$k_1 \sin(\varphi_1(z, \xi)) + k_2 \sin(\varphi_2(z, \xi)) + \alpha \dot{z} + \beta z$
Beam-and-Ball	$-k_0 g \sin(\xi) + \alpha \dot{z} + \beta z$
Cart-Pole	$\tan(\xi) + \alpha \dot{z} + \beta z$
Overhead Crane	$\tan(\xi) - \alpha \dot{z} - \beta z$
Furuta Pendulum	$\tan(\xi) + \alpha \dot{z} + \beta z$
Pendubot	$k \sin(\varphi(z, \xi)) + \alpha \dot{z} + \beta z$

TABLE 6.3: Nonlinear Sliding Manifolds in Actual Coordinates $(q_1, \dot{q}_1, q_2, \dot{q}_2)$

System	$\sigma(q_1, \dot{q}_1, q_2, \dot{q}_2)$
IWP	$\alpha (\dot{q}_1 + k_2 \dot{q}_2) + k_1 \sin(q_1) + \beta (q_1 + k_2 q_2)$
TORA	$k_2 \sin(q_2) + \alpha \left(\dot{q}_1 + \frac{m_2 r}{m_1 + m_2} \dot{q}_2 \cos(q_2) \right)$
Acrobot	$k_1 \sin(q_1) + k_2 \sin(q_1 + q_2) + \alpha \dot{q}_1 + \alpha \dot{q}_2 (1 + h_0) / 2 + \beta \left(q_1 + \frac{q_2}{2} + w_1 \tan^{-1}(w_2 \tan(q_2/2)) \right)$
BB	$-k_0 g \sin(q_1) + \alpha \dot{q}_2 + \beta q_2$
CP	$\alpha \dot{q}_1 + \alpha k_1 \dot{q}_2 \sec(q_2) + \beta q_1 + \beta k_1 \ln(\sec(q_2) + \tan(q_2)) + \tan(q_2)$
OC	$-\alpha \dot{q}_1 - \alpha L \dot{q}_2 \sec(q_2) - \beta q_1 - \beta L \ln(\sec(q_2) + \tan(q_2)) + \tan(q_2)$
FP	$\alpha \dot{q}_1 + \alpha k_4 \dot{q}_2 \sec(q_2) + \beta q_1 + \beta k_4 \ln(\sec(q_2) + \tan(q_2)) + \tan(q_2)$
Pendubot	$k \sin(q_1 + q_2) + \alpha (\dot{q}_1 + h_0 \dot{q}_2) + \beta \left(q_1 + w_1 \tan^{-1}(w_2 \tan(q_2/2)) \right)$

TABLE 6.4: Control Coefficient $b(q_1, \dot{q}_1, q_2, \dot{q}_2)$ in Eq. (6.24)

System	$b(q_1, \dot{q}_1, q_2, \dot{q}_2)$
IWP	$k_1 k_2 \cos(q_1)$
TORA	$k_2 \cos(q_2)$
Acrobot	$\frac{1}{2} k_1 (-1 - h_0) \cos(q_1) + \frac{1}{2} k_2 (+1 - h_0) \cos(q_1 + q_2) + \frac{\alpha b (2\dot{q}_1 + \dot{q}_2 (1 + h_0)) \sin(q_2)}{2a + 2b \cos(q_2)}$
BB	$2k_0 \alpha q_2 \dot{q}_2 - k_0 g \cos(q_1)$
CP	$\sec^2(q_2) + 2\alpha k_1 \dot{q}_2 \sec(q_2) \tan(q_2)$
OC	$\sec^2(q_2) - 2\alpha L \dot{q}_2 \sec(q_2) \tan(q_2)$
FP	$\sec^2(q_2) + 2\alpha \dot{q}_2 (k_4 + k_2 k_3^2) \sec(q_2) \tan(q_2) - 2\alpha k_2 k_3 (\dot{q}_1 + k_4 \dot{q}_2 \sec(q_2)) \sec(q_2) \tan(q_2)$
Pendubot	$\frac{2\alpha b c \sin(q_2) ((\dot{q}_1 + h_0 \dot{q}_2) (a + 2b \cos(q_2)) - c \dot{q}_2 + (a + 2b \cos(q_2)) \dot{q}_2)}{(a + 2b \cos(q_2))^3} + k(1 - h_0) \cos(q_1 + q_2)$

6.6 Chapter Summary and Conclusions

We presented a comprehensive robust and smooth control design framework for underactuated mechanical systems. The framework builds on the design of novel nonlinear sliding manifolds for underactuated mechanical systems and the application of smooth HOSM control to achieve both smooth control and global results. The design framework was applied and the results were compared to standard ones for the following benchmark underactuated mechanical systems:

A. Class-I Underactuated Mechanical Systems:

1. The Inertia-Wheel Pendulum
2. The TORA System
3. The Acrobot

B. Class-II Underactuated Mechanical Systems:

1. The Furuta Pendulum
2. The Overhead Crane
3. The Cart-Pole System
4. The Pendubot
5. The Beam-and-Ball System

Based on the results, the following conclusions are drawn.

1. The proposed smooth HOSM framework addresses the control problem of underactuated mechanical systems in a comprehensive way.
2. The framework makes the complex control design problem of underactuated mechanical systems much simple.

3. The framework achieves global convergence of underactuated mechanical systems.
4. The designed control laws have enhanced stabilization and tracking (set-point regulation) response for benchmark underactuated mechanical systems.
5. The results are in agreement with and improved to standard results reported in the literature.
6. The framework is robust to wide parametric variations and disturbance in contrast to other works.
7. The control action is smooth.
8. The design procedure is simple compared to other approaches.

The design framework presented in this chapter utilizes no local assumptions and hence achieves global results. But the nature of dynamics and singularities are hurdles in the global convergence of underactuated mechanical systems as was noted for the IWP. Similarly, other pendulum-like underactuated mechanical systems such as the Furuta Pendulum, the Acrobot, the Pendubot, and the Cart-Pole system suffer from this problem. In Chapter 7, Swingup Control laws are designed for underactuated mechanical systems and use the smooth HOSM control laws developed in this chapter as balancing control and hence achieve global swingup and stabilization.

Chapter 7

Swingup and Balancing of Underactuated Mechanical Systems

In this chapter, the swingup control problem of underactuated mechanical systems is addressed. Pendulum-like underactuated mechanical systems such as the IWP, the Acrobot, Furuta Pendulum, and the Pendubot need swingup, from the downward stable equilibrium position to bring the system near the upward unstable equilibrium position, and then switching to a balancing control to stabilize the system. Although not the primary focus of this research, Swingup Controls are designed for these system in a more classical way and use the smooth HOSM controls developed in chapter 6 as balancing controls to demonstrate successful swingup and balancing. The design concepts are illustrated for the following underactuated mechanical systems:

A. Class-I Underactuated Mechanical Systems:

1. The Inertia-Wheel Pendulum
2. The Acrobot

B. Class-II Underactuated Mechanical Systems:

1. The Furuta Pendulum
2. The Pendubot

7.1 Class-I Underactuated Mechanical Systems

Consider Class-I underactuated mechanical systems described by:

$$m_{11}(q_2)\ddot{q}_1 + m_{12}(q_2)\ddot{q}_2 + c_1(q, \dot{q}) + g_1(q_1, q_2) = 0 \quad (7.1a)$$

$$m_{21}(q_2)\ddot{q}_1 + m_{22}(q_2)\ddot{q}_2 + c_2(q, \dot{q}) + g_2(q_1, q_2) = u \quad (7.1b)$$

The Inertia-Wheel Pendulum with Eq. (3.10) and the Acrobot with Eq. (3.8) are described by Eq. (7.1).

7.1.1 Inertia-Wheel Pendulum (IWP)

The dynamics of IWP are described by (7.1) with the following

$$\begin{aligned} m_{11}(q_2) &= I_1 + I_2 + m_1 l_1^2 + m_2 L_1^2 \\ m_{12}(q_2) &= I_2 \\ m_{21}(q_2) &= m_{12}(q_2) \\ m_{22}(q_2) &= m_{12}(q_2) \\ c_1(q, \dot{q}) &= 0 \\ c_2(q, \dot{q}) &= 0 \\ g_1(q_1, q_2) &= -(m_1 l_1 + m_2 L_1)g \sin(q_1) \\ g_2(q_1, q_2) &= 0 \end{aligned} \quad (7.2)$$

Noted that smooth HOSM control w given by (6.25) cannot stabilize the IWP from below the horizontal axis due to singularity at $\cos(q_1 = \frac{\pi}{2}) = 0$ in Eq. (6.33). To stabilize the IWP from the downward stable equilibrium position $q_1 = \pi$ to the upward unstable equilibrium position $q_1 = 0$, we design Swingup Control. The

controller w in Eq. (6.25) can then be used as a balancing controller. We use the same physical parameters for the IWP as in the previous chapters.

To stabilize the Pendulum position from $q_1 = \pi$ to $q_1 = 0$, partially linearize the dynamics of IWP with respect to q_1 . Solving Eq. (7.1a) for \ddot{q}_2 as

$$\ddot{q}_2 = -m_{12}^{-1}(c_1 + g_1 + m_{11}\ddot{q}_1) \quad (7.3)$$

putting the result in Eq. (7.1b) and using the following noncollocated Partial Feedback Linearizing control

$$u = u_{PFL} = (m_{21} - m_{22}m_{12}^{-1}m_{11})v_{swingup} + c_2 + g_2 - m_{22}m_{12}^{-1}(c_1 + g_1) \quad (7.4)$$

where $v_{swingup}$ is a new control to be designed, the dynamics of the IWP become:

$$\ddot{q}_1 = v_{swingup} \quad (7.5a)$$

$$m_{12}\ddot{q}_2 + c_1 + g_1 = -m_{11}v_{swingup} \quad (7.5b)$$

Equation (7.5a) is linear, a double integrator, and is simple to stabilize. Choose the following state feedback control law

$$v_{swingup} = -K_d\dot{q}_1 - K_pq_1 \quad (7.6)$$

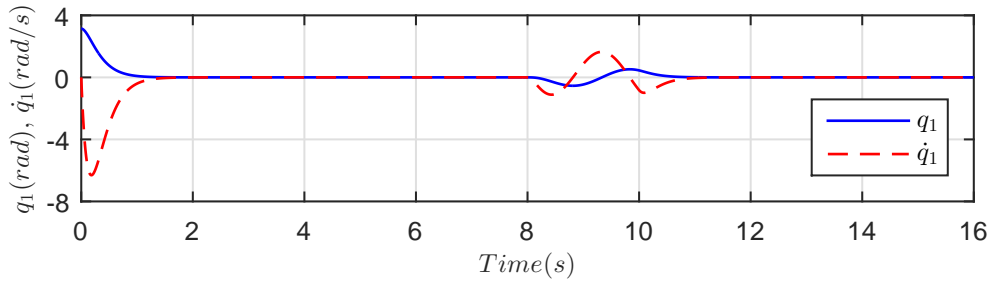
with K_d , K_p as positive design constants. The control $v_{swingup}$ combined with u_{PFL} (7.4) can stabilize q_1 from $q_1 = \pi$ to $q_1 = 0$, however the q_2 -dynamics, obviously, become unstable. Once q_1 is stabilized, $v_{swingup}$ becomes zero, which is obvious, however, the PFL control u_{PFL} also becomes zero in accordance with the expression in Eq. (7.4). This implies the q_2 -dynamics, in accordance with Eq. (7.3) (equivalently Eq. (7.5b)), become

$$\ddot{q}_2 = 0 \quad (7.7)$$

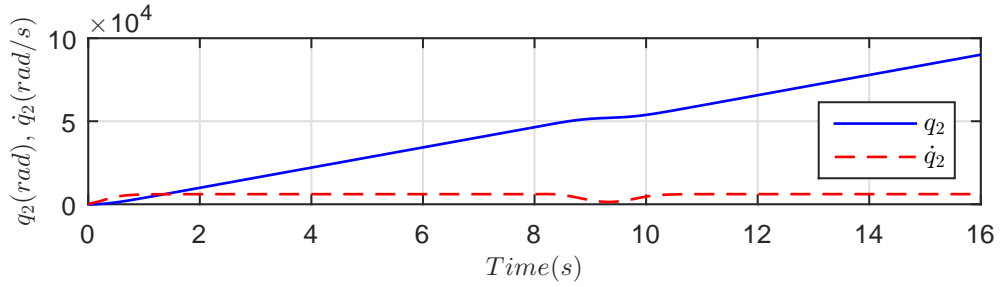
Figure 7.1 shows closed loop response of the with $v_{swingup}$ (7.6) with $K_d = 11$, $K_p = 30$ for the initial condition $q(0) = [\pi, 0, 0, 0]^T$. The q_1 -dynamics are stabilized as

shown in Fig. 7.1a. The linear double integrator behavior (7.7) of the q_2 -dynamics is shown Fig. 7.1a. The system closed with state feedback law (7.6) is more vulnerable to the adverse effects of the disturbance.

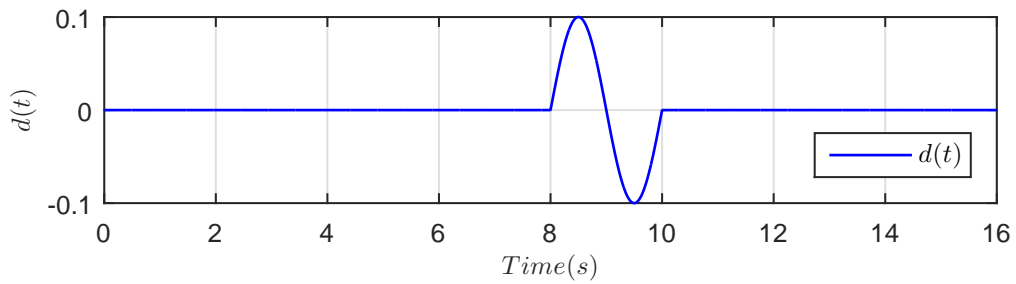
The strategy is to use $v_{swingup}$ (7.6) to swing up the pendulum and once q_1 becomes within the domain of attraction of the HOSM control w in Eq. (6.25), the control action is switched to stabilize the system. Figure 7.2 shows a successful swing up, from $q_1 = \pi$ to $q_1 = 0$, and balancing in the presence of external disturbance. The HOSM control (6.25) takes control of the system motion at $q(t = .5) = [0.7652, -3.044, 1151, 4487]^T$, $\sigma(t = .5) = 151.5$ and balance it to $q(t) = [0, 0, 0, 0]^T$ in 8 seconds. System response with HOSM control is robust to disturbance.



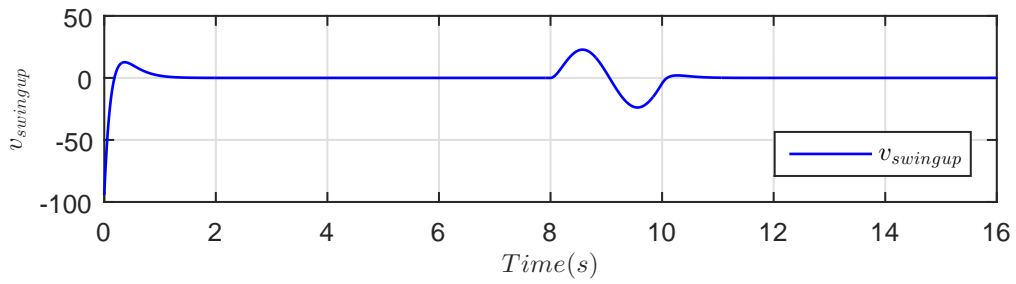
(A) Pendulum position q_1 (rad) and velocity \dot{q}_1 (rad/s)



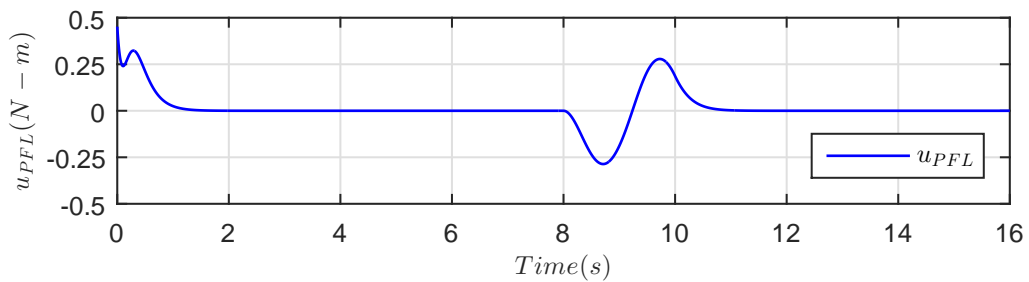
(B) Wheel position q_2 (rad) and velocity \dot{q}_2 (rad/s)



(C) Disturbance $d(t) = 0.1 \sin(\pi t)$



(D) Swingup control $v_{swingup}$



(E) Control effort u_{PFL} (N-m)

FIGURE 7.1: IWP - Closed loop response with control law (7.6) ($K_d = 11$, $K_p = 30$), $q(0) = [\pi, 0, 0, 0]^T$

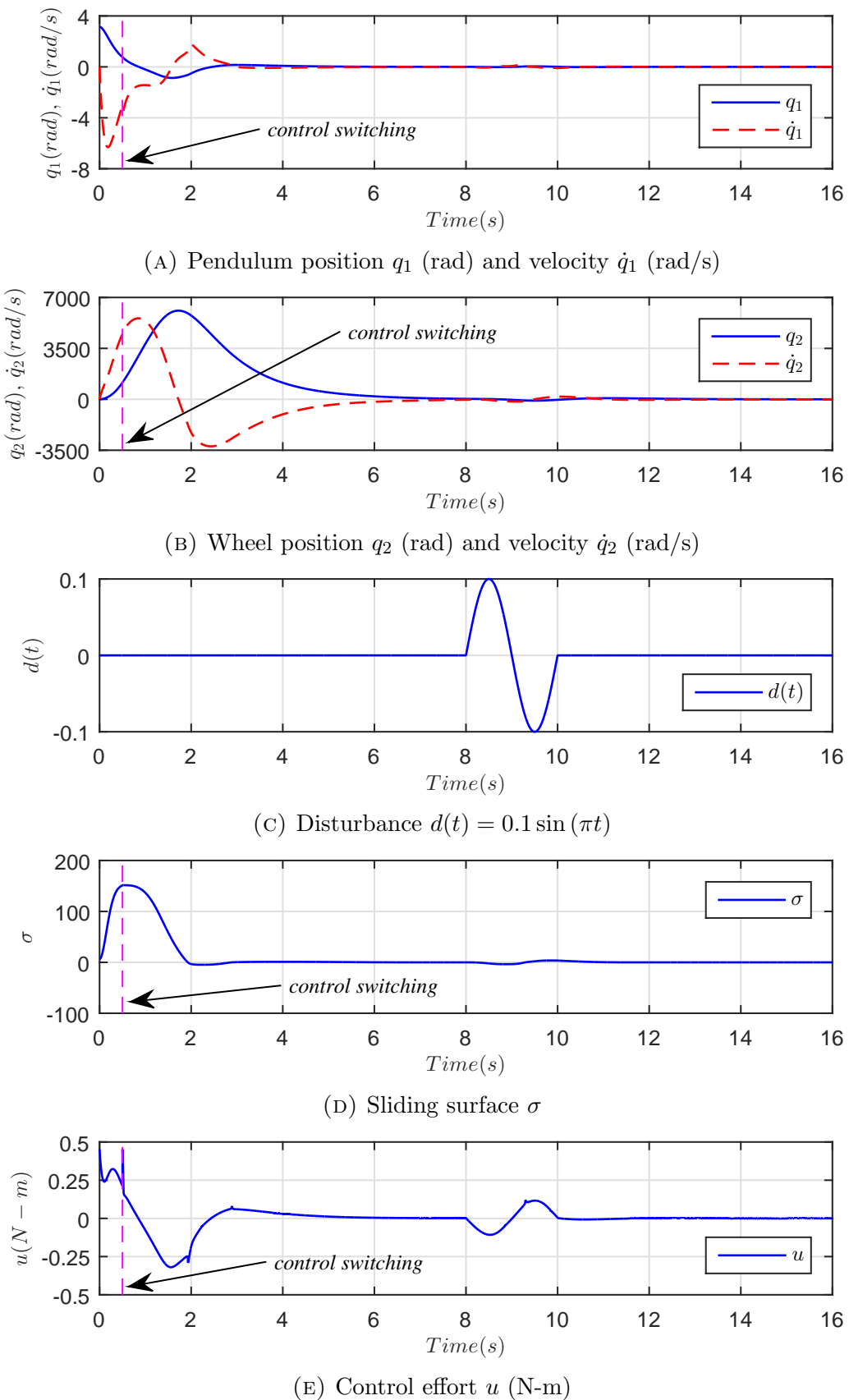


FIGURE 7.2: IWP - Swingup with control law (7.6) ($K_d = 11$, $K_p = 30$) and balancing with HOSM control law (6.25) ($K_1 = 500$, $K_2 = 400$) and observer (6.26) ($\lambda_1 = 2$, $\lambda_2 = 3$), sliding parameters ($\alpha = 3$, $\beta = 2$), $q(0) = [\pi, 0, 0, 0]^T$

7.1.2 The Acrobot

The dynamics of Acrobot are described by (7.1) with the following

$$\begin{aligned}
m_{11}(q_2) &= m_1 \ell_1^2 + m_2(L_1^2 + \ell_2^2) + I_1 + I_2 + 2m_2 L_1 \ell_2 \cos(q_2) \\
m_{12}(q_2) &= m_2 \ell_2^2 + I_2 + m_2 L_1 \ell_2 \cos(q_2) \\
m_{21}(q_2) &= m_{12} \\
m_{22}(q_2) &= m_2 \ell_2^2 + I_2 \\
c_1(q, \dot{q}) &= -m_2 L_1 \ell_2 \sin(q_2)(2\dot{q}_1 \dot{q}_2 + \dot{q}_2^2) \\
c_2(q, \dot{q}) &= m_2 L_1 \ell_2 \sin(q_2) \dot{q}_1^2 \\
g_1(q) &= -(m_1 \ell_1 + m_2 L_1)g \sin(q_1) - m_2 \ell_2 g \sin(q_1 + q_2) \\
g_2(q) &= -m_2 \ell_2 g \sin(q_1 + q_2)
\end{aligned} \tag{7.8}$$

The Acrobot has the following four natural equilibrium points:

- P1: $(q_1, \dot{q}_1, q_2, \dot{q}_2) = (0, 0, 0, 0)$, both link 1 and link 2 up; unstable
- P2: $(q_1, \dot{q}_1, q_2, \dot{q}_2) = (0, 0, \pi, 0)$, link 1 up and link 2 down; unstable
- P3: $(q_1, \dot{q}_1, q_2, \dot{q}_2) = (\pi, 0, \pi, 0)$, link 1 down and link 2 up; unstable
- P4: $(q_1, \dot{q}_1, q_2, \dot{q}_2) = (\pi, 0, 0, 0)$, both link 1 and link 2 down; stable

The control objective is to drive the system from P4 to P1 and balance it there afterward.

Note that the synthesis of smooth HOSM control w given by (6.25) for the Acrobot is based on the assumption $-\frac{\pi}{2} < \xi = q_2 < \frac{\pi}{2}$, and hence cannot stabilize the Acrobot from below the horizontal axis $q_2 = \frac{\pi}{2}$. To stabilize the Acrobot from the downward stable equilibrium position $q_1 = \pi$ to the upward unstable equilibrium position $q_1 = 0$, design Swingup Control. The controller w in Eq. (6.25) can then be used as a balancing controller. We use the same physical parameters for the Acrobot as in the previous chapters.

To stabilize the Pendulum from P4 to P1, the following two approaches are presented for the swingup problem and discuss their merits and demerits.

Partial linearization w.r.t q_1 :

To stabilize the the first link position from $q_1 = \pi$ to $q_1 = 0$, partially linearize the dynamics of the Acrobot with respect to q_1 . Solving Eq. (7.1a) for \ddot{q}_2 as

$$\ddot{q}_2 = -m_{12}^{-1} (c_1 + g_1 + m_{11}\ddot{q}_1) \quad (7.9)$$

putting the result in Eq. (7.1b) and using the following noncollocated Partial Feedback Linearizing (PFL) control

$$u = u_{PFL1} = (m_{21} - m_{22}m_{12}^{-1}m_{11})v_{swingup} + c_2 + g_2 - m_{22}m_{12}^{-1}(c_1 + g_1) \quad (7.10)$$

where $v_{swingup}$ is a new control to be designed, the dynamics of the Acrobot become:

$$\ddot{q}_1 = v_{swingup} \quad (7.11a)$$

$$m_{12}\ddot{q}_2 + c_1 + g_1 = -m_{11}v_{swingup} \quad (7.11b)$$

Equation (7.11a) is linear, a double integrator, and is simple to stabilize. Choose the following control law

$$v_{swingup} = -K_d\dot{q}_1 - K_pq_1 \quad (7.12)$$

with K_d , K_p as positive design constants. The control $v_{swingup}$ combined with u_{PFL1} (7.10) can stabilize q_1 from $q_1 = \pi$ to $q_1 = 0$, however the q_2 -dynamics, obviously, become unstable. Once q_1 is stabilized, $v_{swingup}$ becomes zero and the q_2 -dynamics, in accordance with Eq. (7.9) (equivalently, Eq. (7.11b)), become

$$(m_2\ell_2^2 + I_2 + m_2L_1\ell_2 \cos(q_2)) \ddot{q}_2 - m_2\ell_2 (g + L_1\dot{q}_2^2) \sin(q_2) = 0 \quad (7.13)$$

Linearization and stabilization w.r.t. to q_1 led to the above complex dynamics in Eq. (7.13) for q_2 that strongly depend on the velocity, i.e., \dot{q}_2^2 . Figure 7.3 shows closed loop response of the Acrobot with $v_{swingup}$ (7.12) with $K_d = 3.0$, $K_p = 2.0$ for the initial condition $q(0) = [\pi, 0, 0, 0]^T$. The nonlinear behavior in Eq. (7.13) is shown Fig. 7.3b.

A simple choice of K_d , and K_p resulting in stable and real only closed loop poles (-2,-1 in this case) of (7.11a) can achieve the desired response for q_1 -dynamics as shown in Fig. 7.3a. But as predicted by Eq. (7.13) and verified by Fig. 7.3b, the response of q_2 -dynamics exhibits large peak in velocity and in control efforts. This response is not helpful in stabilization by the HOSM controller. For a successful swingup and stabilization using this case needs some oscillatory behavior and crucially depends on the values of K_d , and K_p . Figure 7.4 shows such a response of the Acrobot using $v_{swingup}$ (7.12) with $K_d = 1.0$, $K_p = 20.0$ for the initial condition $q(0) = [\pi, 0, 0, 0]^T$. Figure 7.5 shows a successful using $v_{swingup}$ (7.12) with $K_d = 1.0$, $K_p = 20.0$ and then balancing by HOSM control (6.25) in the presence of external disturbance for the initial condition $q(0) = [\pi, 0, 0, 0]^T$.

Figures 7.3 and 7.4 show that system response is more sensitive to disturbance under state feedback control law (7.12). Figures 7.5 shows the great advantage of using HOSM control that rejects the same disturbance. 7.4b shows how the disturbance induces a positive shift of 4π in the Link 2 position q_2 and make it stable around it. This is a positive sign of sinusoidal disturbance and is used as control input to excite oscillatory motion and capture by balancing control.

As we noted that the strong dependence \dot{q}_2^2 in (7.13) results in the control effort. The reason is that this dependence results in strong peaks in the Coriolis term $c_1(q, \dot{q})$ in Eq. (7.8) that in turn results in strong peaks in the u_{PFL} control in Eq. (7.10). So the best approach is to stabilize the q_2 -dynamics first to get rid of this strong dependence \dot{q}_2^2 and in Coriolis term and further in control effort. This is achieved in the next paragraph.

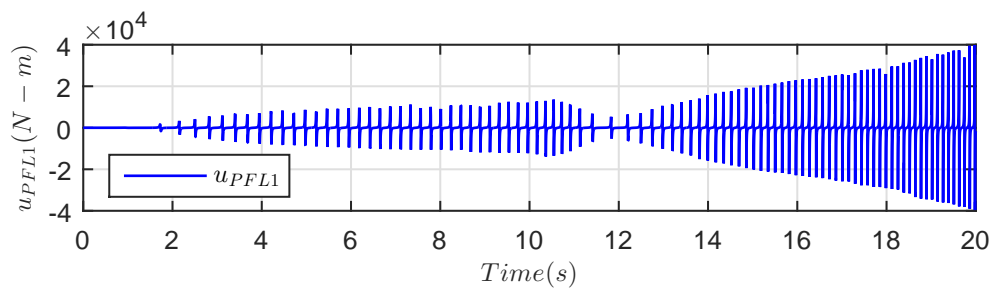
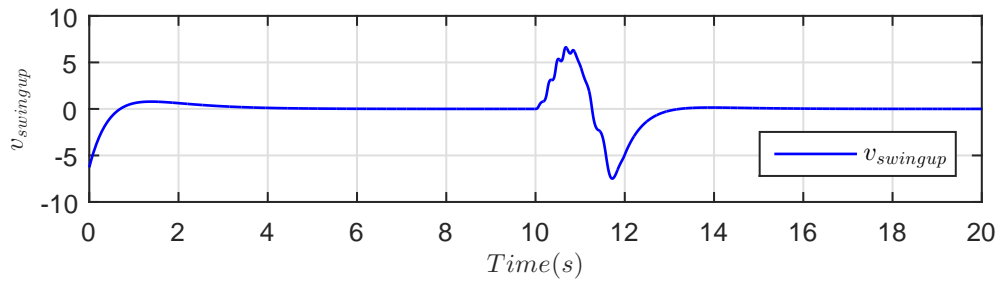
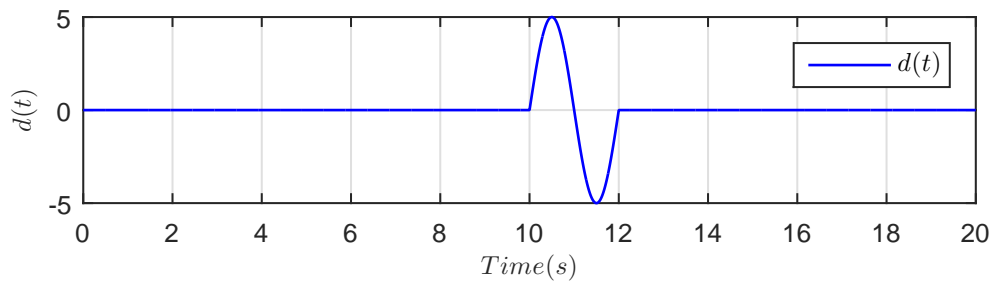
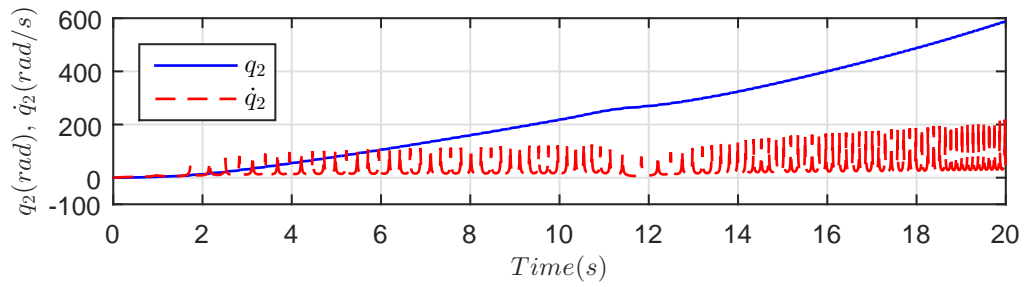
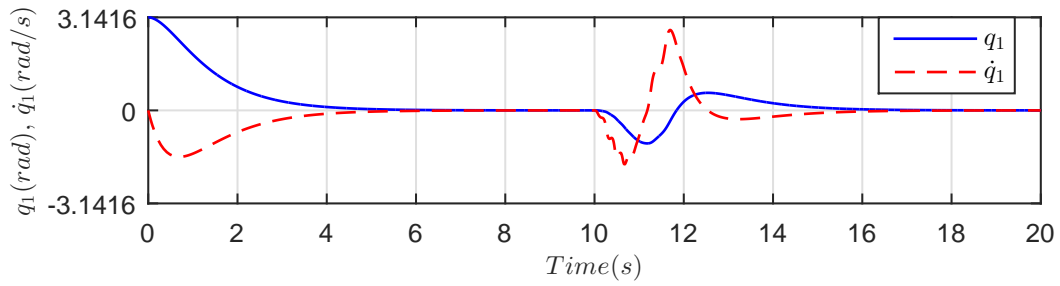


FIGURE 7.3: Acrobot - Closed loop response with control law (7.12) ($K_d = 3$, $K_p = 2$), $q(0) = [\pi, 0, 0, 0]^T$

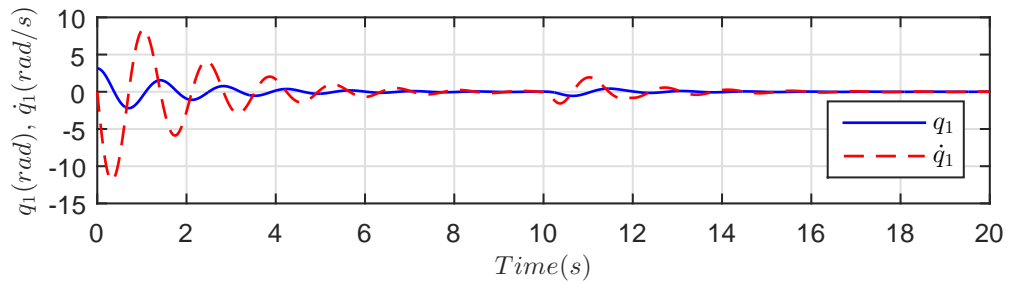
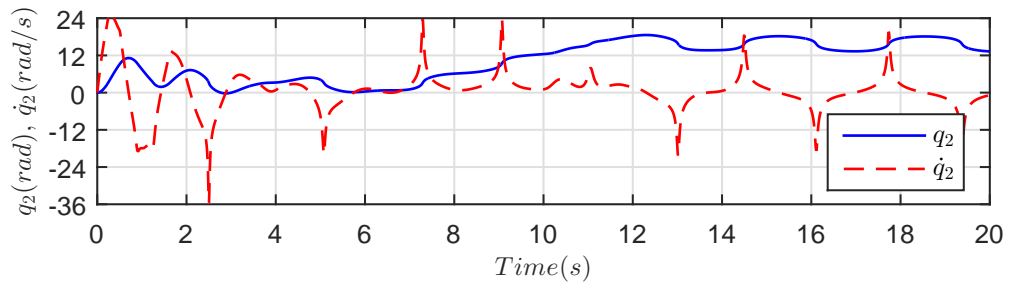
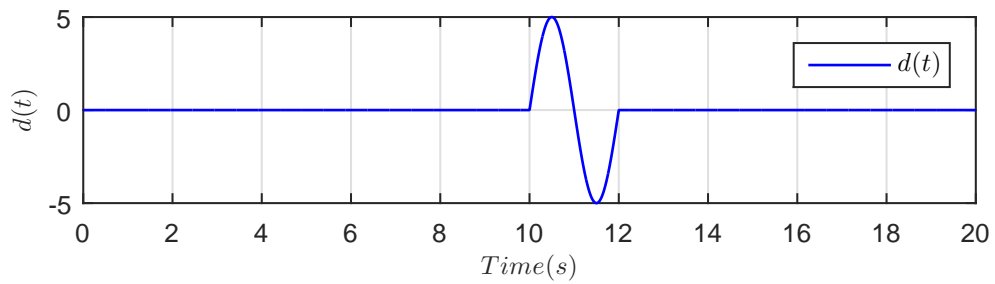
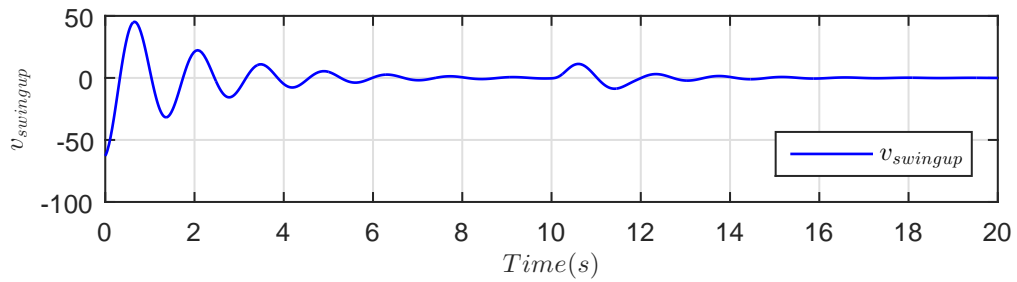
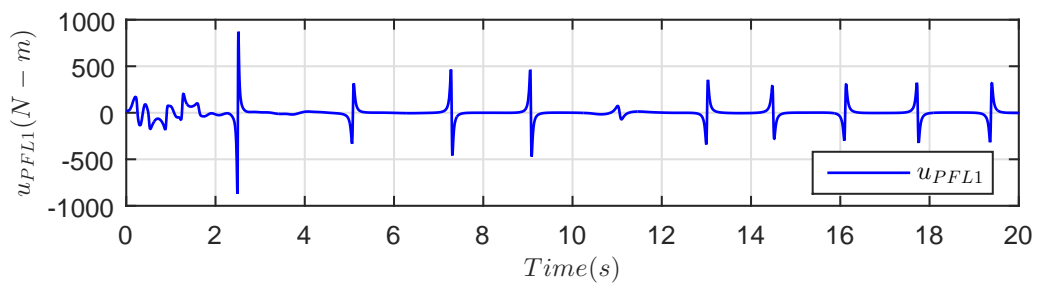
(A) Link 1 position q_1 (rad) and velocity \dot{q}_1 (rad/s)(B) Link 2 position q_2 (rad) and velocity \dot{q}_2 (rad/s)(C) Disturbance $d(t) = 5 \sin(\pi t)$ (D) Swingup control $v_{swingup}$ (E) Control effort u_{PFL1} (N-m)

FIGURE 7.4: Acrobot - Closed loop response with control law (7.12) ($K_d = 1$, $K_p = 20$), $q(0) = [\pi, 0, 0, 0]^T$

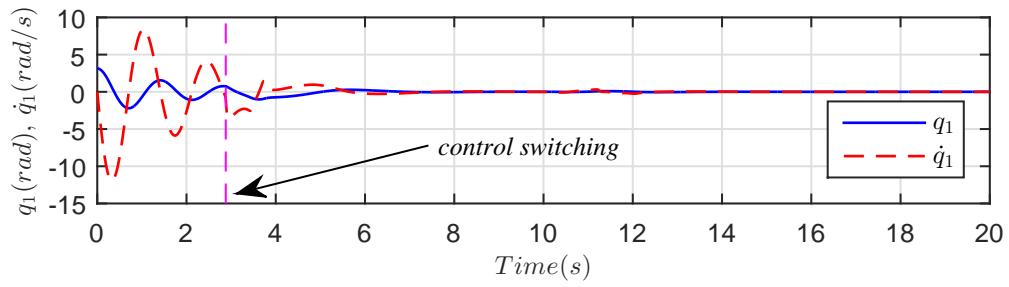
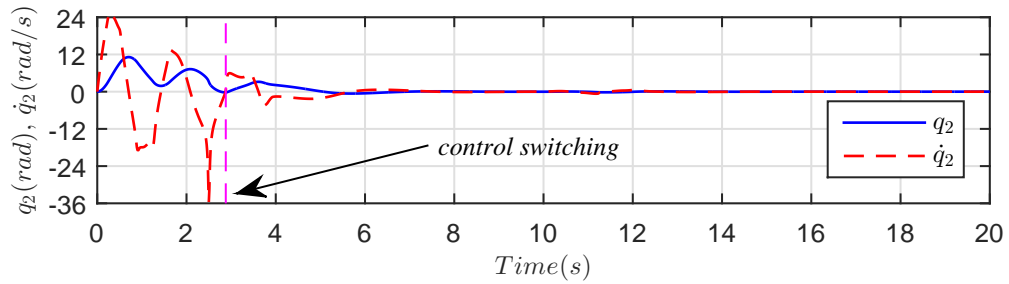
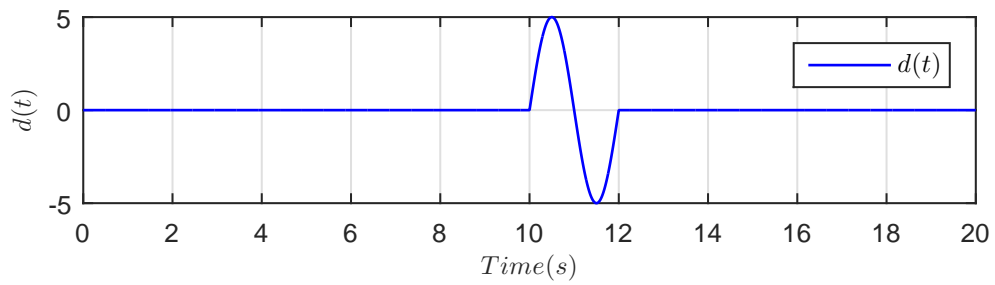
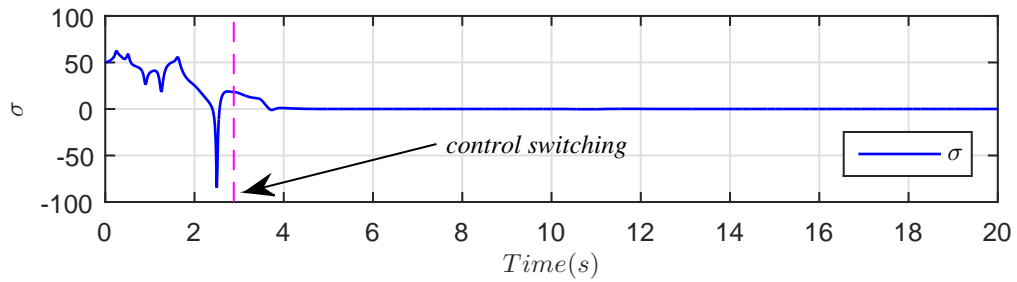
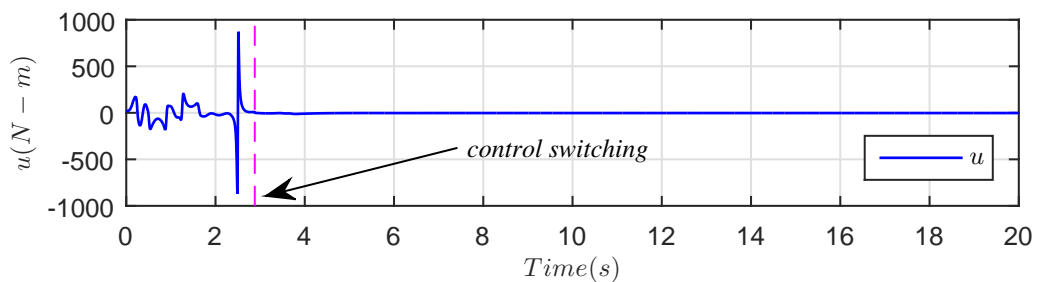
(A) Link 1 position q_1 (rad) and velocity \dot{q}_1 (rad/s)(B) Link 2 position q_2 (rad) and velocity \dot{q}_2 (rad/s)(C) Disturbance $d(t) = 5 \sin(\pi t)$ (D) Sliding surface σ (E) Control effort u (N-m)

FIGURE 7.5: Acrobot - Swingup with control law (7.12) ($K_d = 1$, $K_p = 20$) and balancing with HOSM control law (6.25) ($K_1 = 75$, $K_2 = 50$) and observer (6.26) ($\lambda_1 = 1$, $\lambda_2 = 3$), sliding parameters ($\alpha = 8$, $\beta = 16$), $q(0) = [\pi, 0, 0, 0]^T$

Partial linearization w.r.t q_2 :

Partially linearize the dynamics of the Acrobot with respect to q_2 . Solving Eq. (7.1a) for \ddot{q}_1 as

$$\ddot{q}_1 = -m_{11}^{-1}(c_1 + g_1 + m_{12}\ddot{q}_2) \quad (7.14)$$

putting the result in Eq. (7.1b) and using the following collocated Partial Feedback Linearizing (PFL) control

$$u = u_{PFL2} = (m_{22} - m_{21}m_{11}^{-1}m_{12})v_{swingup} + c_2 + g_2 - m_{21}m_{11}^{-1}(c_1 + g_1) \quad (7.15)$$

where $v_{swingup}$ is a new control to be designed, the dynamics of the Acrobot become:

$$m_{11}\ddot{q}_1 + c_1 + g_1 = -m_{12}v_{swingup} \quad (7.16a)$$

$$\ddot{q}_2 = v_{swingup} \quad (7.16b)$$

Equation (7.16b) is linear, a double integrator, and is simple to stabilize. Choose the following control law

$$v_{swingup} = -K_d\dot{q}_2 - K_pq_2 \quad (7.17)$$

with K_d , K_p as positive design constants. The control $v_{swingup}$ combined with u_{PFL2} (7.15) can stabilize q_2 , however the q_1 -dynamics, obviously, become unstable. Once q_2 is stabilized, $v_{swingup}$ becomes zero and the q_1 -dynamics, in accordance with Eq. (7.14) (equivalently, Eq. (7.16a)), become

$$(m_1\ell_1^2 + m_2(L_1^2 + \ell_2^2) + I_1 + I_2 + 2m_2L_1\ell_2)\ddot{q}_1 - g(m_1\ell_1 + m_2L_1 + m_2\ell_2)\sin(q_1) = 0 \quad (7.18)$$

Linearization and stabilization w.r.t. to q_2 led to the above dynamics in Eq. (7.18) for q_1 that represent the simple pendulum. Figure 7.6 shows closed loop response of the Acrobot with $v_{swingup}$ (7.17) with $K_d = 12.0$, $K_p = 36.0$ for the initial condition $q(0) = [\pi, 0, 2\pi, 0]^T$. The pendulum behavior in Eq. (7.18) is shown Fig. 7.6a.

A simple choice of K_d , and K_p resulting in stable and real only closed loop poles (-6,-6 in this case) of (7.16b) can achieve the desired response for q_2 -dynamics as shown in Fig. 7.6b and a pendulum behavior for q_1 that is helpful in stabilization by the HOSM controller. Figure 7.7 shows a successful using $v_{swingup}$ (7.17) with $K_d = 12.0$, $K_p = 36.0$ and then balancing by the balancing by HOSM control (6.25) in the presence of external disturbance for the initial condition $q(0) = [\pi, 0, 2\pi, 0]^T$. Figure 7.6 shows that system response is more sensitive to disturbance under state feedback control law (7.17). Figures 7.7 shows the great advantage of using HOSM control that rejects the same disturbance. Figure 7.6a shows how the disturbance induces a negative shift of 2π in the Link 1 position q_1 crossing the upward equilibrium point $q_1 = 0$ and making it attractive for the balancing controller. Again note the advantage of sinusoidal disturbance as control input to excite oscillatory motion and capture by balancing control.

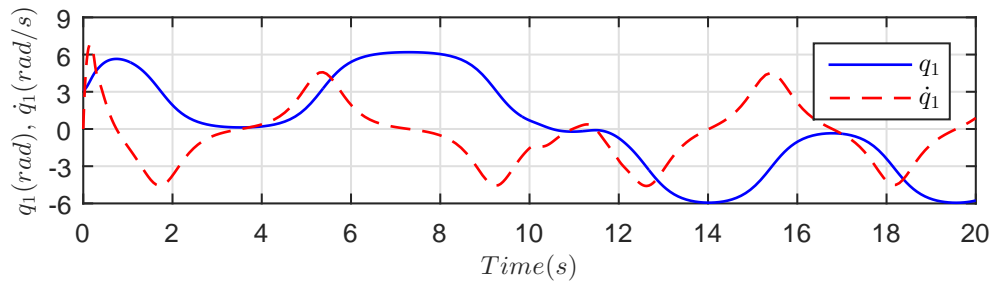
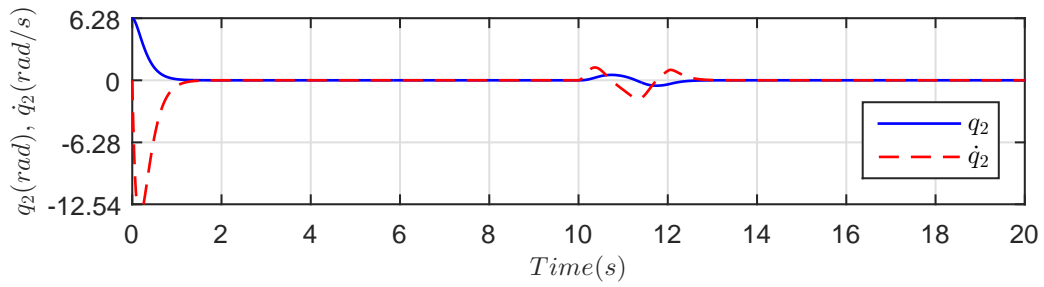
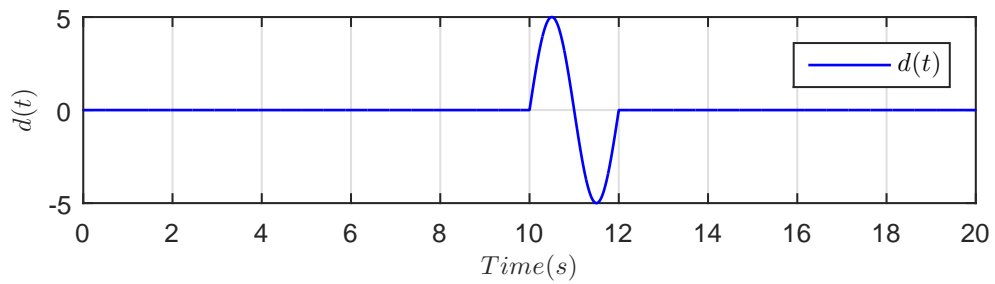
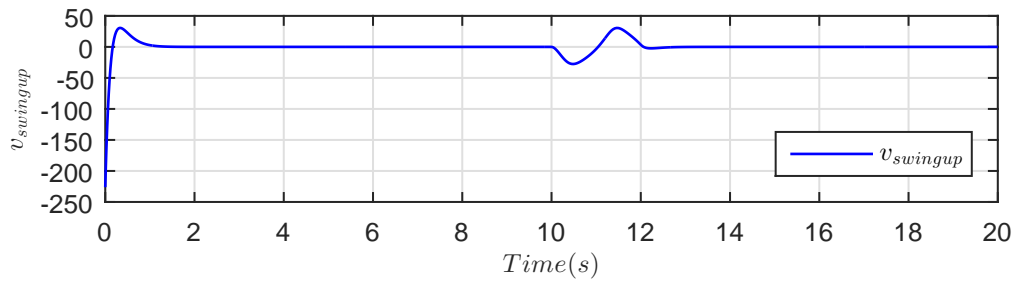
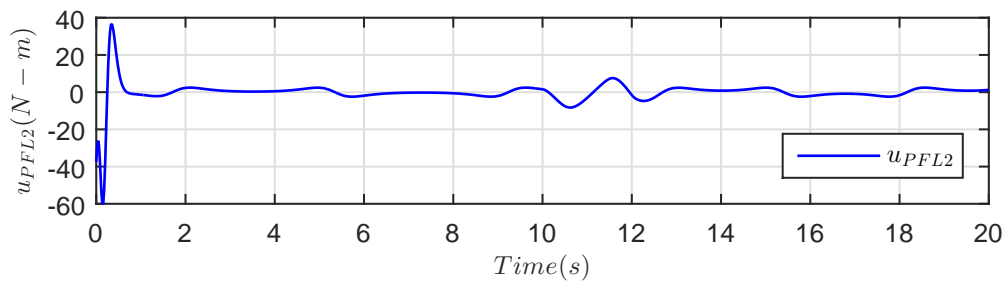
(A) Link 1 position q_1 (rad) and velocity \dot{q}_1 (rad/s)(B) Link 2 position q_2 (rad) and velocity \dot{q}_2 (rad/s)(C) Disturbance $d(t) = 5 \sin(\pi t)$ (D) Swingup control $v_{swingup}$ (E) Control effort u_{PFL2} (N-m)

FIGURE 7.6: Acrobot - Closed loop response with control law (7.17) ($K_d = 12$, $K_p = 36$), $q(0) = [\pi, 0, 2\pi, 0]^T$

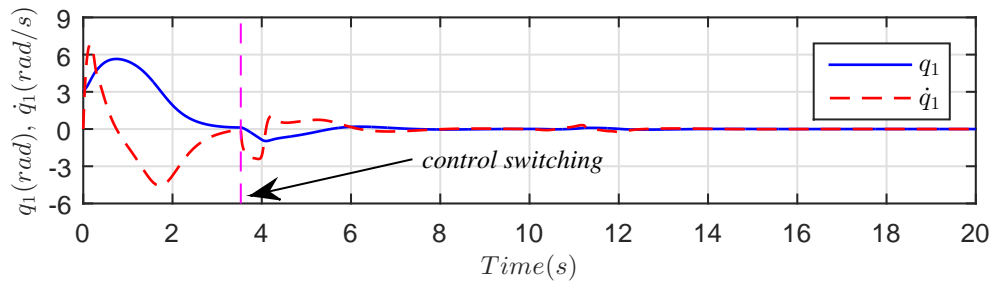
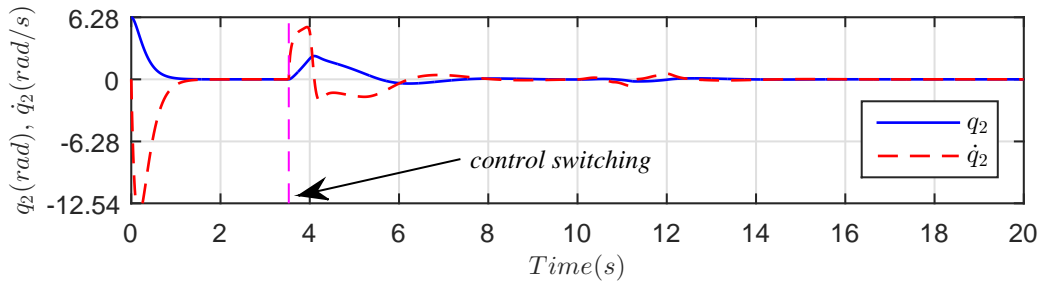
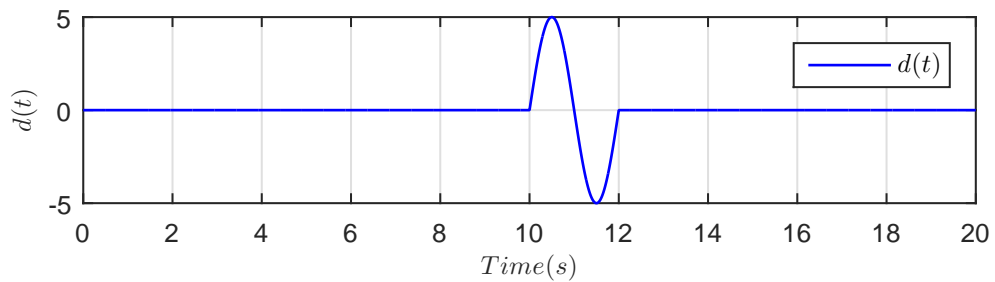
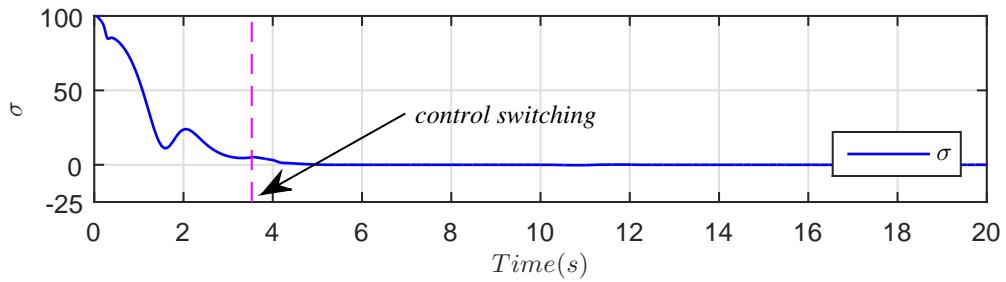
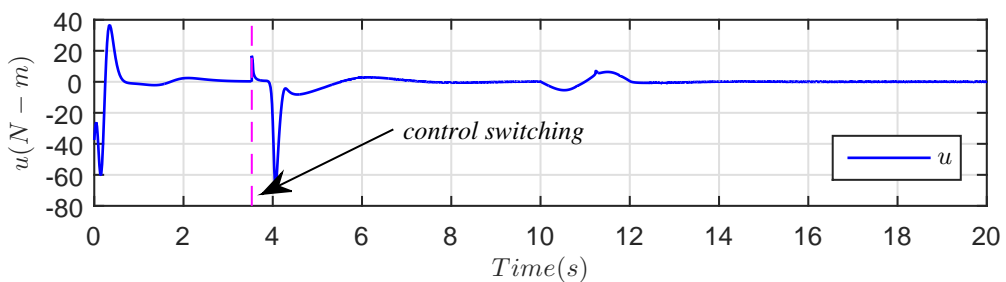
(A) Link 1 position q_1 (rad) and velocity \dot{q}_1 (rad/s)(B) Link 2 position q_2 (rad) and velocity \dot{q}_2 (rad/s)(C) Disturbance $d(t) = 5 \sin(\pi t)$ (D) Sliding surface σ (E) Control effort u (N-m)

FIGURE 7.7: Acrobot - Swingup with control law (7.17) ($K_d = 12$, $K_p = 36$) and balancing with HOSM control law (6.25) ($K_1 = 75$, $K_2 = 50$) and observer (6.26) ($\lambda_1 = 1$, $\lambda_2 = 3$), sliding parameters ($\alpha = 8$, $\beta = 16$), $q(0) = [\pi, 0, 2\pi, 0]^T$

7.2 Class-II Underactuated Mechanical Systems

Consider Class-II underactuated mechanical systems described by:

$$m_{11}(q_2)\ddot{q}_1 + m_{12}(q_2)\ddot{q}_2 + c_1(q, \dot{q}) + g_1(q_1, q_2) = u \quad (7.19a)$$

$$m_{21}(q_2)\ddot{q}_1 + m_{22}(q_2)\ddot{q}_2 + c_2(q, \dot{q}) + g_2(q_1, q_2) = 0 \quad (7.19b)$$

The Furuta Pendulum with Eq. (3.13) and the Pendubot with Eq. (3.12) are described by Eq. (7.19).

7.2.1 The Furuta Pendulum

The dynamics of Furuta Pendulum are described by (7.19) with the following

$$\begin{aligned} m_{11}(q_2) &= I_1 + m_1 l_1^2 + m_2 L_1^2 + m_2 l_2^2 \sin^2(q_2) \\ m_{12}(q_2) &= m_2 L_1 l_2 \cos(q_2) \\ m_{21}(q_2) &= m_{12}(q_2) \\ m_{22}(q_2) &= I_2 + m_2 l_2^2 \\ c_1(q, \dot{q}) &= 2m_2 l_2^2 \sin(q_2) \cos(q_2) \dot{q}_1 \dot{q}_2 - m_2 L_1 l_2 \sin(q_2) \dot{q}_2^2 \\ c_2(q, \dot{q}) &= -m_2 l_2^2 \sin(q_2) \cos(q_2) \dot{q}_1^2 \\ g_1(q_1, q_2) &= 0 \\ g_2(q_1, q_2) &= -m_2 l_2 g \sin(q_2) \end{aligned} \quad (7.20)$$

Note that the HOSM control in (6.25) cannot stabilize the Furuta Pendulum globally first due to the assumption $-\frac{\pi}{2} < \xi = q_2 < \frac{\pi}{2}$ in its synthesis and second due to a singularity in the PFL control in (6.48) at $q_2 = \frac{\pi}{2}$. For global stabilization we design swingup control law.

The above mentioned singularity problem also dictate us to partially linearize the dynamics of Furuta Pendulum with respect to q_1 . Solving Eq. (7.19b) for \ddot{q}_2 as

$$\ddot{q}_2 = -m_{22}^{-1} (c_2 + g_2 + m_{21}\ddot{q}_1) \quad (7.21)$$

putting the result in (7.19a) and using the following collocated Partial Feedback Linearizing control

$$u = u_{PFL} = (m_{11} - m_{12}m_{22}^{-1}m_{21})v_{swingup} - m_{12}m_{22}^{-1}(c_2 + g_2) + c_1 + g_1 \quad (7.22)$$

where $v_{swingup}$ is a new control to be designed, the dynamics of the Furuta Pendulum become:

$$\ddot{q}_1 = v_{swingup} \quad (7.23a)$$

$$m_{22}\ddot{q}_2 + c_2 + g_2 = -m_{21}v_{swingup} \quad (7.23b)$$

To stabilize (7.23a), choose the following control law

$$v_{swingup} = -K_d\dot{q}_1 - K_pq_1 \quad (7.24)$$

with $K_d > 0$, $K_p > 0$ as design constants. Once q_1 is stabilized, $v_{swingup}$ becomes zero and the q_2 -dynamics become:

$$(I_2 + m_2\ell_2^2)\ddot{q}_2 - m_2\ell_2g\sin(q_2) = 0 \quad (7.25)$$

Fig. 7.8 shows closed loop response of the Furuta Pendulum with $v_{swingup}$ (7.24) with $K_d = 8$, $K_p = 10$ for the initial condition $q(0) = [-5, 0, \pi, 0]^T$. The pendulum behavior in (7.25) is shown Fig. 7.8b. Fig. 7.9 shows a successful swing up from $q_2 = \pi$ to $q_2 = 0$ using $v_{swingup}$ (7.24) and then balancing by HOSM control (6.25) in the presence of external disturbance. Fig. 7.8

Fig. 7.8 shows the effect of disturbance is prominent on system response under the state feedback control and Fig. 7.9 shows the system response is robust to the same disturbance under the HOSM control.

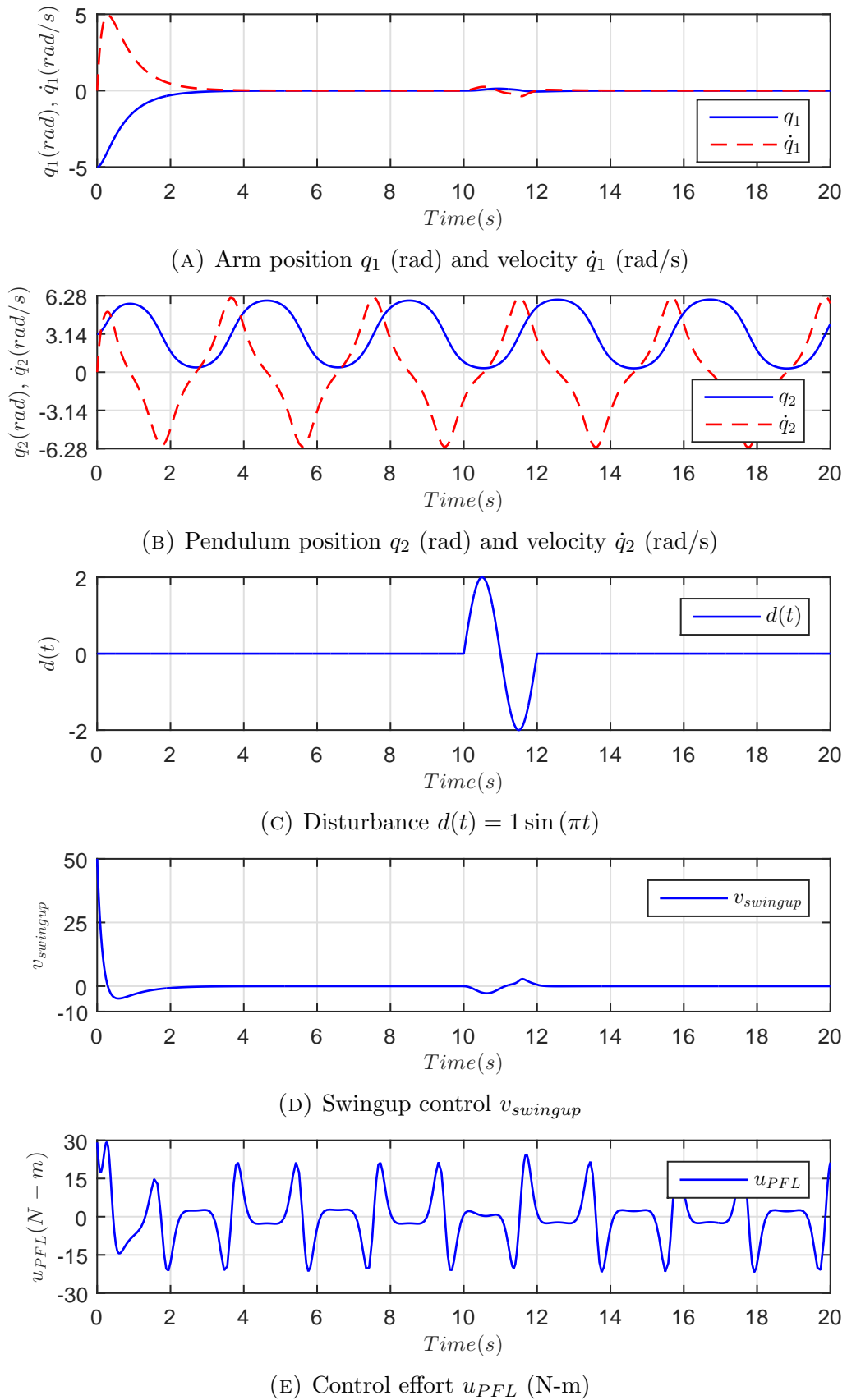


FIGURE 7.8: Furuta Pendulum - Closed loop response with control law (7.24) ($K_d = 8$, $K_p = 10$), $q(0) = [-5, 0, \pi, 0]^T$

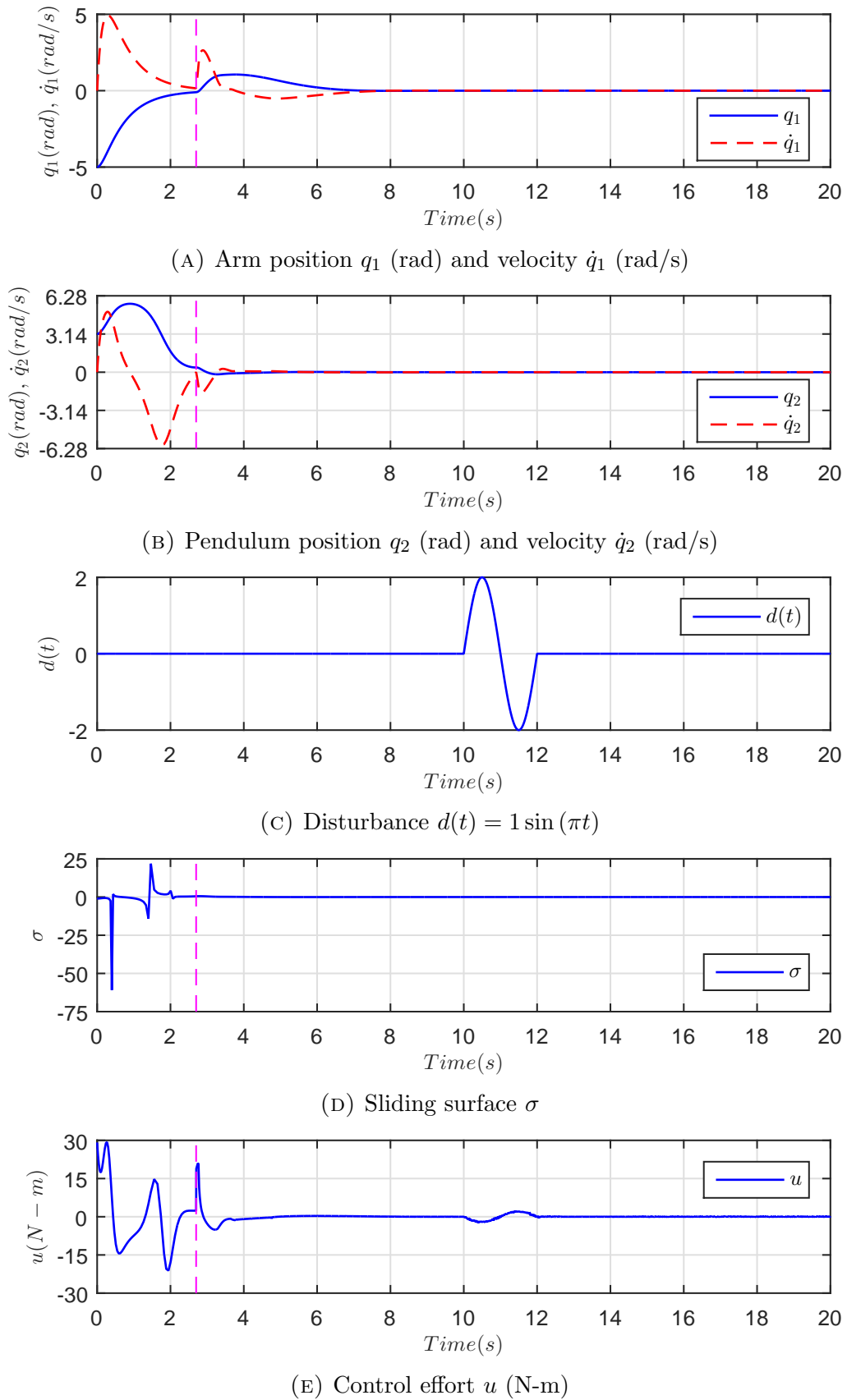


FIGURE 7.9: Furuta Pendulum - Swingup with control law (7.24) ($K_d = 8$, $K_p = 10$) and balancing with HOSM control law (6.25) ($K_1 = 8$, $K_2 = 10$) and observer (6.26) ($\lambda_1 = 1$, $\lambda_2 = 3$), sliding parameters ($\alpha = 8$, $\beta = 16$), $q(0) = [-5, 0, \pi, 0]^T$

7.2.2 Pendubot

The dynamics of Pendubot are described by (7.19) with the following

$$\begin{aligned}
m_{11}(q_2) &= m_1\ell_1^2 + m_2(L_1^2 + \ell_2^2) + I_1 + I_2 + 2m_2L_1\ell_2 \cos(q_2) \\
m_{12}(q_2) &= m_2\ell_2^2 + I_2 + m_2L_1\ell_2 \cos(q_2) \\
m_{21}(q_2) &= m_{12} \\
m_{22}(q_2) &= m_2\ell_2^2 + I_2 \\
c_1(q, \dot{q}) &= -m_2L_1\ell_2 \sin(q_2)(2\dot{q}_1\dot{q}_2 + \dot{q}_2^2) \\
c_2(q, \dot{q}) &= m_2L_1\ell_2 \sin(q_2)\dot{q}_1^2 \\
g_1(q) &= -(m_1\ell_1 + m_2L_1)g \sin(q_1) - m_2\ell_2g \sin(q_1 + q_2) \\
g_2(q) &= -m_2\ell_2g \sin(q_1 + q_2)
\end{aligned} \tag{7.26}$$

The Pendubot has the following four natural equilibrium points:

- P1: $(q_1, \dot{q}_1, q_2, \dot{q}_2) = (0, 0, 0, 0)$, both link 1 and link 2 up; unstable
- P2: $(q_1, \dot{q}_1, q_2, \dot{q}_2) = (0, 0, \pi, 0)$, link 1 up and link 2 down; unstable
- P3: $(q_1, \dot{q}_1, q_2, \dot{q}_2) = (\pi, 0, \pi, 0)$, link 1 down and link 2 up; unstable
- P4: $(q_1, \dot{q}_1, q_2, \dot{q}_2) = (\pi, 0, 0, 0)$, both link 1 and link 2 down; stable

The control objective is to drive the system from P4 to P1 and balance it there afterward.

Note that the synthesis of smooth HOSM control v given by (6.25) for the Pendubot is based on the assumption $-\frac{\pi}{2} < \xi = q_2 < \frac{\pi}{2}$, and hence cannot stabilize the Pendubot from below the horizontal axis $q_2 = \frac{\pi}{2}$. To stabilize the Pendubot from the downward stable equilibrium position $q_1 = \pi$ to the upward unstable equilibrium position $q_1 = 0$, we design Swingup Control. The controller v in Eq. (6.25) can then be used as a balancing controller. We use the same physical parameters for the Pendubot as in the previous chapters.

To stabilize the Pendulum from P4 to P1, the following two approaches are presented for the swingup problem and discuss their merits and demerits.

Partial linearization w.r.t q_1 :

To stabilize the the first link position from $q_1 = \pi$ to $q_1 = 0$, partially linearize the dynamics of the Pendubot with respect to q_1 . Solving Eq. (7.19b) for \ddot{q}_2 as

$$\ddot{q}_2 = -m_{22}^{-1} (c_2 + g_2 + m_{21}\ddot{q}_1) \quad (7.27)$$

putting the result in Eq. (7.19a) and using the following collocated Partial Feedback Linearizing (PFL) control

$$u = u_{PFL1} = (m_{11} - m_{12}m_{22}^{-1}m_{21})v_{swingup} + c_1 + g_1 - m_{12}m_{22}^{-1}(c_2 + g_2) \quad (7.28)$$

where $v_{swingup}$ is a new control to be designed, the dynamics of the Pendubot become:

$$\ddot{q}_1 = v_{swingup} \quad (7.29a)$$

$$m_{22}\ddot{q}_2 + c_2 + g_2 = -m_{21}v_{swingup} \quad (7.29b)$$

Equation (7.29a) is linear, a double integrator, and is simple to stabilize. Choose the following control law

$$v_{swingup} = -K_d\dot{q}_1 - K_pq_1 \quad (7.30)$$

with K_d , K_p as positive design constants. The control $v_{swingup}$ combined with u_{PFL1} (7.28) can stabilize q_1 from $q_1 = \pi$ to $q_1 = 0$, however the q_2 -dynamics, obviously, become unstable. Once q_1 is stabilized, $v_{swingup}$ becomes zero and the q_2 -dynamics, in accordance with Eq. (7.27) (equivalently, Eq. (7.29b)), become

$$(m_2\ell_2^2 + I_2) \ddot{q}_2 - m_2\ell_2g \sin(q_2) = 0 \quad (7.31)$$

Linearization and simple stabilization w.r.t. to q_1 led to the above pendulum dynamics in Eq. (7.31). Figure 7.10 shows closed loop response of the Pendubot with $v_{swingup}$ (7.30) with $K_d = 10.0$, $K_p = 125.0$ for the initial condition $q(0) = [\pi, 0, 0, 0]^T$. The Pendulum behavior in Eq. (7.31) is shown Fig. 7.10b.

A simple choice of K_d , and K_p resulting in stable and real only closed loop poles of

(7.29a) can achieve the desired response for q_1 -dynamics as shown in Fig. 7.10a. Figure 7.11 shows a successful using $v_{swingup}$ (7.30) with $K_d = 10.0$, $K_p = 125.0$ and then balancing by the HOSM control (6.25) in the presence of external disturbance for the initial condition $q(0) = [\pi, 0, 0, 0]^T$.

Fig. 7.10 shows the visible effect of disturbance on system response under the state feedback control (7.30) and Fig. 7.11 shows the system response is robust to the same disturbance under the HOSM control (6.25).

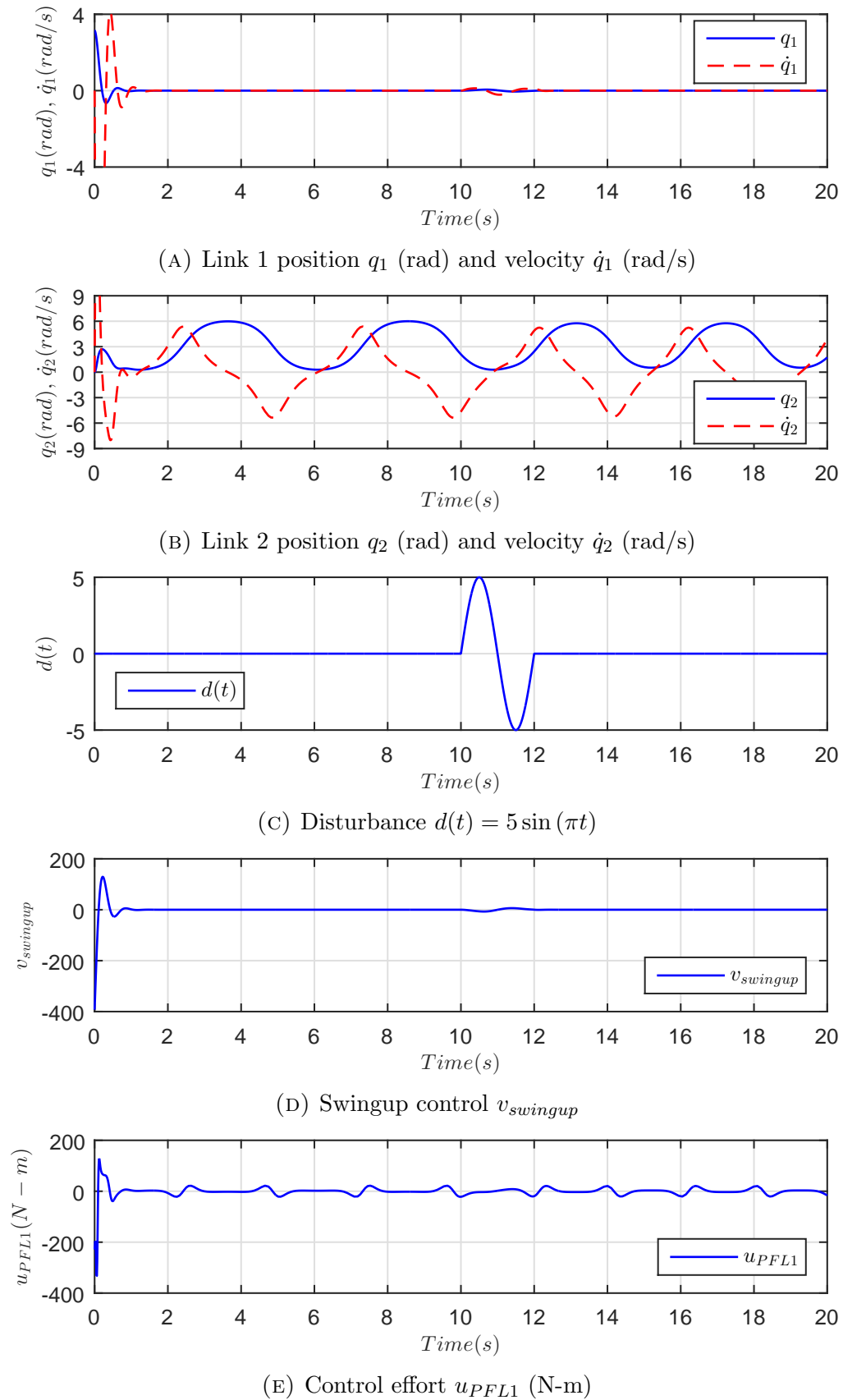


FIGURE 7.10: Pendubot - Closed loop response with control law (7.30) ($K_d = 10$, $K_p = 125$), $q(0) = [\pi, 0, 0, 0]^T$

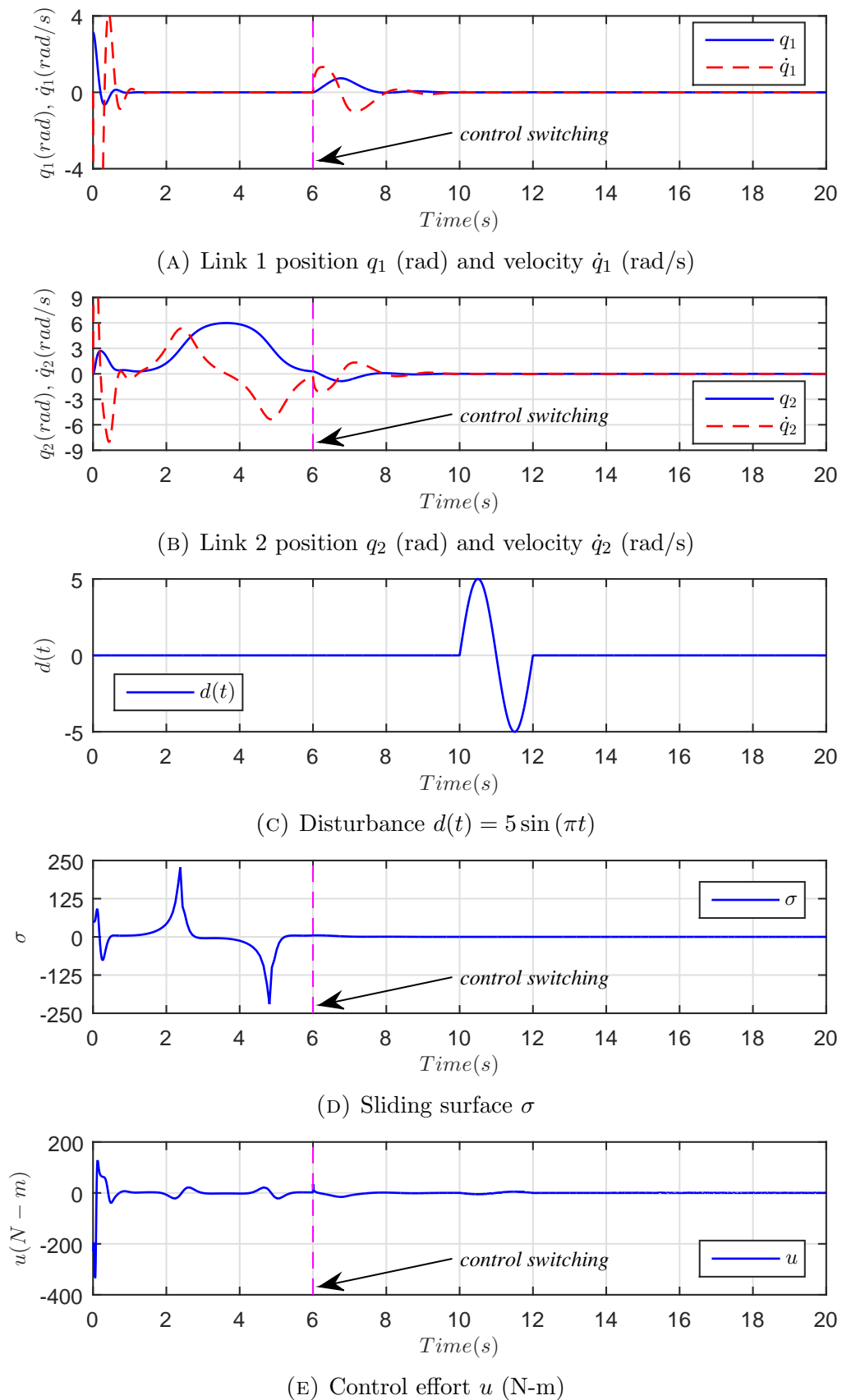


FIGURE 7.11: Pendubot - Swingup with control law (7.30) ($K_d = 10$, $K_p = 125$) and balancing with HOSM control law (6.25) ($K_1 = 125$, $K_2 = 100$) and observer (6.26) ($\lambda_1 = 3$, $\lambda_2 = 5$), sliding parameters ($\alpha = 8$, $\beta = 16$), $q(0) = [\pi, 0, 0, 0]^T$

Partial linearization w.r.t q_2 :

Partially linearize the dynamics of the Pendubot with respect to q_2 . Solving Eq. (7.19b) for \ddot{q}_1 as

$$\ddot{q}_1 = -m_{21}^{-1}(c_2 + g_2 + m_{22}\ddot{q}_2) \quad (7.32)$$

putting the result in Eq. (7.19a) and using the following noncollocated Partial Feedback Linearizing (PFL) control

$$u = u_{PFL2} = (m_{12} - m_{11}m_{21}^{-1}m_{22})v_{swingup} + c_1 + g_1 - m_{11}m_{21}^{-1}(c_2 + g_2) \quad (7.33)$$

where $v_{swingup}$ is a new control to be designed, the dynamics of the Pendubot become:

$$m_{21}\ddot{q}_1 + c_2 + g_2 = -m_{22}v_{swingup} \quad (7.34a)$$

$$\ddot{q}_2 = v_{swingup} \quad (7.34b)$$

Equation (7.34b) is linear, a double integrator, and is simple to stabilize. Choose the following control law

$$v_{swingup} = -K_d\dot{q}_2 - K_pq_2 \quad (7.35)$$

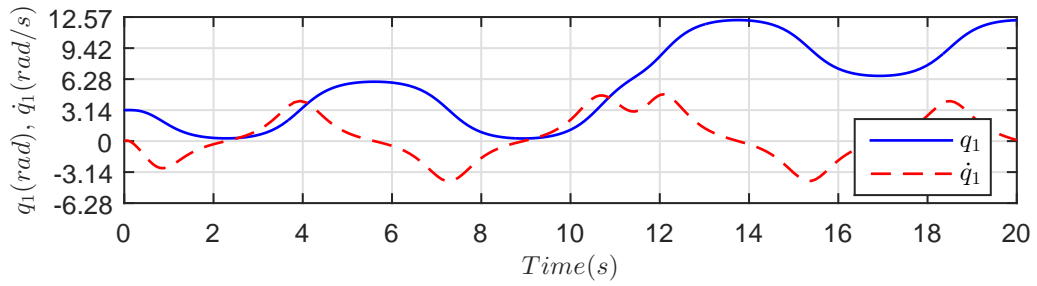
with K_d , K_p as positive design constants. The control $v_{swingup}$ combined with u_{PFL2} (7.33) can stabilize q_2 , however the q_1 -dynamics, obviously, become unstable. Once q_2 is stabilized, $v_{swingup}$ becomes zero and the q_1 -dynamics, in accordance with Eq. (7.32) (equivalently, Eq. (7.34a)), become

$$(m_2\ell_2^2 + I_2 + m_2L_1\ell_2)\ddot{q}_1 - m_2\ell_2g\sin(q_1) = 0 \quad (7.36)$$

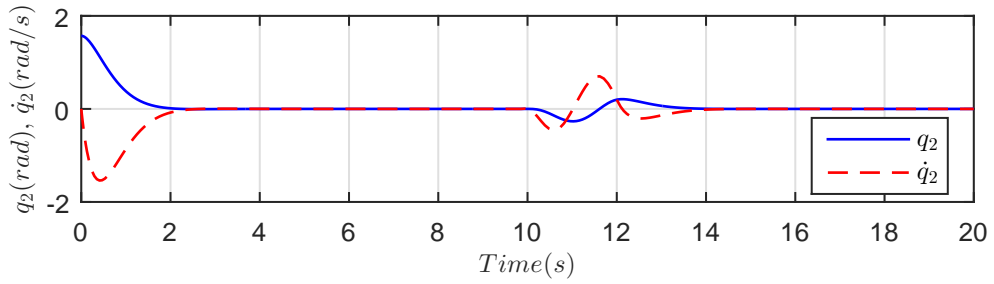
Linearization and simple stabilization w.r.t. to q_2 led to the above dynamics in Eq. (7.36) for q_1 that represents a simple pendulum. Figure 7.12 shows closed loop response of the Pendubot with $v_{swingup}$ (7.35) with $K_d = 4.3$, $K_p = 6.0$ for the initial condition $q(0) = [\pi, 0, \frac{\pi}{2}, 0]^T$. The pendulum behavior in Eq. (7.36) is shown Fig. 7.12a.

A simple choice of K_d , and K_p resulting in stable closed loop poles of (7.34b) can achieve the desired response for q_2 -dynamics as shown in Fig. 7.12b and a pendulum behavior for q_1 that is helpful in stabilization by the HOSM control. Figure 7.13 shows a successful using $v_{swingup}$ (7.35) with $K_d = 4.3$, $K_p = 6.0$ and then balancing by the HOSM control (6.25) in the presence of external disturbance for the initial condition $q(0) = [\pi, 0, \frac{\pi}{2}, 0]^T$.

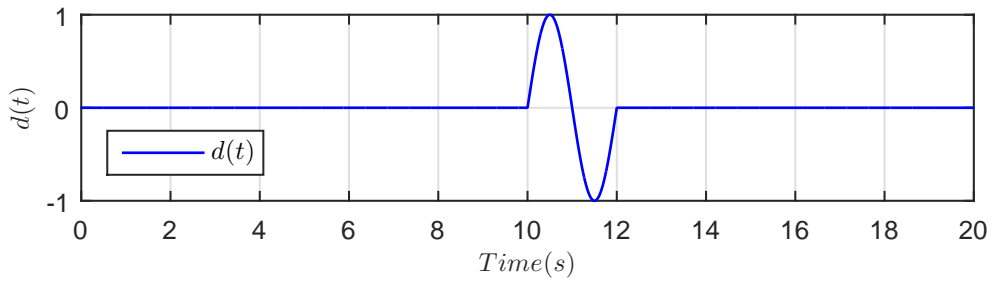
Fig. 7.12 shows the adverse effect of even a smaller disturbance on system response under the state feedback control (7.35) and Fig. 7.13 shows the system response is robust to even a larger disturbance under the HOSM control (6.25). Having a large attractive region and robustness to large disturbance are the two main and crucial properties of a balancing control.



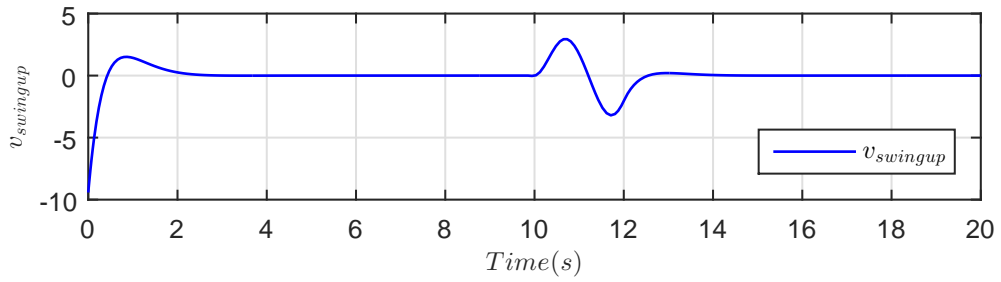
(A) Link 1 position q_1 (rad) and velocity \dot{q}_1 (rad/s)



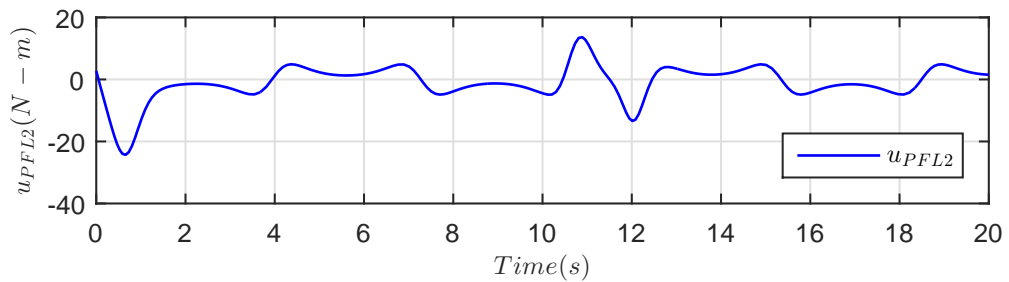
(B) Link 2 position q_2 (rad) and velocity \dot{q}_2 (rad/s)



(C) Disturbance $d(t) = 1 \sin(\pi t)$



(D) Swingup control $v_{swingup}$



(E) Control effort u_{PFL2} (N-m)

FIGURE 7.12: Pendubot - Closed loop response with control law (7.35) ($K_d = 4.3$, $K_p = 6$), $q(0) = [\pi, 0, \frac{\pi}{2}, 0, 0]^T$

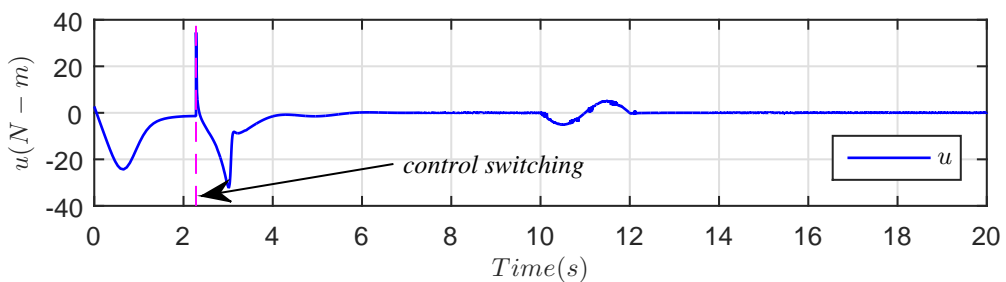
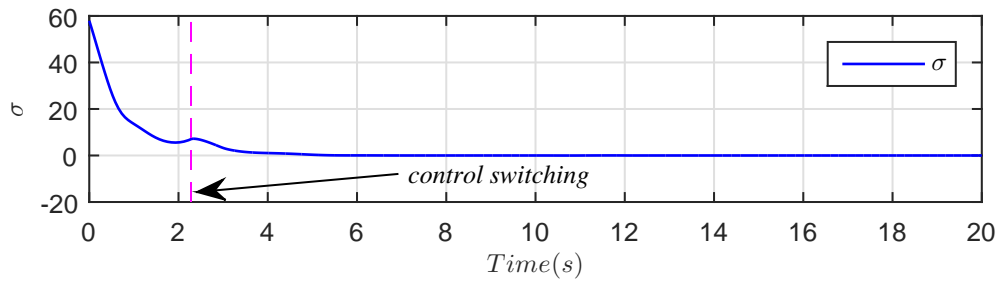
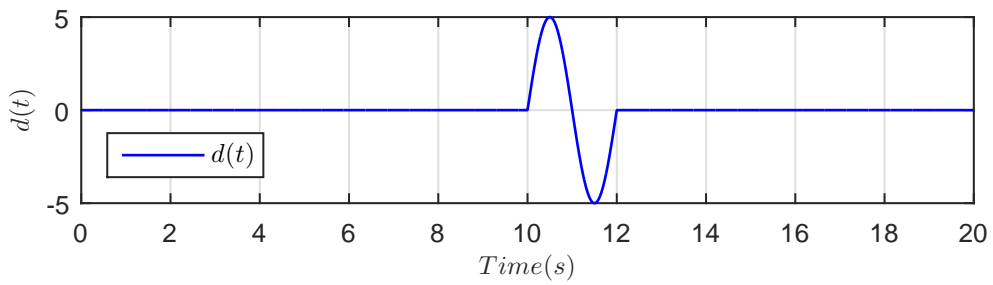
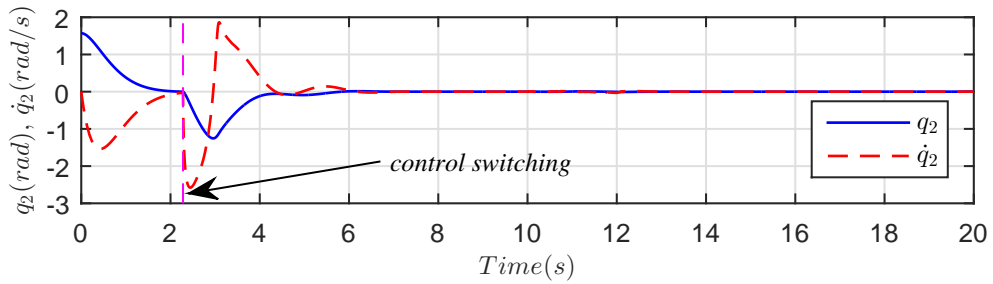
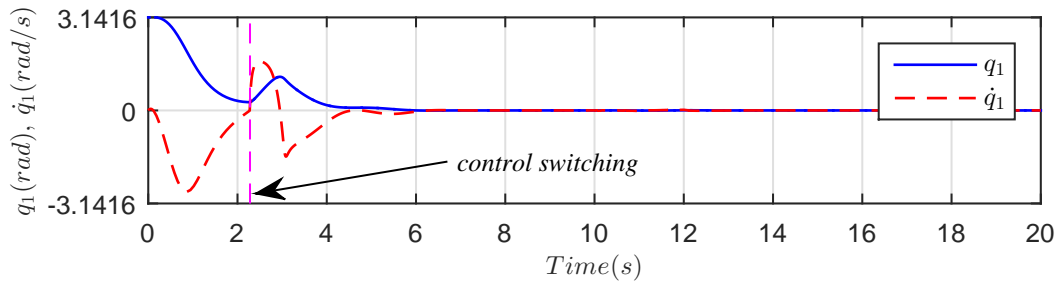


FIGURE 7.13: Pendubot - Swingup with control law (7.35) ($K_d = 4.3$, $K_p = 6$) and balancing with HOSM control law (6.25) ($K_1 = 125$, $K_2 = 100$) and observer (6.26) ($\lambda_1 = 3$, $\lambda_2 = 5$), sliding parameters ($\alpha = 8$, $\beta = 16$), $q(0) = [\pi, 0, \frac{\pi}{2}, 0]^T$

7.3 Chapter Summary and Conclusions

Swingup control problem of underactuated mechanical systems was addressed using classical considerations of the partial feedback linearization. The result were applied to the IWP, the Acrobot, Furuta Pendulum, and the Pendubot. Successful swingups with the designed Swingup Control laws and balancing with the HOSM control were demonstrated for the following systems.

A. Class-I Underactuated Mechanical Systems:

1. The Inertia-Wheel Pendulum
2. The Acrobot

B. Class-II Underactuated Mechanical Systems:

1. The Furuta Pendulum
2. The Pendubot

Chapter 8

Conclusion and Future Work

A comprehensive robust control design framework for underactuated mechanical systems was developed on the basis of sliding mode control theory. First, conventional linear sliding surfaces were introduced. Then novel nonlinear sliding manifolds based on the Lagrangian zero dynamics were introduced. The proposed framework provides the following sliding mode solutions to the control problem of underactuated mechanical systems:

1. Standard SMC design for underactuated mechanical systems
2. HOSM design for underactuated mechanical systems
3. Smooth HOSM design for underactuated mechanical systems
4. Swingup control design for underactuated mechanical systems

The framework was applied to the following benchmark underactuated mechanical systems:

1. The Inertia-Wheel Pendulum
2. The TORA System
3. The Acrobot

4. The Furuta Pendulum
5. The Overhead Crane
6. The Cart-Pole System
7. The Pendubot
8. The Beam-and-Ball System

8.1 Conclusion

Based on the results, the following conclusions are drawn.

1. The proposed framework addresses the control problem of underactuated mechanical systems in a comprehensive way.
2. The designed control laws have enhanced stabilization and tracking (set-point regulation) response for the above benchmark underactuated mechanical systems.
3. The results are in agreement and improved to standard results reported in the literature.
4. Being sliding mode, the framework is robust to parametric variations and disturbance in contrast to other works mentioned in the comparisons.
5. The design procedure is simple compared to other approaches the results were compared to.
6. Chattering free and smooth control action needed for mechanical control systems is achieved with HOSM techniques.

Underactuated mechanical systems are more vulnerable than fully actuated system to disturbances due to absence of actuators for some of the configuration variables and the effects of disturbances are more complex due to coupling. Both

the matched and unmatched disturbances are taken care of explicitly in the design procedure. A detailed analysis of the results supports the following findings.

1. The effect of the matched disturbance remains the same and can be fully rejected by the controller by utilizing the discontinuous gain of the controller embodied explicitly in the control law.
2. The effect of the unmatched disturbance is scaled to a lower or a higher value depending on the elements of the inertia matrix of the system.
3. The unmatched disturbance cannot be rejected by the controller by utilizing the discontinuous gain of the controller embodied explicitly in the control law.
4. When both matched and unmatched disturbances are applied at the same time, they may cancel their effects depending on the nature of the disturbances and the the elements of the inertia matrix of the system.

8.2 Future Work

Based on the research work, the following directions are recommended for future work.

1. Extension and application of the theory to higher order underactuated mechanical systems.
2. Application of sliding mode control theory to swingup control problems of underactuated mechanical systems.
3. Application of sliding mode observation techniques to underactuated mechanical systems.
4. Practical implementation of the theory on prototype underactuated mechanical systems.

Bibliography

- [1] A. Isidori, *Nonlinear Control Systems*. Springer, 1995.
- [2] I. Kolmanovsky and N. H. McClamroch, “Developments in nonholonomic control problems,” *IEEE Control Syst. Mag*, vol. 15, pp. 20 – 36, 1995.
- [3] R. W. Brockett, “Asymptotic stability and feedback stabilization,” in *Differential geometric control theory*, R. W. Brockett, R. S. Millman, and H. J. Sussman, Eds. Boston, MA: Birkhauser, 1983.
- [4] G. Oriolo and T. Nakamura, “Control of mechanical systems with second-order nonholonomic constraints: underactuated manipulators,” in *Proc. IEEE Int. Conf. Decision and Control*, Brighton, UK, 1991, pp. 2398–2403.
- [5] K. Y. Wichlund, O. J. Sordalen, and O. Egeland, “Control of vehicles with second-order nonholonomic constraints: Underactuated Vehicles,” in *European Control Conf*, Rome, Italy, 1995, pp. 3086–3091.
- [6] M. Reyhanoglu, A. Schaft, N. H. McClamroch, and I. Kolmanovsky, “Dynamics and control of a class of underactuated mechanical systems,” *IEEE Trans. Autom. Control*, vol. 44, pp. 1663 – 1671, 1999.
- [7] Y. L. Gu, “A direct adaptive control scheme for underactuated dynamic systems,” in *Proc. Conf. Decision and Control*, San Antonio, Texas, USA, 1993, pp. 1625–1627.
- [8] M. W. Spong, “Partial feedback linearization of underactuated mechanical systems,” in *Proc. IEEE/RSJ/GI Int. Conf. Intelligent Robots and Systems*, Munich, Germany, 1994, pp. 314–321.

-
- [9] —, “Energy based control of a class of underactuated mechanical systems,” in *Proc. IFAC World Congress*, San Francisco, CA, USA, 1996, pp. 431–435.
- [10] —, “Underactuated mechanical systems,” in *Control problems in robotics and automation*, B. Siciliano and K. P. Valavanis, Eds. London: Springer-Verlag, 1998.
- [11] G. Bartolini, A. Pisano, E. Punta, and E. Usai, “A survey of applications of second-order sliding mode control to mechanical systems.” *Int. J. Control*, vol. 76, no. 9/10, pp. 875–892, 2003.
- [12] Y. Liu and H. Yu, “A survey of underactuated mechanical systems,” *IET Control Theory Appl.*, vol. 7, pp. 921–935, 2013.
- [13] M. W. Spong, P. Corke, and R. Lozano, “Nonlinear control of the Inertia Wheel Pendulum,” *Automatica*, vol. 37, pp. 1845–1851, 2001.
- [14] R. Olfati-Saber, “Global stabilization of a flat underactuated system: the Inertia Wheel Pendulum.” in *Proceedings of the 40th IEEE Conference on Decision and Control*, vol. 4, Orlando, Florida, USA, 2001, pp. 3764–3765.
- [15] H. Ye, H. Wang, and H. Wang, “Stabilization of a PVTOL aircraft and an Inertia Wheel Pendulum using saturation technique,” *IEEE Trans. Control Syst. Technol.*, vol. 15, pp. 1143–1150, 2007.
- [16] R. T. Bupp, D. S. Bernstein, and V. T. Coppola, “A benchmark problem for nonlinear control design,” *Int. J. Robust Nonlinear Control*, vol. 8, pp. 307–310, 1998.
- [17] C.-J. Wan, D. S. Bernstein, and V. T. Coppola, “Global stabilization of the oscillating eccentric rotor,” *Nonlinear Dyn.*, vol. 10, pp. 49–62, 1996.
- [18] M. Jankovic, D. Fontaine, and P. V. Kokotovic, “TORA example: cascade and passivity-based control designs,” *IEEE Trans. Control Syst. Technol.*, vol. 4, pp. 292–297, 1996.

-
- [19] Z. P. Jiang, D. J. Hill, and Y. Guo, "Stabilization and tracking via output feedback for a nonlinear benchmark system," *Automatica*, vol. 34(7), pp. 907–915, 1998.
- [20] Z. P. Jiang and I. Kanellakopoulos, "Global output-feedback tracking for a benchmark nonlinear system," *IEEE Trans. Autom. Control*, vol. 45(5), pp. 1023–1027, 2000.
- [21] A. Pavlov, B. Janssen, N. Van de Wouw, and H. Nijmeijer, "Experimental output regulation for a nonlinear benchmark system," *IEEE Trans. Control Syst. Technol.*, vol. 15, pp. 786–793, 2007.
- [22] I. Kolmanovsky and N. H. McClamroch, "Hybrid feedback stabilization of rotational translational actuator (rtac) system," *Int. J. Robust Nonlinear Control*, vol. 8, pp. 367–375, 1998.
- [23] C. P. Mracek and R. C. James, "Control designs for the nonlinear benchmark problem via the state-dependent Riccati equation method," *Int. J. Robust Nonlinear Control*, vol. 8, pp. 401–433, 1998.
- [24] S. Dussy and L. El Ghaoui, "Measurement-scheduled control for the RTAC problem: an LMI approach." *Int. J. Robust Nonlinear Control*, vol. 8, pp. 377–400, 1998.
- [25] T. Mahdi, H. D. Taghirad, and M. Abrishamchian, "Identification and robust H control of the rotational/translational actuator system," *Int. J. Control. Autom. Syst.*, vol. 3, pp. 387–396, 2005.
- [26] P. Tsiotras, M. Corless, and M. A. Rotea, "An L2 disturbance attenuation solution to the nonlinear benchmark problem," *Int. J. Robust Nonlinear Control*, vol. 8, pp. 311–330, 1998.
- [27] M. W. Spong, "The swing up control problem for the acrobot," *IEEE control systems*, vol. 15, no. 1, pp. 49–55, 1995.

- [28] X. Xin and M. Kaneda, “Analysis of the energy-based swing-up control of the acrobot,” *International Journal of Robust and Nonlinear Control*, vol. 17, no. 16, pp. 1503–1524, 2007.
- [29] S. C. Brown and K. M. Passino, “Intelligent control for an acrobot,” *Journal of intelligent & robotic systems*, vol. 18, no. 3, pp. 209–248, 1997.
- [30] R. Jafari, F. B. Mathis, and R. Mukherjee, “Swing-up control of the acrobot: An impulse-momentum approach,” in *American Control Conference (ACC), 2011*. IEEE, 2011, pp. 262–267.
- [31] X.-Z. Lai, J.-H. She, S. X. Yang, and M. Wu, “Comprehensive unified control strategy for underactuated two-link manipulators,” *IEEE Transactions on Systems, Man, and Cybernetics, Part B (Cybernetics)*, vol. 39, no. 2, pp. 389–398, 2009.
- [32] M.-S. Park and D. Chwa, “Swing-up and stabilization control of inverted-pendulum systems via coupled sliding-mode control method,” *IEEE Trans. Ind. Electron.*, vol. 56, no. 9, pp. 3541–3555, 2009.
- [33] I. Fantoni and R. Lozano, “Stabilization of the Furuta Pendulum around its homoclinic orbit,” *Int. J. Control*, vol. 75, pp. 390–398, 2002.
- [34] A. S. Shiriaev, L. B. Freidovich, A. Robertsson, R. Johansson, and A. Sandberg, “Virtual-holonomic-constraints-based design of stable oscillations of Furuta Pendulum: theory and experiments,” *IEEE Trans. Robot.*, vol. 23, pp. 827–832, 2007.
- [35] L. B. Freidovich, A. S. Shiriaev, F. Gordillo, F. Gómez-Estern, and J. Aracil, “Partial-energy-shaping control for orbital stabilization of high frequency oscillations of the Furuta Pendulum,” *IEEE Trans. Control Syst. Technol.*, vol. 17, pp. 853–858, 2009.
- [36] J. Aracil, J. A. Acosta, and F. Gordillo, “A nonlinear hybrid controller for swinging-up and stabilizing the Furuta Pendulum,” *Control Engineering Practice*, vol. 21, no. 8, pp. 989–993, 2013.

- [37] N. Sun, Y. Fang, and H. Chen, “A continuous robust anti-swing tracking control scheme for underactuated crane systems with experimental verification,” *J. Dyn. Syst. Meas. Control*, 2016.
- [38] N. Sun, Y. Fang, Y. Zhang, and B. Ma, “A novel kinematic coupling-based trajectory planning method for overhead cranes,” *IEEE/ASME Transactions on Mechatronics*, vol. 17, no. 1, pp. 166–173, 2012.
- [39] Y. Fang, B. Ma, P. Wang, and X. Zhang, “A motion planning-based adaptive control method for an underactuated crane system,” *IEEE Trans. Control Syst. Technol.*, vol. 20, no. 1, pp. 241–248, 2012.
- [40] B. Ma, Y. Fang, and Y. Zhang, “Switching-based emergency braking control for an overhead crane system,” *IET Control Theory Appl.*, vol. 4, no. 9, pp. 1739–1747, 2010.
- [41] N. B. Almutairi and M. Zribi, “Sliding mode control of a three dimensional overhead crane,” *J. Vib. Control*, vol. 15, pp. 1679–1730, 2009.
- [42] B. Kolar, H. Rams, and K. Schlacher, “Time-optimal flatness based control of a gantry crane,” *Control Engineering Practice*, vol. 60, pp. 18–27, 2017.
- [43] Z. Zhang, Y. Wu, and J. Huang, “Differential-flatness-based finite-time anti-swing control of underactuated crane systems,” *Nonlinear Dynamics*, vol. 87, no. 3, pp. 1749–1761, 2017.
- [44] J. Zhao and M. W. Spong, “Hybrid control for global stabilization of the cart–pendulum system,” *Automatica*, vol. 37, no. 12, pp. 1941–1951, 2001.
- [45] N. Muškinja and B. Tovornik, “Swinging up and stabilization of a real inverted pendulum,” *IEEE Trans. Ind. Electron.*, vol. 53, pp. 631–639, 2006.
- [46] M. B. P. Mason and B. Piccoli, “Time optimal swing-up of the planar pendulum,” *IEEE Trans. Autom. Control*, vol. 53, pp. 1876–1886, 2008.
- [47] C. C. Chung and J. Hauser, “Nonlinear control of a swinging pendulum,” *Automatica*, vol. 31, no. 6, pp. 851–862, 1995.

- [48] D. Chatterjee, A. Patra, and H. K. Joglekar, “Swing-up and stabilization of a cart–pendulum system under restricted cart track length,” *Systems & control letters*, vol. 47, no. 4, pp. 355–364, 2002.
- [49] D. Angeli, “Almost global stabilization of the inverted pendulum via continuous state feedback,” *Automatica*, vol. 37, no. 7, pp. 1103–1108, 2001.
- [50] A. Shiriaev, H. Ludvigsen, O. Egeland, and A. Pogromsky, “On global properties of passivity based control of the inverted pendulum,” in *Decision and Control, 1999. Proceedings of the 38th IEEE Conference on*, vol. 3. IEEE, 1999, pp. 2513–2518.
- [51] C. E. Lin and Y. R. Sheu, “A hybrid-control approach for pendulum-car control,” *IEEE Transactions on Industrial Electronics*, vol. 39, no. 3, pp. 208–214, 1992.
- [52] M. W. Spong and D. J. Block, “The pendubot: A mechatronic system for control research and education,” in *Decision and Control, 1995., Proceedings of the 34th IEEE Conference on*, vol. 1. IEEE, 1995, pp. 555–556.
- [53] I. Fantoni, R. Lozano, and M. W. Spong, “Energy based control of the pendubot,” *IEEE Transactions on Automatic Control*, vol. 45, no. 4, pp. 725–729, 2000.
- [54] M. Zhang and T.-J. Tarn, “Hybrid control of the pendubot,” *IEEE/ASME transactions on mechatronics*, vol. 7, no. 1, pp. 79–86, 2002.
- [55] W. Li, K. Tanaka, and H. O. Wang, “Acrobatic control of a pendubot,” *IEEE Transactions on Fuzzy Systems*, vol. 12, no. 4, pp. 549–554, 2004.
- [56] T. Albahkali, R. Mukherjee, and T. Das, “Swing-up control of the pendubot: an impulse–momentum approach,” *IEEE Transactions on Robotics*, vol. 25, no. 4, pp. 975–982, 2009.
- [57] Y. Orlov, L. T. Aguilar, L. Acho, and A. Ortiz, “Swing up and balancing control of pendubot via model orbit stabilization: Algorithm synthesis

- and experimental verification,” in *Decision and Control, 2006 45th IEEE Conference on*. IEEE, 2006, pp. 6138–6143.
- [58] D. Qian, J. Yi, and D. Zhao, “Hierarchical sliding mode control to swing up a pendubot,” in *American Control Conference, 2007. ACC'07*. IEEE, 2007, pp. 5254–5259.
- [59] L. Freidovich, A. Robertsson, A. Shiriaev, and R. Johansson, “Periodic motions of the pendubot via virtual holonomic constraints: Theory and experiments,” *Automatica*, vol. 44, no. 3, pp. 785–791, 2008.
- [60] X. Xin, S. Tanaka, J. She, and T. Yamasaki, “New analytical results of energy-based swing-up control for the pendubot,” *International Journal of Non-Linear Mechanics*, vol. 52, pp. 110–118, 2013.
- [61] D. Xia, L. Wang, and T. Chai, “Neural-network-friction compensation-based energy swing-up control of pendubot,” *IEEE Transactions on Industrial Electronics*, vol. 61, no. 3, pp. 1411–1423, 2014.
- [62] D. Xia, T. Chai, and L. Wang, “Fuzzy neural-network friction compensation-based singularity avoidance energy swing-up to nonequilibrium unstable position control of pendubot,” *IEEE Transactions on Control Systems Technology*, vol. 22, no. 2, pp. 690–705, 2014.
- [63] J. Hauser, S. Sastry, and P. Kokotovic, “Nonlinear control via approximate input-output linearization: the beam and ball example,” *IEEE Trans. Autom. Control*, vol. 37, pp. 392–398, 1992.
- [64] D. Voytsekhovskiy and R. M. Hirschorn, “Stabilization of singleinput nonlinear systems using higherorder term compensating sliding mode control,” *Int. J. Robust Nonlinear Control*, vol. 18, no. 4-5, pp. 468–480, 2008.
- [65] N. B. Almutairi and M. Zribi, “On the sliding mode control of a ball on a beam system,” *Nonlinear Dyn.*, vol. 59, pp. 221–238, 2010.

- [66] F. Andreeva, D. Aucklyb, S. Gosavic, L. Kapitanskib, A. Kelkard, and W. Whitec, “Matching, linear systems, and the ball and beam,” *Automatica*, vol. 38, pp. 2147–2152, 2002.
- [67] Y. Aoustin and A. FormalSkii, “Ball on a beam: stabilization under saturated input control with large basin of attraction,” *Multibody System Dynamics*, vol. 21, no. 1, pp. 71–89, 2009.
- [68] R. M. Hirschorn, “Incremental sliding mode control of the ball and beam,” *IEEE Transactions on Automatic Control*, vol. 47, no. 10, pp. 1696–1700, 2002.
- [69] L. Marton, A. S. Hodel, B. Lantos, and J. Y. Hung, “Underactuated robot control: comparing LQR, subspace stabilization, and combined error metric approaches,” *IEEE Trans. Ind. Electron.*, vol. 50, pp. 3724–3730, 2008.
- [70] A. M. Bloch, N. E. Leonard, and J. E. Marsden, “Controlled Lagrangians and the stabilization of mechanical systems I: the first matching theorem,” *IEEE Trans. Autom. Control*, vol. 45, pp. 2253–2270, 2000.
- [71] A. M. Bloch, D. E. Chang, N. E. Leonard, and J. E. Marsden, “Controlled Lagrangians and the stabilization of mechanical systems II: potential shaping,” *IEEE Trans. Autom. Control*, vol. 46, pp. 1556–1571, 2001.
- [72] R. Ortega, M. W. Spong, F. Gómez-Estern, and G. Blankenstein, “Stabilization of a class of underactuated mechanical systems via interconnection and damping assignment,” *IEEE Trans. Autom. Control*, vol. 47, pp. 1218–1232, 2002.
- [73] R. Fierro, F. L. Lewis, and A. Lowe, “Hybrid control for a class of underactuated mechanical systems,” *IEEE Transactions on Systems, Man, and Cybernetics-Part A: Systems and Humans*, vol. 29, no. 6, pp. 649–654, 1999.
- [74] M. Zhang and T.-J. Tarn, “A hybrid switching control strategy for nonlinear and underactuated mechanical systems,” *IEEE Transactions on Automatic Control*, vol. 48, no. 10, pp. 1777–1782, 2003.

- [75] J. She, A. Zhang, X. Lai, and M. Wu, “Global stabilization of 2-DOF underactuated mechanical systems - an equivalent-input-disturbance approach,” *Nonlinear Dynamics*, vol. 69, no. 1-2, pp. 495–509, 2012.
- [76] R. Xu and U. Özgüner, “Sliding mode control of a class of underactuated systems,” *Automatica*, vol. 44, pp. 233–241, 2008.
- [77] H. Ashrafiuon and R. S. Erwin, “Sliding mode control of underactuated multibody systems and its application to shape change control,” *Int. J. Control*, vol. 81, pp. 1849–1858, 2008.
- [78] W. Wang, J. Yi, D. Zhao, and D. Liu, “Design of a stable sliding-mode controller for a class of second-order underactuated systems,” *IEE Proceedings-Control Theory and Applications*, vol. 151, no. 6, pp. 683–690, 2004.
- [79] S. Riachy, Y. Orlov, T. Floquet, R. Santiesteban, and J.-P. Richard, “Second-order sliding mode control of underactuated mechanical systems i: Local stabilization with application to an inverted pendulum,” *International Journal of Robust and Nonlinear Control*, vol. 18, no. 4-5, pp. 529–543, 2008.
- [80] R. Santiesteban, T. Floquet, Y. Orlov, S. Riachy, and J.-P. Richard, “Second-order sliding mode control of underactuated mechanical systems ii: Orbital stabilization of an inverted pendulum with application to swing up/balancing control,” *International Journal of Robust and Nonlinear Control*, vol. 18, no. 4-5, pp. 544–556, 2008.
- [81] V. I. Utkin, J. Guldner, and J. Shi, *Sliding Mode Control in Electromechanical Systems*. London: Taylor and Francis, 1999.
- [82] V. I. Utkin, *Sliding Modes in Optimization and Control Problems*. New York: Springer, 1992.
- [83] C. Edwards and S. Spurgeon, *Sliding Mode Control: Theory and Applications*. London: Taylor and Francis, 1998.

- [84] A. M. Bloch, M. Reyhanoglu, and N. H. McClamroch, “Control and stabilization of nonholonomic dynamic systems,” *IEEE Trans. Autom. Control*, vol. 37, pp. 1746 – 1757, 1992.
- [85] H. J. Sussmann, “A general theorem on local controllability,” *SIAM J. Control Optim.*, vol. 25, pp. 158–194, 1987.
- [86] A. de Luca, R. Mattone, and G. Oriolo, “Control of underactuated mechanical systems: application to the planar 2R robot,” in *Proc. Conf. Decision and Control*, Kobe, Japan, 1996, pp. 1455–1460.
- [87] H. Arai and S. Tachi, “Position control of a manipulator with passive joints using dynamic coupling,” *IEEE Trans. Robot. Autom.*, vol. 7, pp. 528–534, 1991.
- [88] M. W. Spong, “On the robust control of robot manipulators,” *IEEE Trans. Autom. Control*, vol. 27, pp. 1782–1786, 1992.
- [89] J. H. Shin, “Trajectory planning and robust adaptive control for underactuated manipulators,” *Eletron. Lett.*, vol. 27, pp. 1705–1706, 1998.
- [90] C. Y. Su and Y. Stepanenko, “Adaptive variable structure set-point control of underactuated robots,” *Eletron. Lett.*, vol. 44, pp. 2090–2093, 1999.
- [91] A. de Luca, S. Iannitti, and G. Oriolo, “Control problems in underactuated manipulators,” in *Proc. IEEE/ASME Int. Conf. Advanced Intelligent Mechatronics*, Como, Italy, 2001, pp. 8–12.
- [92] E. Garcia, A. Jimenez, P. Santos, and M. Armada, “The evolution of robotics research: from industrial robotics to field and service robotics,” *IEEE Robot. Autom. Mag.*, vol. 14, pp. 90–103, 2007.
- [93] I. Fantoni and R. Lozano, *Nonlinear control for underactuated mechanical systems*. London: Springer-Verlag, 2001.

-
- [94] R. Olfati-Saber, “Nonlinear control of underactuated mechanical systems with application to robotics and aerospace vehicles,” Ph.D. dissertation, Department of Electrical Engineering and Computer, Massachusetts Institute of Technology, 2001.
- [95] N. P. I. Aneke, “Control of underactuated mechanical systems,” Ph.D. dissertation, Mechanical Engineering, Eindhoven University of Technology, 2003.
- [96] R. Olfati-Saber, “Normal forms for underactuated mechanical systems with symmetry,” *IEEE Trans. Autom. Control*, vol. 47, pp. 305–308, 2002.
- [97] H. Goldstein, *Classical Mechanics*. Addison Wesley, USA, 1981.
- [98] R. Olfati-Saber, “Trajectory tracking for a flexible one-link robot using a nonlinear noncollocated output,” in *Proc. IEEE Conf. Decision Control*, Sydney, Australia, 2000, pp. 4024–4029.
- [99] I. Fantoni, R. Lozano, and M. W. Spong, “Energy based control of the pendubot,” *IEEE Trans. Autom. Control*, vol. 45, pp. 725–729, 2000.
- [100] K. J. strm and K. Furuta, “Swinging up a pendulum by energy control,” *Automatica*, vol. 36, pp. 287–295, 2000.
- [101] X. Z. Lai, J. H. She, S. X. Yang, and M. Wu, “Comprehensive unified control strategy for underactuated two-link manipulators,” *IEEE Trans. Syst. Man Cybern. Part B: Cybern.*, vol. 39, pp. 389–398, 2009.
- [102] B. Gao, X. Zhang, H. Chen, and J. Zhao, “Energy-based control design of an underactuated 2-dimensional tora system,” in *Proc.e IEEE/RSJ Int. Conf. Intelligent Robots and Systems*, St. Louis, USA, 2009, pp. 1296–1301.
- [103] M. W. Spong, J. K. Holm, and D. Lee, “Passivity-based control of bipedal locomotion,” *IEEE Robot. Autom. Mag.*, vol. 14, pp. 30–40, 2007.
- [104] X. Xin and M. Kaneda, “Analysis of the energy-based control for swinging up two pendulums,” *IEEE Trans. Autom. Control*, vol. 50, pp. 679–684, 2005.

-
- [105] W. Zhong and H. Rock, “Energy and passivity based control of the double inverted pendulum on a cart,” in *Proc. IEEE Int. Conf. Control Applications*, Mexico City, Mexico, 2001, pp. 896–901.
- [106] R. Ortega and E. Canseco, “Interconnection and damping assignment passivity-based control: a survey,” *European J. Control*, vol. 10, pp. 432–450, 2004.
- [107] R. Ortega, A. van der Schaft, B. Maschke, and G. Escobar, “Interconnection and damping assignment passivity-based control of port-controlled hamiltonian systems,” *European J. Control*, vol. 38, pp. 585–596, 2002.
- [108] M. Krstic, I. Kanellakopoulos, and P. Kokotovic, *Nonlinear and Adaptive Control Design*. New York: Wiley, 1995.
- [109] J. Ghommam, F. Mnif, A. Benali, and N. Derbel, “Asymptotic backstepping stabilization of an underactuated surface vessel,” *IEEE Trans. Control Syst. Technol.*, vol. 14, pp. 1150–1157, 2006.
- [110] J. Ghommam, F. Mnif, and N. Derbel, “Global stabilisation and tracking control of underactuated surface vessels,” *IET Control Theory Appl.*, vol. 4, pp. 71–88, 2010.
- [111] K. D. Do, Z. P. Jiang, and J. Pan, “Underactuated ship global tracking under relaxed conditions,” *IEEE Trans. Autom. Control*, vol. 47, pp. 1529–1536, 2002.
- [112] F. Y. Bi, Y. J. Wei, J. Z. Zhang, and W. Cao, “Position-tracking control of underactuated autonomous underwater vehicles in the presence of unknown ocean currents,” *IET Control Theory Appl.*, vol. 4, pp. 2369–2380, 2010.
- [113] A. Abdessameuda and A. Tayebi, “Global trajectory tracking control of vtol-uavs without linear velocity measurements,” *Automatica*, vol. 46, pp. 1053–1059, 2010.

-
- [114] R. Olfati-Saber, “Global configuration stabilization for the vtol aircraft with strong input coupling,” *IEEE Trans. Autom. Control*, vol. 47, pp. 1949–1952, 2002.
- [115] K. D. Do, Z. P. Jiang, and J. Pan, “On global tracking control of a vtol aircraft without velocity measurements,” *IEEE Trans. Autom. Control*, vol. 48, pp. 2212–2217, 2003.
- [116] —, “Robust adaptive path following of underactuated ships,” *Automatica*, vol. 40, pp. 929–944, 2004.
- [117] Z. Cai and C. Y. Su, “Real-time tracking control of underactuated pendubot using takagi-sugeno fuzzy systems,” in *Proc. IEEE Int. Symp. Computational Intelligence in Robotics and Automation*, Kobe, Japan, 2003, pp. 73–78.
- [118] C. W. Tao, J. S. Taur, T. W. Hsieh, and C. L. Tsa, “Design of a fuzzy controller with fuzzy swing-up and parallel distributed pole assignment schemes for an inverted pendulum and cart system,” *IEEE Trans. Control Syst. Technol.*, vol. 16, pp. 1277–1288, 2008.
- [119] O. Begovich, E. N. Sanchez, and M. Maldonado, “Takagi-sugeno fuzzy scheme for real-time trajectory tracking of an underactuated robot,” *IEEE Trans. Control Syst. Technol.*, vol. 10, pp. 14–20, 2002.
- [120] W. Li, K. Tanaka, and H. O. Wang, “Acrobatic control of a pendubot,” *IEEE Trans. Fuzzy Syst.*, vol. 12, pp. 549–552, 2004.
- [121] M. I. El-Hawwary, A. L. Elshafei, H. M. Emara, and H. A. Fattah, “Adaptive fuzzy control of the inverted pendulum problem,” *IEEE Trans. Control Syst. Technol.*, vol. 14, pp. 1135–1144, 2006.
- [122] R. J. Wai, M. A. Kuo, and J. D. Lee, “Cascade direct adaptive fuzzy control design for a nonlinear two-axis inverted-pendulum servomechanism,” *IEEE Trans. Syst. Man Cybern. B, Cybern.*, vol. 38, pp. 439–454, 2008.

- [123] S. Aloui, O. Pags, A. Hajjaji, A. Chaari, and Y. Koubaa, “Robust adaptive fuzzy sliding mode control design for a class of mimo underactuated systems,” in *Proc. IFAC World Congress*, Milano, Italy, 2011, pp. 11 127–11 132.
- [124] C. C. Kung, T. H. Chen, and L. C. Huang, “Adaptive fuzzy sliding mode control for a class of underactuated systems,” in *Proc. IEEE Int. Conf. Fuzzy Systems*, Taipei, Taiwan, 2009, pp. 1791–1796.
- [125] E. C. Yang, P. C. Chao, and C. K. Sung, “Optimal control of an underactuated system for landing with desired postures,” *IEEE Trans. Control Syst. Technol.*, vol. 19, pp. 248–255, 2011.
- [126] C. Park, D. J. Scheeres, V. Guibout, and A. M. Bloch, “Global solution for the optimal feedback control of the underactuated heisenberg system,” *IEEE Trans. Autom. Control*, vol. 53, pp. 2638–2642, 2008.
- [127] I. Hussein and A. M. Bloch, “Optimal control of underactuated nonholonomic mechanical systems,” *IEEE Trans. Autom. Control*, vol. 53, pp. 668–682, 2008.
- [128] M. B. P. Mason and B. Piccoli, “Time optimal swing-up of the planar pendulum,” *IEEE Trans. Autom. Control*, vol. 53, pp. 1876–1886, 2008.
- [129] P. Paoletti and R. Genesio, “Rate limited time optimal control of a planar pendulum,” *Syst. Control Lett.*, vol. 60, pp. 264–270, 2011.
- [130] M. Krstic and P. Tsiotras, “Inverse optimal stabilization of a rigid spacecraft,” *IEEE Trans. Autom. Control*, vol. 40, pp. 1042–1049, 1999.
- [131] V. Sankaranarayanan and A. D. Mahindrakar, “Control of a class of underactuated mechanical systems using sliding modes,” *IEEE Trans. Robot.*, vol. 25, pp. 459–467, 2009.
- [132] D. W. Qian, J. Q. Yi, and D. B. Zhao, “Robust control using sliding mode for a class of underactuated systems with mismatched uncertainties,” in

- Proc. IEEE Int. Conf. Robotics and Automation*, Rome, Italy, 2007, pp. 1449–1456.
- [133] S. G. Nersesov, H. Ashrafiuon, and P. Ghorbanian, “On the stability of sliding mode control for a class of underactuated nonlinear systems,” in *Proc. American Control Conf.*, Baltimore, MD, USA, 2010, pp. 3446–3451.
- [134] H. Ashrafiuon, K. R. Muske, L. C. McNinch, and R. A. Soltan, “Sliding mode tracking control of surface vessels,” *IEEE Trans. Ind. Electron.*, vol. 55, pp. 4004–4012, 2008.
- [135] J. Huang, Z. H. Guan, T. Matsuno, T. Fukuda, and K. Sekiyama, “Sliding-mode velocity control of mobile-wheeled inverted-pendulum systems,” *IEEE Trans. Robot.*, vol. 26, pp. 750–758, 2010.
- [136] R. Martinez, J. Alvarez, and Y. Orlov, “Hybrid sliding-mode-based control of underactuated systems with dry frictions,” *IEEE Trans. Ind. Electron.*, vol. 55, pp. 3998–4003, 2008.
- [137] M. Nikkhah, H. Ashrafiuon, and F. Fahimi, “Robust control of underactuated bipeds using sliding modes,” *Robotica*, vol. 25, pp. 367–374, 2007.
- [138] I. Boiko and L. Fridman, “Analysis of chattering in continuous sliding-mode controllers,” *IEEE Trans. Automat. Contr.*, vol. 50, no. 9, pp. 1442–1446, 2005.
- [139] L. Fridman, “The problem of chattering: an averaging approach,” in *Variable Structure, Sliding Mode and Nonlinear Control. Lecture Notes in Control and Information Science*, Y. K. and O. U., Eds. London: Springer, 1999, vol. 247, pp. 363–386.
- [140] —, “An averaging approach to chattering,” *IEEE Trans. Automat. Contr.*, vol. 46, no. 8, pp. 1260–1264, 2001.
- [141] —, “Singularly perturbed analysis of chattering in relay control systems,” *IEEE Trans. Automat. Contr.*, vol. 47, no. 12, pp. 2079–2084, 2002.

- [142] ———, “Chattering analysis in sliding mode systems with inertial sensors,” *Int. J. Control*, vol. 76, no. 9/10, pp. 906–912, 2003.
- [143] K. Furuta and Y. Pan, “Variable structure control with sliding sector,” *Automatica*, vol. 36, no. 2, pp. 211–228, 2000.
- [144] J.-J. Slotine and W. Li, *Applied Nonlinear Control*. New Jersey: Prentice Hall, 1991.
- [145] G. Bartolini, A. Ferrara, and E. Usai, “Chattering avoidance by second-order sliding mode control,” *IEEE Trans. Automat. Contr.*, vol. 43, no. 2, pp. 241–246, 1998.
- [146] I. Boiko, L. Fridman, A. Pisano, and E. Usai, “Analysis of chattering in systems with second order sliding modes,” *IEEE Trans. Automat. Contr.*, vol. 52, no. 11, pp. 2085–2102, 2007.
- [147] A. Levant, “Higher-order sliding modes, differentiation and output-feedback control,” *Int. J. Control*, vol. 76, no. 9/10, pp. 924–941, 2003.
- [148] A. Levant and L. V. Levantovsky, “Sliding order and sliding accuracy in sliding mode control,” *Int. J. Control*, vol. 586, pp. 1247–1263, 1993.
- [149] S. V. Emelyanov, S. K. Korovin, and L. V. Levantovsky, “Higher order sliding modes in the binary control systems,” *Sov. Phys. Dokl.*, vol. 31, no. 4, pp. 291–293, 1986.
- [150] A. Levant, “Quasi-continuous high-order sliding-mode controllers,” *IEEE Trans. Automat. Contr.*, vol. 50, no. 11, pp. 1812–1816, 2006.
- [151] ———, “Construction principles of 2-sliding mode design,” *Automatica*, vol. 43, no. 4, pp. 576–586, 2007.
- [152] ———, “Universal SISO sliding-mode controllers with finite-time convergence,” *IEEE Trans. Automat. Control*, vol. 46, no. 9, pp. 1447–1451, 2001.

- [153] Y. B. Shtessel, I. A. Shkolnikov, and A. Levant, “Smooth second-order sliding modes: Missile guidance application,” *Automatica*, vol. 43, no. 8, pp. 1470–1476, 2007.
- [154] S. Iqbal, C. Edwards, and A. I. Bhatti, “A smooth second-order sliding mode controller for relative degree two systems,” in *IECON 2010 - 36th Annual Conference on IEEE Industrial Electronics Society*, 2010, pp. 2370–2384.
- [155] J. J. E. Slotine, J. K. Hedrick, and E. A. Misawa, “On sliding observers for nonlinear systems,” *Trans. ASME: J. Dyn. Syst. Meas. Control*, vol. 109, pp. 245–252, 1987.
- [156] A. G. Bondarev, S. A. Bondarev, N. Y. Kostilyeva, and V. I. Utkin, “Sliding modes in systems with asymptotic state observers,” *Automatica i telemekhanika (Automat. Rem. Contr.)*, vol. 46, no. 5, pp. 679–684, 1985.
- [157] B. L. Walcott and S. H. Zak, “State observation of nonlinear uncertain dynamical systems,” *IEEE Trans. Automat. Contr.*, vol. 32, no. 2, pp. 166–170, 1987.
- [158] J. Davila, L. Fridman, and A. Levant, “Second-order sliding-mode observer for mechanical systems,” *IEEE Trans. Automat. Control*, vol. 50, no. 11, pp. 1785–1789, 2005.
- [159] Z. E. Cruz, J. A. Moreno, and L. Fridman, “Uniform second-order sliding mode observer for mechanical systems,” in *2010 11th International Workshop on Variable Structure Systems (VSS)*, 2010, pp. 14–19.
- [160] ———, “Uniform robust exact differentiator,” *IEEE Trans. Automat. Control*, vol. 56, no. 11, pp. 2727–2733, 2011.
- [161] C. Edwards, S. K. Spurgeon, and R. J. Patton, “Sliding mode observers for fault detection and isolation,” *Automatica*, vol. 36, no. 4, pp. 541–553, 2000.
- [162] H. Alwi, C. Edwards, and C. P. Tan, *Fault Detection and Fault-tolerant Control Using Sliding Modes.*, ser. Advances in Industrial Control Series. Berlin: Springer, 2011.

- [163] C. P. Tan and C. Edwards, "Sliding mode observers for robust detection and reconstruction of actuator and sensor faults," *Int. J. Robust. Nonlin.*, vol. 13, pp. 443–463, 2003.
- [164] —, "Robust fault reconstruction in linear uncertain systems using multiple sliding mode observers in cascade." *IEEE Trans. Automat. Contr.*, vol. 55, pp. 855–867, 2010.
- [165] R. H. Rand, R. J. Kinsey, and D. L. Mingori, "Dynamics of spinup through resonance," *Int. J. Non-Linear Mech.*, vol. 27, pp. 489–502, 1992.
- [166] R. T. Bupp, C.-J. Wan, V. T. Cappola, and D. S. Bernstein, "Design of a rotational actuator for global stabilization of translational motion," in *Symp. Active Contr. Vibration Noise, ASME Winter Mtg.*, Seattle, WA, USA, 1994, pp. 4363–4367.
- [167] N. Qaiser, N. Iqbal, A. Hussain, and N. Qaiser, "Exponential stabilization of a class of underactuated mechanical systems using dynamic surface control," *Int. J. Control. Autom. Syst.*, vol. 5, pp. 547–558, 2007.
- [168] L. Xu and Q. Hu, "Output-feedback stabilisation control for a class of underactuated mechanical systems," *IET Control Theory Appl.*, vol. 7, no. 7, pp. 985–996, 2013.
- [169] Y. F. Chen and A. C. Huang, "Controller design for a class of underactuated mechanical systems," *IET Control Theory Appl.*, vol. 6, pp. 103–110, 2012.
- [170] I. Shah and F. u. Rehman, "Smooth higher-order sliding mode control of a class of underactuated mechanical systems," *Arabian Journal for Science and Engineering*, vol. 42, no. 12, pp. 5147–5164, 2017.
- [171] M. López, Martínez, J. A. Acosta, and J. M. Cano, "Non-linear sliding mode surfaces for a class of underactuated mechanical systems," *IET Control Theory & Applications*, vol. 4, no. 10, pp. 2195–2204, 2010.

-
- [172] D. E. Chang, “Stabilizability of controlled Lagrangian systems of two degrees of freedom and one degree of under-actuation by the energyshaping method,” *IEEE Trans. Autom. Control*, vol. 55, pp. 1888–1893, 2010.
- [173] M. T. Ravichandran and A. Mahindrakar, “Robust stabilization of a class of underactuated mechanical systems using time scaling and Lyapunov redesign,” *IEEE Trans. Ind. Electron.*, vol. 58, pp. 4299–4313, 2011.
- [174] H. Ye, W. Gui, and Z. P. Jiang, “Backstepping design for cascade systems with relaxed assumption on Lyapunov functions,” *IET Control Theory Appl.*, vol. 5, pp. 700–712, 2011.
- [175] Y. Shtessel, C. Edwards, L. Fridman, and A. Levant, *Sliding mode control and observation*. Springer, 2014.
- [176] I. Shah and F. u. Rehman, “Smooth second order sliding mode control of a class of underactuated mechanical systems,” *accepted for publication in IEEE Access*, pp. 1–12, 2018.